Physiological Response of Plants Grown on Porous Ceramic Tubes

NASA Final Report
Contract #NAG10-112

Submitted to:
NASA Center for Aerospace Information
800 Elkridge Landing Road
Linthicum Heights, MD 21090-2934

By:
David Tsao and Martin Okos
Agricultural and Biological Engineering Department
Purdue University
West Lafayette

ABSTRACT

This research involves the manipulation of the root-zone water potential for the purposes of discriminating the rate limiting step in the inorganic nutrient uptake mechanism utilized by higher plants. This reaction sequence includes the pathways controlled by the root-zone conditions such as water tension and gradient concentrations. Furthermore, plant based control mechanisms dictated by various protein productions are differentiated as well. For the nutrients limited by the environmental availability, the kinetics were modeled using convection and diffusion equations. Alternatively, for the nutrients dependent upon enzyme manipulations, the uptakes are modeled using Michaelis-Menten kinetics. In order to differentiate between these various mechanistic steps, an experimental apparatus known as the Porous Ceramic Tube - Nutrient Delivery System (PCT-NDS) was used. Manipulation of the applied suction pressure circulating a nutrient solution through this system imposes a change in the matric component of the water potential. This compensates for the different osmotic components of water potential dictated by nutrient concentration. By maintaining this control over the root-zone conditions, the rate limiting steps in the uptake of the essential nutrients into tomato plants (*Lycopersicon esculentum* cv. Cherry Elite) were differentiated. Results showed that the uptake of some nutrients were mass transfer limited while others were limited by the enzyme kinetics. Each of these were adequately modeled with calculations and discussions of the parameter estimations provided.

PREFACE

The novel hydroponic system utilized throughout this research consists of ceramic tubes which are normally used for ultrafiltration. Using these tubes for plant growth purposes was originally conceived by Thomas Dreschel of the Bionetics Corporation at Kennedy Space Center (KSC), FL, working under contract for the National Aeronautics and Space Administration (NASA). Although this system has undergone several name changes since it's original conception, it is generally known as the Porous Ceramic Tube - Nutrient Delivery System (PCT-NDS) or the Porous Ceramic Tube Plant Nutrification System (PCTPNS). Throughout this text, it will be referred to by the former abbreviation; however, several of the references quoted refer to the system using the latter abbreviation as well as various others.

TABLE OF CONTENTS

Page

Page

Page

LIST OF TABLES

Table Page

Table Page

Table

Page

Table Page

Table Page

Table | Page

Table Page

Table Page

Table Page

LIST OF FIGURES

Figure Page

Figure Page

Figure Page

LIST OF SYMBOLS

This List of Symbols is alphabetically arranged with the lower case Roman letters listed before the upper case counterparts followed by Greek symbols arranged similarly. The definition of the listed symbol is proceeded by examples of the typical units used in this research thesis. Furthermore, the first occurrence of the symbol is referenced to the equation, if applicable, for which it is initially used. Finally, for scientific constants, the accepted values are given along with the typical units.

Symbol = Definition (Units)	Location
a = Leaf Area Index Correlation - Stanghellini model (unitless)	3.42
a_0 = Regression Constant - enzyme response to temperature (unitless)	3.21
a_1 = Regression Constant - enzyme response to temperature ($°C^{-1}$)	3.21
a_2 = Regression Constant - enzyme response to temperature ($°C^{-2}$)	3.21
a_J = Proportionality Factor for Nutrient Flux ($cm\ s^{-1}$)	3.50
A = Area (Rectangular) - Line-Intersect Method (cm^2)	2.1
A_{leaf} = Total Leaf Area (cm^2)	3.13
A_m = Interfacial Membrane Area (mm^2)	3.29
$A_{void,filled}$ = Total Interfacial Area of Liquid in the Porous Ceramic Matrix (ml)	5.5
A_{wet} = Total Wettable Cross-Sectional Area (cm^2)	5.1
b = Buffering Power of the Solid Soil Phase = dC/dC_{soil} (unitless)	3.61
$b_{0,i}$ = Regression Constant - solubility of nutrient, i, as a function of pH ($\mu g/ml$)	8.41
b_1 = Regression Constant - general transpiration model ($s^2\ m^{-2}$)	3.41

$b_{1,i}$ = Regression Constant - solubility of nutrient, i, as a function of pH (μg/ml) 8.41

b_2 = Regression Constant - general transpiration model (s m^{-1}) 3.41

$b_{2,i}$ = Regression Constant - solubility of nutrient, i, as a function of pH (μg/ml) 8.41

c_0 = Linear Regression Constant - (T_c - T_a) versus vapor pressure deficit (K) 3.47

$c_{0,i}$ = Regression Constant - quantity of nutrient, i, in the plant tissues (unitless) 9.2

c_1 = Regression Constant - leaf area index model (unitless) 3.42

$c_{1,i}$ = Regression Constant - quantity of nutrient, i, in the plant tissues (unitless) 9.2

c_2 = Regression Constant - leaf area index model(unitless) 3.42

$c_{2,i}$ = Regression Constant - quantity of nutrient, i, in the plant tissues (MPa^{-1}) 9.2

c_3 = Regression Constant - leaf area index model(unitless) 3.42

$c_{3,i}$ = Regression Constant - quantity of nutrient, i, in the plant tissues (unitless) 9.2

c_4 = Regression Constant - leaf area index and radiation model(kg s^{-3} K^{-1}) 3.42

c_5 = Regression Constant - leaf area index and radiation model(unitless) 3.42

c_6 = Regression Constant - leaf area index and radiation model(W m^{-2}) 3.42

c_{ww} = Water Vapor Concentration in Air (mol m^{-3}) 2.7

c_{ww}^0 = Saturated Water Vapor Concentration in Air (mol m^{-3}) 2.7

C = General Concentration (mol kg^{-1}, mg g^{-1}, mg ml^{-1}) 3.50

C* = Dimensionless Concentration (unitless) 3.38

$C_{branch,i}$ = Concentration of Nutrient, i, in the Branch Tissues (μg/g) 8.26

C_{CO2} = CO_2 Concentration (g m^{-3}) 3.14

C_f = Final Concentration (mg ml^{-1}) 3.67

C_i = Initial Concentration (mg ml^{-1}) 3.62

C_j^i = Internal Cellular Concentration where j = specific nutrient (mol L^{-1}) 2.8

C_j^o = External Cellular Concentration where j = specific nutrient (mol L^{-1}) 2.8

C_{leaf} = Leaf Solution Osmolarity (mol solute / kg water) 2.6

$C_{leaf,i}$ = Concentration of Nutrient, i, in the Leaf Tissues (μg/g) 8.26

C_{min} = Minimum Nutrient Concentration in Soil where J_c = 0 (mg ml^{-1}) 3.64

C_{O2} = O_2 Concentration (g m^{-3}) 3.16

C_p = Specific Heat Capacity of Air (J kg^{-1} K^{-1}) 3.42

C_{plant} = Nutrient Concentration in Plant (mg g^{-1}) 3.51

$C_{plant,\,0}$ = Initial Nutrient Concentration in Plant (mg g^{-1}) 3.52

C_{root} = Nutrient Concentration in Root (mol kg^{-1}, mg ml^{-1}) 2.5

$C_{root,i}$ = Concentration of Nutrient, i, in the Root Tissues (µg/g) 8.26

C_s = Solution Osmolarity (mol solute / kg water) 2.2

$C_{sample,i}$ = Concentration of Nutrient, i, in a Solution Sample (µg/ml) 8.27

$C_{sample,i,ave}$ = Average Concentration of Nutrient, i, in a Solution Sample (µg/ml) Table 8.8

$C_{sample,i,final}$ = Final Concentration of Nutrient, i, in a Solution Sample (µg/ml) 8.39

$C_{sample,i,init}$ = Initial Concentration of Nutrient, i, in a Solution Sample (µg/ml) 8.38

$C_{sample,i,k}$ = Concentration of Nutrient, i, in Solution Sample, k (µg/ml) 8.39

C_{soil} = Nutrient Concentration in Soil (mol kg^{-1}, mg ml^{-1}) 2.4

$C_{soln,i}$ = Concentration of Nutrient, i, in Solution (µg/ml) 7.4

$C_{soln,i}^{\circ}$ = Concentration of Nutrient, i, in Solution at the Initial pH (µg/ml) 8.35

$C_{soln,i,final}$ = Final Concentration of Nutrient, i, in Solution (µg/ml) 8.29

$C_{soln,i,init}$ = Initial Concentration of Nutrient, i, in Solution (µg/ml) 8.28

$C_{soln,i,k}$ = Concentration of Nutrient, i, Removed in Solution Sample, k (µg/ml) 8.29

$C_{surface}$ = Nutrient Concentration at Root Surface (mg ml^{-1}) 3.53

$C_{surface,i}$ = Nutrient Concentration at Root Surface (µg ml^{-1}) 9.11

$C_{tissue,i,ave}$ = Average Concentration of Nutrient, i, in Plant Tissues (µg/g) Table 8.7

$C_{void,filled}$ = Total Circumference of Liquid in the Porous Ceramic Matrix (cm) 5.4

C_{water} = Volumetric Soil Water Content (cm^3 cm^{-3}) 3.31

$C_{water,max}$ = Volumetric Soil Water Content at Saturating Conditions (cm^3 cm^{-3}) 3.32

C_{α} = Concentration of Initial Photosynthetic Carbon Substrate (kg CO_2 J^{-1}) 3.25

d = Average Pore Diameter of Ceramic Tubes (µm) 5.3

$\bar{d}$ = Average Difference Between Values Calculated from Two Methods (variable) 7.5

d_0 = Linear Regression Constant - (T_c - T_a) versus vapor pressure deficit (K/MPa) 3.47

$d_{0,i}$ = Regression Constant - diffusion of nutrient, i, (µg LS^{-1}) 9.12

d_1 = Regression Constant - Penman-Monteith equation (s^2 m^{-2}) 3.43

$F_{C,max}$ = Maximum CO_2 Assimilation Rate based on CO_2 Conc. (g cm^{-2} day^{-1}) 3.14

$F_f(cn)$ = Frictional Loss for the Flow through a Sudden Contraction (cm^2 s^{-2}) 5.12

$F_f(ex)$ = Frictional Loss for the Flow through a Sudden Expansion (cm^2 s^{-2}) 5.11

$F_f(s)$ = Frictional Loss for the Flow through System Tubing (cm^2 s^{-2}) 5.10

F_g = Force due to Uni-Directional Gravity (N) Fig. 5.6

F_n = Net CO_2 Assimilation Rate (g cm^{-2} day^{-1}) 3.13

$F_{n,C}$ = Net CO_2 Assimilation Rate based on CO_2 Conc.(g cm^{-2} day^{-1}) 3.14

$F_{n,C/O}$ = Net CO_2 Assimilation Rate based on CO_2 and O_2 Conc.(g cm^{-2} day^{-1}) 3.16

$F_{n,R}$ = Net CO_2 Assimilation Rate based on Photosynthesis (g cm^{-2} day^{-1}) 3.18

F_p = Force due to Pressure Differential (N) Fig. 5.6

$F_{R,max}$ = Maximum CO_2 Assimilation Rate based on Photosynthesis (g cm^{-2} day^{-1}) 3.18

F_{st} = Force due to Surface Tension (N) Fig. 5.6

g = Standard Gravity (980.6 cm s^{-2}) 5.6

g* = Effective Non-Standard Gravitational Force (cm s^{-2}) 5.22

g_a = Air Boundary Layer Conductance (m s^{-1}) 3.44

g_c = Canopy Conductance (m s^{-1}) 3.44

g_r = Radial Component of the Effective Gravitational Force (cm s^{-2}) 5.22

g_z = Vertical Component of the Effective Gravitational Force (cm s^{-2}) 5.22

G_c = Free Convection Parameter due to Volumetric Expansion - concentration 3.38

G_r = Free Convection Parameter due to Volumetric Expansion - temperature 3.38

h = Average Height of Liquid in the Porous Ceramic Matricies (cm) 5.2

h_0 = Vertical Height from Reference of the Ceramic Tube Entrance (cm) 5.15

h_A = Vertical Height from Reference for Upstream Point A (cm) 5.9

h_B = Vertical Height from Reference for Downstream Point B (cm) 5.9

h_c = Canopy Height (cm) 3.49

h_{expt} = Experimentally Measured Height of Liquid in the Porous Matricies (cm) 5.21

h_L = Vertical Height from Reference of the Ceramic Tube Exit (cm) 5.16

h_{plant} = Plant Height (cm) 8.2

h_t = Leaf Area Index and Radiation Correlation - Stanghellini model (kg s^{-3} K^{-1}) 3.42

H = Length (Line) - Line-Intersect Method (cm)	2.1
$H_{w,tissue}$ = Plant Tissue Water Retention or Hydration (ml)	7.3
J = General Nutrient Flux (mg cm^{-2} day^{-1})	3.50
J_b = Nutrient Flux due to Mass Convection in Plant Water (mg cm^{-2} day^{-1})	3.55
J_B = Nutrient Flux due to Mass Convection in Soil Water (mg cm^{-2} day^{-1})	3.54
J_c = Nutrient Flux due to Enzyme Carriers/Channels (mg cm^{-2} day^{-1})	3.58
$J_{c,i}$ = Nutrient Uptake due to Enzyme Carriers/Channels (µg LS^{-1})	9.15
$J_{c,max}$ = Maximum Nutrient Flux due to Enzyme Carriers/Channels (mg cm^{-2} day^{-1})	3.58
$J_{c,max,i}$ = Nutrient Uptake due to Enzyme Carriers/Channels (µg LS^{-1})	9.16
$J_{conv,i}$ = Convection Rate of Nutrient, i (µg LS^{-1})	7.4
J_d = Nutrient Flux due to Diffusional Gradients in Plants (mg cm^{-2} day^{-1})	3.56
$J_{diff,i}$ = Convection Rate of Nutrient, i (µg LS^{-1})	9.9
J_D = Nutrient Flux due to Diffusional Gradients in Soil (mg cm^{-2} day^{-1})	3.53
J_i = Experimentally Based Nutrient Uptake Rate (µg LS^{-1})	9.4
J_r = Radial Mass Flux of Diffusable Solute (g min^{-1})	3.60
k = Root Absorbing Power = $J_{c,max}$ / $K_{c,m}$ (cm day^{-1})	3.71
k' = Growth Rate Constant - monomolecular (L mol^{-1} day^{-1})	3.8
$k_{rs,r}$ = Rate Constant - flow from root surface into root (m^2 s^{-1})	3.30
$k_{s,rs}$ = Rate Constant - flow from soil to root surface (m^2)	3.30
K = Light Extinction Coefficient (unitless)	3.27
$K_{c,m}$ = Nutrient Concentration Required for 1/2 $J_{c,max}$ (mg ml^{-1})	3.58
K_g = Linear Coefficient for Growth Metabolism (g g^{-1} TNC^{-1} h^{-1})	3.3
K_i = Inhibition Constant for O_2 on Rubisco (g m^{-3})	3.16
$K_{m,C}$ = Concentration of CO_2 Required for 1/2 $F_{C,max}$ (g m^{-3})	3.14
$K_{m,i}$ = Concentration of Nutrient, i, Required for 1/2 $J_{c,max,i}$ (µg ml^{-1})	9.16
$K_{m,R}$ = Radiation Level Required for 1/2 $F_{R,max}$ (W m^{-2})	3.18
$K_{m,Pmax}$ = Carbon Machinery Required for 1/2 $P_{n,max}$ (kg Pmax-carbon m^{-2})	3.18
$K_{m,\alpha}$ = Concentration of α-Carbon Required for 1/2 α_{max} (kg CO_2 J^{-1})	3.25
K_s = Soil Hydraulic Conductivity (m^2 s^{-1} MPa^{-1})	3.30

$K_{s,max}$ = Soil Hydraulic Conductivity at Saturating Conditions ($m^2\ s^{-1}\ MPa^{-1}$)	3.33
L = Length of the Ceramic Tubes (cm)	5.1
L_p = Plant Hydraulic Conductivity ($mm\ s^{-1}\ MPa^{-1}$)	3.29
L_r = Root Length (cm)	2.1
L_{r0} = Initial Root Length (cm)	3.52
L_s = Length of System Tubing (cm)	5.10
LAI = Leaf Area Index - ratio of leaf area to ground area ($m^2\ m^{-2}$)	3.27
LAR = Leaf Area Ratio - leaf area to plant dry weight ($m^2\ g^{-1}$)	3.4
LS = Leaf Stage (unitless)	8.1
m = Leaf Transmission Coefficient (unitless)	3.27
M_t = Amount of Radioactive Tracer (g)	3.67
n = Number of Experimental Samples (unitless)	7.5
n_R = Richard's Growth Function Parameter (unitless)	3.12
n_p = Theoretical Number of Pores (unitless)	5.3
N = Number of Root Intersection - Line-Intersect Method (unitless)	2.1
N_{Pr} = Prandtl Number (unitless)	3.39
N_{Re} = Reynold's Number (unitless)	Fig. 5.9
N_{Sc} = Schmidt Number (unitless)	3.40
pH = Solution pH (unitless)	8.30
pH_0 = Initial Solution pH (unitless)	8.41
P = Hydrostatic Pressure (MPa)	2.2
P* = Dimensionless Pressure (unitless)	3.37
P_0 = Pressure at the Ceramic Tube Entrance ($cm.H_2O$)	5.13
P_1 = Pressure Upstream of the Ceramic Tube ($cm.H_2O$)	5.13
P_2 = Pressure Downstream of the Ceramic Tube ($cm.H_2O$)	5.14
P_{air} = Total Air Pressure (MPa)	3.42
P_A = Pressure at Upstream Point A ($cm.H_2O$)	5.9
P_B = Pressure at Downstream Point B ($cm.H_2O$)	5.9
P_c = Cavitation Pressure (atm)	5.8

P_f = Pressure Loss due to Friction ($cm.H_2O$)	5.18
P_j = Permeability Coefficients where j = specific nutrient ($cm\ s^{-1}$)	2.8
P_L = Pressure at the Ceramic Tube Exit ($cm.H_2O$)	5.14
P_m = Matric Potential (MPa)	2.3
P_{min} = Min. Pressure Required to Contain Liquid in the Ceramic Tubes ($cm.H_2O$)	5.23
P_n = Rate of Photosynthesis ($g\ CO_2\ m^{-2}\ h^{-1}$)	3.4
$P_{n,max}$ = Maximum Rate of Photosynthesis ($g\ CO_2\ m^{-2}\ h^{-1}$)	3.16
$P_{n,max}(T)$ = Temperature Dependent Rate of Photosynthesis ($g\ CO_2\ m^{-2}\ h^{-1}$)	3.22
$P_{r,max}$ = Maximum Rate of Photorespiration ($g\ O_2\ m^{-2}\ h^{-1}$)	3.26
P_s = Applied Suction Pressure ($cm.H_2O$)	5.6
$P_{soil}(z,t)$ = Soil Hydrostatic Pressure - space and time dependent (MPa)	3.34
P_t = Turgor Pressure (MPa)	2.5
$P_{t,\ leaf}$ = Leaf Turgor Pressure (MPa)	2.6
$P_{t,\ root}$ = Root Turgor Pressure (MPa)	2.5
P_w = Weeping Pressure ($cm.H_2O$)	5.7
$P_{w,\ expt}$ = Experimental Weeping Pressure ($cm.H_2O$)	Table 5.3
$P_{w,\ theo}$ = Theoretical Weeping Pressure ($cm.H_2O$)	Table 5.3
POT = Actual Potentiometer Readings for Syringe Position (V)	Fig. 5.13
POT_{std} = Standardized Potentiometer Readings for Syringe Position (V)	5.20
POT_{zero} = Average Potentiometer Readings used for Standardization (V)	Fig. 5.13
$q_{branch,i}$ = Quantity of Nutrient, i, in the Branch Tissues (μg)	8.26
$q_{input,i}$ = Quantity of Nutrient, i, Supplied to a Test System (μg)	8.28
$q_{leaf,i}$ = Quantity of Nutrient, i, in the Leaf Tissues (μg)	8.26
$q_{output,i}$ = Quantity of Nutrient, i, Not Removed by the Plants (μg)	8.37
$q_{plant,i}$ = Quantity of Nutrient, i, in the Entire Plant (μg)	8.26
$q_{precip,i}$ = Quantity of Nutrient, i, Precipitated a Test System (μg)	8.36
$q_{rem,i}$ = Quantity of Nutrient, i, Remaining or Removed from a Test System (μg)	8.29
$q_{remain,i}$ = Quantity of Nutrient, i, Remaining in a Test System (μg)	8.29
$q_{remain,i}^{\circ}$ = Quantity of Nutrient, i, Remaining in a Test System at the Initial pH (μg)	8.35

$q_{removed,i}$ = Quantity of Nutrient, i, Removed From a Test System (μg)	8.29
$q_{root,i}$ = Quantity of Nutrient, i, in the Root Tissues (μg)	8.26
Q_r = Water Retention Rate (ml day^{-1})	7.3
Q_u = Rate of Solution Uptake (ml day^{-1})	7.3
Q_w = Water Flow Rate (ml s^{-1})	3.28
$Q_{w,rs-rx}$ = Water Flow Rate between Root Surface and Root Xylem (ml s^{-1})	3.35
Q_z = Volumetric Flow Rate - Longitudinal (ml s^{-1})	5.10
r = Radius of Curvature of a Meniscus (μm)	2.3
r* = Velocity Component of Fluid in the Radial Direction (cm s^{-1})	3.36
r_0 = Mean Root Radius (cm)	3.51
r_1 = Distance Away from Root Surface (cm)	3.65
r_{ap} = Air Resistance to Water Vapor Flow (s m^{-1})	3.45
r_{arm} = Length of the Radial Centrifuge Arm (cm)	5.22
r_{cp} = Canopy Resistance to Water Vapor Flow (s m^{-1})	3.45
R = Universal Gas Constant (0.0083143 L MPa mol^{-1} K^{-1})	2.2
R^2 = Correlation Coefficient (unitless)	Fig. 8.3
$R_{1,2}$ = General Flow Resistance between Points 1 and 2 (MPa·s ml^{-1})	3.28
R_e = Effective Radius of the Ceramic Tubes (cm)	5.18
R_g = Rate of Growth Respiration (g CO_2 g^{-1} h^{-1})	3.4
R_i = Light Intensity or Radiation - excluding infra-red (W m^{-2})	3.16
R_m = Rate of Maintenance Respiration (g CO_2 g^{-1} h^{-1})	3.4
R_n = Light Intensity or Radiation - including infra-red (W m^{-2})	3.43
R_{root} = Flow Resistance in thr Root Cellular System (MPa·s ml^{-1})	3.35
$R_{s,r}$ = Flow Resistance between Soil and Roots (MPa·s ml^{-1})	3.30
R_{stem} = Aspect Ratio - stem radius to length (unitless)	3.36
RC = Reserve Carbon (g)	3.5
RH = Relative Humidity (%)	2.7
s = Integration Variable	3.60
s_d = Calculated Standard Deviation (variable)	7.5

S = Substrate Concentration (mol L^{-1})	3.8
$S(z,t)$ = Water Extraction Term - space and time dependent (mg m^{-3} s^{-1})	3.34
S_f = Final Substrate Concentration (mol L^{-1})	3.8
SDM = Structural Dry Matter (g)	3.5
t = Time (sec)	3.1
t_0 = Initial Time (sec)	3.52
t_{calc} = Calculated t-Statistic (unitless)	7.5
t_{DAE} = Time - Days after Emergence (days)	8.1
t_m = Elapsed Time to Mean Dry Matter Distribution (day)	3.10
T = Temperature (K, °C)	2.2
T^* = Dimensionless Temperature (unitless)	3.38
T_0 = Zero Enzymatic Response Temperature (°C)	3.21
T_a = Air Temperature (°C)	3.44
$T_{a,ave}$ = Average Air Temperature (°C)	Table A.1
T_c = Canopy Temperature (°C)	3.46
T_m = Maximum Enzymatic Response Temperature (°C)	3.21
TNC = Total Non-Structural Carbohydrate (g g^{-1})	3.3
u = Integration Variable	3.11
u_1 = Regression Constant - volumetric solution uptake function (day^{-1})	9.10
u_a = Wind Speed (m s^{-1})	3.49
v = Bulk Solution Flow Velocity (cm s^{-1})	3.54
v_0 = Bulk Solution Flow Velocity at the Root Surface (cm s^{-1})	3.61
v_1 = Bulk Solution Flow Velocity at a Distance, r_1, Away from Root (cm s^{-1})	3.66
$v_{A,av}$ = Average Flow Velocity at General Upstream Point A (cm s^{-1})	5.9
$v_{B,av}$ = Average Flow Velocity at General Downstream Point B (cm s^{-1})	5.9
V^* = Actual Volume of Water Contained in the Ceramic Tubes (ml)	5.20
V_{sample} = Volume of a Liquid Solution Sample (20 ml)	8.27
V_{soln} = Volume of Solution in a Sample (19.6 ml)	8.27
V_{sys} = Volume of the Test Bed Unit Including Ceramic Tubes (ml)	8.28

V_{tot} = Total Volume of the Ceramic Tube (ml)	5.20
V_u = Total Solution Uptake Volume (ml)	7.3
$V_{void,filled}$ = Volume of Liquid in the Porous Ceramic Matrix (ml)	5.2
V_w = Specific Volume of Water Vapor (m^3 mol^{-1})	2.7
V_{wet} = Total Wettable Volume (ml)	5.1
W = Tissue Weight (g)	3.1
W_0 = Initial Tissue Weight (g)	3.2
$W_{branch,d}$ = Branch Tissue Dry Weight (g)	8.5
$W_{branch,w}$ = Branch Tissue Fresh Weight (g)	8.13
W_C = Weight of Substrate Carbon (g)	3.17
W_F = Final Tissue Weight (g)	3.9
$W_{leaf,d}$ = Leaf Tissue Dry Weight (g)	8.4
$W_{leaf,w}$ = Leaf Tissue Fresh Weight (g)	8.12
W_M = Weight of Machinery which Assimilates Carbon (g)	3.17
W_p = Weight of Primary Cell Wall Material (g)	3.17
$W_{plant,d}$ = Total Plant Dry Weight (g)	8.7
$W_{plant,w}$ = Total Plant Fresh Weight (g)	8.15
W_{pump} = Work Exerted by a Pump (cm^2 s^{-2})	5.9
W_{Pmax} = Weight of Photosynthetic Machinery (g)	3.17
W_r = Structural Dry Mass of Roots (g)	3.30
$W_{root,d}$ = Root Tissue Dry Weight (g)	8.6
$W_{root,w}$ = Root Tissue Fresh Weight (g)	8.14
W_s = Weight of Secondary Cell Wall Material (g)	3.17
$W_{tissue,d}$ = General Tissue Dry Mass (g)	8.20
$W_{tissue,w}$ = General Tissue Fresh Mass (g)	8.20
W_{tot} = Total Weight of the Plant (g)	3.17
W_x = Weight of Cross-Linked Primary Cell Wall Material (g)	3.17
W_α = Weight of Initial Photosynthetically Converted Carbon Substrate (g)	3.17
z = Root Zone Vertical Depth (cm)	3.34

μ = Viscosity of Liquid Solution (g cm^{-1} s^{-1})	5.10
μ_g = Specific Growth Rate (g g^{-1} day^{-1})	3.1
μ_g' = Specific Growth Rate (g g^{-1} day^{-1})	3.17
μ_{g0} = Initial Specific Growth Rate (g g^{-1} day^{-1})	3.7
π = Osmotic Pressure (MPa)	2.2
π_{soil} = Soil Osmotic Pressure (MPa)	2.4
ρ = Density of Liquid Solution (g cm^{-3})	5.6
ρ_a = Density of Air (kg m^{-3})	3.45
ρ_r = Density of the Roots (kg m^{-3} soil)	3.30
ρ_{wa} = Density of Air Water Vapor (kg m^{-3})	3.43
ρ_{wsa} = Density of Saturated Air Water Vapor (kg m^{-3})	3.43
τ = Tortuosity (unitless)	3.68
τ_c = CO_2 Conductance Rate (mol m^{-2} s^{-1})	3.24
$\tau_{c,max}$ = Maximum CO_2 Conductance Rate (mol m^{-2} s^{-1})	3.24
σ = Standard Deviation	3.10
σ_m = Membrane Thickness (nm)	3.57
σ_r = Solute Reflection Coefficient (unitless)	3.29
ΣF = Sum of the Frictional Losses (cm^2 s^{-2})	5.9
ϕ = Contact Angle (radians)	5.6
χ = Dimensionless Permeability (unitless)	3.37
Ψ = Water Potential (MPa)	2.2
Ψ_{air} = Air Water Potential (MPa)	2.7
Ψ_{leaf} = Leaf Water Potential (MPa)	2.5
Ψ_{root} = Root Water Potential (MPa)	2.5
Ψ_{rs} = Water Potential at the Root Surface (MPa)	3.35
Ψ_{rx} = Water Potential in the Root Xylem (MPa)	3.35
Ψ_{soil} = Soil Water Potential (MPa)	2.4
$\Psi_{soil,max}$ = Soil Water Potential at Saturating Conditions (MPa)	3.32

Ψ_{space} = Water Potential of Air in Leaf Spaces (MPa)	Table 2.2
Ψ_{xylem} = Root Xylem Water Potential (MPa)	3.34
ω = Rotational Speed (s^{-1})	5.22
ω_j = Mobility in Membrane where j = specific nutrient	3.57
∇ = Gradient Operator (cm^{-1})	3.31

LIST OF ABBREVIATIONS

3-PGA = 3-Phosphoglycerate

ANOVA = Analysis of Variance

ATP = Adenosine Triphosphate

ATPase = Adenosine Triphosphatase

BC1 = Boundary Condition 1

BC2 = Boundary Condition 2

C2 = 2 Carbon Compound

C3 = 3 Carbon Compound

C4 = 4 Carbon Compound

CELSS = Closed Ecological Life Support System

CERES = Capillary Effect Root Environment System

CI = Statistical Confidence Interval

DNA = Deoxyribonucleic Acid

DOF = Degrees of Freedom

DTPA = Diethylene Triamine Pentaacetic Acid

EDDHA = Ethylene Diamine Dihydroxyphenylacetic Acid

EDTA = Ethylene Diamine Tetraacetic Acid

GAL-P = Glyceraldehyde-3-Phosphate

HEDTA = N-(2-Hydroxyethyl)Ethylene Diamine Triacetic Acid

IC = Initial Condition

ICP-AES = Inductively Coupled Plasma - Atomic Emissions Spectrometry

KSC = Kennedy Space Center

NAD+/NADH = Nicotinamide Adenine Dinucleotide

NADP+/NADPH = Nicotinamide Adenine Dinucleotide Phosphate

NASA = National Aeronautics and Space Administration

NFT = Nutrient Film Technique

PAR = Photosynthetically Active Radiation

PCA = Photosynthetic Carbon Assimilation

PCO = Photorespiratory Carbon Oxidation

PCR = Photosynthetic Carbon Reduction

PCT-NDS = Porous Ceramic Tube - Nutrient Delivery System

PCTPNS = Porous Ceramic Tube Plant Nutrification System

PEG = Polyethylene Glycol

PEP = Phosphoenolpyruvate

PPF = Photosynthetic Photon Flux

PPFD = Photosynthetic Photon Flux Density

PSI = Photosystem I

PSII = Photosystem II

PVC = Polyvinyl Chloride

RNA = Ribonucleic Acid

Rubisco = Ribulose Bisphosphate Carboxylase/Oxygenase

RuBP = Ribulose-1,5-Bisphosphate

RZT = Root Zone Temperature

RZWQM = Root Zone Water Quality Model

TBU = Test Bed Unit

TCA = Tricarboxylic Acid

UDP = Uridine Diphosphate

VPD = Vapor Pressure Deficit

WAS = Water Availability Sensor

WCSAR = Wisconsin Center for Space Automation and Robotics

WDS = Water Delivery System

CHAPTER 1 - INTRODUCTION

This initial chapter begins with a description of the common taxonomic nomenclature used throughout the text. This will include the scientific names of the various agronomic crops including tomato as well as the cultivar names of the multitude of plant sub-species used as examples in this thesis. The next section provides a general description of the growth stages of tomatoes including some of the varietal differences between sub-species. This will include several brief descriptions of the various plant tissues that develop during the growth of tomato plants. The conclusion of this chapter contains a description of the contents for the remainder of this thesis.

1.1 Common Nomenclature

In order to aid the reader, this section provides the abbreviations used throughout this text during the naming and identification of the various plant species and sub-cultivars. This includes plants from various families as well as the within the tomato family of Solanaceae itself [Taylor, 1986]. The formats presented in each sub-section below will be systematically used during the presentation of examples. In general, most of the examples cited specifically for tomato plants belong to the commercial variety, *Lycoperison esculentum*.

1.1.1 Naming Plant Species

During the presentation of examples throughout this thesis, several other agronomically important crops will be cited. Consistently, only the common names will be provided with the specific cultivar name (if provided in the literature) given in parentheses. These cultivar names will be proceeded by the abbreviation, 'cv.', in order to denote the word, cultivar. The taxonomic names of these non-tomato examples are provided in Table 1.1 along with the common names that will appear in the text. This table follows the format: *Genus - Species* based on the Linnean methodology of naming plant species.

Table 1.1 Common and Taxonomic Names of Various Agronomic Crops

Common Name	Taxonomic Name
alfalfa	*Medicago sativa*
bean (kidney)	*Phaseolus vulgaris*
bean (pinto)	*Phaseolus vulgaris*
bean (snap)	*Phaseolus vulgaris*
cabbage	*Brassica oleracea*
corn/maize	*Zea mays*
cucumber	*Cucumis sativus*
eggplant	*Solanum melongena*
lettuce	*Lactuca sativa*
oat	*Avena sativa*
peas	*Pisum sativum*
potato	*Solanum tuberosum*
rice	*Oryza sativa*
ryegrass	*Lolium perenne*
sorghum	*Sorghum bicolor*
soybean	*Glycine max*
sugarcane	*Saccharum officinarum*
tobacco	*Nicotiana tabacum*
wheat	*Triticum aestivum*

1.1.2 Naming Tomato Species

Within the Solanaceae family, tomato comprises the genus, *Lycopersicon*. However, some controversy has arisen based on the nomenclature that should be used in order to identify tomato plants [Taylor, 1986]. Originally, tomatoes were categorized in the genus - species taxonomy of, *Solanum lycopersicum* L., where the abbreviation, 'L.', represents the Linnean name for the species. In 1768, Miller derived the following name based on the development of a new genus - species category of, *Lycopersicon esculentum* Mill. where the abbreviation, 'Mill.', represents the name, Miller. This new genus was developed based on the differences in floral morphology between tomatoes and other members of the Solanaceae family. Finally, in 1900, Karsten developed the name, *Lycopersicon lycopersicum* (L.) Karsten, which is actually the correct nomenclature that should be used. However, due to the popular usage of Miller's nomenclature, this has been retained to this day in the literature and is used throughout this text. An additional abbreviation that is utilized in this thesis is the abbreviation of the genus name using the first letter in italicized face (*L.* = *Lycopersicon*).

There are also several closely related species of tomato based on their ability to be crossed with the commercial variety [Taylor, 1986]. These consist of the 'esculentum-complex' which readily form crosses with the *esculentum* species and the 'peruvianum-complex' which do not. For the tomatoes in the 'esculentum-complex', there are several species within the genus including *L. esculentum*, *pimpinellifolium*, *cheesmanii*, *parviflorum*, *chmielewskii*, *hirsutum*, and *pennellii*. As for the 'peruvianum-complex', these consist of only *L. peruvianum* and *L. chilense*. In addition to these scientific means of differentiating the various tomato species, a more common form based on size is also used where small fruits are called cherry tomatoes. These small sized tomatoes (1 to 2.5 cm) originated from the *L. esculentum* species and are known as the variety (var.), *cerasiforme* which distinguishes them from the regularly sized fruit [Taylor, 1986]. For most of the examples that are cited in this text, the tomatoes belong to the *L. esculentum* Mill. variety. In this case, only the cultivar name is provided in parentheses. In the case of different tomato species given in an example, each species name will be provided.

1.2 Tomato Growth Stages

Under amicable conditions, tomato plants pass through four basic developmental stages [IPM Manual Group, 1982]. These begin with the germination and emergence stage followed by the main vegetative growth stage. During these two stages, the tomato plant establishes itself and proceeds to produce sufficient foliage in order to begin reproduction. Once adequate vegetation has been produced, the tomato plants proceed into the flowering and then finally, the fruiting stages. These last two stages consist of the reproduction of the tomato plants through the production of flowers which are pollinated in order to produce seed-bearing fruit.

1.2.1 Establishment and Vegetative Stages

The initial growth stage involves the germination and emergence of the seed which leads to the main root apex or radicle (region of active cell division) entering the soil and the main shoot apex emerging from the seed coat. Initially during this stage, the seed will imbibe a sufficient quantity of moisture in order to hydrate these primordial structures. After imbibition and radicle protrusion are complete, tomato seedlings establish a complex rooting system consisting of a main tap root and additional branch roots. In order to increase the total surface area of the rooting system, microscopic root hairs are produced from the root epidermal (external) cells. Typically, these are established at the zone of elongation just after the meristematic region (primary and secondary regions of actively dividing cells). In total, these root hairs can constitute as much as 60% of the root surface area [Taiz and Zeiger, 1991]. Under normal growth conditions, tomatoes remain in the germination and emergence stage during the first 3 to 4 days of growth [Pickens, et al., 1986]. As for the terrstrial portion, the seed coat or aria is shed upon emergence revealing the hypocotyl with the cotyledons on top. These cotyledons contain enough chlorophyll to begin the production of photosynthates. In dicotylenous plants such as tomatoes, there are two such initiating structures as compared to monocots such as grasses and grains which contain only one cotyledon [Taiz and Zeiger, 1991].

Upon entering the main vegetative stage (second stage), root growth slows in conjunction with a rapid increase in leaf and stem biomass [IPM Manual Group, 1982]. The vegetative portion of the plant consists of a main shoot with the apex at the top. From this region of active cell division, secondary branches emerge along with the various levels of true leaves. The locations along the main stem where secondary branches emerge are called nodes while the regions in between are internodes. A distinction is made between true leaves and the cotyledons, both of which contain chlorophyll. Furthermore, the leaves produced by tomatoes are generally compound leaves with a terminal leaflet and several lateral leaflets on the same tertiary branch. After approximately 7 to 11 true leaf nodes are formed, generally within 4 to 7 weeks after seeding, the shoot apical meristem can be transformed into either a terminal or lateral inflorescence which generates the reproductive tissues of the plant [Pickens, et al., 1986]. In 'determinate' type tomato plants, this terminal inflorescence marks the end of the growth for the main shoot whereas 'indeterminate' varieties may continue main shoot extension. Further vegetative growth is also accomplished through the axillary meristems located at the pit between the main stem and secondary branches. These leaf axils proceed in a similar manner as the main shoot producing an inflorescence in conjunction with vegetative biomass.

1.2.2 Reproductive Stages

During the next two stages of flowering and fruit production, vegetative growth also slows as plant resources and energy are dedicated towards fruit development [IPM Manual Group, 1982]. During the flowering stage, buds are initially formed as clusters or trusses typically emerging from either the apical meristem of the main shoot or as a node along the axillary growths of the plant [Pickens, et al., 1986]. The axillary productions can give rise to either additional vegetative biomass or inflorescence clusters depending upon the developmental demands of the tomato plant. Whether a particular genotype of tomato can continue producing reproductive organs depends on the growth behavior [Atherton and Harris, 1986]. For tomatoes that have a 'determinate' type of growth behavior, the

number of inflorescences produced is limited by the resources available to support additional reproductive development. Once this biochemical limit is reached, 'determinate' tomato plants abort the remaining flowers produced. On the other hand, 'indeterminate' tomato species can continue to produce bud clusters even after several have been aborted due to the biochemical limitations. Furthermore, the main shoot can continue to grow vegetatively giving rise to lateral inflorescences instead of a terminal one as well as form additional axillary growths. These types of tomato plants can achieve vertical heights of upto 10 meters whereas the 'determinate' types generally develop into more of a bush form [Pickens, et al., 1986].

Once the buds open, yellow flowers are produced usually containing 5 petals reflexed away from the central pistil (reproductive organs) [Smith, 1977]. Pollination occurs either by automatic self-pollination such as by the *L. esculentum, pimpinellifolium, cheesmanii,* and *parviflorum* representatives of tomatoes or by insect pollination such as by *L. chmielewskii, hirsutum, peruvianum,* and *chilense* tomatoes [Taylor, 1986]. Flowers generally remain receptive to pollination only 4 to 6 days after complete expansion [Ho and Hewitt, 1986]. The process of pollination and fertilization of the ovary involves viable pollen initially being transferred to the stigma (tip) of the floral structure. Once accomplished, pollen tubes begin to grow until they reach the ovules located at the base of the pistil inside of the style (tubular structure). Once there, the pollen fertilizes the ovary (base of the pistil) leading to the production of the tomato fruit.

After pollination, the fruit development stage begins. This can proceed for up to an additional 2 months depending upon the variety of tomato produced [Geisenberg and Stewart, 1986]. As stated previously, several tomato genotypes produce reddish colored fruit whereas others produce green fruit. In several varieties, the transition from green fruit to red, ripened fruit is caused by the release of the plant hormone, ethylene.

1.3 Overview of Thesis Contents

This thesis is separated into three distinct parts. The first emphasizes the background material necessary to conduct research in the area of plant nutrition modeling. The next part describes the short-comings of the current methods and how this research provides useful information to the current state of this field. Finally, the last part is dedicated towards presenting and discussing the ramifications of the results obtained in this doctoral research.

1.3.1 Chapters Providing Background Descriptions

The background section of this thesis is split into two portions. The first portion begins in Chapter 2 with the nutrient uptake requirements of higher plants with an emphasis on tomato growth. This will include general descriptions of the processes involved in both organic and inorganic nutrition. This is followed up with Chapter 3 reviewing the current plant growth and nutrient uptake models that have been developed for agronomically important crops. This will include the various models that have been devised to interrelated the plant processes of overall growth, photosynthesis, water uptake, transpiration, and inorganic nutrient absorption. Once the nutrient uptake requirements have been reviewed, the methods which are utilized to supply plants hydroponically are discussed in the second portion of this background section. In Chapter 4, a general review of the conventional techniques that have been developed for hydroponic agriculture is provided. This will include a description of the hydroponic solutions that are available as well as the systems and designs that have been utilized in the past. Finally, the background portion of this thesis will conclude with Chapter 5 reviewing the specialized hydroponic system known as the Porous Ceramic Tube - Nutrient Delivery System (PCT-NDS). This chapter describes the construction of physical and mathematical models for the PCT-NDS, the theoretical development for the operation and control of the system, and the experimental verifications of both the model and control equations.

1.3.2 Chapters on the Current State of Plant Nutrition Modeling

With this background information on the current state of the field of plant nutrition modeling complete, Chapter 6 describes the rationale and significance of conducting research on modeling the nutrient uptake kinetics into tomato plants grown on the Porous Ceramic Tube - Nutrient Delivery System. In addition to the basic scientific advantages of this novel hydroponic system for the study of root-zone environmental effects on plant growth, several practical applications are presented as well. This includes applications to conventional and hydroponic agriculture as well as the endeavors of the National Aeronautic and Space Administration (NASA) to produce plants in space. Once the reasons for this research are presented, Chapter 7 presents the experimental protocols used for growing plants as well as analyzing the subsequent results. This will include the development of the plant growth chamber, the design of the test units, the experimental design, and the analytical procedures used to produce the nutrient uptake models.

1.3.3 Chapters on the Discussion of Results

With the description of the investigative methods complete, Chapters 8 and 9 are dedicated towards presenting the experimental results and discussing their implications, respectively. This will include a description of the plant growth chamber conditions throughout the experimentation, the growth and development responses of the tomato plants on the PCT-NDS, and the development of the nutrient uptake models. Finally, this thesis concludes Chapter 10 describing the contribution of this research to the current state of the field as well as provide some future recommendations for this type of research.

CHAPTER 2 - PLANT NUTRIENT UPTAKE

This chapter provides a background for the current state of the field of plant nutrition with an emphasis on tomato plants. In Section 2.1, the concentrations of the elements required for general plant growth are provided along with a description of the criteria for essentiality. Common plant biological functions for the organic nutrients are presented next in Section 2.2 in addition to the methods by which plants obtain and assimilate these nutrients. This includes a description of the carbon and oxygen fixation process of the Calvin-Bensen cycle and the photosynthetic "Z-scheme" for hydrogen evolution from water. Special emphasis is then afforded in Section 2.3 to the countercurrent gas exchange process of transpiration which is directly involved in both organic and inorganic nutrition. This section begins with a description of the pathways in which water is acquired in the root system continuing with a review of the factors affecting transpiration. These include species variations, atmospheric conditions, and the water potential gradients that form throughout the soil-plant-atmosphere continuum. As with the organic constituents, the major biological functions of the inorganic nutrients are presented next in Section 2.4 In addition to the mechanisms of uptake from the transpirational stream, this section will also include descriptions of several factors affecting uptake in the plants such as composition, concentration, pH, water potential, and temperature of the soil environment. Finally, this section will conclude with the deficiency and toxicity symptoms associated with inorganic nutrition.

2.1 Essential Plant Nutrients

There are 16 different elements that are required by all higher plants. These include carbon (C), hydrogen (H), oxygen (O), nitrogen (N), phosphorus (P), potassium (K), calcium (Ca), magnesium (Mg), sulfur (S), iron (Fe), chlorine (Cl), manganese (Mn), boron (B), zinc (Zn), copper (Cu), and molybdenum (Mo). This section of this chapter reviews the common terminology used in plant biotechnology to classify these nutrients as well as the criteria used to determine their essentiality. This determination distinguishes these 16 nutrients from the other elements that are generally available to the plant. These include, amongst others, arsenic, lead, silicon, cobalt, selenium, aluminum, and sodium.

2.1.1 Classification of Nutrients

There are several means of classifying plant nutrients. The organic constituents consist of C, H, and O while the inorganic nutrients consist of the other 13 remaining plant required elements listed above. A further classification of the inorganic nutrients distinguishes these elements by the relative amounts in which they are found in the tissues [Resh, 1978]. The macro-(inorganic)-nutrients are elements present in quantities ranging greater than 1,000 parts per million parts of plant tissue (ppm), including N, P, K, Mg, Ca, and S. These differ from the micro-nutrients which have sufficient concentration ranges of approximately 100 ppm in plant tissues and include, Fe, Cl, Mn, B, Zn, Cu, and Mo. The general concentration levels and classifications of these 16 essential plant nutrients are summarized in Table 2.1 [Salisbury and Ross, 1985; Taiz and Zeiger, 1991].

Table 2.1 Adequate Concentrations of Essential Plant Nutrients

Classification	Element	Symbol	Concentration (ppm)	in Dry Tissue (%)
Organic Constituents	Carbon	C	450,000	45
	Hydrogen	H	60,000	6
	Oxygen	O	450,000	45
Macro-Nutrients	Nitrogen	N	15,000	1.5
	Phosphorus	P	2,000	0.2
	Potassium	K	10,000	1.0
	Magnesium	Mg	2,000	0.2
	Calcium	Ca	5,000	0.5
	Sulfur	S	1,000	0.1
Micro-Nutrients	Iron	Fe	100	0.01
	Chlorine	Cl	50	0.005
	Manganese	Mn	50	0.005
	Boron	B	20	0.002
	Zinc	Zn	20	0.002
	Copper	Cu	6	0.0006
	Molybdenum	Mo	0.1	0.00001

2.1.2 Criteria for Essentiality

The 16 elements listed in Table 2.1 are considered essential plant nutrients due to their ability to meet three criteria [Salisbury and Ross, 1985; Resh, 1978; Taiz and Zeiger, 1991]. The first is that higher plants cannot survive in the absence of the nutrient which indicates that the nutrient must be present and accessible either in the atmosphere or in the nutrient solution of the soil. The second criteria is that the element must have a specific physiological function in the reproduction or growth of the plant that cannot be completely duplicated by using another nutrient. The third criteria is that the element must be acting directly in a plant process and not simply allowing another element to become more available or inhibit any toxic actions of the other elements.

For the organic constituents, these criteria are fairly stright forward as they comprise of approximately 96% of the total plant biomass. The three elements, C, H, and

O, form the basic skeletons for the starch, sugars, cellulose, phospholipid membranes, carbohydrates, amino acids, enzymes, proteins, genetic material, and all other compounds constituent to plants. As for the macro-nutrient elements, these are generally contained within these major compounds as well or perform some other major plant biological role that cannot be completely replaced with another element. The involvement of the micro-nutrients in the physiological development of the plant is generally as enzyme activators, cofactors, or electron carriers. Elaboration of the major plant biological functions for each of these nutrients are presented in later sections of this chapter.

2.2 Organic Nutrition

Comprising approximately 96% of the total weight of the organic plant matter, C and O are obtained by higher plants from carbon dioxide while water contributes H as well as additional O. The mechanisms by which these essential nutrients are acquired are by two related processes [Salisbury and Ross, 1985; Taiz and Zeiger, 1991]. Carbon dioxide enters through the stomates of the leaves (openings on the leaf underside) and is utilized through the bio-actions of photosynthesis (light-dependent reactions) and carbon fixation (light-independent or dark reactions). In addition, while these stomatal openings allow CO_2 influx, water vapor can simultaneously escape into the atmosphere. This countercurrent gas exchange process is termed transpiration and generally occurs during the lighted periods of the daily growth cycle. In order to balance the loss of water by the terrestrial portion, simultaneous water uptake is achieved by the root system.

2.2.1 Carbon Fixation - Carbon and Oxygen Assimilation

Carbon and oxygen entering through the plant stomates as CO_2 are fixed into the bulk biomass by the reactions of the Calvin-Benson or photosynthetic carbon reduction (PCR) cycle [Salisbury and Ross, 1985; Taiz and Zeiger, 1991]. There are two classifications of higher plants which are denoted by the pathway in which they conduct

this carbon dioxide fixation. A C3 plant initially fixes the CO_2 into a five carbon compound called ribulose-1,5-bisphosphate (RuBP) through the carboxylation actions of the enzyme, ribulose bisphosphate carboxylase/oxygenase (Rubisco), and forms an unstable six carbon compound. This C6 compound then splits into two components of a stable compound called 3-phosphoglycerate (3-PGA). This C3 compound is then dehydrogenated to form glyceraldehyde-3-phosphate (GAL-P). It is this C3 compound which is involved in the major reactions of the PCR cycle which ultimately leads to the production of sugars, carbohydrates, starch, amino acids, etc. Examples of plants that utilize the C3 carbon reduction cycle include wheat, oat, rice [Salisbury and Ross, 1985], kidney bean, potato, cabbage, eggplant [Sage, et al., 1989], and tomato [Martin and Thorstenson, 1988].

These plants are differentiated from their C4 counterparts due to the pathway in which they fix CO_2. Instead of initially forming stable 3-PGA, C4 plants store newly obtained carbon dioxide in a four-carbon compound such as malate or aspartate. These compounds are formed through the combination of CO_2 with a compound called phosphoenolpyruvate (PEP), a three carbon unit. The PEP is regenerated from the malate or aspartate with the concomitant release of CO_2 to the Calvin-Bensen cycle. Therefore, the difference between C3 and C4 plants is that the C4 plants utilize a cyclic reaction, known as the photosynthetic carbon assimilation (PCA) cycle, prior to the normal carbon dioxide fixing mechanisms of the C3 plants. The effect that this C4 PCA cycle has is to concentrate CO_2 at the active sites on Rubisco. Examples of typical C4 plants include corn, sugarcane, and sorghum [Salisbury and Ross, 1985].

Under normal atmospheric conditions, C4 plants have higher assimilation rates as compared to their C3 counterparts [Taiz and Zeiger, 1991]. This is due to the concentrating mechanism present in the C4 plants which increases the CO_2 available to the active sites on Rubisco. In C3 plants and, to a much smaller degree, in C4 plants, the active sites on Rubisco are competing for both CO_2 and oxygen. The oxygenation reaction termed, photorespiration or the C2 photorespiratory carbon oxidation (PCO) cycle, decreases the efficiencies of photosynthesis and carbon assimilation [Taiz and Zeiger, 1991]. This is due to the substrates utilized in this PCO process. Specifically, when RuBP

is oxygenated, it yields one 3-PGA and one C2 compound, 2-phosphoglycolate. This C2 compound is eventually split into a CO_2 molecule with the remaining carbon combining with glycine (another C2 compound) to produce a second 3-PGA. Therefore, the cost of oxygenating RuBP to form two molecules of 3-PGA are, amongst other resources, two previously fixed carbon atoms (glycine) plus a CO_2 that will have to be fixed again.

After CO_2 has entered the Calvin-Benson cycle, it can lead to the formation of other organic compounds [Salisbury and Ross, 1985; Taiz and Zeiger, 1991; Galtier, et al., 1995]. One component in this cycle is a phosphorylated fructose which can be isomerized into a phosphorylated glucose. This second compound can lead to the formation of sucrose (a C12 sugar) and starch (a multi-glucose compound) which are the principle leaf storage compounds. These stores are utilized in a process known as respiration where the production of adenosine triphosphate (ATP), the major energy carrying compound of biological systems, is accomplished. Additionally, inorganic phosphate is regenerated during sucrose and starch synthesis which eventually leads to the regeneration of RuBP for the carbon reduction cycle [Sage, 1990]. Another fate of C and O is the formation of amino acids. In particular, serine, glycine, and cysteine are derived from 3-PGA while phenylalanine, tyrosine, and tryptophan are synthesized from PEP and erythrose-4-phosphate, another intermediate in the PCR cycle [Stryer, 1988]. As for other amino acids, these are derived from other products of this CO_2 metabolizing cycle as well.

In 1994, the ambient CO_2 levels were measured to be approximately 350 ppm or 0.035% [Galtier, et al., 1995] and has been steadily increasing by about 1 ppm per year [Taiz and Zeiger, 1991]. Comparing this value to the 20-21% oxygen concentration in ambient air, the competition between CO_2 and O_2 for active sites is much higher in C3 plants as compared to C4 plants which have the PCA concentrating mechanism favoring carbon. However, increasing the carbon dioxide concentration above ambient conditions, which is often the case in greenhouses [Romero-Aranda and Longuenesse, 1995; Galtier, et al., 1995], leads to higher carbon reduction rates in C3 plants as compared to the C4 counterparts. This is due to the key C4 enzyme, PEP carboxylase, becoming saturated at the elevated CO_2 levels leading to a limitation in the Rubisco supply rate. In C3 plants this

rate limiting step is eliminated since Rubisco can accept the CO_2 directly from the enriched atmosphere. However, a CO_2 compensation point is eventually reached due to the saturation of the photosynthetic apparatus within the leaves which supplies regenerated RuBP for the carbon fixation processes [Sage, et al., 1989; Galtier, et al., 1995].

In order to illustrate the effects of carbon dioxide concentration on the assimilation and photosynthesis rates in tomato plants, a C3 plant [Macler, et al., 1990], the following examples are provided. Four hybrid cultivars (cv.) of *Lycopersicon esculentum* Mill. (Early Cascade, Ohio-Michigan, Sonato, and Virosa) each showed approximately 15% increases in growth rates (total plant matter) when cultivated under enriched CO_2 levels of 1,000 ppm as compared to ambient levels [Gent, 1984]. Similarly, tomatoes (cv. Rondello) were subjected to five levels of CO_2 ranging from 200 to 1,100 ppm resulting in net photosynthesis that increased from 5 to 35 $\mu mol/m^2/s$ in order to meet the increasing supply of carbon [Romero-Aranda and Longuenesse, 1995]. Carbon dioxide enrichment can also affect the growth and development of the individual plant parts. For example, while stems of tomatoes (cv. Calypso) increased from 12.8 to 13.4% dry matter content and fruits increased from 9.7 to 10.7 kg/m^2 when CO_2 levels were changed from 350 to 550 ppm, leaf area decreased from 0.174 to 0.158 m^2 per plant [Nederhoff, et al., 1992].

2.2.2 Photosynthesis - Hydrogen Assimilation

Although oxygen also enters through the absorption of water at the root surfaces, this source is not metabolized but is released back into the atmosphere as molecular oxygen. This process is achieved during the initial steps involved in photosynthesis occurring in the leaf chloroplasts [Taiz and Zeiger, 1991]. Water is first broken down into elemental H and O when photonic energy in the form of red light (680 nm) energizes the reaction center, Photosystem II (PSII). Two electrons are eventually transferred to an iron-sulfur containing protein complex which has a more positive redox potential. This energy transfer from a lower to a higher (more positive) potential is the basis of the "Z-scheme" used to describe the photosynthetic process [Salisbury and Ross, 1985; Taiz and

Zeiger, 1991]. With this loss of electrons, two H^+ ions are evolved along with half of a molecule of O_2. This oxygen exits through the gas exchange process of plant transpiration.

There are many fates for these hydrogen ions such as their incorporation into the Calvin-Benson cycle achieved during the reaction converting 3-PGA into GAL-P. Involved in this reaction step is a proton carrier called nicotinamide adenine dinucleotide phosphate (NADP+) which can be reduced to NADPH and a proton during a second light-dependent reaction occurring in Photosystem I (PSI), energized by far-red light (>680 nm). It is this reduced form which transfers its hydrogen ion to 3-PGA in the synthesis of the aldehyde and requires the expenditure of ATP energy. Once the hydrogen is contained within the key triose phosphate compound, the processes described above for the utilization and metabolism of carbon and oxygen are applicable. Other important physiological functions of hydrogen ions include ATP production and cation exchange.

Plants contain several types of light absorbing pigments including chlorophyll *a* and *b* which primarily absorb at 670 and 650 nm (red light), respectively, and a group of pigments known as carotenoids which absorb between 400 and 500 nm (blue light). These wavelengths of visible light (400-700 nm) are termed, photosynthetically active radiation (PAR) [Taiz and Zeiger, 1991]. The changes in wavelengths between the absorption capabilities of the chlorophylls and the reaction centers, PSI and PSII, results in the release of heat as does the energy transfer from the carotenoids to the chlorophylls. Compensation of this heat is achieved during the evaporative cooling process in plant transpiration.

During normal plant growth, the light intensity and quality of the PAR varies according to the time of day, weather patterns, shading, and plant density. These changes in the light greatly affect the rates of various plant biological processes. A previous example showed that although carbon assimilation increased by 15% when four tomato cultivars (Early Cascade, Ohio-Michigan, Sonato, and Virosa) were subjected to increased CO_2 levels, the magnitude of these differences were reduced but with an overall increase in the absolute growth when the PAR level was increased from 2.3 to 4.3 $MJ/m^2/day$ [Gent, 1984]. These results were probably due to a balancing between the photosynthesis and carbon fixation rates. Similarly, an increase in photosynthetic photon flux density (PPFD)

from 400 to 800 μmol/m^2/s increased the net carbon uptake in tomatoes (cv. UC82B) from 15 to 20 μmol/m^2/s at ambient CO_2 levels [Galtier, et al., 1995].

For the transpiration rates, changes in PPFD from 900 to 1300 μmol/m^2/s resulted in transpiration rates in maize (cv. Pioneer 3949) from 45 to 88 mg/m^2/s [Berard and Thurtell, 1991]. In tomato plants (cv. Counter), continuous monitoring of the global radiation and transpiration using a weighing lysimeter system [Van Ieperen and Madery, 1994] was accomplished over a 24 hour period. This experiment was conducted during a period of fluctuating radiation (i.e partly cloudy) which resulted in measurements between 200 and 1000 W/m^2 during the daylight hours. The corresponding transpiration rates directly followed the changes in radiation whereas the changes in fresh weight during the day were reversed from transpiration. This indicated a change in plant water status dictated by this environmental input [Van Ieperen and Madery, 1994]. Furthermore, subjecting plants to different wavelengths of light causes different degrees of stimulation of the stomatal aperture. Blue light was shown to be more effective than red followed by green [Matsui, et al., 1981]. This could be due to the compensation of the higher internal heat generated during the energy transfer from carotenoids (400-500 nm) to chlorophyll (650-670 nm) as opposed to chlorophyll to the PSI or PSII reaction centers (680+ nm).

When tomato plants (cv. Duranto) were grown in an artificial environment under three different types of lamps with differing light spectral qualities, inorganic nutrient uptake was also shown to be affected [Tremblay, et al., 1988]. Radioactive rubidium (^{86}Rb) uptake which utilizes the same mechanism as K [Wrona and Epstein, 1985; Peterson and Jenson, 1988] was shown to be reduced when the tomato plants were grown with either deficit or low blue light. Specifically, high pressure sodium lamps which lack blue light altogether but have a high quantity of red light yielded 8.01 cpm x 10^6/g dry weight while white deluxe fluorescent lamps which contain low levels of both blue and red lights resulted in a value of 8.10. These results differed when Gro-lux fluorescent lamps, which contain higher red and blue light quantities than the white deluxe, were utilized. In this case, the rubidium uptake was significantly increased to 10.27 cpm x 10^6/g dry weight. Similarly for Ca uptake (measured using ^{45}Ca), the sodium lamps reduced the capacity

while either fluorescent lamp resulted in significantly higher rates. Therefore, the light spectral quality of these three lamps affected the nutrient uptake capacities in the tomato plants even though the PPF was maintained at 300 $\mu E/m^2/s$. Other nutrients that were investigated included Fe and Mn but did not lead to any significant differences in uptake.

2.3 Transpiration

In addition to the introduction of CO_2 into the plant, the process of transpiration has several other functions [Salisbury and Ross, 1985; Taiz and Zeiger, 1991]. This includes the release of water vapor which serves to maintain the internal temperature particularly during the day by utilizing the evaporative cooling by the water vapor from the leaf stomata. This process contributes to the majority of the water loss from plants but is used to maintain hydration through the continuous column of water absorbed at the root surface, transferred through the main shoot and branching system, and out the leaves.

2.3.1 Water Uptake Pathways

The methods in which water enters the roots are the apoplastic, symplastic, and transcellular pathways [Salisbury and Ross, 1985; Taiz and Zeiger, 1991; Maggio and Joly, 1995]. The apoplast is the continuous system of cell walls and intracellular air spaces in plant tissues where water can enter and move without crossing membranes. The transcellular pathway consists of water moving from one cell to another where it crosses at least two plasma membranes. However, when the water is between the cells, the symplastic pathway can be utilized. The symplasm consists of the entire continuous network of cell cytoplasms interconnected by plasmodesmata, small channels connecting adjacent cells [Molz, 1981; Taiz and Zeiger, 1991]. These pathways are depicted in Figure 2.1 along with the overall root structure. During water uptake, each pathway is utilized to some degree; however, at the endodermis, the apoplastic pathway is blocked due to the Casparian strip which are highly suberized cell walls (not shown) interrupting this route.

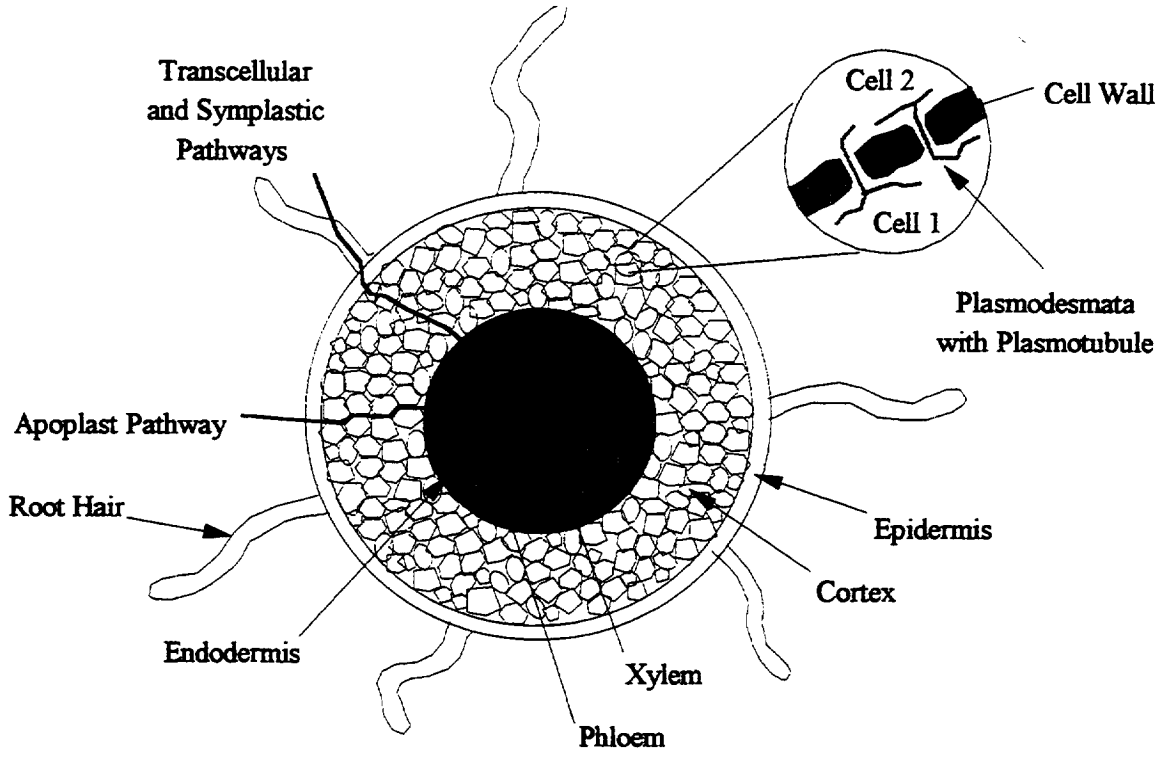

Figure 2.1 Root Structures and Water Transport Pathways

The flow rate across the root membrane is determined as a function of the water potential gradient (see Section 2.3.4), the area of the root membrane, and the hydraulic conductivity, L_p. Root length can be estimated using a microscope and the line-intersection method [Newman, 1966]. Utilizing a rectangular plate of known area, A, with randomly placed straight lines of known total length, H, the number of intersections, N, that the root placed on the plate makes with the lines can be counted using the microscope. This number is then used in Equation (2.1) to estimate the root length, L_r.

$$L_r = \pi NA / 2H \qquad (2.1)$$

Using this method, errors of approximately 10% were achieved when compared to the actual measurements of the roots; however, the times required to make these measurements were substantially lower than the direct method. In order to estimate the hydraulic conductivity, L_p, de-topped roots systems are placed in a pressure vessel filled with nutrient solution. When a pressure is applied, xylem sap from the cut stump is

exuded. Measuring the rate of exudation at pressures above 0.15 MPa yields a linear relationship with the slope equaling L_p. In this case, L_p defines the capacity of roots to supply water to the shoot. It describes the degree that a given water potential gradient can move water through the root frictional resistances [Boyer, 1985]. This technique yields an average L_p for the entire root surface but is not able to resolve local differences in L_p along the root length [Joly, 1989]. Using this procedure, tomato roots (cv. Ailsa Craig) were found to have a hydraulic conductivity of 18.95 $mm^3\ s^{-1}\ MPa^{-1}$ [Jackson, et al., 1996].

2.3.2 Species Varietal Differences

The absolute transpiration from plants varies with species, cultivars, and growth conditions. For example, wheat plants (cv. Yecora rojo) transpired 6.9 ml/day per plant when grown on a porous tube hydroponic system which was one-third the loss when grown conventionally [Dreschel and Sager, 1989]. For lettuce (cv. Waldmann's Green and Grand Rapids), air moisture derived from transpiration and collected as condensate from growth chamber heat exchangers averaged over 325 kg over a 30 day period for 960 plants [Edeen and Henninger, 1990; Barta, et al., 1992]. In tomato plants, transpiration can account for as much as 90% of the total water intake [IPM Manual Group, 1982]. Using a weighing lysimeter, 2 meter tall tomato plants (cv. Counter) were found to transpire 3.0 g/min per plant at peak global radiation levels while this level decreased to 0.15 g/min per plant during the night [Van Ieperen and Madery, 1994].

In a direct comparison between plant species, the sap flow rates in the vascular tissues known as xylem were measured using the heat-pulse method [Cohen, et al., 1988]. In this experiment, the sap flow rates in soybean (cv. Williams) and maize (cv. Pioneer 3377) plants were measured to be 26 and 21 mm^3/s, respectively [Cohen, et al., 1990]. Furthermore, the sap flow rates were shown to be directly proportional in a 1-to-1 relationship to the transpiration rates which can be calculated to be 1.56 and 1.26 ml/min, respectively, averaged over the time of measurement. For the differences within a species, two soybean cultivars (OX922 and OX942) exhibited significantly different transpiration

rates based on measured sap flow rates [Tan and Buttery, 1995]. Genetically, these two isolines differed by the number of stomates (4 vs. 155 per mm^2 leaf area, respectively) leading to maximal transpiration measurements of 677 and 1193 g/day per plant.

2.3.3 Factors Affecting Transpiration

The factors controlling transpiration include the stomatal conductance, the leaf surface boundary layer resistance, and the atmospheric temperature [Taiz and Zeiger, 1991]. The first factor is dependent upon the plant's ability to control the stomatal aperture while the last two factors are controlled through the atmospheric conditions. This stomatal control is necessary in order to balance the plant water status and is affected by the availability (i.e. moisture) in the soil [Lafolie, et al., 1991]. It has been hypothesized that the hormone, abscisic acid, is transmitted from the root to the guard cells of the leaf stomata [Johnson, et al., 1991; Bruckler, et al., 1991; Trejo, et al., 1995]. During hot, dry climates, this 'message' reduces the stomatal conductance by transferring K^+ and Cl^- from the guard to the mesophyll cells [Johnson, et al., 1991]. This transfer reduces the stomatal pore, thus, reducing transpiration. Therefore, as water transpires from the leaves, a decrease in the leaf water content develops. This change leads to a gradient between the leaf and the connecting branch xylem causing an increase in the water transport to the leaf. As water exits the branch xylem, a continuous supply is maintained from the main shoot xylem which is subsequently supplied by the roots. Finally, as the root water content decreases, the rate of transport from the soil solution to the root surface increases. This whole process assumes a sufficient supply of water at the root-zone. In order to increase water absorption, microscopic root hairs are produced from the root epidermal cells. Typically, these are established at the zone of elongation and constitute as much as 60% of the total root surface area [Taiz and Zeiger, 1991].

The leaf surface boundary layer resistance is affected by wind speed, planting density, canopy height, and leaf structure [Taiz and Zeiger, 1991; Johnson, et al., 1991]. The resistance to water vapor diffusion is proportional to the thickness of the boundary

layer. Therefore, as the amount of air passing over the leaves increases either by increased wind speeds or by decreased leaf surface area per unit volume of air, the film of stagnant air surrounding the leaf becomes thinner, reducing the resistance. As for leaf structure, differences in morphology and orientation can affect how the leaves intercept the wind.

The effects of atmospheric temperature, in general, range from the developmental threshold of about 10°C to between 25 to 32°C for optimum growth. The upper limit for growth is approximately 44°C [IPM Manual Group, 1982] with half maximal growth rates occurring at 13 and 36°C [Gent, 1986]. Under low temperature conditions, plant growth can become inhibited due to a decrease in cell membrane fluidity. At the other extreme, growth becomes inhibited primarily due to the change in enzyme activity [Salisbury and Ross, 1985; Taiz and Zeiger, 1991]. In order to protect against these extreme fluctuations, plants control transpiration through the stomatal conductance. When it is cold, the stomates will remain closed in order to conserve the internal heat whereas when it is hot, transpiration serves to cool the plant [Salisbury and Ross, 1985; Taiz and Zeiger, 1991; IPM Manual Group, 1982]. Therefore, as the surrounding temperature rises, the rates of transpiration and nutrient uptake significantly increase through the plant cooling process.

2.3.4 Water Potential Gradients

As stated earlier, water transfers from one region of the plant to the next through the vascular tissues known as the xylem. This transpirational stream begins at the root surfaces where the water is first absorbed and subsequently loaded into the xylem of the root tissues. It then proceeds upwards through the xylem of the main shoot and branching system eventually being unloaded into the cells of the leaves. At this point, the water exits the leaf stomates through evaporation into the atmosphere. The driving force for this transport process is based upon the water potential gradients that form between one region and another. The water potential, Ψ, is defined below [Salisbury and Ross, 1985; Rudich and Luchinsky, 1986; Taiz and Zeiger, 1991] as the difference between the hydrostatic pressure, P, in excess of ambient conditions and the osmotic potential, π. This

second quantity reduces the water concentration due to the presence of solutes; thus, it reduces Ψ. This quantity is further defined in Equation (2.2) where R is the universal gas constant (0.0083143 L MPa mol^{-1} K^{-1}), T is absolute temperature (in Kelvins), and C_s is the solution osmolality (moles of all solutes, regardless of form, per kg of water).

$$\Psi = P - \pi = P - RTC_s \qquad (2.2)$$

Therefore, the gradient between a region of higher to lower potential, $\Delta\Psi = \Psi_{hi} - \Psi_{lo}$, can be determined from these quantities. In general, the resulting hydrostatic pressure gradient, ΔP, represents the driving force for bulk flow while the concentration gradient, $\Delta\pi$, represents the driving force for nutrient diffusion.

For the soil, the hydrostatic component, P, arises from the water adhesion to the soil matricies and is, thus, referred to as the matric potential, $P = P_m$. This arises from the attractive forces between water and soil which tends to cause water to form concave microfilms around the particle surfaces particularly in the intersticies of the matricies. This quantity can be estimated using the surface tension of water, $\gamma = 7.275 \times 10^{-8}$ MPa m, along with the radius of curvature, r, that the meniscus makes between the liquid and the soil colloids [Taiz and Zeiger, 1991; Bromberg, 1984].

$$P_m = -2\gamma / r \qquad (2.3)$$

Therefore, Equation (2.2) can be rewritten as the following with the substitution of $\Psi = \Psi_{soil}$ for the soil solution with osmolality, C_{soil}, and Equation (2.3) substituted for $P = P_m$.

$$\Psi_{soil} = P_m - \pi_{soil} = -2\gamma / r - RTC_{soil} \qquad (2.4)$$

Since both quantities in Equation (2.4) are negative, this indicates that water is always under tension when contained in a soil matrix. Furthermore, ionic interactions between the nutrients and the fixed charges on the soil colloids cause a localization of the osmotic pressure. This effectively increases the magnitude of the soil water potential and becomes more pronounced when the soil water content decreases.

In order to measure the soil water potential, methods such as lysimetry, gamma densitometry, neutron moderation, time-domain reflectometry [Wraith and Baker, 1991], and the microtensiometer [Vetterlein, et al., 1993] have been designed. However, these techniques generally have poor spatial and/or temporal resolutions, range, and precision. Typical values for Ψ_{soil} range from -0.05 MPa for moist conditions where the major contribution is due to the osmotic component to -0.5 MPa for dry conditions where the matric potential becomes dominant [Lafolie, et al., 1991]. For saline soils, π can attain values as high as 0.2 MPa [Taiz and Zeiger, 1991]. Extremely dry soil conditions can attain values for Ψ_{soil} of -3 MPa; however, most plants cannot be sustained under this soil water potential as plants reach a permanent wilting point at about this same level [Taiz and Zeiger, 1991]. Another measure of the water content within soils is the field capacity which is the moisture holding capacity in relation to the soil itself (measured in quantity of water per quantity of soil). Determinations of this quantity is achieved by saturating a particular soil with water and allowing the excess to drain away. The difference in wet and dry weights leads to the field capacity [Taiz and Zeiger, 1991]. Since soil properties vary greatly based on particle size, microporous spaces, surface area, degree of compaction, and depth, field capacities are dependent upon the particular soil. For example, a clay loam soil had a field capacity of 0.23 kg/kg [Bruckler, et al., 1991] while fine sand measured at 0.13 and high surface area Andosols measured upto 0.70 [Cox and Barber, 1992].

For plant tissues, this matric potential is considered negligible [Rudich and Luchinsky, 1986]. However, rigid cell walls contribute to the hydrostatic component in the form of turgor pressure, $P = P_t$, by maintaining cell volume especially during periods of dehydration. This quantity can be measured in plant tissues using several different techniques along with the water potential, Ψ, and the osmotic potential, π. This includes the psychrometer (Ψ), cryoscopic osmometer (π), pressure probe (P_t), and pressure chamber (P_t) [Breace and Kohl, 1970; Prager and Bowman, 1963; Taiz and Zeiger, 1991]. Substitution of $P_{t,root}$ or $P_{t,leaf}$ for P and C_{root} or C_{leaf} for C_s in Equation (2.2) yields the following water potentials for the roots ($\Psi = \Psi_{root}$) and leaves ($\Psi = \Psi_{leaf}$), respectively.

$$\Psi_{root} = P_{t,root} - RTC_{root} \quad (2.5)$$

$$\Psi_{leaf} = P_{t,leaf} - RTC_{leaf} \quad (2.6)$$

Taking the difference between Equation (2.4) for the soil potential and Equation (2.5) for the root potential, the gradient for water and nutrient absorption at the root surface can be determined. Specifically, water absorption occurs when $(\Psi_{soil} - \Psi_{root}) > 0$ MPa.

Unlike soils, the typical values of root water potentials vary according to the diurnal cycle of the plant and the overall plant-soil water status. For dry soils (Ψ_{soil} = -0.5 MPa), root water potentials range from approximately -0.5 MPa (equilibrium) during the night to -1.5 MPa during the day when transpiration is peaking. Subsequent measurements as the soil dried out lead to a trend of decreasing maximum root potentials at night which did not equilibrate with the soil levels. Conversely, for moist soils (Ψ_{soil} = -0.05 MPa), Ψ_{root} equilibrated with the soil conditions during the night but continually decreased in magnitude as the soil dried. Furthermore, the gradient between the moist soil and the roots continued to increase as the soil water content decreased [Lafolie, et al., 1991].

The growth, nutrient uptake, transpiration, and developmental rates of a plant is highly dependent upon the water relations at the root-zone [Glass, 1989]. Using an increase in salinity to reduce soil water potential, tomato (cv. Micro-Tom) plants exhibited decreased leaf area, shoot length, root area, and fruit development [Smith, et al., 1992]. In rice (cv. IR 36), maize (cv. DMR-2), and soybean (cv. Clark 63), root and shoot dry weights and leaf elongation rates decreased when soil Ψ declined. However, an earlier reduction was caused in rice as compared to the other two test species. As for the transpiration rates of these plants, each exhibited a decrease starting at various times after water was withheld [Tanguilig, et al., 1987]. The importance of the soil-root water potential gradient on the rate of transpiration becomes evident during a direct comparison of plants grown under different moisture levels. Specifically, maize (cv. Pioneer 3949) plants were subjected to three levels of moisture of 0.11, 0.15, and 0.26 m^3/m^3 resulting in transpiration rates of 25.1, 37.4, and 57.4 $mg/m^2/s$, respectively [Berard and Thurtell, 1991]. This translates into a rate of water loss of 2.2, 3.2, and 5.0 l/day for every square

meter of growing area. Similarly, tomato plants (cv. Capello) were subjected to soil moisture levels of 95 and 55% of field capacity and responded by transpiring at 42.4 and 28.7 $mg/m^2/s$, respectively [Xu, et al., 1995]. To illustrate varietal differences, three genotypes of tomato, *L. esculentum* Mill. cv. UC82B, *L. pennellii* (Cor.) D'Arcy, and their F_1 hybrid were grown under three soil moisture levels rated as 100, 50, and 25% of field capacity [Martin and Thorstenson, 1988]. For each moisture level, the hybrid absorbed more water than either parent with the *L. esculentum* tomatoes absorbing more than the drought tolerant, *L. pennellii*. Furthermore, each type utilized 45 and 15% of the water used at 100% field capacity when subjected to 50 and 25% of the soil moisture, respectively. Specific water use for the plants grown for 60 days at 100% field capacity were 63.5, 33.3, and 82.2 kg for the standard, tolerant, and hybrid varieties, respectively.

For the air outside of the leaf cells, the water potential, Ψ_{air}, results from the actual water vapor concentration in the air, c_{wv}. In Equation (2.7), R is the gas constant, V_w is the specific volume of water vapor and c_{wv}^0 is the concentration in air saturated with water vapor at the given absolute temperature, T. Furthermore, the water potential of the air can be determined in terms of the relative humidity, RH [Taiz and Zeiger, 1991].

$$\Psi_{air} = \frac{RT}{V_w} \ln (c_{wv}/c_{wv}^0) = \frac{RT}{V_w} \ln (RH) \qquad (2.7)$$

For the air just inside of the leaf spaces, the water potential can be assumed to be close to equilibrium with the leaf, $\Psi_{space} \approx \Psi_{leaf}$, where the relative humidity is near saturation. Leaf Ψ generally ranges between -0.2 to -0.6 MPa for well watered plants and can be as low as -5 MPa for extreme conditions [Taiz and Zeiger, 1991]. For comparison, the air inside the leaf spaces at 20°C (293 K) with relative humidities of 99.5, 99.0, or 95.0% have water potentials that can be calculated from Equation (2.7) to be -1.56, -3.12, and -15.95 MPa, respectively. When the exterior humidity is relatively low, the air moisture within the leaf spaces evaporates leading to a transient water potential gradient with the leaf cells. This gradient is also known as the vapor pressure deficit, VPD. Therefore, the driving force for

transpiration can be estimated from the gradient between the air surrounding the leaf and the air inside of the leaf spaces, $\Delta\Psi = \Psi_{space} - \Psi_{air}$. Corresponding water potentials for the surrounding air at 20°C (293 K) with relative humidities of 90,75, and 50% can be similarly calculated from Equation (2.7) to be -33, -89, and -216 MPa, respectively.

The values for the water potentials of the various regions of the soil-plant-atmosphere continuum are reviewed in Table 2.2 for both moist and dry conditions. Upon comparing these water potentials, it can be seen that the largest gradient is formed between the inner space of the leaf and the surrounding air. Therefore, the rate of transpiration can become substantial depending upon the water status of the plant and the relative humidity of the surrounding atmosphere. This dependency is illustrated in the following examples. In the experiment presented earlier where maize (cv. Pioneer 3949) plants were subjected to three levels of soil moisture of 0.11, 0.15, and 0.26 m^3/m^3, chamber RH was also varied between 20-25 and 75-80% [Berard and Thurtell, 1991]. The effect that the low humidity had on the transpiration rates was to cause increases in the quantity of water transpired by 1.8, 1.7, and 1.5 times the high humidity levels reported earlier for the dry to moist soils, respectively. These non-uniform changes indicated that even though the humidity change caused substantial increases in transpiration, the soil water content dictated the degree to which the increases occurred. This is due to the stomates being controlled by the soil water potential through the transmission of abscisic acid in the transpirational stream [Trejo, et al., 1995]. Similarly, high humidities of 0.1 kPa vapor pressure deficits (vs. 0.8 kPa) were shown to cause increases in the transpiration and nutrient uptake rates in tomatoes (cv. Counter) as well [Adams and Holder, 1992].

Table 2.2 Water Potentials in the Soil-Plant-Atmosphere Continuum

		Water Potential (MPa)	
Region	Symbol	Moist	Dry
Atmospheric Air	Ψ_{air}	-33	-216
Inner Air Spaces	Ψ_{space}	-1.56	-15.95
Leaf Cells	Ψ_{leaf}	-0.2	-5
Root Xylem	Ψ_{root}	-0.05	-1.5
Soil Solution	Ψ_{soil}	-0.05	-0.5

2.4 Inorganic Nutrition

As water enters the root environment, the dissolved nutrients can be carried in as well. In order to illustrate the essentiality of the 13 inorganic macro- and micro-nutrients listed in Table 2.1, some of the more well known plant physiological roles and involved processes are given in Table 2.3 for the macro-nutrients and Table 2.4 for the micro-nutrients [Salisbury and Ross, 1985; Adams, 1986; Ho and Hewitt, 1986; Resh, 1978; Stryer, 1988; Taiz and Zeiger, 1991; Kiss, et al., 1991; Barrachina, et al., 1994; Awada, et al., 1995]. These lists are to serve as means to illustrate essentiality of these elements and are by far incomplete lists of how plants utilize these nutrients.

Table 2.3 Physiological Roles and Processes for the Essential Inorganic Macro-Nutrients

Classification	Element	Physiological Roles and Involved Processes
Macro-Nutrients	N	all amino acids, proteins, and enzymes, chlorophyll, NADP+, ATP, deoxyribonucleic acid (DNA), ribonucleic acid (RNA), uridine diphosphate (UDP) glucose used in sucrose synthesis
	P	all sugar phosphate intermediates in the PCR cycle, NADP+, ATP, UDP-glucose, DNA, RNA, phospholipids
	K	coenzyme or activator for many enzymes such as pyruvate kinase, involved in stomatal control, controls fruit development and acidity, involved in protein synthesis and sugar transport
	Mg	chlorophyll, activates certain enzymes such as hexokinases
	Ca	calcium pectate cements together primary walls of adjacent cells, regulates salinity stress, component of peroxidase
	S	cysteine, methionine, FeS protein used in the photosynthetic "Z-scheme", coenzyme A carries acyl groups, thiamine and biotin vitamins, thioredoxin reduces disulfide bridges to activate certain enzymes such as phosphotransferases

Table 2.4 Physiological Roles and Processes for the Essential Inorganic Micro-Nutrients

Classification	Element	Physiological Roles and Involved Processes
Micro-Nutrients	Fe	activates certain enzymes in chlorophyll synthesis, component of cytochromes, FeS protein, peroxidases, and ferrodoxin used in the photosynthetic "Z-scheme"
	Cl	enzyme activator during oxygen production from water, involved in the opening and closing of stomates, maintenance of electrical potentials during ion exchange
	Mn	Mn protein accepts electron from water during photosynthesis, activates certain enzymes involved in DNA and RNA synthesis, coenzyme or activator of enzymes such as enolase, phosphokinase, and phosphotransferase
	B	borate complexes form with carbohydrates during transport, regulates carbohydrate synthesis
	Zn	activates certain enzymes such as alcohol and glutamic acid dehydrogenases, regulates cysteine-to-cystine transformation
	Cu	plastocyanin used in the photosynthetic "Z-scheme", activator of enzymes such as phenolase and laccase
	Mo	electron carrier in the conversion of nitrate to ammonium, component of nitrogenase essential for N_2 reduction

2.4.1 Mechanisms of Uptake

As the inorganic nutrients are transported to the root surfaces through the transpirational stream, integral membrane protein channels and carriers facilitate their uptake [Taiz and Zeiger, 1991; Van Den Honert and Hooymans, 1955; Wheeler, et al., 1994]. This uptake from the solution is either active or passive depending upon whether the transport through the membrane requires metabolic energy [Salisbury and Ross, 1985; Taiz and Zeiger, 1991]. This energy can come from the hydrolysis of an ATP compound through an enzyme known as an ATPase or from the energy stored in the proton motive force determined by the gradient in H^+ ions set up across the membrane.

For passive uptake, protein channels which act as selective pores are often utilized. This selectivity is derived from the size of the pore as well as the surface charges on the pore walls. During this type of transport, a nutrient ion specific for that particular channel is generally transferred across the membrane along its electrochemical gradient. However, this depends upon the diffusion potential of the barrier membrane, ΔE_m, which can be calculated using Equation (2.8), the Goldman equation. In this equation, R is the universal gas constant, T is absolute temperature, F is Faraday's constant (23.06 kcal V^{-1} mol^{-1}), and C_j^i and C_j° are the internal and external concentrations of nutrient, j, respectively.

$$\Delta E_m = \frac{RT}{F} \ln \frac{P_K C_K^\circ + P_{Na} C_{Na}^\circ + P_{Cl} C_{Cl}^i}{P_K C_K^i + P_{Na} C_{Na}^i + P_{Cl} C_{Cl}^\circ} \qquad (2.8)$$

Although terms for all solutes passing through the membrane should be included in the Goldman equation, K, Na, and Cl have the largest permeabilities, P_j, and cellular concentrations, C_j^i [Taiz and Zeiger, 1991]. Therefore, the electrochemical gradient of a particular ion would have to overcome the membrane potential in order for transport to occur through the protein channel. In order to calculate the electrochemical potential that the nutrient ion has for diffusion, Equation (2.9), the Nernst equation, can be utilized.

$$\Delta E_{nj} = \frac{2.3RT}{z_j F} \log \frac{C_j^\circ}{C_j^i} \qquad (2.9)$$

In this equation, R, T, and F are as described for the Goldman equation while z_j is the electrostatic charge of the ion, j. If the Nernst potential calculated from Equation (2.9) is relatively equal to the membrane potential calculated from Equation (2.8), then the transport of the ionic species through the transmembrane protein channel is considered passive. For water, the uptake is considered passive [Cortes, 1992] utilizing integral membrane proteins as specific water channels called, aquaporins [Maggio and Joly, 1995].

Another mode of passive transport utilizes a enzyme carrier in the membrane lipid bilayer which binds to a particular nutrient. This occurs through an active binding sites on

the enzyme that is specific for the substrate, either by size restriction, electrical charge, or other method of recognition. Once a correct union forms, the enzyme undergoes a conformational change moving the nutrient to the other side of the membrane. Once there, the nutrient is passively released completing the transport cycle which is called facilitated diffusion. Again, this type of transport generally occurs down the electrochemical gradient of the nutrient ion. Therefore, this carrier mediated transport occurs when the membrane and electrochemical potentials as determined from Equations (2.8) and (2.9), respectively, are relatively equal. Nutrient uptake studies have revealed that passive uptake mechanisms exist for K^+ in tomato [Peterson and Jensen, 1988], K^+, Ca^{2+}, and Mg^{2+} in pea root tissues [Higinbotham, et al., 1967], and Ca^{2+}, Na^+, and Cl^- in snapbean [Awada, et al., 1995].

When there are large differences between ΔE_{nj} and ΔE_m , this would indicate that the uptake of nutrient, j, is active since energy would be required to transport the ion either against the electrochemical gradient (in the opposite direction) or in addition to the diffusion potential (in the same direction). One type of active transport mechanism utilizes an enzyme carrier similar to the facilitated diffusion mechanism described earlier. However, after the particular nutrient binds to the carrier enzyme causing the conformational change transporting it to the other side of the membrane, the enzyme requires some input of energy. Typically, this energy is derived from ATP which causes the enzyme (known as an ATPase) to return to its original conformation, releasing the nutrient on the other side of the membrane. This mechanism which utilizes the expenditure of energy is called an electrogenic pump [Taiz and Zeiger, 1991]. One of the most common electrogenic pumps is the H^+-ATPase present in the plasma membrane of plant cells [Wheeler, et al., 1994]. Some inorganic nutrients requiring a primary ATPase for transport include Ca^{2+} and Mg^{2+}. The Ca^{2+}-ATPase which regulates calcium levels in the cytosol [Kauss, 1987] may be responsible for Mg^{2+} uptake as well based on inhibition studies conducted on maize plants [Brauer, 1994]. However, a separate ATPase was concluded as the likely means of transport for Mg^{2+} in sorghum plants [Wilkinson and Duncan, 1993]. Furthermore, Mn^{2+} has been speculated to at least partially compete for the active sites on the Ca^{2+}-ATPase in tomato [Le Bot, et al., 1990].

Indirectly associated with the ATP hydrolysis during the electrogenic transport of a proton across a membrane is the formation of an H^+ gradient. This not only contributes to the electrochemical potential across the membrane due to the positive charge but also causes a pH gradient to form as well. In order to maintain adequate levels of protons on either side of a membrane, plant cell have developed special transport proteins [Taiz and Zeiger, 1991]. These are classified as symports or antiports and are utilized to not only transport protons through this proton motive force, but to carry other nutrients as well. An antiport transports a proton in the opposite direction of the other nutrient in association while a symport transports both constituents in the same direction. Example of these include the H^+/Cl^- symport, the H^+/Na^+ antiport [Taiz and Zeiger, 1991], and the H^+/NO_3^- symport [Wheeler, et al., 1994]. Although there is no direct expenditure of energy, these modes of transport are considered active due to their secondary association with the H^+-ATPase's which originally established the proton motive force.

Nutrient uptake mechanisms that have been linked to this proton gradient in tomatoes include NH_4^+ [Peterson and Jensen, 1988], K^+ [Janes, et al., 1988], inorganic phosphate ($H_2PO_4^-$, HPO_4^{2-}, and Pi) [Goldstein, et al., 1988a], and Fe [Brown, 1978; Beinfait, 1988; Holden, et al., 1995]. Furthermore, the enzyme responsible for Fe uptake, Fe-chelate reductase, also requires the expenditure of energy in the form of nicotinamide adenine dinucleotide, NADH [Holden, et al., 1991], a compound similar to NADPH. Experiments conducted on tomato roots which contain this enzyme [Holden, et al., 1991] revealed that the transport of similarly charged cations such as Cu may be attributed to this reductase as well [Holden et al., 1995]. Furthermore, Zn^{2+} absorption in tomato, rice, and sugarcane have been shown to occur through the same mechanism or carrier sites as Cu^{2+} [Bowen, 1987]. This could indicate that Zn^{2+} uptake may even be attributed to this same enzyme. Similarly, in snapbean, Mn was found to compete with Fe during uptake [Awada, et al., 1995] indicating that this nutrient may by competing for binding sites on this enzyme as well. However, in tomato, Mn^{2+} was shown not to be competing with Cu^{2+} or Zn^{2+} during uptake [Bowen, 1987] leading to the conclusion that the specific uptake mechanism utilized is highly dependent upon plant species as well as the nutrient.

For inorganic phosphate nutrition, when levels are deficit, there has been evidence that cation uptake increases in conjunction with the uptake of the anionic P compounds [Heuwinkel, et al., 1992]. This could suggest a possible cation (in)/phosphate (in) symport present in the root cell plasma membrane. Furthermore, P starvation leads many plant root cells including tomato [Goldstein, et al., 1988b] to respond by actively releasing an acid phosphatase [Garcia and Ascencio, 1992]. This protein converts organic P into the more readily absorbed inorganic forms [Goldstein, et al., 1988a]. The organic phosphates in the rooting medium are derived from excreted organic acids such as citric acid. Furthermore, root cells also respond to P deficit conditions by lowering the pH of the external rooting medium by a net proton efflux [Heuwinkel, et al., 1992]. This leads to a more favorable environment for the acid protein which has an optimum pH between 4 and 6 [Goldstein, et al., 1988a]. This also suggests possible proton (out)/cation (in) antiports causing the enhanced cation uptake associated with P starvation. Due to the similarities between MoO_4^{2-}, SO_4^{2-}, and HPO_4^{2-}, it has also been postulated that Mo and S uptake may occur through the same P uptake mechanism in tomato root cells [Heuwinkel, et al., 1992].

In order to determine experimentally whether a nutrient is acquired actively or passively, the membrane potential, ΔE_m, can be measured using a microelectrode inserted into the cell. Substituting this value in for the Nernst potential, ΔE_{nj}, described in Equation (2.9), the internal concentration, C_j^i, can be determined from a known external concentration, C_j^o, and compared to that which is measured. Large differences between the measured and predicted internal concentrations indicate an active uptake. Using this procedure, it was discovered that for pea root tissues, the uptake of K^+ was passive while the other nutrients present in the solution, Ca^{2+}, Mg^{2+}, Cl^-, NO_3^-, $H_2PO_4^-$, and SO_4^{2-} were active [Higinbotham, et al., 1967]. Furthermore, the anionic concentrations were higher than predicted indicating active uptake mechanisms as compared to Ca^{2+} and Mg^{2+} which were lower internally than predicted. Therefore, these cations passively entered the cells and were then actively extruded. However, the region of the root (i..e. cortex vs. xylem) or the cellular compartment (i.e. cytosol vs. vacuole) of the root tissues where the internal concentrations are measured changes these calculations [Cortes, 1992].

2.4.2 Factors Affecting Nutrient Uptake

The factors reviewed earlier that affect plant transpiration also affect the capacity for inorganic nutrient uptake. These factors included the plant's stomatal control, leaf structure, wind speed, planting density, canopy height, leaf surface boundary layer resistance, atmospheric temperature, and the soil-plant-atmosphere water status which dictates the water potential gradients. Concurrent with the reduction in transpiration, the rate of nutrient uptake in tomatoes was also shown to have decreased [Glass, 1989]. In addition to these terrestrial factors, several other factors at the root-zone also affect the ability of plants to acquire nutrients. These include the nutrient solution composition, concentration, and pH, the root-zone water potential, and the temperature of the soil environment.

Although the essential nutrients listed in Tables 2.3 and 2.4 are presented as elemental symbols, plants require these chemicals to be in particular compositional forms in order for uptake to occur [Resh, 1978]. Furthermore, these nutrients need to enter the aqueous phase in order for the plant roots grown in the vicinity to absorb [Taiz and Zeiger, 1991]. When plants are grown in the soil, the nutrients are present in many ionic forms including simple ions and complex charged compounds from which the plant selectively absorbs. This is different from the hydroponic production of plants which utilizes salt solutions that are generally of known composition and ionic charges. In this discussion, the more prevalent forms available to plants in the soil are presented first.

On the surfaces of soil particles, positively charged cations such as Ca^{2+}, Mg^{2+}, Cu^{2+}, Cu^{+}, K^{+}, Zn^{2+}, Mn^{2+}, Fe^{2+}, Fe^{3+}, and NH_4^{+} are bound to the negatively charged core consisting of heavy metals such as aluminum (Al) and silicon (Si). These are generally arranged in a crystal lattice structure and become negatively charged when these cations (Al^{3+} and Si^{4+}) are replaced in the lattice core with a lesser charged group in a process known as isomorphous replacement. In order for the nutrient cations on the surface to enter the soil solution, a process known as cationic exhange needs to occur. In addition to those listed above, one of the main cations used in this exhange process is hydrogen ions (H^{+}) originating from the water present in the soil. Balancing the positively charged

cations in the soil solution are negative ionic groups such as hydroxyls (OH^-), carbonates (HCO_3^-, CO_3^{2-}), sulfates (SO_4^{2-}), phosphates ($H_2PO_4^-$, HPO_4^{2-}, PO_4^{3-}), borates (BO_3^{3-}, $B_4O_7^{2-}$), and molybdates (MoO_4^{2-}). Although these anions can also become bound to the soil particle, contributing to the negative surface charge, they generally remain in the soil solution due to the repulsion by the negative charges already present on the soil. Two additional anionic nutrients that do not associate with the soil particle surfaces at all and generally remain in the soil solution are chloride (Cl^-) and nitrate (NO_3^-). Other ions that can be found in the solid or aqueous phases of the soil that are not essential plant nutrients include selenium (Se), cobalt (Co), arsenite (As), and sodium (Na).

One particular nutrient that requires special attention is nitrogen nutrition. Deemed as one of the more important nutrients affecting the growth and yield of agronomic crops [Bellaloui and Pilbeam, 1991], N is a standard fertilizer applied to fields in various forms. The exact form is dependent upon plant species as some prefer NH_4^+ while others prefer NO_3^- and still others require N_2-fixing bacteria. Furthermore, various forms of nitrogen can be supplied from different sources such as urea [Barker and Corey, 1990], controlled released fertilizers containing urea [Csizinszky, 1994], nettle water (NH_4^+) [Peterson and Jensen, 1988], and NH_4NO_3 as well as other forms of salts. In tomato plants, NO_3^- is preferred over NH_4^+ although both can be assimilated [Ikeda, et al., 1992]. Nitrate-N is readily translocated in the xylem after uptake and is assimilated mainly in the leaves but does occur in the roots and shoot as well [Bellaloui and Pilbeam, 1990]. This occurs through a nitrate reductase enzyme which catalyzes the formation of nitrite from NO_3^-. This nitrite is then reduced to ammonium which is incorporated into free amino acids.

Even though nitrate is eventually converted into ammonium, the former source is still preferred since the accumulation of NH_4^+ can have toxic results in tomato cells [Barker and Corey, 1990] while nitrate-N can be regularly stored. Therefore, the ammonium-N accumulated by tomato root cells must be immediately metabolized into glutamine, followed by glutamate, aspartate, and asparagine which can be safely stored in the cells [Ikeda, et al., 1992]. The acceptors of this ammonium-N are oxaloacetate and α-ketoglutarate, two intermediates in the tricarboxylic acid cycle (TCA) which regenerates

ATP and NADH [Taiz and Zeiger, 1991]. The main substrate of the TCA cycle is pyruvate generated from stored sucrose and starch. Therefore, although NH_4^+ can be assimilated in tomato roots, this decreases the energy resources available for growth and is, thus, less favored. Furthermore, evidence has been provided that the ammonium-N taken up by the roots and subsequently assimilated, remain primarily in the root and shoot cells [Magalhaes, 1991]. This could lead to an insufficient supply to the leaves of the tomato plant if ammonium-N is the only source available. As for the differences in growth, tomato plants (cv. Ailsa Craig) supplied with NH_4^+ yielded shoot and root dry weights that were 74 and 67% lower than when supplied with NO_3^- [Qasem and Hill, 1993].

In addition to the compositional form of the nutrients, the concentration plays an important role in the rate of uptake and subsequent development of the plants as well. In general, higher nutrient concentrations increase the plant's uptake capacity [Adams and Holder, 1992; Bellaloui and Pilbeam, 1991; Coltman, 1987; De Kreij, et al., 1992]. For example, nitrate levels of 8.0 mol/m^3 in nutrient solution stimulated an increased accumulation in storage pools of tomato plants (cv. Ailsa Craig) to await assimilation by nitrate reductase [Bellaloui and Pilbeam, 1991]. Nitrate levels were measured to be 70.59 μmol per gram fresh weight (gfw) in the leaves compared to 37.67 μmol/gfw when supplied 2.0 mol/m^3. Furthermore, the leaf weights became higher under the high nitrate level when the plants were allowed to continue growing (6.318 vs. 3.970 g, respectively).

Similarly for other nutrients, increased P levels in solution from 7 to 25 μm caused a corresponding increase in uptake for various tomato strains (cv. Kewalo, Epoch, Balkan, Tidling Bush, and others) from 9 to 29 mg, respectively [Coltman, 1987]. Root fresh weights were also shown to increase but depended upon the cultivar. For potassium uptake, a higher solution concentration of 20 mM KCl resulted in greater accumulations than 0.5 mM solutions [Wrona and Epstein, 1985]. The corresponding uptake rates for the 30 minute exposure times resulted in 14 and 0.71 μmol/gfw, respectively, for *L. esculentum* Mill. cv. Walter tomato plants and 10.5 and 0.34 μmol/gfw, respectively, for a wild relative tomato strain, *L. cheesmanii* ssp. *minor* (Hook.) C.H. Mull. For calcium, concentrations of 4.0 and 11.2 mM resulted in accumulations in tomato (cv. Spectra) of

88 and 180 in young leaves, 763 and 1076 in older leaves, and 19.5 and 24.0 mmol/kg in fruits [De Kreij, et al., 1992]. In two tomato cultivars (Kewalo and Sel 7625-2), Zn uptake increased to 4.0 and 1.25 μmol/g, respectively, with increasing concentrations until saturation occurred in each strain at approximately 0.2 mM Zn [Bowen, 1987]. Similar results were obtained with Cu during these experiments which varied concentrations between 0.01 and 0.5 mM Cu resulting in saturated uptake rates of 3.45 and 1.24 μmol/g for the respective cultivars. When Mn concentrations were varied from 10 to 300 μM, accumulation increased between 2.5 and 15 times, depending upon the tissues analyzed in the tomato plant (cv. Ailsa Craig) [LeBot, et al., 1990].

Not only do direct increases in supply lead to higher uptake rates, but interactions between nutrients can cause similar effects. When P concentrations were increased from 0.4 to 4.2 mM while Ca contents were maintained, Ca uptake was shown to nearly double in young and old leaves of tomato plants (cv. Spectra). On the other hand, higher K and Mg levels suppressed Ca uptake [De Kreij, et al., 1992]. As stated previously, Mg may be competing directly with Ca for binding sites on a common ATPase responsible for maintaining the appropriate levels in the cytosol. Furthermore, K has often been shown to directly affect Ca and Mg uptake. Specifically, increasing the K concentration by 0.05 mM in solutions used to grown maize seedlings (cv. WF9 x Mo17) resulted in an 11% decrease in Ca uptake and nearly 50% drop in Mg uptake [Brauer, 1994]. This may be attributed to the acid-base characteristics of each nutrient where K and Mg are both hard acids making them more similar and their competition greater while Ca is a slightly weaker acid. Direct competitions indicate a preferential uptake of Ca over K or Mg which may be due to the existence of weak base characteristics on the nutrient binding site. Similarly, small amounts of Mn in the range of 10 to 300 μM competes with Mg and to a lesser extent, Ca, on more than a 1:1 basis even though the concentrations of Mg and Ca were substantially higher at 0.75 and 2.0 mM, respectively [LeBot, et al., 1990]. However, while the uptake of the divalent cations in tomato (cv. Ailsa Craig) decreased roughly 25% each, K uptake increased by about 20% as the Mn concentrations were raised. Other nutrient interactions that have been studied in tomato plants include enhanced Mo uptake

by decreased P levels [Heuwinkel, et al., 1992], decreased Zn uptake by higher Cu concentrations [Bowen, 1987], slower Ca and Mg uptake capacities caused by increasing NO_3^-/NH_4^+ ratios [Qasem and Hill, 1993], enhanced P uptake by greater Zn levels [Parker, et al., 1992], and increased Ca uptake by lower B levels [Yamauchi, et al., 1986]. Furthermore, non-essential nutrients such as sodium (Na) have been shown to interact with essential nutrients, particularly K [Wrona and Epstein, 1985].

As for the soil pH, this factor is closely linked to the concentration and ionic forms of various nutrients. Specifically, slightly acidic conditions (pH 5-6) tend to favor root and shoot growth and fruit yield as well as nutrient uptake [Adams, 1986]. This is due to the cations such as K^+, Mg^{2+}, Ca^{2+}, Fe^{2+}, Mn^{2+}, Zn^{2+}, and Cu^{2+} forming more soluble salts, albeit at different pH levels [Taiz and Zeiger, 1991]. This increase in solubility facilitates nutrient absorption. The change in soil pH can be controlled through a combination of effects dictated by the acidity of the water, amount of applied fertilizers or other substances such as lime, the soil constituents, and the ability of the plant to transport protons across the plasma membranes into the surrounding root environment. For example, when tomato plants (cv. Dansk) were grown in nettle water (pH 6.8) and compared to nutrient solution grown plants (pH 5.3), the uptake of nitrogen was significantly higher by 0.225 mmol/plant at the elevated pH [Peterson and Jensen, 1988]. However, the uptakes of all of the cations listed above were substantially higher at the more acidic pH level. The most pronounced increase in uptake was exhibited by Mn which increased by about 400%. Similar results were obtained for alfalfa and corn when the soil pH was maintained at 5.0, 5.9, 6.8, or 7.9 by applying lime [York, et al., 1954]. For both alfalfa and corn, each reached maximum yields at pH 5.9; however, the increases in uptake of Ca, K, Mg, and Mn at these different pH levels varied for each species as well as for each nutrient. Again, the most pronounced enhancements on uptake for both species were for Mn at pH 5.0 where solubility was the greatest [Taiz and Zeiger, 1991].

In addition to these artificial means of adjusting the pH of the rooting medium, plants have the capability to alter the pH as well by transporting protons into or out of the root cells through H^+-ATPases [Wheeler, et al., 1994]. In order to increase the uptake of

iron from the soil environment, tomato plants decrease the pH. This acidification by tomato roots is conducted in order to reduce ferric iron (Fe^{3+}) into the more readily absorbed ferrous form (Fe^{2+}). This is accomplished through the plasma membrane bound enzyme, Fe-chelate reductase [Holden, et al., 1991; Holden, et al., 1995]. Similarly, when tomatoes are experiencing P deficit conditions, the root cells respond by lowering the pH of the external rooting medium by a net proton efflux [Heuwinkel, et al., 1992]. This leads to a more favorable environment for the acid phosphatase used to breakdown organic P for absorption which has an optimum pH between 4 and 6 [Goldstein, et al., 1988a].

Another factor that greatly affects the nutrient uptake characteristics of tomato plants is the root-zone water potential [Glass, 1989]. As illustrated previously, the entire plant water status, starting with the soil moisture content, affects the water uptake and growth rates of tomato plants (see Section 2.3.4). According to Equation (2.4), Ψ_{soil} can be altered by either changing the matric potential, $P_m = -2\gamma / r$, of the soil or by altering the solute content in the soil solution. The addition of solutes decreases the osmotic component, $-\pi_{soil} = -RTC_{soil}$. Concurrent with this change in osmotic potential, the saline conditions increase as does the electrical conductivity of the nutrient solution. In the reports investigating the effects of different water potentials, researchers often utilize these alternative means of measurement.

In order to illustrate the affect of the soil water potential, Ψ_{soil}, on the nutrient uptake capacity of tomato plants, the following examples are provided. Using the first method of changing soil water potential, tomato plants (cv. Ailsa Craig) exhibited decreased nutrient uptake capacities for P, K, Ca, and S but increased rates for N when subjected to drier soil conditions [Jackson, et al., 1996]. The drier soil condition decreases the root-zone water potential by decreasing (more negative) the matric potential, $P_m = -2\gamma / r$. Using the second method of altering Ψ_{soil}, tomato plants (cv. Micro-Tom) were subjected to increased electrical conductivities by adding NaCl to the nutrient solution. This increase in NaCl content increases the solute concentration which, in turn, decreases (more negative) the osmotic potential, $-\pi_{soil} = -RTC_{soil}$. An increase from 2.4 to 18 dS/m resulted in a decreased uptake capacity for Ca and K but increased uptakes of Na, Cu, and

Zn [Knight, et al., 1992]. For the high Na versus the low K uptake, a direct antagonism between these similar ions probably accounted for the differences [Wrona and Epstein, 1985]. For calcium, the depressed uptake may be the result of the decreased water uptake since Ca may be transported passively into the roots [Higinbotham, et al., 1967]. Furthermore, Ca transport into tomato fruits (cv. Counter) has also been shown to decrease with increasing salinity from 5 to 7 mS/cm [Adams and Holder, 1992]. As for the nutrients exhibiting increased uptakes, these may be due to the interactions caused by other nutrients. Specifically, in tomato plants subjected to more saline conditions, P uptake was shown to decrease [Adams, 1986]. Furthermore, low P uptake can lead to an enhanced uptake of both Cu and Zn [Parker, et al., 1992; Barrachina, et al., 1994].

The last factor that influences the rate of water and inorganic nutrient uptake is the root-zone temperature (RZT). In general, tomatoes respond best at temperatures between approximately 25 and 30 °C. For example, when two cultivars of tomatoes (cv. Shuki and Sataan) were subjected to RZT's of 15, 20, 25, and 30 °C while the atmospheric temperature was maintained at 22 °C during the day, the uptake capacities for N, P, K, Mg, and Ca were each greater at the highest temperature and steadily declined at the lower temperature ranges [Nkansah and Ito, 1995]. As for the differences between these cultivars, in all cases, the heat tolerant cultivar (cv. Shuki) responded with higher uptake capacities than the intolerant strain (cv. Sataan). Furthermore, this pattern was repeated when the day time atmospheric temperature was raised to 40 °C except that the magnitude of the uptake quantities were larger. Similarly, when a different strain of tomato (cv. Burpee 'Big Boy Hybrid') was grown at RZT's of 10, 15.6, 21.1, 26.7, 32.2, and 37.8 °C, the uptake of each of these macro-nutrients peaked at 26.7 °C and rapidly declined at the extreme temperatures [Tindall, et al., 1990]. As for the responses of the micro-nutrients to these root-zone conditions, Zn, Mn, and Cu each peaked at the same level as the macro-nutrients (26.7 °C) while B, Fe, and Mo did not respond at all to the different conditions. Furthermore, root and shoot dry weights as well as total water uptake and overall plant heights each peaked at the 26.7 °C mark.

2.4.3 Deficiency and Toxicity Symptoms

Adequate plant inorganic nutrition is a balance between sink demands in the plant and source supplies in the soil environment. When supplies are limited compared to the demands in the tomato plants, deficiency symptoms may develop which include visual markers such as chlorosis (yellowing), dark necrotic lesions (browning), mottling, discolorations, reduced growth, premature death, poor development, and brittleness [Resh, 1978; Taiz and Zeiger, 1991; Adams, 1986]. While these symptoms are generally diagnosed on the terrestrial portions of the plants, particularly the leaves, additional physiological markers may also be used in determining the exact deficiency disorder. These include poor root development, particularly the actively growing regions at the tips, weak stems and branches, poor fruit quality, and unbalanced chemical (organic) compositions [Adams, 1986]. On the other hand, when tomato plants acquire excess inorganic nutrition compared to demands, toxicity symptoms may develop. Although this is typically less of a problem than deficiency conditions, the physiological markers for inorganic nutrient toxicities include reduced growth, excess foliage, decreased leaf size, leaf abscission, and discolorations [Taiz and Zeiger, 1991; Adams, 1986].

In order to accurately diagnose the nutritional disorder at hand, the locations of the symptoms is an important means of differentiation. This can include the age of the leaves (younger leaves higher on plant), section of leaf (margins, tips, veins, underside), and the tissues (leaves, stems, roots) analyzed. Furthermore, the length of time that the nutritional disorder persists can aid in the diagnoses as the symptoms on the plant develop. After the inorganic nutrients are assimilated into the tomato plant, they can be retranslocated depending upon whether the nutrient is classified as mobile or immobile [Resh, 1978]. The mobile nutrients, which can be redirected to the active growing sites (younger leaves) from their original location of deposition in the older leaves, are N, P, K, Mg, and Zn. As for the immobile nutrients, these are Ca, S, Fe, Mn, B, and Cu. Since the mobile nutrients can be retranslocated, deficiency symptoms will generally occur on the older leaves whereas the younger leaves are more subjected to deficiencies of the immoblie nutrients.

The symptoms of nitrogen deficiency include reduced overall growth and chlorosis of the older leaves [Adams, 1986]. This second symptom is due to a reduced amount of chlorophyll present in the leaves although in younger leaves, this condition could develop when N deficiency is prolonged. Furthermore, in tomatoes, nitrogen deficiency can lead to the petioles, stems, and lower leaf surfaces becoming purple [Resh, 1978]. Additionally, N deficiencies lead to increased nitrate reductase activity which assimilates nitrate in tomatoes [Bellaloui and Pilbeam, 1991]. Increased root/shoot weight ratios [Peterson and Jensen, 1988] and reduced fruit formation [Adams, 1986] are also nitrogen deficiency symptoms. As for the toxicity symptoms, plants usually become dark green in appearance with abundant foliage. However, the rooting systems of these plants grown under this condition can be substantially decreased in extent [Resh, 1978]. Furthermore, N toxicity, particularly when supplied in the form of ammonium, can lead to an excess release of ethylene [Barker and Corey, 1990].

During phosphorus deficient conditions, tomato plants are often stunted in growth and appear to be dark green in color. This symptom is usually first exhibited in older leaves with younger leaves being slow to mature [Resh, 1978]. Therefore, a differentiation between excess N conditions and P limitations can be made through an analysis of the overall growth of the plant. Although both conditions would result in dark green colorations, abundant foliage would indicate the former nutritional status while reduced leaf growth would indicate the latter symptom. This example illustrates the importance of a diagnosing all of the available symptoms in order to implement a proper remedy. Additional P deficiency symptoms include excess root elongation, root hair proliferation, increased extracellular phosphatase activity, proton excretion [Heuwinkel, et al., 1992], decreased root/shoot weight ratios [Garcia and Ascencio, 1992], stiff leaves which become purple underneath, form brown (necrotic) spots, and die prematurely [Adams, 1986].

Another problem that can arise when diagnosing the nutritional status of a plant is that an excess quantity of one element can lead to a deficiency in another by simply antagonizing its uptake. This problem is demonstrated in phosphorus toxicity which can

sometimes lead to copper and zinc deficiencies [Parker, et al., 1992; Barrachina, et al., 1994]. Phosphorus toxicity may be diagnosed when interveinal chlorosis symptoms appear; however, this may be the result of the Zn or Cu deficiencies. Conversely, deficiency conditions can also lead to the increased, potentially toxic, uptake of other nutrients. This is evident during Mo uptake under P deficient conditions which can be increased as much as 10 times normal uptake rates [Heuwinkel, et al., 1992]. Therefore, the attributes of P deficiencies may be a result of Mo toxicities as well.

The symptoms of tomato plants grown in a reduced K environment appear first in older leaves which initially become chlorotic at the margins and then form dark necrotic lesions at random locations [Resh, 1978]. Additional symptoms of K deficiency include restricted growth, uneven fruit ripening, and poor fruit development. As with excess P levels, toxic quantities of potassium may not lead to symptoms directly, but may result in Mg, Fe, Mn, or Zn deficiencies by antagonizing uptake [Adams, 1986]. The symptoms indicating these particular nutritional problems will be discussed later but it should be kept in mind that they could be indications of K toxicity as well.

Low calcium levels in tomato plants results in the occurrence of interveinal chlorosis mainly in the younger leaves which may develop around the margins if the deficiency persists [Adams, 1986]. Although this form of chlorosis is similar to K deficient conditions, the age of the leaf distinguishes between these disorders. Since leaves obtain their calcium directly from the transpirational stream, factors which affect water uptake such as high humidity can compound this affect. Furthermore, bud development is usually inhibited and the root tips often die during calcium deficiency [Resh, 1978]. As for the fruit, low Ca levels often give rise to a condition known as blossom-end rot which is a blackening around the stylar scar [Adams, 1986]. At the other extreme, high Ca levels can lead to the formation of calcium salt crystals in tomato fruit walls. Visually, this appears as gold specks on the fruit surfaces [De Kreij, et al., 1992].

When interveinal chlorosis starts at older leaf tips or margins and progress inwardly, this usually infers magnesium deficiency [Adams, 1986]. As the condition persists, the yellowing can spread to all other leaves. Although these symptoms can also

imply K deficiency as was stated previously, the main leaf veins remain green under low Mg whereas in low K, the veins undergo chlorosis as well. Furthermore, necrotic lesions may form between the veins prior to the chlorotic incursion caused by decreased Mg levels. For low potassium levels, the necrosis occurred after the chlorosis. For Mg toxicity, since this nutrient may compete directly with calcium for uptake, the symptoms indicative of Ca deficiency may be attributed to this Mg nutritional disorder as well.

Although sulfur deficiency conditions are not often encountered, the symptoms include yellowing of the younger leaves first [Resh, 1978] and the veins becoming red [Taiz and Zeiger, 1991]. Furthermore, the petioles tend to become twisted and/or vertically positioned. As for the symptoms implying S toxicity, reduced growth and leaf size are accompanied by interveinal chlorosis similar to Mg deficiencies [Resh, 1978]. Therefore, it is again illustrated that diagnosing all of the available symptoms is of the utmost importance in determining the correct remedy for the tomato plant disorder.

The interveinal chlorosis which appears similar to the effects of Mg deficiency, is an implication of iron deficiency as well [Adams, 1986]. However, instead of the symptoms appearing on older leaves, the effects are first shown on younger leaves. Again, both of these symptoms can be indicative of potassium deficiency. Therefore, plants which exhibit interveinal chlorosis in older leaves would imply either the K disorder or Mg deficiency while symptoms of the younger leaves would imply Fe deficiency. However, as this deficiency persists, the younger leaves become entirely yellow or nearly white while growth ceases. This is due to the veins becoming chlorotic as well [Taiz and Zeiger, 1991]. As for the toxicity symptoms for iron, although it is not evident naturally, foliar sprays have caused necrotic lesions on the leaves applied [Resh, 1978].

Implications of chlorine deficient plants include wilted leaves which become chlorotic and necrotic, and roots which are stunted in growth and have thickened tips [Resh, 1978]. In addition, leaves with a bronze coloration can imply this deficiency as can its toxicity counterpart [Taiz and Zeiger, 1991]. However, an accompanying burning or firing of leaf tips or margins would imply toxic levels of chlorine. Similarly, reduced leaf size, slow growth rate, and leaf abscission are symptoms of this chlorine nutritional status

as well. For the fruit, high Cl levels in relation to other anions in the nutrient solution can give rise to the gold speck disorder indicative of Ca toxicity [De Kreij, et al., 1992].

Another nutritional deficiency which can be lead to interveinal chlorosis occurs when there are low levels of Mn present in the plant nutrient medium [Adams, 1986]. As with iron deficient plants, these symptoms are restricted to younger leaves as well. Furthermore, Mn uptake has been shown to decrease Mg and Ca uptakes, possibly leading to deficiency levels which also result in interveinal chlorosis [LeBot, et al., 1990]. Additional symptoms which would indicate Mn deficiency would be necrotic lesions or leaf shedding occuring later as well as a disorganization of the chloroplast lamellae [Resh, 1978]. The toxic symptoms for this element include a reduction in growth, chlorosis, and an uneven distribution of chlorophyll. Furthermore, the main veins of older leaves can become brown, black, or reddish-black with interveinal chlorosis and premature death [Adams, 1986; LeBot, et al., 1990]. Finally, necrotic lesions form on the stems and petioles when Mn toxicity persists.

When boron deficiency occurs, stem and root apical meristems (actively dividing cell regions) often die reducing growth. In addition, root tips can become swollen and discolored while the internal tissues can sometimes disintegrate as well as discolor [Resh, 1978]. Furthermore, when tomato plants are experiencing this nutritional problem, the leaves can thicken, become brittle, curled, or wilted, or can develop chlorotic spots [Adams, 1986; Taiz and Zeiger, 1991]. Internally, B deficient plants have been shown to generate higher quantities of lignin and cellulose in the cell walls [Yamauchi, et al., 1986]. The toxicity symptoms associated with B nutrition are also well defined. A yellowing of the leaf tips followed by a progessive necrosis of the leaves starting at the tips or margins and proceeding toward the midribs is indicative of this problem [Resh, 1978]. Internally, excess B concentrations can lead to an decreased levels of sugars in root cells [Estaban, et al., 1985].

Another nutritional deficiency which could lead to interveinal chlorosis is a decreased amount of Zn present in the tomato plants. When this occurs, a reduction in internode length and leaf size as well as a distortion or puckering of the leaf margins can

be accompanying [Resh, 1978]. Furthermore, Zn-deficient tomatoes exhibit reddish-brown patches and white incrustations (exudates) at the leaf margins [Parker, et al., 1992], low auxin hormone content in the meristems, and thickened leaves which remain primarily green [Barrachina, et al., 1992]. The toxic symptoms of an over abundant supply of zinc are identical to the results of iron deficiency [Resh, 1978].

As was stated previously, excess P levels can interfere with the Cu uptake abilities of tomato plants [Barrachina, et al., 1994]. The deficiency symptoms which can be used to diagnose this problem include the younger leaves becoming dark green, twisted, or deformed and usually accompanied by necrotic spots. These necrotic spots usually occur in the veins [Taiz and Zeiger, 1991]. This is differentiated from zinc deficiency by the absence of interveinal chlorosis and the presence of the dark green young leaves. Therefore, if both sets of symptoms are present on a given tomato plant, then this would indicate phosphorus toxicity which can lead to the zinc and copper deficiencies. Additional symptoms of Cu deficiency include decreased lignification, brittleness, and wilting [Barrachina, et al., 1994]. When excess quantities of Cu are present in the plant environment, reduced and stunted growth followed by iron chlorosis symptoms can develop [Resh, 1978]. In addition, a reduction in branching along with a thickening and abnormal darkening of the rootlets can also occur.

Symptoms similar to nitrogen deficiency can also be indicative of molybdenum deficiency. However, marginal scorching and cupping of the leaves can also occur under this nutritional condition [Resh, 1978]. Furthermore, gradual drying of the interveinal areas leading to complete tissue desiccation accompanies Mo deficient conditions [Taiz and Zeiger, 1991]. Although molybdenum toxicity is rarely encountered, tomato leaves can become discolored turning golden yellow [Resh, 1978]. Furthermore, the deficiency symptoms attributed to low P levels may be contributed in part or wholly by Mo toxicities [Heuwinkel, et al., 1992].

CHAPTER 3 - MODELING PLANT GROWTH AND NUTRITION

This chapter reviews the models describing the processes involved in plant growth and nutrient absorption as well as the methods for which the parameter values are determined. In Section 3.1, general plant models based on the overall growth and development of higher plants are presented. These will include models defining the specific growth rate (μ_g) in terms of substrate availability or the amount of growth machinery (biomass) present. The relationships of the specific growth rate to physiological processes within the plant are also reviewed. Since the accumulation of biomass is highly dependent upon the net CO_2 assimilation and photosynthetic rates, these processes in relation to growth are specially addressed. In Section 3.2, models detailing the plant water relations in the soil-plant-atmosphere continuum are presented. Specifically, models such as the Darcy-Richards type water uptake models, the Bestman sap flow model, and the Penman-Monteith based equations for transpiration are reviewed. Finally, Section 3.3 presents the two main inorganic nutrient uptake models that have been developed. These are referred to as the Nye-Tinker type models which utilize the macroscopic view of a whole plant while the Barber-Cushman model uses the microscopic approach. Furthermore, this section opens with a description of the vaious methods used to analyze the nutrient content of plant tissues as well as in the nutrient solution.

3.1 Modeling General Plant Growth and Development

There are several means in which to measure the overall growth and development of a plant. Using the statistical approach, the responses of plants to variations in

environmental factors are modeled based on correlation. Models of this sort do not infer causes or mechanisms behind the responses but do generalize the results in order to obtain empirical behaviors. Examples of these types of models include allometric (power) relationships, exponential polynomials, statistical correlations, and probability models [Gent, 1986; Tindall, et al., 1990; Overman, et al., 1995]. On the other hand, mechanistic based plant models are derived from the biochemical processes involved leading to a direct cause and response relationship [Landa and Nokes, 1994]. However, in most cases in plant physiological studies, these exact processes are not fully understood. Therefore, a combination between the empirical and mechanistic approaches to plant modeling are often utilized [France and Thornley, 1984].

In most cases, the growth progression of higher plants is evaluated based on the dry weight gain, ΔW, over some time interval, Δt. However, other measures of growth such as fresh weight, cell volume, cell number, leaf area, crop height, and others could easily be substituted for the dry weight [France and Thornley, 1984; Taiz and Zeiger, 1991]. In this section, the growth models presented will be given in terms of the dry weight, W. However, several examples of the various models are provided in original terms. Furthermore, since the bulk of the plant biomass is derived from the products of carbon reduction cycle and photosynthesis (see Sections 2.2.1 and 2.2.2), then the models describing the affects of these two processes are emphasized.

3.1.1 General Growth Models

The measurement of growth can be conducted at the cellular, organ, tissue, or whole plant levels [France and Thornley, 1984]. The two approaches that are generally utilized are based after limitations caused by substrate availability or the amount of growth machinery (biomass) present. One of the most common and simplest methods of gauging the progress of a plant is the use of the specific growth rate, μ_g. This particular model, presented below, measures the differential rate of increase in dry matter per unit of dry matter present. Therefore, this model fits into the growth machinery category. Again, any

other measure of growth could easily be substituted for the dry weight in Equation (3.1) where W represents the weight of the plant at time, t.

$$dW/dt = \mu_g W \tag{3.1}$$

By rearranging Equation (3.1) and solving for W by integration, the exponential growth function in Equation (3.2) is obtained where W_0 represents the weight at time, t = 0.

$$W = W_0 \exp(-\mu_g t) \tag{3.2}$$

Since Equation (3.2) predicts the weight of the biomass, W, at any time, t, then this simple model, like all growth models, is deterministic and dynamic [France and Thornley, 1984]. Although tomato plants undergo different developmental stages (see Sections 1.2.1 and 1.2.2), this specific growth equation is more useful than an absolute growth rate for comparing the biomass production of plants at different stages. Furthermore, when different sets of experimental conditions are utilized on different sets of plants such as variations in radiation levels, temperature, humidity, and/or nutrition, the specific growth rate can be used to compare the resulting effects [Pickens, et al., 1986]. Using this method of measurement, μ_g for tomato plants (cv. Dombito) at the fifth leaf stage was calculated to be 0.073 (g g^{-1}) day^{-1} [Al-Harbi, 1995]. However, similar tomato plants subjected to saline conditions of two or four times control levels (2.0 mS/cm) yielded relative rates of 0.068 and 0.064 day^{-1}, respectively. For comparison, the specific growth rate for younger tomato plants was calculated to be 0.6 day^{-1} [Pickens, et al., 1986].

Several modifications have been made to this simple growth equation. One such model incorporates the production of total non-structural carbohydrates (TNC). These carbohydrates include starch and sucrose, the primary plant carbon storage compounds, as well as their intermediate components, fructose and glucose. An assumption was made that the TNC concentration was linearly related to the specific growth rate, μ_g [Gent, 1986]. This assumption has been validated through chemical analysis of leaves from four different hybrids of tomato (cv. Early Cascade, Michigan-Ohio, Sonato, and Virosa) [Gent, 1984]. Furthermore, these experiments revealed that this linear trend also applied to tomato

plants subjected to CO_2 concentrations of 1,000 ppm instead of ambient levels. This analysis has also been extended to include the effects of temperature on growth [Gent, 1986]. Equation (3.3) was developed for this relationship where K_g equals the linear coefficient for growth metabolism (0.065 $g\,g^{-1}\,TNC^{-1}\,h^{-1}$) and T is temperature (in °C).

$$\mu_g = K_g\,(TNC)\,\exp[0.0693(T - 25)] \qquad (3.3)$$

In order to quantify the change in TNC concentration, a semi-empirical equation was derived which took into account the dependency on the rates of net CO_2 exchange, photosynthesis, and the production of growth machinery. This is shown in Equation (3.4).

$$\frac{d(TNC)}{dt} = 0.68[P_n\,(LAR) - R_m - R_g\mu_g\,] - 0.92\mu_g \qquad (3.4)$$

In Equation (3.4), P_n represents the rate of photosynthesis (in g CO_2 m^{-2} h^{-1}), LAR equals Leaf Area Ratio (ratio of leaf area to plant dry weight in m^2/g), R_m defines the quantity of maintenance respiration (in g CO_2 g^{-1} h^{-1}), and R_g is the growth respiration (in g CO_2 g^{-1} structural material synthesized). Again, μ_g equals the specific growth rate (but in h^{-1}). Therefore, substituting Equations (3.3) amd (3.4) into Equation (3.2) allows for the dry weight of the tissues to be calculated based on these physiological dependencies.

During the development of Equations (3.3) and (3.4), several parameters were fitted statistically based on experimental measurements. These included the changes in the TNC levels as a function of specific growth (μ_g), respiration (R_g and R_m), and photosynthesis (P_n). In order to obtain these empirical relationships, the TNC levels were measured from tissues digested in α-amylase and measured colormetrically through reduction of $K_3Fe(CN)_6$ [Gent, 1984]. This procedure revealed the TNC levels in terms of glucose equivalents while the specific carbohydrate levels were determined using High Performance Liquid Chromotography (HPLC). In order to measure the rates of respiration and photosynthesis, the plants were placed in a sealed chamber where inlet and outlet CO_2 levels were monitored [Penning De Vries, et al., 1979]. Changes between these levels

indicated the total respiration while the amount of CO_2 respired for growth versus maintenance was distinguished based on reserve carbon and structural dry mattermeasurements as well. This is presented in Equation (3.5) below where RC equals reserve carbon (TNC) and SDM stands for structural dry matter (weight).

$$1.02 \text{ g RC} + 0.27 \text{ g amino acids} \rightarrow 1.00 \text{ g SDM} + 0.47 \text{ g } CO_2 \qquad (3.5)$$

Therefore, for every gram of SDM produced, 0.47 g CO_2 are produced representing the growth respiration. Subtracting this respiration from the total gives the maintenance respiration rate. Since photosynthesis provides the substrates for both of these respirations, then P_n was measured using the total respiration rate divided by the total leaf area. Therefore, using this procedure, each component of Equation (3.4) was determined.

Another modification that has been made to Equation (3.1) defining μ_g is the incorporation of a decay term which can account for enzyme degradation, leaf senescence, or tissue differentiation [France and Thornley, 1984]. This decay term is defined in Equation (3.6) where D represents the decay constant.

$$d\mu_g/dt = -D\mu_g \qquad (3.6)$$

By rearranging and integrating this equation is a manner similar to that used to derive Equation (3.2), an exponential equation is obtained for μ_g based on D and t and an initial condition, μ_{g0}. Combining this resulting equation (not shown) with Equation (3.1), yields the following growth model after a second integration. In Equation (3.7), all parameters are as defined earlier with μ_{g0} equaling the specific growth rate at t = 0.

$$W = W_0 \exp[\mu_{g0}(1 - e^{-Dt})/D] \qquad (3.7)$$

Equation (3.7) is known as the Gompertz equation and assumes that all required substrates are non-limiting [France and Thornley, 1984]. Therefore, this model is completely dependent upon the amount of growth machinery present. When applied to the growth of tomato (cv. Kingley Cross) leaves at the fifth leaf stage, values for μ_{g0} and D were estimated from data to be 4.44 and 0.208 day^{-1}, respectively [Thornley, et al., 1981].

Since the growth of higher plants is dependent upon several substrates such as photosynthetically active radiation (PAR), atmospheric CO_2, and inorganic nutrition, substrate dependent growth models have also been derived. The simplest of these are analogous to monomolecular chemical reactions where a constant of proportionality, k, dictates the rate of conversion of substrate, S, into biomass, W. However, since a single substrate is rarely the only limiting component for the entire growth of a plant, these types of models are generally combined with some form of growth dependent relationship. For example, the logistic growth function shown as Equation (3.8) utilizes the assumption that growth is proportional to both substrate concentration, S, and the amount of growth machinery present, W, through the constant, k' [France and Thornley, 1984].

$$dW/dt = k'WS \tag{3.8}$$

The constant, k', is related to the specific growth rate, $\mu_g = k'W_f$, where W_f determines the final weight of the plant tissue when all substrate is utilized ($S_f = 0$). Since substrate is converted into biomass, then $S = W_f - W$. Substituting these relations into Equation (3.8) and integrating leads to the logistics growth model.

$$W = \frac{W_0 W_f}{W_0 + (W_f - W_0)\exp(-\mu_g t)} \tag{3.9}$$

Plots of Equation (3.9) result in a smooth sigmoidal curve exhibiting the characteristic phases of lag, exponential, and stationary growth. Since the growth and development of plants is exemplified by this continuous sigmoid shaped curve starting from a minimum value, W_0, and reaching an asymptotic maximum, W_f, then a probability density function which incorporates a distribution of responses has also been developed [Overman, et al., 1995]. In this case, the dry weight, W, is related to the final weight, W_f, using the well known error function, erf, as shown in Equation (3.10).

$$W = \{W_f / 2\}\ \{1 + \mathrm{erf}[(t - t_m) / \sigma\sqrt{2}\,]\} \tag{3.10}$$

In Equation (3.10), t_m equals the elapsed time to mean of dry matter distribution and σ is the standard deviation of dry matter distribution. The error function used in Equation (3.10) is generally defined for any variable, x, as shown by Equation (3.11).

$$\text{erf}\, x = 2/\sqrt{\pi} \int_0^x \exp(-u^2)\, du \qquad (3.11)$$

The value of erf x attains values between -1 and +1 for x between $-\infty$ to $+\infty$. Therefore, Equation (3.10) ranges from 0 and reaches an asymptotic value of W_f at $t >> t_m$. This probability model has been used to describe the growth of several crops including corn, tobacco, and soybeans [Overman, et al., 1995].

The major problem with these growth equations is that knowledge of the final weight, W_f, would be needed beforehand [Thornley, 1990]. Furthermore, the use of the logistics growth function or probability model is restricted to identical conditions for which the value of this parameter was determined. Therefore, using Equation (3.9) or (3.10) to compare the growth of plants experiencing different environmental conditions is inadequate. However, these functions have been reformulated to allow the growth rate and final weight to change with different growth conditions. This was accomplished by introducing a second rate equation describing the change in another biologically significant quantity which affects the specific growth rate in terms of weight, μ_g. The final tissue weight, W_f, then becomes dependent upon both of these rates and can change values based on a second growth rate. An example of this is the specific growth of leaves in terms of dry weight as the primary function and the leaf area as the second rate equation [Thornley, 1990]. Similarly, the (primary) rate of dry matter accumulation may be determined from the (secondary) rate of nitrogen uptake [Overman, 1995].

There are several other growth models which have been developed to incorporate both substrate and growth machinery terms. This includes Chanter's equation [Chanter, 1976] which is a hybrid between the Gompertz (growth machinery) and logistics (substrate) growth equations. Specifically, Chanter's equation incorporates a linear term for substrate dependence multiplied by an exponential decay term. Similarly, Richard's growth function also encompasses the logistics and Gompertz equations but also includes

monomolecular reactions [France and Thornley, 1984]. This is accomplished using the parameter, n_R, in the differential equation which attains a value of 1, 0, or -1, leading to the three respective models. The Richard's growth function is shown in Equaiton (3.12).

$$\frac{dW}{dt} = \frac{kW(W_f^{nR} - W^{nR})}{n_R W_f^{nR}} \tag{3.12}$$

A third substrate and growth machinery model utilizes a dual substrate format which includes both carbon and nitrogen concentration terms multiplied by the tissue weight [Johnson and Thornley, 1987]. Furthermore, this dual substrate model also takes into consideration the partitioning of these subtrates into root and shoot (and leaves) structural matter and can be extended to include multiple substrates acquired through the roots.

3.1.2 Net CO_2 Assimilation Models

Since the assimilation of carbon dioxide comprises the major portion of the biomass of higher plants [Taiz and Zeiger, 1991], the simple growth models reviewed above can be related to the net CO_2 assimilation rate, F_n. As shown in Equation (3.13) below, F_n represents a measure of the rate of dry weight increase per unit of total leaf area, A. Furthermore, since carbon fixation operates in tandem with photosynthesis, this parameter quantifies the efficiency of light use by plants on a per unit leaf area basis. Therefore, the factors which affect this assimilation rate include the leaf and stem net photosynthesis rates, the rates of dark respiration in all plant tissues, and the rate of inorganic nutrient uptake [Pickens, et al., 1986]. By substituting in Equation (3.1) defining μ_g into Equation (3.13), the leaf area ratio (LAR) becomes a measure of the photosynthetic capacity for a plant under constant conditions.

$$F_n = \frac{1}{A_{leaf}} \frac{dW}{dt} = \mu_g / LAR \tag{3.13}$$

When plants are younger, both the specific growth and net CO_2 assimilation rates have been shown to be highest due to the self-shading, leaf senescence, and maintenance energies required as the plants age [Pickens, et al., 1986]. However, the assimilation rate tends to increase faster than the specific growth since the weight of the plant, W, includes non-leaf structures while the surface area term, A_{leaf}, does not account for the thickening of older leaves [Hurd and Thornley, 1974].

One factor that does substantially affect the net assimilation rate, F_n, and, thus, μ_g, is the atmospheric CO_2 concentration, C_{CO2}. Except at saturating levels, F_n has been measured to be directly proportional to the CO_2 concentration. However, saturation conditions do occur when light levels are low, particularly for plants utilizing the C3 carbon assimilation pathway such as tomatoes (see Section 2.2.1) [Martin and Thorstenson, 1988]. This saturation behavior has been modeled similar to Michaelis-Menten kinetics where $F_{C,max}$ is the maximum assimilation rate for saturating CO_2 levels and $K_{m,C}$ is the concentration required for half maximal assimilation. Under test conditions for CO_2 levels when light levels are maintained, the kinetic equation for the assimilation rate based on CO_2 concentration, $F_{n,C}$, can be written as follows. The kinetic constants in Equation (3.14) can be determined using Lineweaver-Burke plots of $1/F_{n,C}$ versus $1/C_{CO2}$.

$$F_{n,C} = \frac{F_{C,max}\, C_{CO2}}{K_{m,C} + C_{CO2}} \qquad (3.14)$$

Results from this type of experimentation conducted on tomato (cv. Minibelle) yielded values for the kinetic constants of 14.9 g m^{-2} day^{-1} and 1.0 g/m^3, respectively, for $F_{C,max}$ and $K_{m,C}$ for 19 day old plants. Similarly, 35 day old tomato plants yielded kinetic constants of 7.8 g m^{-2} day^{-1} and 0.35 g/m^3, respectively, when subjected to the same constant irradiance of 50 W/m^2 [calculated from data obtained from Hurd and Thornley, 1974]. In order to measure the CO_2 concentration in the air, commercial gas analyzers are available. Therefore, combining Equations (3.13) and (3.14) results in Equation (3.15) for μ_g which can be substituted into the growth equations reviewed earlier.

$$\mu_g = (LAR)\frac{F_{C,max}\, C_{CO2}}{K_{m,C} + C_{CO2}} \qquad (3.15)$$

Since carbon dioxide and oxygen compete for the same active sites on the main carbon reduction enzyme, Rubisco, inhibition kinetics have been incorporated into the net CO_2 assimilation rate, $F_{n,C/O}$ [Heath, et al., 1990; Sage, 1990]. This is shown in Equation (3.16).

$$F_{n,C/O} = \frac{P_{n,max} \exp(-\alpha_e R_i/P_{n,max})\, C_{CO2}}{C_{CO2} + [K_{m,C}/(C_{O2} + K_i)]} \qquad (3.16)$$

In Equation (3.16), $P_{n,max}$ equals the maximum photosynthetic rate (in g CO_2 m^{-2} h^{-1}), R_i is the light intensity (in W m^{-2}), α_e is the quantum yield or light use efficiency (in g CO_2 J^{-1}), C_{O2} represents the concentration of oxygen, and K_i equals the competitive inhibition constant for O_2. All other parameters are as defined earlier. This model was used to predict the leaf growth of bean plants (cv. Pinto) cultivated under controlled environment conditions. This resulted in an assimilation rate, $F_{n,C/O}$, of 122.3 $\mu g/m^2 s$ using a kinetic constant, $K_{m,C}$, of 123 mg/m^3 and an inhibition constant, K_i, of 8.0%. In order to measure the amount of photosynthetically active radiation, R_i, commercial light meters (also known as solarimeters, quantum sensors, and spectroradiometers) are available which can measure the levels at specific frequencies. Furthermore, since the electron transport chain supplies substrates for this carbon fixation process, models which consider these possible rate limiting steps have also been developed [Sage, 1990].

There have also been comprehensive models which incorporate the complete partitioning of substrate carbon from source (atmosphere) into their ultimate fates (structural) or functions (pools) [Thornley, 1991]. The structural components include the carbon utilized in the machinery which assimilates carbon (W_M) such as the compounds involved in the PCR and PCA cycles (see Section 2.2.1), carbon based machinery involved in the photosynthetic process (W_α and W_{Pmax}) such as those required in the "Z-scheme" (see Section 2.2.2), primary (W_p) and secondary (W_s) cell wall material, and cross-linked primary cell wall material (W_x). For the carbon pool, this includes the substrate carbon

(W_C) transported in the phloem (i.e. TNC). Therefore, the dynamic growth equation incorporates the sum of each time dependent component as shown in Equation (3.17).

$$dW_M/dt + dW_\alpha/dt + dW_{Pmax}/dt + dW_p/dt + dW_s/dt + dW_x/dt + dW_C/dt = \mu_g' W_{tot} \quad (3.17)$$

The set of equations defining each differential component of Equation (3.17) has been solved for the leaves of wheat plants (cv. Marquis) [Thornley, 1991]. A similar adaptation of this partitioning approach to modeling has also been successfully applied to ryegrass (cv. S321) roots [Brugge and Thornley, 1985]. Furthermore, this analysis can be extended to water consumption, nitrogen partitioning, and other inorganic nutrients.

3.1.3 Photosynthesis Models

As with the contribution of the net CO_2 assimilation, the production of plant biomass is also dependent upon the photosynthetic capabilities. This is illustrated in Equations (3.4) and (3.16) which contain terms for the rate of photosynthesis, P_n or $P_{n,max}$, respectively. Furthermore, the behavior of the net assimilation rate to irradiation levels, R_i, is similar to the saturation kinetics for CO_2. Therefore, analogous to Equation (3.14), the photosynthetic contribution to carbon assimilation, $F_{n,R}$, can be derived as Equation (3.18).

$$F_{n,R} = \frac{F_{R,max}\, R_i}{K_{m,R} + R_i} \quad (3.18)$$

In Equation (3.18), $F_{R,max}$ represents the maximum CO_2 assimilation rate at saturating photosynthetically active radiation (PAR) levels and $K_{m,R}$ represents the radiation level required for half maximal assimilation. Again, these kinetic constants can be determined using Lineweaver-Burke plots of $1/F_{n,R}$ versus $1/R_i$. Results from this type of experimentation conducted on tomato (cv. Minibelle) yielded values for the kinetic constants of $F_{R,max} = 25.0$ g m^{-2} day^{-1} and $K_{m,R} = 139.5$ W/m^2 for 19 day old plants. When conducted under similar conditions of a constant CO_2 concentration of 0.73 g/m^3 on 35 day old plants, $F_{R,max}$ and $K_{m,R}$ attained values of 10.3 g m^{-2} day^{-1} and 51.6 W/m^2,

respectively [calculated from data obtained from Hurd and Thornley, 1974]. Therefore, combining Equations (3.13) and (3.18) results in Equation (3.19) for μ_g which can be substituted into the various growth equations reviewed earlier.

$$\mu_g = (LAR)\frac{F_{R,max}\, R_i}{K_{m,R} + R_i} \tag{3.19}$$

A frequently used relationship between photosynthesis rate, P_n, and irradiation level or intensity, R_i, was initially developed by Acock and is presented below. In Equation (3.20), α_e represents the efficiency while $P_{n,max}$ is equivalent to P_n at saturating PAR levels [France and Thornley, 1984; Thornley, 1991].

$$P_n = \frac{\alpha_e R_i\, P_{n,max}}{\alpha_e R_i + P_{n,max}} \tag{3.20}$$

Since the maximum photosynthetic rate, $P_{n,max}$, is dependent upon temperature, photosynthetic carbon machinery present [Thornley, 1991], and CO_2 levels [France and Thornley, 1984], equations for these relationships have been derived. Specifically, in Equation (3.21), the temperature dependency is based on the enzymatic response to temperature, $f_{T,enz}$, which is modeled empirically using the following quadratic relation. The coefficients, a_i, are defined so that $f_{T,enz} = 1$ at $T = 20$ °C, $f_{T,enz} = 0$ at $T = T_0$ °C, and $f_{T,enz}$ is maximum at $T = T_m$.

$$f_{T,enz} = a_0 + a_1 T + a_2 T^2 \tag{3.21}$$

Equation (3.21) is related to $P_{n,max}$ using Equation (3.22) where $P_{n,max}(20)$ equals the rate of photosynthesis at 20 °C.

$$P_{n,max}(T) = f_{T,enz}\, P_{n,max}(20) \tag{3.22}$$

Typical values for the maximum P_n at 20 °C has been estimated for C_3 plant leaves to be 1.0×10^{-6} kg CO_2 m^{-2} s^{-1} [Acock, et al., 1976]. Therefore, this temperature dependency

term can be combined with the dependency on light saturated photosynthetic machinery using Michaelis-Menten style kinetics [Thornley, 1991], as shown in Equation (3.23).

$$P_{n,max} = P_{n,max}(T) \frac{W_{Pmax}/A_{leaf}}{W_{Pmax}/A_{leaf} + K_{m,Pmax}} \quad (3.23)$$

In Equation (3.23), W_{Pmax} equals the quantity of light saturated photosynthetic carbon machinery, A_{leaf} is leaf area, and $K_{m,Pmax}$ represents the level of carbon machinery per unit area required for 1/2 maximum photosynthesis at a specific temperature, $P_{n,max}(T)$. A typical value of this kinetic constant was estimated to be 3×10^{-4} kg Pmax-carbon m^{-2}.

In order to compensate for the effects of CO_2, a conductance term, τ_c, has often been utilized as shown in Equation (3.24) [France and Thornley, 1984].

$$P_{n,max} = \tau_c C_{CO2} \quad (3.24)$$

This conductance term is a measure of the rate at which CO_2 enters the leaf to be assimilated and is dependent upon the leaf level or maturity and air vapor pressure deficit (VPD) [Romero-Aranda and Longuenesse, 1995]. Both of these dependencies have been modeled as empirical exponential functions based on the maximum conductance, $\tau_{c,max}$, obtained for young leaves. For tomato (cv. Rondello), this value was calculated to be approximately 0.12 mol m^{-2} s^{-1}. Therefore, Equation (3.24) or Equations (3.21) to (3.23) can be substituted into Equation (3.20) in order to determine the photosynthetic rate based on controllable quantities such as radiation levels, CO_2 concentration, and temperature.

Another relationship for the dependency of $P_{n,max}$ on CO_2 takes into account the initial photosynthetic conversion into substrate carbon as utilized in Equation (3.17) [Thornley, 1991]. In this case, the efficiency of light use, α_e, becomes dependent upon the availability of this α-carbon which is subject to photorespiration (see Section 2.2.1). This relationship has been modeled, in Equation (3.25), using Michaelis-Menten kinetics where α_{max} represents the maximum efficiency, $K_{m,\alpha}$ equals the concentration of α-carbon required for 1/2 α_{max}, and C_α equals the amount of substrate available per unit area.

$$\alpha_e = \frac{\alpha_{max} C_\alpha}{C_\alpha + K_{m,\alpha}} \tag{3.25}$$

A typical value for α_{max} and $K_{m,\alpha}$ for C_3 plants has been calculated to be 1.6 x10^{-8} kg CO_2 J^{-1} and 10.0 x10^{-6} kg α-carbon m^{-2} [Acock, et al., 1976]. Therefore, Equation (3.25) can also be incorporated into Equation (3.20) during the determination of the photosynthesis rate, P_n. Since some of the α-carbon may be used in photorespiration, then the efficiency can also include this phenomenon [Nederhoff and Vegter, 1994a]. This is shown in Equation (3.26).

$$\alpha_e = \alpha_{max} (1 - P_{r,max} / P_{n,max}) \tag{3.26}$$

In Equation (3.26), all parameters are as previous defined plus $P_{r,max}$ represents the maximum photorespiration rate (in g O_2 m^{-2} h^{-1}). In tomato plants (cv. Blizzard), a typical value for $P_{r,max}$ was determined to be 111 μg m^{-2} s^{-1} [Nederhoff and Vegter, 1994b].

Other factors affecting the efficiency of light use include the individual leaf light use efficiency, α_{le}, the leaf area index, LAI, which represents the ratio of leaf to ground area, and the characteristics of the leaves to transmit, reflect, and absorb light. These characteristics are dependent upon the leaf morphology, structure, angle with respect to the light source, degree of shading from other leaves on the same plant (self-shading), and the degree of shading from surrounding plants [France and Thornley, 1984]. In order to quantify these spectral qualities, two coefficients are often used. The first if the light extinction coefficient, K, which represents the fraction of light that is intercepted by the leaves versus the amount passing through the canopy and intercepting the ground. As for the second, the leaf transmission coefficient, m, represents the fraction of incident light reflecting off of the leaves to be intercepted by others. Therefore, the relationship between total and individual leaf light use efficiency can be written as Equation (3.27) and is known as a modified Monsi-Saeki equation [Nederhoff and Vegter, 1994a].

$$\alpha_e = \alpha_{le} \{1 - \exp[-K(LAI)] / (1 - m)\} \tag{3.27}$$

Individual tomato leaves (cv. Blizzard) have an estimated light use efficiency of 21.1 $\mu g\ J^{-1}$ [Nederhoff anf Vegter, 1994b]. The values for K range from the theoretical value of 1.0 for randomly spaced, opaque, horizontally oriented leaves to practical values of 0.9 for planophiles and 0.3 for erectophiles to approximately zero for emerging leaves [Goudriaan and Monteith, 1990]. These values are generally obtained empirically from experimental data [France and Thornley, 1984]. For tomato leaves (cv. Blizzard), the light extinction coefficient has been estimated at 0.94 [Nederhoff and Vegter, 1994b]. Furthermore, the typical amount of incident light that is reflected by tomato leaves averages about 10% (m = 0.10). Therefore, the efficiency, α_e, determined from any one of Equations (3.25) to (3.27) can be substituted into Equation (3.20) when quantifying the net photosynthesis, P_n.

3.2 Modeling Plant Water Relations

Plant water relations include the uptake and transport of water throughout the soil-plant-atmosphere continuum. In this section, the water taken up by the plant will be followed from the soil into the roots, through the vascular (xylem) tissues within the plant traversing upwards to the leaves, and then out of the plant through transpiration. Therefore, the models describing the water relations in plants can be divided into water uptake models, sap flow models, and transpiration models.

3.2.1 Water Uptake Models

In general, most of the water uptake models deal with the macroscopic level of the root system. This is due to the complex nature and impracticality of determining the transport to each individual rootlet in an entire rooting system. This is further complicated by the fact that the roots can be either active or inactive in terms of uptake depending on the growth stage of the plant [Molz, 1981a]. In addition, the properties of the roots as well as the soil change based on the rate of flow of the transpirational stream occurring through the soil-plant-atmosphere continuum. These include the hydraulic conductivities,

solute concentration gradients, differences between solutes (i.e. inorganic ions versus organic components) and water content [Johnson, et al., 1991; Passioura, 1984]. However, there are several microscopic models which have been developed as well which do take these consideration into account. These microscopic model are becoming more prevalent as the understanding into the soil-plant water relationship increases.

The macroscopic models describing water uptake by plant roots take into account the overall water potential gradients between the soil and the plant root. Using the analogy to an electrical circuit, Ohm's law states that the rate of flow is proportional to the driving force taking into account the resistances along the pathway. This is illustrated in Equation (3.28) where Q_w represents the flow rate (in cm^3/s), $\Delta\Psi$ equals the driving force (water potential gradient, in MPa), and $R_{1,2}$ determines the resistances in the flow pathway between points 1 and 2 [Passioura, 1984].

$$Q_w = \Delta\Psi / R_{1,2} = (\Psi_1 - \Psi_2) / R_{1,2} \qquad (3.28)$$

For water transport from the soil into the root, $\Psi_1 = \Psi_{soil}$ and $\Psi_2 = \Psi_{root}$, respectively, while $R_{1,2} = R_{s,r}$ represents the resistances between the soil and root interior. Although Equation (3.28) is a linear relationship between Q_w and $\Delta\Psi$, the linearity is lost when factors such as solute and temperature gradients as well as the dependency of the soil hydraulic conductivity, K_s, on the water content, C_{water}, are taken into account [Passioura, 1984]. Furthermore, Ψ_{soil} depends on the specific location in the soil with respect to the root surface. Therefore, spacial factors such as soil depth must be taken into account.

For the non-linearities of Equation (3.28) induced by the presence of solutes, Equation (2.2), defining the water potential, Ψ, in terms of the hydrostatic, P, and osmotic components, π, has been combined with a solute reflection coefficient, σ_r [Passioura, 1984]. This coefficient takes into account the permeability of the root membrane to a specific solute. For the temperature dependence, the resistance to flow is often defined as the inverse of the hydraulic conductivity of the membrane, L_p (in $m\ s^{-1}\ MPa^{-1}$), multiplied by the interfacial membrane area, A_m. This conductivity is dependent upon temperature, T,

based on membrane fluidity [Tindall, et al., 1990; Nkansah and Ito, 1995]. Therefore, Equation (3.28) can be rewritten as Equation (3.29).

$$Q_w = A_m L_p(T) [\Delta P - \sigma_r \Delta\pi] \tag{3.29}$$

The techniques used to measure the individual components of Equation (3.29) were reviewed earlier (see Section 2.3.4).

A more empirically based modeling approach to describe the transport of water (and solutes) from the soil into the root also utilizes the resistances, $R_{1,2} = R_{s,r}$, between these two flow points. This has been done using the density of the roots, ρ_r (kg m^{-3} soil), defined as the root structural dry mass, W_r, divided by the root depth, d_r. Furthermore, the soil hydraulic conductivity, K_s (in m^2 s^{-1} MPa^{-1}), quantifies the permeability of the particular soil type to water movement. This is shown in Equation (3.30).

$$R_{s,r} = \frac{k_{s,rs}\,\rho_r}{K_s\,W_r} + \frac{k_{rs,r}}{W_r} \tag{3.30}$$

In Equation (3.30), the constants, $k_{s,rs}$ (in m^2), which represents the flow from the soil to the root surface and $k_{rs,r}$ (in m^2/s), which represents the flow through the root membrane into the root are determined empirically [Johnson, et al., 1991]. As for the soil conductivity, large particle soils such as sand have large values while finer media have smaller values. Furthermore, K_s changes as the water content changes, decreasing from saturated values to the field capacity (see Section 2.3.4), down to the permanent wilting point which occurs when Ψ_{soil} falls below the root water potential [Taiz and Zeiger, 1991].

Since the rate of transport of water is dependent on the soil water potential, many models have been developed describing this parameter in relation to various factors. One of the most widely developed relationships between the soil water potential and water content is the Darcy-Richards equation shown as Equation (3.31) [Molz, 1981a].

$$\delta C_{water} / \delta t = \nabla \cdot (K_s \nabla \Psi_{soil}) \tag{3.31}$$

In Equation (3.31), C_{water} represents the volumetric soil water content, t is time, and ∇ is the gradient operator. All other variables are as defined earlier. In order to obtain a single differential equation in terms of C_{water}, several empirical relationships for K_s and Ψ_{soil} have been developed [Johnson, et al., 1991] such as Equations (3.32) and (3.33), respectively.

$$\Psi_{soil} = \Psi_{soil,max} \frac{1}{(C_{water} / C_{water,max})^{\beta}} \tag{3.32}$$

$$K_s = K_{s,max} (C_{water} / C_{water,max})^{2\beta+3} \tag{3.33}$$

In Equation (3.32) and (3.33), $\Psi_{soil,max}$ and $K_{s,max}$ represent the respective parameters at saturating conditions when C_{water} equals $C_{water,max}$, and β is the empirical constant.

Another approach to modeling the water transport rate caused by the gradient in water potentials was to incorporate a water extraction term, S, with the Darcy-Richards equation. Many researchers producing relationships for S were successful in describing experimental data; however, these were generally approached in a completely empirical manner where S was calibrated from data [Molz, 1981a]. The factors for which S has been correlated include the transpiration rate, root length, root depth in the soil, soil water content, soil water diffusivity [Molz and Remsen, 1970], plant wilting point, soil pressure head [Feddes, et al., 1978], and soil hydraulic conductivity [Selim and Iskandar, 1978].

Other more mechanistic water extraction terms have also been derived based on soil and root properties [Herkelrath, et al., 1977; Molz, 1981b]. An example of this is shown below indicating (only) a dependency upon individual root depth, z, and time, t. The microscopic model shown in Equation (3.34) was derived without calibration.

$$S(z,t) = \frac{E_t(t) \cdot C_{water}(z,t) \cdot L_r(z,t) \cdot [P_{soil}(z,t) - \Psi_{xylem}(t)]}{\int_0^{d(t)} C_{water}(z,t) \cdot L_r(z,t) \cdot [P_{soil}(z,t) - \Psi_{xylem}(t)]dz} \tag{3.34}$$

In Equation (3.34), $E_t(t)$ equals the transpiration rate per unit soil surface area, $C(z,t)$ equals the volumetric soil water content, $L_r(z,t)$ equals the length of roots per unit soil volume, $d(t)$ equals the root zone depth, $P_{soil}(z,t)$ equals the soil pressure potential, and

$\Psi_{xylem}(t)$ equals the xylem root water potential. This one-dimensional model is also known as the root-zone water quality model (RZWQM) [Landa and Nokes, 1994]. There are also two- and three-dimensional problems (including x and y directions) which have been solved using finite element analysis [Lafolie, et al., 1991]. With the soil-root water relationship defined mathematically in both space and time, computer generated maps of the soil water content at any time can be generated [Bruckler, et al., 1991]. The spatial distribution of the roots was determined by mapping the soil-root contact points using a trench dug into the soil. These contact points generated the finite element grids.

With the advent of more accurate methods of measuring the spatial variations in the soil water potential, these microscopic models are becoming more popular for the study of soil-plant communications during the transpirational process. These methods include gamma densitometry, neutron moderation, time-domain reflectometry [Wraith and Baker, 1991], and the microtensiometer [Vetterlein, et al., 1993].

3.2.2 Sap Flow Models

The transport of water and inorganic nutrients throughout the plant is conducted in the vascular tissue known as the xylem. This connective tissue begins in the root system, travels through the main stem and into the branches, and concludes at the leaves where transpiration occurs. There are several models which have been derived for the various portions throughout this continuous pathway. For the transport of water from the surface of the roots into the root xylem itself, the general resistance model presented in Equation (3.28) has often been applied. In this situation, $Q_{w,\,rs\text{-}rx}$ equals the water transport rate, Ψ_{rs} and Ψ_{rx} are the root surface and root xylem water potentials, respectively, and R_{root} represents the resistance of the root cells to water flow. This is shown in Equation (3.35).

$$Q_{w,\,rs\text{-}rx} = (\Psi_{rs} - \Psi_{rx}) / R_{root} \tag{3.35}$$

These resistances include the various plant membranes which must be crossed as well as the electrochemical gradients between the cellular compartments and adjacent cells

[Cortes, 1992]. These include the cylindrical layers of cells from epidermis, cortex, endodermis, stelar parenchyma, and xylem (see Figure 2.1). Furthermore, these resistances vary with the rate of transpiration [Molz, 1981a].

The application of this type of resistance flow equation (Equation 3.28) is not restricted to the root surface and the xylem. This general equation has also been applied to the flow of water from the roots into the shoots and from the shoots into the leaves [Johnson, et al., 1991]. Again, the resistances are derived empirically using the dry weights of the shoot structural matter. Furthermore, this type of equation can be applied throughout the entire plant from the roots (point 1) to the leaves (point 2) taking into account all of the resistance in series [Landa and Nokes, 1994].

Since the xylem is a continuous conduit for which water flows, models have been derived which assume that the xylem consists of cylindrical tubes of known radius with perforated valves located intermittently along its length. These valves have been further approximated as the flow through porous media [Bestman, 1992a]. Using these assumptions, the governing equations of continuity, momentum, energy, and mass concentration have been developed based on the aspect ratio, R_{stem}, which is the ratio of stem radius to length. These equations have been solved for various (boundary and initial) conditions. These include the simplified case of fully developed flow within the plant stems [Bestman, 1992a], non-fully developed flow which exists in plants due to relatively large aspect ratios [Bestman, 1992b], and when the plant is experiencing dehydration leading to a change in the flow diameter [Bestman, 1992c]. This set of equations is shown below as Equations (3.36) to (3.40) in dimensionless form with the assumption of axisymmetry.

$$\frac{1}{r}\frac{\delta}{\delta r}(r r^*) + R_{stem}\frac{\delta z^*}{\delta z} = 0 \tag{3.36}$$

$$\frac{\delta r^*}{\delta t} = -\frac{\delta P^*}{\delta r} + \left(\frac{\delta^2}{\delta r^2} + \frac{1}{r}\frac{\delta}{\delta r} - \frac{1}{r^2} - \chi^2\right) r^* + R_{stem}{}^2\frac{\delta^2 r^*}{\delta z^2} \tag{3.37}$$

$$\frac{\delta z^*}{\delta t} = -R_{stem}\frac{\delta P^*}{\delta z} + \left(\frac{\delta^2}{\delta r^2} + \frac{1}{r}\frac{\delta}{\delta r} - \chi^2\right) z^* + R_{stem}^2\frac{\delta^2 z^*}{\delta z^2} + G_r T^* + G_c C^* \qquad (3.38)$$

$$N_{Pr}\frac{\delta T^*}{\delta t} = \left(\frac{\delta^2}{\delta r^2} + \frac{1}{r}\frac{\delta}{\delta r}\right) T^* + R_{stem}^2\frac{\delta^2 T^*}{\delta z^2} \qquad (3.39)$$

$$N_{Sc}\frac{\delta C^*}{\delta t} = \left(\frac{\delta^2}{\delta r^2} + \frac{1}{r}\frac{\delta}{\delta r}\right) C^* + R_{stem}^2\frac{\delta^2 C^*}{\delta z^2} \qquad (3.40)$$

In this set of equations, r* and z* represent the velocity components of the fluid in the r and z directions (polar coordinate system), respectively, while P*, T*, and C* equal the dimensionless pressure, temperature, and concentration. The parameter χ is the dimensionless permeability calculated as the ratio of the stem radius to the square root of the permeability coefficient while G_r and G_c represent the free convection parameters caused by the volumetric expansion due to temperature and concentration, respectively. The two additional dimensionless parameters included in this equation set are the standard Prandtl (N_{Pr}) and Schmidt (N_{Sc}) numbers.

3.2.3 Transpiration Models

Typical models predicting transpiration are based upon correlations with climatic conditions such as solar radiation (excluding infra-red radiation), R_i, and air vapor pressure deficit from saturation, $e_{sa} - e_a$ [Jolliet, 1994]. This is shown in Equation (3.41) where E_t equals the transpiration rate (in mg m^{-2} s^{-1}) and b_1 and b_2 are constants.

$$E_t = b_1 R_i + b_2(e_{sa} - e_a) \qquad (3.41)$$

The limitations of these correlation models are that they are specific for particular crop species, growth stages, and climatic conditions [Jolliet, 1994]. In order to generalize these models, b_1 and b_2, have been calculated as functions of the leaf area index, LAI, which is the ratio of the leaf area to ground area. The Stanghellini model shown below is based

after this generalization and has been used to accurately predict the transpiration from tomatoes (cv. Counter) [Stanghellini, 1987]. In Equation (3.42), λ equals the latent heat of water vaporization (in MJ/kg) and the psychrometric constant (in MPa/K), γ_p, is defined as the ratio of the specific heat capacity of air (in J kg^{-1} K^{-1}), C_p, times the total air pressure, P_{air}, over λ times the ratio of the molecular weights of water vapor and air, η (= 0.622) [France and Thornley, 1984].

$$E_t = \frac{a}{\lambda} R_i + \frac{h_t}{\lambda \gamma_p}(e_{sa} - e_a) \qquad \text{where } a = c_1 \ln [1 + c_2 (LAI)^{c_3}] \tag{3.42}$$

$$h_t = c_4 (LAI)[1 - c_5 \exp(-R_i / c_6)]$$

In Equation (3.42), c_1 to c_6 are constants that were determined through non-linear regression analysis on 168 transpirations determined from different climatic conditions (i.e. different R_i, LAI, and $e_{sa} - e_a$) [Jolliet, 1994]. Although this model is more generalized than Equation (3.41), the constants, c_1 to c_6, were still determined empirically.

Another generalization that has been widely used is the Penman-Montieth equation which replaces R_i with the net radiative exchange including infra-red radiation, R_n, and ($e_{sa} - e_a$) is replaced with the corresponding difference in the water density, ($\rho_{wsa} - \rho_{wa}$). The constants, d_1 and d_2, in Equation (3.43) are calculated as functions of LAI, canopy conductance, g_c, and air boundary layer conductance, g_a [Jolliet, 1994].

$$E_t = d_1 R_n + d_2 (\rho_{wsa} - \rho_{wa}) \tag{3.43}$$

An example of these functional relationships is presented in Equation (3.44) where T_a equals air temperature and all other variables are as defined earlier [Johnson, et al., 1991].

$$E_t = \frac{(d\rho_{wsa}/dT)}{\lambda[(d\rho_{wsa}/dT) + \gamma_p(1 + g_a/g_c)]} R_n + \frac{\gamma_p \, g_a}{[(d\rho_{wsa}/dT) + \gamma_p(1 + g_a/g_c)]}[\rho_{wsa}(T_a) - \rho_{wa}] \tag{3.44}$$

The main differences between transpiration models utilizing this type of equation are due to the methods in which R_n, g_c, and g_a are calculated [Jolliet, 1994].

Another semi-empirical model that has been developed also utilzes the general resistance flow equation presented earlier (see Equation 3.28). Instead of explicitly using the water potential gradient, the driving force of this model is written as the vapor pressure deficit between the saturated canopy and the surrounding air, $e_{sc} - e_a$ [Sammis and Jernigan, 1992]. In each of these transpiration models, the vapor pressure deficits can be converted into relative humidities and used in Equation (2.7) to calculate the air water potential. Furthermore, the transpiration rate, E_t' (in J m^{-2} s^{-1}), measures the rate of energy loss instead of mass and is based on the energy balance between the plant and the environment [Campbell, 1977] as illustrated in Equation (3.45).

$$E_t' = \rho_a C_p (e_{sc} - e_a) / \gamma_p (r_{ap} + r_{cp}) \tag{3.45}$$

In Equation (3.45) ρ_a equals the density of air, C_p represents the heat capacity, γ_p is the psychrometric constant, and r_{ap} and r_{cp} represent the air and canopy resistances, respectively. In order to convert these calculated energy fluxes due to transpiration into the mass rate of water loss (in kg m^{-2} s^{-1}), Equation (3.45) is divided by $C_p (T_c - T_a)$. This temperature gradient between the canopy and the surrounding air is determined from Equation (3.46) where all parameters are as defined earlier.

$$T_c - T_a = \frac{r_{ap} R_n}{\rho C_p} \frac{\gamma_p (1 + r_{cp} / r_{ap})}{\Delta_{air} + \gamma_p (1 + r_{cp} / r_{ap})} - \frac{e_{sc} - e_a}{\Delta_{air} + \gamma_p (1 + r_{cp} / r_{ap})} \tag{3.46}$$

The parameter, Δ_{air}, in this equation represents the average slope of the relation between the water saturation vapor pressure and air temperature [Sammis and Jernigan, 1992].

The resistances of the previous two equations are the reciprocal of the conductances of Equation (3.44) where $g_c = 1/r_{cp}$ and $g_a = 1/r_{ap}$. Determined empirically, r_{cp} and r_{ap} are calculated from the linear regression constants, c_0 and d_0, obtained from a plot of the difference between the canopy and air temperatures, $T_c - T_a$, versus the vapor pressure deficit [Sammis and Jernigan, 1992]. These resistances are shown in Equations (3.47) and (3.48).

$$r_{ap} = \frac{\rho_a C_p c_0}{R_n d_0 (\Delta_{air} + 1/d_0)} \tag{3.47}$$

$$r_{cp} = -r_{ap} \left[\frac{\Delta_{air} + 1/d_0}{\gamma_p} - 1\right] \tag{3.48}$$

An alternative means of determining the air boundary layer conductance, g_a (or $1/r_{ap}$) is to consider the differences caused by wind speed, canopy structure, and reference height above the canopy. This is calculated using Equation (3.49) [Johnson, et al., 1991].

$$g_a(h_c) = \frac{\kappa^2 u_a}{\ln[(z_c + \zeta - d_c)/\zeta] \ln[(z_c + \zeta_m - d_c)/\zeta_m]} \tag{3.49}$$

In Equation (3.49), u_a equals the wind speed, κ is von Karman's constant (= 0.4), z_c is the reference height above the canopy, and d_c is the depth below the canopy level, h_c, for which the air current does not penetrate ($d_c = 0.77h_c$). The roughness parameters for vapor and heat exchange, ζ, and for turbulent momentum transport, ζ_m, are determined as a portions of the canopy height as well. Respectively, these are $0.026h_c$ and $0.13h_c$. Therefore, Equation (3.49) depends upon wind speed, reference height and canopy height.

3.3 Modeling Plant Nutrient Uptake

Included with the flow of water in the transpirational stream, inorganic nutrients are carried in as well as charged ions. In order to model these nutrient uptake kinetics, several types of experiments and measurement techniques are often utilized. This includes using various concentrations of nutrients and following the depletion rate with time in order to obtain Michaelis-Menten type kinetics [Barber and Cushman, 1981]. Another is the split root experiments where a single rooting system is divided into two distinctly different nutrient solutions for a relative short amount of time after which a chemical analysis is performed to determine the differential uptake rates by the two portions

[Johnson, et al., 1991]. Similarly, radioactive tracers such as ^{86}Rb for K, ^{15}N, ^{32}P, ^{45}Ca, ^{65}Zn, and ^{99}Mo have been used extensively by several researchers to measure the short term uptake rates, diffusion rates in soil, and the localizations of the nutrients in the tissues [Warncke and Barber, 1972; Wrona and Epstein., 1985; Petersen and Jensen, 1988; Tremblay, et al., 1988; Bowen, 1987; Heuwinkel, et al., 1992]. These short-term methods are useful for determining the uptake kinetics of plants at specific growth stages. However, the nutrient demands of a plant change with the stage of development.

3.3.1 Measuring Nutrient Quantities

In order to measure the changes in nutrient concentrations within the solutions as well as in the plant tissues themselves, several methods are available. This includes established chemical techniques such as the micro-Kjeldahl method for the analysis of nitrogen containing compounds [Nelson and Sommers, 1973], the turbidimetric determination of sulfate as $BaSO_4$ [Blanchar, et al., 1965], and ion chromatography methods for S and Cl determination [Busman, et al., 1983; Hafez, et al., 1991]. In fact, prior to the more sophisticated spectrophotometric techniques now widely being used, chemical analysis for all essential plant inorganic nutrients have been developed [Bould, et al., 1960]. The techniques which have become dominant include atomic absorption, flame photometer, mass spectrometry, nuclear magnetic resonance imagery, and inductively coupled plasma atomic emissions spectrometry (ICP-AES) [Baker, et al., 1963; O'Neill and Webb, 1970; Boss and Fredeen, 1989; Pritchard and Lee, 1984].

Of these various techniques, the ICP-AES system offers several distinct advantages. Using this system, many of the essential inorganic plant nutrients (see Section 2.4) can be quantified simultaneously from a single sample. Of the 13 macro- and micro-nutrients listed in Table 2.1, eleven can be directly analyzed including P, K, Ca, Mg, S, Fe, Mn, Cu, Mo, B, and Zn [Boss and Fredeen, 1989]. Furthermore, the resolutions of many of the nutrients are down to the parts per billion (ppb) range while most are in the parts per million (ppm) range. Other advantages include automated analysis and single-pass

multi-element capability. The disadvantages of the ICP-AES system include the high maintenance of sample purity, extensive solid sample preparations (i.e. acid digestion, purification), possible spectral interferences between analyzed nutrients, and expensive capital investment. Furthermore, the ICP-AES method is not capable of analyzing for all of the essential plant nutrients such as N, S, and Cl. Therefore, complementary methods are required for total inorganic nutrient determination.

For the plant tissues, these can generally be chemically analyzed using the same techniques and equipment as solution samples; however, they generally have to be acid digested prior to analysis [Nelson and Sommer, 1973; Blanchar, et al., 1965]. In order to facilitate the acid digestion process, the tissues are usually dried and then ground to pass through, typically, a 40-mesh stainless steel screen. Usually, all of the plant material can be digested unless appreciable quantities of aluminum are present.

3.3.2 Inorganic Nutrient Uptake Model

The simplest nutrient uptake models relate the flux of nutrient, J, to the concentration gradient, ΔC, using some sort of proportionality factor, a_J, such as root permeability or conductivity [Nye and Tinker, 1969; Akeson and Munns, 1990]. This is shown in Equation (3.50). This type of model is analogous to a driving force divided by resistance (or multiplied by conductance) [Wheeler, et al., 1994].

$$J = a_J \Delta C \tag{3.50}$$

Equation (3.50) fails to take into account the variations in the proportionality factor caused by changes in plant age, growth rates, water status, and concentrations [Wheeler, et al., 1994]. An improvement to Equation (3.50) expressed J as a function of the growth rate, dW/dt, and the internal concentration, C_{plant}, as shown in Equation (3.51) [Nye and Tinker, 1969; Willits, et al., 1992].

$$J = (C_{plant}\, dW/dt + W\, dC_{plant}/dt)/2\pi r_0 L_r \tag{3.51}$$

In Equation (3.51), W is plant weight, t is time, r_0 is the mean root radius, and L_r equals total root length. The problem with this model is that dC_{plant}/dt, r_0, and L_r are often difficult to measure in practice [Wheeler, et al., 1994]. Further improvements have related the growth and uptake rates to the age of the plant using the relative growth rate, $\mu_g = (1/W)dW/dt$, and the relative uptake rate, $(1/C_{plant})dC_{plant}/dt$, respectively [Nye and Tinker, 1969; Bhat, et al., 1979a; Bhat, et al., 1979b]. In these equations, C_{plant} can be the concentration in any specific plant tissue at time, t.

A similar model of nutrient uptake takes into consideration the differing effects caused by variations in root growth stage. Assuming that root growth follows a first order differential equation and assuming that the root growth is exponential [Silberbush and Gbur, 1994], then Equation (3.52) can be derived. This equation is presented in similar form to Equation (3.50) and is known as the William's Equation.

$$J = \frac{\ln(L_r / L_{r0})}{2\pi r_0(L_r - L_{r0})(t - t_0)} (C_{plant} - C_{plant,0}) \qquad (3.52)$$

In Equation (3.52), L_r represents the length of roots at times, t and t_0, when the concentration of the nutrients in the plant are C_{plant}, and $C_{plant,0}$, respectively. Uptake rates for the macro-nutrients (N, P, K, Mg, and Ca) have been confirmed for corn plants (cv. Pioneer 3516) albeit under several assumptions and short time scales [Warncke and Barber, 1974].

Using a mass balance approach, taking into account the individual mechanisms responsible for the transport of nutrients towards and away from the root surface, the following model has been developed [France and Thornley, 1984]. Nutrients are carried to the root surface through the transpirational stream utilizing the mechanisms of bulk flow, J_B, and diffusional gradients, J_D. On the other hand, these nutrients are translocated into the root itself and to the upper portions of the plants through three distinct mechanisms. This includes bulk flow, J_b, diffusion, J_d, and active uptake by root membranes proteins, J_a. Using an effective diffusion coefficient for the soil based on geometrical characteristics of

the soil structure, D_{eff}, the transport to the root surface due to diffusion can be written as Equation (3.53), where the C_{soil} and $C_{surface}$ are the respective nutrient concentrations.

$$J_D = D_{eff} (C_{soil} - C_{surface}) \tag{3.53}$$

For the bulk flow rates to the surface and into the plant, the mass flux of the nutrient solution, v, is an equivalent quantity. Therefore, J_B and J_b can be determined using Equations (3.54) and (3.55) with the respective nutrient concentration terms.

$$J_B = vC_{soil} \tag{3.54}$$

$$J_b = vC_{surface} \tag{3.55}$$

As for the diffusion of nutrients from the root surface into the root cells, an equation identical to the Nye and Tinker model (Equation 3.50) can be utilized, as shown in Equation (3.56).

$$J_d = J = a_J (C_{surface} - C_{root}) \tag{3.56}$$

The membrane permeability coefficient, P_j, has been substituted for the correlation coefficient, a_J, in this equation. This permeability coefficient has subsequently been defined based on the mobility of the particular ion in the membrane, ω_j, the membrane-water partition coefficient, K_j, and the membrane thickness, σ_m (usually taken to be 4 nm) [Akeson and Munns, 1990]. This is demonstrated in Equation (3.57)

$$a_J = P_j = RT\omega_j K_j / \sigma_m \tag{3.57}$$

Finally, for the active uptake of nutrients by the membrane bound proteins, a Michaelis-Menten equation can be utilized. This is shown in Equation (3.58) where $J_{c,max}$ and $K_{c,m}$ are the usual kinetic constants.

$$J_c = \frac{J_{c,max} C_{surface}}{K_{c,m} + C_{surface}} \tag{3.58}$$

Combining Equations (3.53) to (3.58) in a mass balance taken at the surface of the roots leads to Equation (3.59), a quadratic relationship in terms of $C_{surface}$.

$$J_B + J_D = J_b + J_d + J_c$$

$$vC_{soil} + D_{eff}(C_{soil} - C_{surface}) = vC_{surface} + a_J (C_{surface} - C_{root}) + \frac{J_{c,max}\, C_{surface}}{K_{c,m} + C_{surface}} \qquad (3.59)$$

Therefore, since C_{soil} and C_{root} are easier to measure using the techniques described earlier, $C_{surface}$ can be determined assuming all other parameters are known or can be estimated.

The application of these uptake models are based upon macroscopic quantities such as overall root length, mean radius, total growth, average nutrient concentrations, etc. This differs for the microscopic models which deal with the immediate vicinity around the root [Barber and Cushman, 1981]. The two main focal points for the microscopic approach to nutrient uptake are based on the rate of depletion from the soil and the enzymatic uptake capacity by the plant cells.

For the soil portion of this model, the rate of depletion is described using classical convection and diffusion equations for flow through porous media (i.e. soil). The mass flow of water is driven by the transpiration stream where the nutrients are dissolved and the diffusion occurs due to the differential accumulation of nutrients by the root surface. In order to derive a mathematical model, a radial control volume, $r+\Delta r$, around the root is utilized with the principle of mass conservation. This is depicted in Equation (3.60).

$$\int_0^t (2\pi r J_r)|_{(r+\Delta r,s)}\, ds - \int_0^t (2\pi r J_r)|_{(r,s)}\, ds + 2\pi \int_0^t \int_r^{r+\Delta r} \alpha_m(u,s) u\, du\, ds = \int_r^{r+\Delta r} C(u,t)\, u\, du \qquad (3.60)$$

In Equation (3.60), J_r is the radial mass flux of diffusable solute, C equals the total concentration of the diffusable solute, and α_m represents the mass of diffusable solute produced per unit time per unit volume in the control volume. This leads to the following linear, parabolic equation [Nye and Marriott, 1969; Barber and Cushman, 1981].

$$\frac{1}{r}\frac{\delta}{\delta r}\left(rD_{eff}\frac{\delta C_{soil}}{\delta r} + \frac{v_0 r_0}{b} C_{soil}\right) = \frac{\delta C_{soil}}{\delta t} \qquad (3.61)$$

The left hand side of Equation (3.61) is equivalent to the sum of the diffusive flux as described by Fick's Law and the convective flux. Fick's Law is defined with D_{eff} as the

effective diffusivity of the nutrient through the soil and C_{soil} as the concentration of the nutrient in the soil solution. For the convective flux, v_0 equals the mass-water flux at the outer root radius, r_0, and b represents the buffering power of the solid soil phase to replenish the nutrients in the solution phase taken up by the roots ($b = dC/dC_{soil}$). During the derivation of this equation, several assumptions were used [Nye and Marriott, 1969]. These included assuming that nutrient transport occurs only in the radial direction, D_{eff} was independent of v, the parameters, b and D_{eff} are independent of concentration, root hairs were taken as the outer root radius (r_0 and v_0 refer to the cylinder where the tips of the hairs are located, not the main root), the root radius remains constant, and the absorbing power, k (defined later), remains constant with the age of the root. Additional assumptions have been subsequently imposed in order to simplify the computation of exact solutions. These included assuming that the soil is homogeneous and isotropic, moisture conditions are at a steady state, there is no production or depletion by microbial or other such activity, and the radial concentration gradient is linear [Barber and Cushman, 1981].

In order to solve Equation (3.61), two boundary and one initial condition are required [Nye and Marriott, 1969; Cushman, 1979; Barber and Cushman, 1981]. The initial condition, IC, utilizes an initial concentration, C_i, as explained in Equation (3.62).

$$\text{IC)} \qquad C_{soil} = C_i \qquad (t = 0) \qquad (3.62)$$

For the inner boundary condition, BC1, the rate of convection and diffusion of nutrients to the root surface at r_0 is equal to the rate of uptake. This rate of uptake can be described as shown in Equation (3.63) using Michaelis-Menten style kinetics where $J_{c,max}$ is the maximum rate of influx and $K_{c,m}$ represents the concentration at one-half $J_{c,max}$.

$$\text{BC1)} \qquad D_{eff} b \frac{\delta C_{soil}}{\delta r} + v_0 C_{soil} = \frac{J_{c,max} C_{surface}}{K_{c,m} + C_{surface}} \quad (r = r_0,\ t > 0) \qquad (3.63)$$

The adoption of this boundary condition stems from the second focal point for the microscopic approach to nutrient uptake based on the enzymatic capacity by the plant cells [Nielsen, 1972]. It is assumed that the rate limiting step in the absorption of nutrients is

due to the transport across the cellular membranes in the epidermis and xylem of the root tissue. This transport is carried out by various membrane associated enzymes (see Section 2.4.1) each of which reach a maximum uptake, $J_{c,max}$, at saturating concentrations. In order to calculate the root absorbing power, k, $J_{c,max}$ is divided by $K_{c,m}$ ($k = J_{c,max}/K_{c,m}$) [Cushman, 1979; Barber and Cushman, 1981].

Slight modifications to BC1 were made in order to consider the fact that a nutrient is not completely absorbed even after an infinite time. One method to compensate for this occurrence was to assume that an efflux of nutrient occurred based on the concentration gradient ($C_{surface}$ becomes greater than C_{soil}) that developed after substantial amount of soil nutrient was absorbed [Classen and Barber, 1974; Jungk and Barber, 1975]. This efflux rate, E, can be simply subtracted from the right hand side of BC1. A second method of compensation was to specify a minimum soil concentration, C_{min}, where the uptake into the roots, J_c, was equal to zero. This is demonstrated in Equation (3.64).

$$J = \frac{J_{c,max}\,(C_{surface} - C_{min})}{K_{c,m} + C_{surface} - C_{min}} \qquad (3.64)$$

In this case, $K_{c,m}$ equals ($C_{surface} - C_{min}$) where J_c equals 1/2 $J_{c,max}$ [Silberbush and Barber, 1983]. As for BC1, Equation (3.64) would be substituted into Equation (3.63).

As for the outer boundary condition, BC2, several possibilities exist. One of the common assumptions is that there exists no inter-root competition for a particular nutrient. Therefore, the concentration of the nutrient at some distance, r_1, away from the root is relatively constant as shown in Equation (3.65). For relatively immobile nutrients such as potassium, this assumption is reasonable [Barber and Cushman, 1981].

$$\text{BC2)} \qquad C_{soil} = \text{constant} \qquad (r = r_1,\ t > 0) \qquad (3.65)$$

On the other hand, if there exists inter-root competition for a nutrient such as phosphate, the diffusion as described by Fick's Law combined with the convective term with a mass flux, v_1, taken at r_1 away from the root can be assumed to be zero, as shown in Equation

(3.66). This is due to the lack of competition for water and the assumption that the nutrient cannot cross the cylinder of radius, r_1 [Cushman, 1979].

$$\text{BC2)} \qquad D_{eff} b \frac{\delta C_{soil}}{\delta r} + v_1 C_{soil} = 0 \qquad (r = r_1,\ t > 0) \qquad (3.66)$$

This uptake model and corresponding initial and boundary conditions have been solved analytically using separation of variables [Cushman, 1979] and series approximations [De Willigen and Van Noordwijk, 1994a] as well as numerically using the Crank-Nicolson method [Classen and Barber, 1976]. The Barber-Cushman equations have been validated experimentally for N, P, and K in corn [Barber and Cushman, 1981; Schenk and Barber, 1979; Claasen and Barber, 1976], P and K for soybeans [Silberbush and Barber, 1983], and N for pennygrass [Barber and Cushman, 1981]. However, since these solutions are based on relatively short time frames (1-2 weeks) as compared to the entire plant life (months), then several experiments are required to develop the total nutrient uptake capacity of the plant. This can be accomplished by integrating the uptake rates from each growth stage over the entire plant life cycle [De Willigen and Van Noordwijk, 1994b].

For each of these nutrient uptake models, the parameters must be estimated using experimental data. For the bulk flow velocities, v, this can be determined based on the change in soil moisture content. This can be determined either as the change in weight of the moist soil or as a change in the water potential as measured using the methods described earlier. In order to estimate the diffusion coefficient, D_{eff}, for each nutrient through the soil, radioactive tracers placed into a test soil can be absorbed into cation exchange resin paper [Warncke and Barber, 1972]. The amount of radioactive tracer, M_t, absorbed onto the paper after time, t, can be used to determine D_{eff} as shown in Equation (3.67) as long as the initial, C_i, and final, C_f, interface tracer concentrations in the soil can be measured. If taken to completion, then C_f can be eliminated from the equation.

$$D_{eff} = M_t^2 \pi / [4(C_i - C_f)^2 t] \qquad (3.67)$$

Assuming that the ionic species diffuses completely through the liquid, then D_{eff} can be related to the diffusion coefficient through pure water, D_{AB}. This is desired since these pure coefficients are readily available. Therefore, D_{eff} can be related using D_{AB} multiplied by some transmission factor. This transmission factor has been correlated to several parameters such as the moisture content of the soil, C_{water}, the tortuosity through the porous soil, τ, and the buffering capacity of the soil, $b = dC/dC_{soil}$ [Warncke and Barber, 1972; Bar-Tal, et al., 1993]. This relationship is shown in Equation (3.68).

$$D_{eff} = D_{AB} C_{water} \tau / b \tag{3.68}$$

If the soil does not contain a buffering capacity such as is the case for hydroponic systems (see Sections 4.1.1 and 4.2.2), then the effective diffusion coefficient can be estimated based on the porosity of the media, ε, as shown in Equation (3.69) [Geankoplis, 1983].

$$D_{eff} = D_{AB} (\varepsilon / \tau) \tag{3.69}$$

In order to estimate the tortuosity for either Equations (3.68) or (3.69), the following correlation, Equation (3.70), to the soil volumetric water content has often been used [Oates and Barber, 1987; Cox and Barber, 1992].

$$\tau = 1.58\, C_{water} - 0.17 \qquad (C_{water} > 0.12) \tag{3.70}$$

Finally, for the Michaelis-Menten kinetic parameters, $J_{c,max}$ and $K_{c,m}$, these can be estimated using standard procedures where the uptake rates into plants, J_c, are measured as a function of various solution concentrations, C [Taiz and Zeiger, 1991]. By graphing these results on a Lineweaver-Burke plot of $1/J_c$ versus $1/C$, the kinetic constants can be determined from the slope ($= K_{c,m} / J_{c,max}$) and y-intercept ($= 1/J_{c,max}$). This relationship is shown in Equation (3.71) where the root absorbing power, k, has been substituted in for the inverse of the slope ($k = J_{c,max} / K_{c,m}$).

$$\frac{1}{J_c} = \frac{K_{c,m}}{J_{c,max}} \frac{1}{C_{surface}} + \frac{1}{J_{c,max}} = \frac{1}{k} \frac{1}{C_{surface}} + \frac{1}{J_{c,max}} \tag{3.71}$$

CHAPTER 4 - CONVENTIONAL HYDROPONIC SYSTEMS

This chapter provides the background information specific for the production of plant biomass utilizing conventional hydroponic solutions and systems. In Section 4.1, a review of basic hydroponic solutions is provided. This starts with a description of some standard formulations followed by a discussion of the common methods of altering these mixes for specific purposes. Special attention is given to maintaining the osmotic potential after modifying a nutrient solution. In Section 4.2, a review of the conventional hydroponic systems that are used both experimentally in research as well as practically in greenhouse industry is provided. This will include descriptions of various soil-like media as well as soil-less culturing techniques.

4.1 Hydroponic Solutions

From the background information provided in Chapter 2 on plant nutrient uptake, the successful growth and cultivation of plants requires the adequate and specific supply of 13 inorganic nutrients. These include the macro-nutrients of ammonium or nitrate nitrogen (NH_4^+ or NO_3^-), phosphate ($H_2PO_4^-$, HPO_4^{2-}, PO_4^{3-}), potassium (K^+), calcium (Ca^{2+}), magnesium (Mg^{2+}), and sulfate (SO_4^{2-}). Similarly, the micro-nutrients of iron (Fe^{2+}, Fe^{3+}), chlorine (Cl^-), manganese (Mn^{2+}), borate ($B_4O_7^{2-}$, BO_3^{3-}), zinc (Zn^{2+}), copper (Cu^+, Cu^{2+}), and molydate (MoO_4^{2-}) are required to be supplied at specific concentrations as well. In order to supply these essential nutrients, several hydroponic solutions have been devised and modified for the specific needs of the plants grown.

4.1.1 Standard Nutrient Solutions

There are several mixes of hydroponic nutrient solutions that can be concocted based on the different types of salts and concentrations used. One of the original solutions, Sachs' solution, was developed as early as 1860 but only consisted of KNO_3, $Ca_3(PO_4)_2$, $MgSO_4$, $CaSO_4$, NaCl, and $FeSO_4$ [Hoagland and Arnon, 1950]. Although this solution mainly consisted of macro-nutrients, successful plant growth was probably achieved due to the presence of the micro-nutrients as water impurities. This solution, along with another developed at approximately the same time by Knop, was subsequently used mainly as a means to study plant nutrition. In 1938, Hoagland's #1 solution was developed which contained all of the inorganic elements essential for plant growth [Resh, 1978]. This formulation was further refined to include the ammonium ion as is preferred by some plants. This second solution is referred to as Hoagland's #2 solution, differentiating it from the previous mixture [Hoagland and Arnon, 1950]. With the advent of these solutions that were considered to be complete with all the essential nutrients, commercial hydroponic cultivation began to receive attention. This was particularly true for agromonically significant crops produced in areas where the land is non-arable or limited [Resh, 1978; Schwarz, 1995]. Today, over 300 different nutrient solutions of various formulations have been developed and are widely used in scientific research as well as commercial practice. A review of some of these nutrient solutions are presented in Table 4.1 [Resh, 1978; Hoagland and Arnon, 1950; Mackowiak, et al., 1989; Hewitt and Smith, 1974].

The typical salts that are used to produce these nutrient solutions can be of various composition [Resh, 1978]. Anionic species such as sulfate, chloride, nitrate, and phosphates are generally associated with the essential cationic nutrients to form the salt. For example, Ca can be supplied as calcium sulfate ($CaSO_4$), calcium chloride ($CaCl_2$), calcium nitrate ($Ca(NO_3)_2$), or monocalcium phosphate ($Ca(H_2PO_4)_2$), among others. Furthermore, these salts can be of different grades such as commercial, reagent, greenhouse, or food grades. The differences in the grades of fertilizer salts are the levels of impurites that are present. Similarly, the quality of water that is used to dissolve the salts such as distilled, irrigation, or tap water can also introduce significant impurities. These

impurities can increase the quantity of a nutrient, particularly the micro-nutrients, above the desired levels [Schwarz, 1995]. Furthermore, non-essential nutrients such as sodium and fluorine may be introduced into the solution causing deleterious effects to the plant [Hoagland and Arnon, 1950]. Finally, the lower grade salts can contain inert carriers such as clays or silt particles which can clog the hydroponic system [Resh, 1978].

Table 4.1 Nutrient Solution Formulations

Forumulation Nutrient	Sachs' (1860)	Knop's (1865)	Hoagland's #1 (1938)	Hoagland's #2 (1938)	NASA's (1989)
Macro: (mM)					
NH_4^+-N	-----	-----	-----	1.0	-----
NO_3^--N	10.0	12.0	15.0	14.0	15.0
P	3.2	1.5+	1.0	1.0	1.0
K	10.0	3.5	6.0	6.0	6.0
Mg	2.0	0.8	2.0	2.0	2.0
Ca	7.7	5.0	5.0	4.0	5.0
S	5.0+	0.8	2.0	2.0	2.0
Micro: (μM)					
Fe	Trace	Trace	50.0	50.0	100.0
Cl	4300	-----	18.0	18.0	*
Mn	-----	-----	9.0	9.0	8.0
B	-----	-----	46.0	46.0	80.0
Zn	-----	-----	0.8	0.8	0.8
Cu	-----	-----	0.3	0.3	0.3
Mo	-----	-----	0.1	0.1	0.1
Non-Essential: (mM)					
Na	4.3	-----	-----	-----	-----
Si	-----	-----	-----	-----	0.3

+ Additional quantity of these nutrients due to their combination as trace iron salts.
* Added with the micro-nutrients as chlorine salts but concentration not reported.

Another consideration when choosing the appropriate nutrient components is the quantity of water that is present in the base fertilizer salt. They can be in the anhydrous form such as $MgSO_4$ or $CaSO_4$ or the hydrated form such as $MgSO_4.7H_2O$ or $CaSO_4.2H_2O$. When concocting the nutrient solution, the difference in molecular weight

due to the hydration (18.0 g/mol for each water molecule) will effect the concentration when a specific amount of the salt is weighed. Therefore, the exact salt composition utilized needs to be carefully monitored. This factor has often gone uncorrected when nutrient solutions are prepared [Owens and Miller, 1992]. Furthermore, these errors are often perpetuated when cited in the literature. For example, Knop's solution often has $MgSO_4$ listed [Hoagland and Arnon, 1950] while the actual formulation requires the hydrated form. If the anhydrous form were used at the quantities quoted, then this would result in increases from 0.8 to 1.7 mM for both Mg^{2+} and SO_4^{2-} concentrations.

Another important factor to consider when using nutrient solutions to cultivate plants in a hydroponic system is the solubility of the salts that are utilized [Resh, 1978]. This is particularly true for iron which is highly susceptible to precipitation (low solubility), particularly due to changes in the pH [Hoagland and Arnon, 1950]. In order to maintain appropriate levels of Fe in the solution, chelated iron often has to be utilized as the source of this essential nutrient. Typical artificially produced chelating compounds include ethylene diamine tetraacetic acid (EDTA), ethylene diamine dihydroxyphenylacetic acid (EDDHA) [Resh, 1978], N-(2-hydroxyethyl)ethylene diamine triacetic acid (HEDTA) [Mackowiak, et al., 1989], and diethylene triamine pentaacetic acid (DTPA) [Parker, et al., 1992]. In terms of natural plant metabolism, tomatoes were shown to increase the production of oxalate and citrate which also chelate Fe under deficient conditions [Holden, et al., 1991]. These soluble organic components bind the nutrient ion and maintain the solubility even when the pH levels change. Other chelated nutrients that are sometimes used in hydroponic solutions include Zn [Parker, et al., 1992] and Mn [Resh, 1978].

Since pH has such a profound effect on the solubility of the nutrient ions, this factor needs to be expressly monitored and controlled from the onset of hydroponic plant production. In general, nutrient solutions are initially set at a pH ranging from 5.5 to 6.5 [Resh, 1978] with the optimum pH determined by the plant species grown and the composition of the rooting medium. For tomato plants, this value has often been set to approximately 5.8 which is the average value found to be optimum for root (pH 5.5) and shoot (pH 6.0) growth [Adams, 1986]. This initial pH is usually accomplished by adding

an acid or base which contains essential elements such as HNO_3, H_2SO_4, KOH, NH_3, etc. However, as plants are cultivated on the solution, the roots selectively absorb nutrients at different rates [Hoagland and Arnon, 1950]. This is due to the different demands based on the plant growth stage as well as environmental factors affecting the growth, including the volume of solution available. This differential uptake can alter the acid-base characteristics of the solution leading to a substantial change in the pH. This can lead to the precipitation of certain nutrients as was discussed earlier. In order to correct this occurrence, the acids and bases listed above can be added as appropriate. Furthermore, buffering components containing a combination of either a weak acid and a basic salt or a weak base and an acidic salt can be added to the nutrient solution in order to counteract the changes in pH.

4.1.2 Alterations of Standard Nutrient Solutions

Although a single solution is not superior to the rest [Hoagland and Arnon, 1950], much research has been conducted on optimizing a formulation based on the specific crop produced. This has been widely accomplished by commercial greenhouses and is particularly true for nitrogen nutrition as NO_3^- or NH_4^+ since some plant species prefer one nitrogen form over the other. In tomato plants, nitrate is preferred over ammonium; therefore, formulations modified from solutions such as Hoagland's #1 hydroponic solution are often utilized [Ikeda, et al., 1992]. Furthermore, the nutrient mixtures presented in Table 4.1 have also been adjusted based on the specific experimental conditions under examination for nutrient studies.

One important factor to consider when altering the composition of a nutrient solution is the effect on the water potential, Ψ. Specifically, a change in water potential at the root-zone can have a profound effect on the nutrient uptake capacity of plants [Glass, 1989]. As determined in Equation (2.2), the osmotic component, $-\pi$, of this water potential, equals $-RTC_s$ where C_s is the osmolality measured as moles of solute per kg of water, regardless of the solute composition [Taiz and Zeiger, 1991]. In order to balance Ψ, this total solute concentration must be maintained at the control levels even though the

concentration of the individual nutrients can be altered. Experiments conducted that do not take this stipulation into account may lead to erroneous conclusions simply by attributing the results to the changes in nutrient levels instead of to the altered solution transport characteristics caused by the water potential changes. This is illustrated in the following example where the effects of nitrogen form (NO_3^- or NH_4^+) on the assimilation rates in tomatoes (cv. Fukuju Nigo) were examined [Ikeda, et al., 1992]. During this experiment, 100 mg/L of nitrogen were supplied as $NaNO_3$ (two solutes), $(NH_4)_2SO_4$ (three solutes), or NH_4NO_3 (two solutes). The different solute counts for these three salts contribute 14.3, 10.7, and 7.1 mmol/kg, respectively, to the total solute concentration, C_s. According to Equation (2.2), the soil water potential, Ψ_{soil}, would become less negative with the NH_4^+-containing solutions as compared to the nitrate-only solution. When compared to Equation (2.5) for the root water potential, Ψ_{root}, which is more negative than the soil potential, faster uptake rates should result with the two NH_4^+ salts since the water potential gradient between the roots and the soil would be larger. These differences were not taken into consideration during these experiments which did report uptake rates that were greater with the two ammonium treatments. However, whether the observed effects can be attributed to the differences in the form of nitrogen or to the different water potentials is not separable. Therefore, the conclusions obtained may be suspect since the total osmotic potential of the nutrient solution was altered which leads to different nutrient uptake capacities anyway [Glass, 1989]. Unfortunately, this problem is far more prevalent during macro-nutrient studies than during the micro-nutrient counterparts simply due to the concentrations involved and their respective contributions to the osmotic potential.

Another factor to consider during nutrient uptake studies is the form of the various replacement salts that can be used in the standard solution to change the composition of a particular essential element. In conjunction with the changes in composition, these alterations in the formulation lead to changes in the concentrations of various other elements in solution in addition to the target nutrient. These additional variations have also been ignored in several cases as the possible reasons for the observed effects which are usually only attributed to the nutrient specifically examined. As an example, during

another study involving the effects of different ratios of NO_3^-/NH_4^+ concentrations on tomato plants (cv. Ailsa Craig), modified full strength Long Ashton solutions were utilized but with constant osmotic potentials [Qasem and Hill, 1993]. The original formulation for this solution containing only nitrate-N [Hewitt and Smith, 1974] is reviewed in Table 4.2 along with the total solute content contributed by the inorganic ions. In order to modify this solution to contain 3:1, 2:2, 1:3, or 0:4 ratios of nitrate to ammonium concentrations, different salts containing sodium, chloride, and sulfate were utilized to replace the nitrate with ammonium and to maintain the osmotic potentials. However, in order to maintain the solute level as calculated in Table 4.2 while subjecting the tomato plants to the various nitrogen ratios, the concentration of the other essential elements would have to be altered as well. This is illustrated below for the 0:4 solution and reviewed in Table 4.2.

Table 4.2 Comparison of Long Ashton Nutrient Solutions Modified for Ammonium Nitrogen Only (Concentrations in mmol/kg)

	Nutrient	Original: Standard NO_3^- Only	Modified: NH_4^+ Only (Constant Osmolarity)	Modified: NH_4^+ Only (Constant Conc.)
Macro-Nutrients	NH_4^+-N	----	8.0	12.0
	NO_3^--N	12.0	----	----
	P	1.33	1.33	1.33
	K	4.0	1.8	4.0
	Mg	1.5	1.5	1.5
	Ca	4.0	1.8	4.0
	S	1.5122	6.4122	9.5122
Micro-Nutrients	Fe	0.1	0.1	0.1
	Cl	0.1	3.7	8.1
	Mn	0.01	0.01	0.01
	B	0.05	0.05	0.05
	Zn	0.001	0.001	0.001
	Cu	0.001	0.001	0.001
	Mo	0.0005	0.0005	0.0005
Non-Essential	Na	1.431	1.431	1.431
	Co	0.0002	0.0002	0.0002
TOTAL:	Solutes	26.0359	26.1359	42.0359

For the nitrate-only solution presented in the third column from the left in Table 4.2, KNO_3 and $Ca(NO_3)_2$ both supply NO_3^--N to a concentration of 12.0 mmol/kg. Additionally, the K^+ and Ca^{2+} ions from these compounds both contribute 4.0 mmol/kg to the total osmolarity. Using the assumption that the osmolarity was maintained as stated [Qasem and Hill, 1993], then the concentrations of these macro-nutrients would have to be substantially altered. Since the micro-nutrients and non-essential elements represent less than 10% of the total 26.0 mmol/kg osmolarity, then these levels will be assumed to be maintained during this modification. This is also suggested in the literature during the modification of the Long Ashton solution to contain ammonium-N either partially or wholly [Hewitt and Smith, 1974]. In order to maintain the total solute concentration contributed by the macro-nutrients, $(NH_4)_2SO_4$, a three solute compound, was suggested to supply the replacement nitrogen. Similarly, K_2SO_4 and $CaCl_2$ are suggested as replacement salts for the potassium and calcium requirements in the solution, both of which contain three solutes as well. As for the magnesium and phosphate levels, these can be maintained according to original formulations using the same salts of $MgSO_4.7H_2O$ and $NaH_2PO_4.2H_2O$ [Hewitt and Smith, 1974]. As illustrated in Table 4.2, maintaining these individual nutrient levels contributes approximately 6.0 mmol/kg while the remaining 20.0 mmol/kg needs to be contributed by the K^+, SO_4^{2-}, Cl^-, and NH_4^+ ions of the replacement salts. If nitrogen levels were to be maintained at the original 12.0 mmol/kg, then 6.0 mmol/kg of $(NH_4)_2SO_4$ would have to be used. This would contribute 18.0 mmol/kg (12.0 NH_4^+ + 6.0 SO_4^{2-}) leaving only 2.0 mmol/kg of total solutes from the other two replacement salts. This would substantially decrease both K^+ and Ca^{2+} levels in the solution. On the other hand, if these two cations were maintained at their original levels, then the K_2SO_4 and $CaCl_2$ levels would have to be 2.0 and 4.0 mmol/kg, respectively. This would also provide 18.0 mmol/kg in total solute contributions (4.0 K^+ + 4.0 Ca^{2+} + 2.0 SO_4^{2-} + 8.0 Cl^-) leaving only 2.0 mmol/kg of total solutes from the ammonium salt. Again, this would be a substantially deficit solution. Using only 4.0 mmol/kg of the ammonium salt yields 8.0 NH_4^+ and 4.0 mmol/kg SO_4^{2-}. This total of 12.0 mmol/kg of solutes leaves 8.0 mmol/kg to be contributed by the other two replacement salts. Since the original

formulation called for equal quantities of Ca^{2+} and K^+, then approximately 0.9 of K_2SO_4 and 1.8 mmol/kg $CaCl_2$ can be utilized, which actually yields 8.1 mmol/kg of total solutes. This is illustrated in the fourth column from the left of Table 4.2. These calculations illustrate that the suggested replacement salts used during these experiments radically altered the entire solution composition even though the osmotic potential was maintained. Similar results can be obtained for solution containing mixtures of nitrate and ammonium.

If it is assumed that the maintenance of all concentration levels was the goal for modifying the Long Ashton solution, then this would also lead to substantial compositional changes as well. At the same nitrogen concentration, $(NH_4)_2SO_4$, contributes 12.0 mmol/kg NH_4^+ and 6.0 mmol/kg SO_4^{2-}. In order to maintain the original potassium and calcium levels of 4.0 mmol/kg each, K_2SO_4 and $CaCl_2$ would lead to an additional 2.0 mmol/kg SO_4^{2-} and 8.0 mmol/kg Cl^- ions, respectively. These choices for replacement salts increases the osmotic component, π, of the solution water potential from the original 20.0 mmol/kg contributed by the potassium and calcium nitrates to 36.0 mmol/kg. This modified formulation is presented in the last column of Table 4.2.

Under both calculation procedures of conserved osmolarity or conserved concentrations, the levels of sulfate and chloride are significantly increased which could have caused the observed results of decreased growth and nitrogen uptake on the ammonium only solution. Originally, these were attributed to the differences in nitrogen form [Qasem and Hill, 1993]. However, the increased Cl^- concentration may be particularly relevant since, as discussed earlier (see Section 2.4) and illustrated in Table 2.4, this essential nutrient plays a substantial role in the maintenance of the electropotentials across membranes during ion (nutrient) transport [Salisbury and Ross, 1985; Resh, 1978; Taiz and Zeiger, 1991; Adams, 1986]. Therefore, significant changes in the levels of this ion can alter the transport characteristics at the root surface. Furthermore, by simple charge distibution, increasing the negative charge outside of the root by increasing Cl^- and SO_4^{2-} levels in the solution needs to be balanced by either a similar increase internally or a positive ion remaining outside of the root. This positive ion may have been the ammonium ion. Thus, NH_4^+ uptake may have been depressed due to

the increased external anionic levels instead. Furthermore, when plants experience salt stress conditions, the tissues undergo osmotic regulation either by altering the uptake of inorganic nutrients or by producing organic solutes (amino acids, organic acids, and soluble sugars) internally [Perez-Alfocea, et al., 1993].

One method that has been widely used to modify the osmotic potential of a hydroponic solution is the addition of non-penetrating solutes such as high molecular weight polyethylene glycols (PEG) or mannitol [Hohl and Schopfer, 1991]. The PEGs that have been used as hydroponic solution osmotica range in molecular weights from 1,000 to 20,000 [Yaniv and Werker, 1983]. However, the lower molecular weight PEGs as well as the mannitol have been shown to enter the root apoplast and even the symplast which can lead to the transport of the solutes in the transpirational stream [Yaniv and Werker, 1983; Hohl and Schopfer, 1991]. Therefore, the results obtained from these experiments may be suspect due to the altered transport characteristics imposed by the supposedly non-penetrating solutes. Using a higher molecular weight PEG (6000), leaf dry weights, plant biomass, tissue hydration, and internal nitrate and potassium concentrations were shown to decrease in several *Lycopersicon esculentum* Mill. tomato cultivars (Pera, P-73, and Volgogradskij) and a wild relative, *L. pennellii* (Corr.) D'Arcy accession PE-47, subjected to -0.50 MPa osmotic stress for 3 weeks [Perez-Alfocea, et al., 1993]. However, it has not been excluded that the higher molecular weight PEGs may behave in the same manner during long term experiments as the lower molecular weight PEGs during short term experiments [Hohl and Schopfer, 1991]. In fact, eight different plant species including tomato were subjected to different molecular weight PEGs for 24 hrs leading to the deposition of white material on the leaves. This material was later identified as the osmotica indicating the presence in the transpirational stream [Yaniv and Werker, 1983]. Furthermore, root morphology was altered when subjected to these osmotica by decreasing root length and increasing diameter [Materechera, et al., 1992].

Since plants grown in the soil are often subjected to additional elements present, some studies have been conducted using hydroponic solutions to investigate their effects on plants. In order to study these effects of typically non-essential nutrients on the growth

and development of plants, the standard or optimally modified hydroponic solutions can be supplemented with additional quantities of the element. Some elements that have been found to be beneficial to plants, yet non-essential, include silicon, sodium, cobalt, and selenium [Mackowiak, et al., 1989; Miyage and Takahashi, 1983; Menzies, et al., 1991]. Conversely, others lead to detrimental results such aluminum and fluorine [Akeson and Munns, 1990; Barrachina, et al., 1994]. These elements are added as various salts as well.

4.2 Conventional Hydroponic Systems

From the discussion of the previous chapter, it becomes evident that a tight control of the plant nutrient environment is required in order to maintain growth at an optimum level. For the conventional growth of plants, the inorganic nutrients are present in the soil itself. However, these crops are subject to other environmental factors such as climatic conditions, growth seasons, and diseases and pests. On the other hand, the inorganic nutrient requirements of plants grown hydroponically are maintained through the use of the non-limiting nutrient solutions presented earlier. Furthermore, hydroponic systems can be maintained indoors which allows for the optimal control of the growth environment.

There are two main types of hydroponic systems, ones that utilize an artificial soil-like medium in conjunction with the nutrient solution and those that are completely soilless, utilizing only the nutrient solution. The systems that are categorized in latter of these two types are considered true hydroponics according to the definition of the word (*hydros* = having to do with water + *ponos* = labor) [Schwarz, 1995]. Common to all is their ability to simulate the growth of plants as if maintained in soil. There are three soil characteristics which must be replicated in order for the plants to survive. These are root aeration, root-zone darkness, and plant support [Salisbury and Ross, 1985; Resh, 1978].

In order to obtain root aeration which is necessary for the normal respiration processes required for growth, several methods can be employed. These include direct aeration or agitation of the nutrient solution or by utilizing a rapid continuous flow system to maintain an adequate dissolved oxygen content [Schwarz, 1995; Bugbee and Salisbury,

1988]. In some systems, this requirement is obtained using an ebb and flow design where nutrient solution is introduced into the rooting medium and then drained to allow the aeration to occur [Resh, 1978; Schwarz, 1995]. Alternatively, the Nutrient Film Technique (NFT) can be employed which utilizes a continuous flow design. However, slower flow rates, larger surface area, and shallower solution levels are utilized. The increased surface area provides for higher oxygen transfer rates in the solution while the shallow liquid levels insures that some roots are always exposed to air [Cooper, 1979].

For the second criterion of root-zone darkness, opaque building or covering materials can be employed to contain the plant roots in the dark. This criterion is necessary in order to prevent the excess growth of algae which will compete directly for the nutrients present in solution [Resh, 1978]. One of the inherent disadvantages is that this severely restricts the building materials which can be used. An early impetus to the wide-spread commercialization of hydroponic growth systems was that the necessary building materials were expensive and required excess maintenance. However, with the introduction of light weight plastics such as polyvinylchloride (PVC) tubing and polyethylene sheets, these problems have been for the most part solved [Resh, 1978].

In addition to supplying root-zone darkness, the cover materials also provide the plants with physical support. Furthermore, the use of artificial soil mediums such as sand, peat, gravel, vermiculite, rockwool, sawdust, and others provide a physical structure for which the roots can adhere to in order to support the plants. The differences between the various rooting matricies that are utilized include the water holding capacity, leaching capacities, durability, porosity, and the ease of sterilization [Resh, 1978; Schwarz, 1995].

4.2.1 Comparisons between Hydroponic and Soil-Based Agriculture

In order to determine whether soil or hydroponic cultivation of plants is more advantageous, a cost analysis can be used [Pena, 1985; Schwarz, 1995]. This is generally based on several cost factors including the amount of land present, the initial investment for constructing the facility, and the costs of maintaining a controlled environment

throughout the repeated life cycles of the plants. This is balanced by factors such as the growth and yield of the crop grown under normal and controlled environments as well as the value and demand for the crop commercially.

When land space and irrigation are in ample supply, the use of the conventional farming may be more advantageous due to lower economic costs. Although the majority of the nutrients are present in the soil, depletion can become a problem when successive cropping over several generations is maintained. One method which is widely used to compensate for this problem in the short term is the use of crop rotation procedures [Oyer and Touchton, 1990]. Since plant species usually have a differential accumulation of certain nutrients, the growth of one species may not deplete the nutrient required during the growth of another species maintained later on the same soil. In addition, nutrients utilized by one crop can be replenished by another which could be used to reduce the fertilizers that would normally be required to maintain a single crop. Although this crop rotation technique may replenish certain nutrients while producing high yielding crops, fertilization cannot be avoided entirely. For a more long term solution to the problem of nutrient depletion, application of fertilizers to the crop rotation cycle is widely practiced.

When land area is limited or vast regions are non-arable, the use of a hydroponic growth system to cultivate crops may be more advantageous. Comparable studies between soil-grown and nutrient culture-grown plants reveal that there are several advantages of the latter growth method over the conventional means. These include increased production yields, faster growth times, absence of competitive organisms, decreased growth area per plant [Resh, 1978], and little or no stress resulting from water, nutrient, soluble salts, oxygen, or pH status [Schwarz, 1995]. In addition, the growth conditions such as light requirements, pH, relative humidity, temperature, and carbon dioxide concentration in the air are more easily controlled and maintained [Romero-Aranda and Longuenesse, 1995; Galtier, et al., 1995]. The harvesting of crops from a hydroponic system is easier than the soil-grown method since roots and leaves are cleaner and the changes to new crops can be done fairly rapidly [Cooper, 1979]. Adequate growth chambers have been built which can supply plants with the necessary conditions for

growth [Wheeler, et al., 1990]. Perhaps the most important aspect of a nutrient culture system is that the delivery of nutrients and water is no longer limited by climatic conditions such as those present on Earth. Since the nutrients supplied in hydroponic solutions are adequate to sufficiently grow many plant types, application in a multiple crop hydroponic system would be possible [Stroup and Schwartzkopf, 1992].

The initial costs to construct and set up a hydroponic system, excluding the housing facility, ranges upto $83,000 per hectare, depending on system type and location [Schwarz, 1995]. In the United States, a complete medium sized greenhouse facility can cost $400,000 [Carpenter, 1985]. As for the operating costs of maintaining a growth environment, this depends upon the amount and efficiency of control desired or required based on the ambient atmospheric conditions at the location. An example of extremely high construction and operating costs would be NASA's Closed Ecological Life Support System Breadboard Project which utilizes a complete control of the environment [Averner, et al., 1987]. Furthermore, this ongoing project has the goals of producing crops on a space station where all environmental components will be provided artificially. On the other hand, the production capabilities with hydroponics can be substantially higher than with soil on a per acre basis. For example, 60-300 tons of tomatoes can be produced hydroponically compared to 5-10 tons using soil [Resh, 1978]. Similar results have been obtained many other crops such as soybeans, peas, wheat, rice, oats, potatoes, cabbage, lettuce, and cucumbers [Resh, 1978] as well as ornamental flowers [Schwarz, 1995]. Today, hydroponics are utilized in the United States, Italy, France, the Netherlands, Germany, England, Belgium, the former USSR, Japan, Canada, Israel, Singapore, India, Kuwait, and the Canary Islands [Schwarz, 1995; Van de Vooren, et al., 1986]. Furthermore, tomatoes are one of the most widely produced hydroponic crops [Van de Vooren, et al., 1986]. These production facilities such as those established by Archer-Daniels Midland, PhytoFarm, and Geniponics are becoming more economical and efficient leading to increased commercialization [Field, 1988]. Increases in technology leading to optimized growth environments, recirculation and regeneration of nutrient solutions, and automation have caused these endeavors to become financially applicable.

4.2.2 Soil-Like Cultures

In addition to the factors such as location, ambient atmospheric conditions, and available land, the choice to use hydroponic also depends upon the type of system utilized. There is quite a diverse selection of hydroponic systems which have been developed over the past century. These include the systems that utilize a soil-like medium such as those classified as sand and gravel systems. The difference between these two types of soil-like hydroponic systems is in the relative size of the particles utilized [Schwarz, 1995]. The sand systems have particle diameters upto 3 mm and utilize substrates such as sand, vermiculite (magnesium aluminum silicate), perlite (siliceous volcanic rock), plastics (polystyrene, polyurethane, urea-formaldehyde, polysterene), rockwool granules (various inorganic oxides), and others. The gravel type systems such as gravel, basalt, pumice, lava, and others utilize particles with diameters greater than 3 mm. Furthermore, these inorganic substrates have also been mixed with known quantities of organic components such as peat (sphagnum, sedge, hyphum), bark, sawdust, and manure. The use of these additives is practiced due to their pH-buffering effects and water and air holding capacities.

The utilization of these various soil-like media provide the three characteristic requirements of a hydroponic system of root aeration, root-zone darkness, and plant support. Another advantage to using these alternative mediums is that a continuous flow system can be utilized as well. Typically, both of these systems utilize above ground irrigation systems such as distribution sprayers or perforated pipes. Additionally for the gravel type systems, sub-surface irrigation has also been applied where the entire bed is filled with nutrient solution and then drained in the ebb and flow design [Schwarz, 1995]. The common reservoir utilized with these systems can be used to regenerate the nutrient solution from the returned mixture as well as to alter the composition in the middle of the growth cycle as plant demands change. An additional advantage of this particular system is that it can support relatively tall plants such as tomatoes and cucumbers [Cooper, 1979]. As to whether a particular growth medium is better than another, conclusions are difficult to make since the responses by different plant species varies with the media.

There are also several disadvantages associated with these types of hydroponic systems. These soil-like media generally require repeated sterilization using steam at 180 °F or chemical means such as chloropicrin, methyl bromide, and formaldehyde pumped through the irrigation system [Resh, 1978]. Furthermore, these systems require a large amount of material handling particularly during set-up and some times during sterilization. Another disadvantage to using soil-like substrates is that the turnover rate between crops can be substantially slowed by complex rooting systems intermixed with the particulates. Inefficient separation methods can lead to a reduction in material, requiring replacement. Since the particles are soil-like, they can also contain substantial quantities of essential and non-essential solutes which can be leached in to the nutrient solutions [Resh, 1978]. For example, the composition of rockwool which is artificially produced include SiO_2, Al_2O_3, CaO, MgO, Fe_2O_3, Na_2O, K_2O, MnO, and TiO_2 [Schwarz, 1995].

4.2.3 Soilless Cultures

As stated earlier, true hydroponics is the growth of plants without the benefit of a soil or soil-like medium. Typical water culture methods include floating systems, trough systems, Nutrient Film Technique (NFT), and aeroponics [Cooper, 1979; Resh, 1978; Schwarz, 1995]. Each of these systems can utilize some sort of support medium such as perforated plastic sheets, wood, wire, or rockwool slabs. These materials provide the necessary plant support as well as root-zone darkness. In order to provide the necessary aeration, several methods are available depending upon the system utilized. The general advantages of these water culturing techniques over the soil-like media include the elimination of sterilizations, rapid turnover, and precise solution control [Resh, 1978].

A typical floating system utilizes a light weight synthetic medium such as styrofoam, plastics, or rockwool slabs for support and root-zone darkness [Resh, 1978; Schwarz, 1995]. In this design, the plants are grown in holes made through the support medium and floated on top of the nutrient solution. These materials, particularly the rockwool slabs, are constructed such that the plants roots can grow directly into the

support medium itself yet remain in contact with the solution contained in the pores. Two types of system configurations can be utilized with these floating devices. This includes the tank cultures which utilizes a single solution or the continuous systems which circulates the nutrient solution from a common reservoir. In order to supply proper aeration to the roots, air can be directly bubbled into the solution or rapidly flowed to promote oxygen transfer. However, this represents the major disadvantage of these flooded type hydroponic systems as proper aeration can be difficult to achieve [Resh, 1978]. Furthermore, for the rockwool systems, these materials are generally not reused. The advantages to these types of hydroponic systems are relative cheap costs for materials and the applicability to a conveyor type design where plants are initiated at one end and floated down to the other end where they are harvested [Schwarz, 1995].

Typical systems which utilizes troughs for growing plants include open and closed designs. The basic concept behind these systems utilizes the effects of gravity to pull liquid down a sloping gradient. For the closed systems, the solution is drained into a nutrient reservoir and then pumped back up to the top of the gradient [Cooper, 1979]. This large amount of pumping can be a source of considerable economic input. Alternatively, the open systems do not reuse the solution once though the trough but utilize considerably slower flow rates to promote nutrient depletion [Schwarz, 1995]. The troughs in which the solution flows can be dug directly into the ground and lined with a water-proof material, or the material can simply be suspended above ground. In order to reduce algal growth and maintain root-zone darkness, the water-proof material can be enclosed at the top with just the terrestrial portion of the plant exposed.

The advantages of these systems include easy construction and operation, maintained solution levels, accommodation of large root systems, and high plant densities [Cooper, 1979; Schwarz, 1995]. On the other hand, a major disadvantage is that the plants cannot be initiated in this system but must be transplanted from some other source. A problem with this is that plants can undergo transplanting shock which can severely reduce the rate of growth of the plants [Resh, 1978]. Similarly, deficiency and toxicity symptoms have often been seen after such procedures have been conducted [Bugbee and Salisbury,

1988]. Another disadvantage to these water culturing techniques is that the pH buffering capacity is very low leading to sudden and possibly extreme shifts in pH [Schwarz, 1995].

A variant of the trough system is the NFT system which is widely used in research as well as commercial practice. This technique utilizes a thin film of solution where the roots grow directly into the solution forming an approximate two dimensional system. These two dimensional root mats can be sufficient to provide the plant with the required support without the use of additional support systems. The large surface area to volume ratios associated with this design allows for proper oxygen transfer into the solution to occur without the need for extra aeration [Cooper, 1979]. Furthermore, as the plants develop in this system, aeration is achieved due to the upper surface of the roots being in continuous contact with the moist air while the lower half remains submerged. This has the added advantage over conventional trough systems in that aeration is maintained without excessive flow rates or supplemental air pumping. Inherent disadvantages of this system include the requirements for a uniform downward gradient, larger areas for the root mats, and maintanance of the thin film after the root mats develop in the channel.

The last type of water culturing technique is aeroponics which utilizes a closed environment for the roots which are periodically moistened with a fine mist of nutrient solution [Schwarz, 1995]. The enclosures used to confine the roots in the dark can be constructed of the light weight plastics presented earlier. The high relative humidites that are maintained within the chamber provides the plant roots with the proper aeration with simultaneous nutrition. In order to provide the appropriate misting within the system, sprayers are located evenly throughout the periphery of the container. The obvious disadvantages of this type of system is the complex fluid handling and misting devices that have to be installed as well as transplantation requirements. Furthermore, each container can only accommodate a limited number of plants. Of all of the hydroponic systems reviewed, this system is the only one which has not been implemented commercially.

CHAPTER 5 - CAPILLARY EFFECT ROOT ENVIRONMENT SYSTEMS

In order to facilitate the investigation into the effects of root-zone water potential on nutrient uptake, this chapter reviews a special category of nutrient delivery systems, known as the Capillary Effect Root Environment Systems (CERES). In Section 5.1, the theoretical concept for the capillary supply of nutrients from these systems to plant roots is described. This includes a review of the various materials tested and the different designs that have been implemented. Next, Section 5.2 describes the physical and mathematical models developed for a specific CERES system known as the Porous Ceramic Tube - Nutrient Delivery System (PCT-NDS). This includes the characterization of the porous tubes used as an artificial root environment as well as a description of the affecting forces developed into a mathematical model. This is followed with Section 5.3 reviewing the experiments accomplished on verifying this model equation for the PCT-NDS. This includes a review of the theoretical development of the operational limits for the system as well as a description of the static experiments used for verification. Furthermore, the results of the steady state flow experiments conducted to examine the effects of pressure drop through the ceramic tubes are reviewed. Finally, Section 5.4 presents the experiments performed to verify the control equation that was developed for this system. Specifically, dynamic experiments were conducted which subjected the system to non-standard gravities ranging from near-zero to twice standard gravity. Furthermore, this control equation was tested and verified experimentally under sustained hyper-gravities ranging upto 10 g's using artificial gravitational fields.

5.1 Theoretical Concept and Initial Designs

The Capillary Effect Root Environment Systems (CERES) were originally developed for use by the National Aeronautics and Space Adminstration (NASA). In order to produce higher plants in space, adequate nutrient solution and oxygen need to be supplied to the plant roots just as under conventional conditions such as here on Earth. However, since surface tension forces become dominant in the absence of a substantial gravitational field, liquid would tend to form globular clusters and literally float around within the growth chamber. This could cause potentially fatal accidents particularly with the highly sensitive electrical systems onboard a space capsule or shuttle. Therefore, the development of the CERES was prompted as a unique means to overcome the fluid handling and gas separation problems experienced in micro-gravity [Wright and Bausch, 1984]. Furthermore, these systems have been designed to satisfy the soil characteristics required for plant survival of root aeration, root-zone darkness, and plant support. Finally, these membrane systems allow for the discrete control of the water potential right at the root-zone making an effective tool for research purposes [Dreschel and Sager, 1989].

5.1.1 Theoretical Concepts

As a variation of a Nutrient Film Technique (NFT) system, the CERES concept is based on utilizing the physical separation of the liquid and gas phases through the use of semi-rigid or rigid, micro-porous, hydrophilic membranes [Wright and Bausch, 1984]. In order to produce plants on this type of hydroponic system, seeds can be directly germinated on the membrane surface [Dreschel and Sager, 1989]. This compensates for the transplantation problems encountered with the standard NFT systems. In order to ensure proper aeration, the plant roots are contained on the gas phase side but in direct contact with the membrane. Instead of flowing the nutrient solution in a thin film over the root mat as in the NFT system, the solution is contained within the matricies and on the surface of the membrane. The effect of capillary rise caused by the dominant surface tension forces through the matricies allows for the solution contained on the liquid phase

side to form a thin stagnant film on the gas phase side of the membrane. In order to retain the liquid phase, a slight suction must be applied to draw solution from a reservoir [Wright and Bausch, 1984]. As the plants grow, the roots are maintained in direct contact with the porous matrix and absorb the required nutrients in that manner. Since the formation of the film is relatively thin, the roots are also exposed to the air which provides the necessary aeration. In order to maintain the root-zone darkness, this system can be covered with a polyethylene sheet which also provides the plant with the necessary support. By using micro-porous membranes with average pore diameters that are less than the size of the root hairs, root penetration into the matricies is restricted [Bausch and Wright, 1985].

When dealing with an altered gravitational environment which is the original application for these systems, the flow characteristics of a nutrient delivery system will be seriously affected [Wright and Bausch, 1984]. First and foremost, there can be no free liquid entering or leaving the system since it would literally just float away [MacElroy, 1991]. Therefore, the entire nutrient solution must be in a self-contained vessel. This further complicates the ability to supply the roots with adequate aeration since normal gravity dependent gas separation processes (bouyancy) would no longer occur. In particular, the normal functions of root aeration to supply oxygen for respiration processes [Bausch and Wright, 1985] and carry away excess carbon dioxide will cause an accumulation of these gases in the liquid phase. This accumulation will effectively interfere with the flow of the liquid as well as reduce the contact between the roots and the nutrient solution. Therefore, a complete separation of the gases from the liquid medium is required when the influences of gravity are reduced. In order to overcome this situation, the membrane based CERES systems were developed.

5.1.2 Flat Plate Designs

Initial constructions of this type of hydroponic system utilized 10 by 10 cm plates supported by a coarse plastic screen laid in the flowing solution [Wright and Bausch, 1984]. A schematic design of this system is reprinted in Figure 5.1 along with an

adjustment that was made to remove excess air bubbles from the solution [Bausch and Wright, 1985]. In this modified design, a hydrophobic membrane is laid parallel to the hydrophilic membrane separated by another mesh screen. Any air bubbles in the nutrient solution will be drawn towards the hydrophobic plane and subsequently removed. This can be accomplished as long as the pressure beneath the hydrophobic membrane is less than the pressure of the flowing solution. The materials used in the construction of this CERES system were a polysulfone hydrophilic membrane (0.45 microns), a Teflon hydrophobic membrane (same pore size), and polyethylene coarse mesh screens.

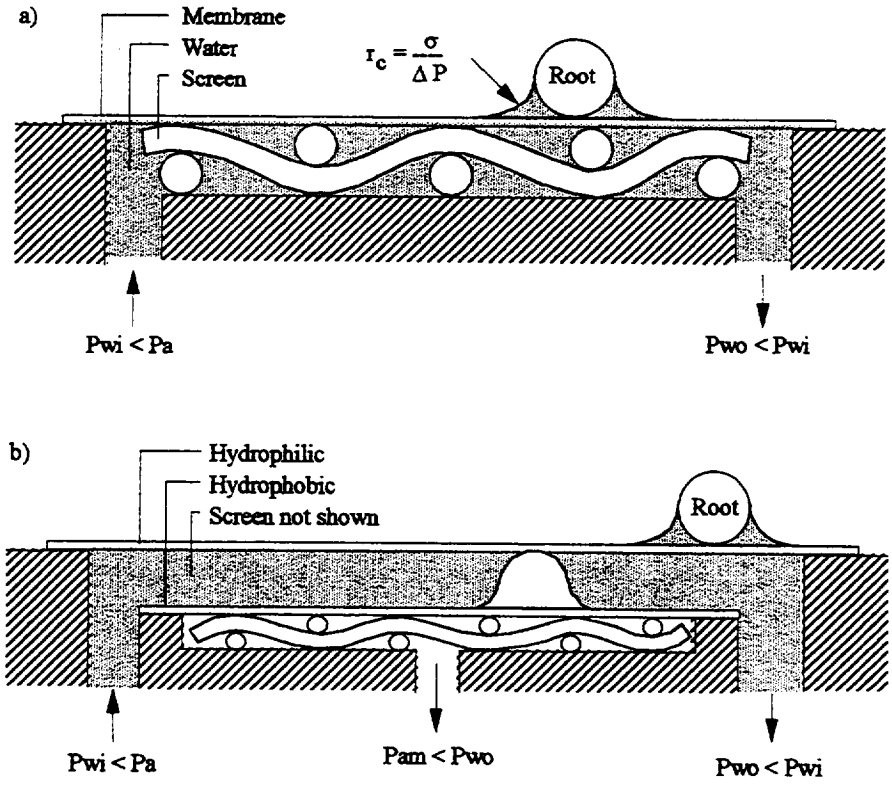

Figure 5.1 Reprints from Wright and Bausch, 1984: (a) A Cross Section Illustrating the Operational Principles of the Capillary Effect Root Environment System and (b) The Hydrophilic/Hydrophobic System for Removing Air Bubbles from the Hydroponic Solution in Micro-Gravity

Several modifications such as the utilization of different materials and altered geometrical designs have been made to this initial design. Problems due to the lack of material durability [Dreschel, et al., 1988; Koontz, et al., 1990] as well as possible leaching of toxic substances or absorption of organic contaminants [Averner, et al., 1987] prompted closer examination of the construction of these systems. Porous stainless steel plates (type 316) mounted on a PVC framework were substituted into the initial design of this system [Koontz, et al., 1990]. This alleviated the lack of durability and allowed for continuous reuse but also introduced the possible absorption of contaminants by the PVC. This can be particularly dangerous in that these contaminants may be released into the nutrient solution or onto the root surfaces [Averner, et al., 1987]. A second problem also arose due to the uneven distribution of nutrient solution leading to localized drying [Bausch and Wright, 1985]. This lead to a further modification of the initial design which utilized two stainless steel plates sandwiched together. The concept behind this design is that the larger pore sized plate (100 microns) would have a more even distribution of solution and could equalize the delivery of nutrients to the smaller pore sized plate (0.5 microns) above it. The top plate acted as the root growth surface while the bulk solution flowed beneath the bottom plate, wetting each plate through capillary action.

A similar adaptation to this original flat plate design utilized two parallel plates oriented with the longitudinal axis of the plant shoot instead of perpendicular [Wright and Bausch, 1984]. Each plate was supplied in a parallel configuration with flowing nutrient solution with the plant roots placed in between. This supplied the necessary aeration while increasing the root growth surface area and, thus, the contact area with nutrient solution. A schematic of this parallel plate design is reprinted in Figure 5.2. This particular CERES configuration was designed to fit into a space shuttle middeck stowage locker [Wright and Bausch, 1984]. In addition to the size limitations and complex flow control, the problem of an uneven distribution of solution also occurred.

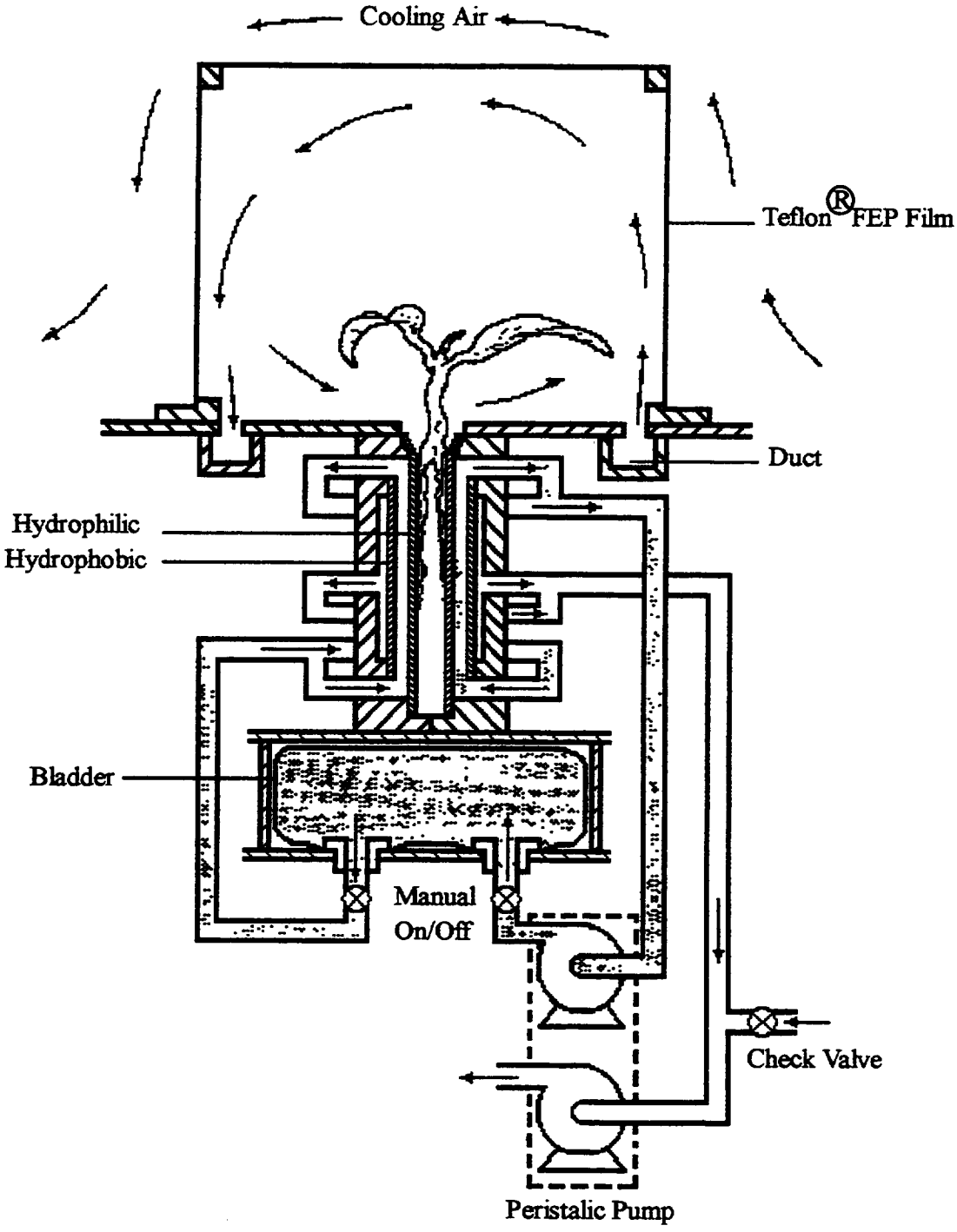

Figure 5.2 Reprint from Wright and Bausch, 1984: Schematic Diagram of a Single Plant Growth Chamber

5.1.3 Tubular CERES Designs

In order to compensate for the uneven distribution of solution, another configuration which utilized a tubular design was conceptualized [Dreschel, et al., 1987; Dreschel, et al., 1988]. The initial construction of this tubular CERES utilized an acrylic (Versapor) membrane material formed into a tube and internally supported by a semi-rigid plastic screen. This cylindrical membrane was then encased in PVC tubing which contained a slot to accommodate emerging plants. The acrylic material provided a more durable construction [Dreschel, et al., 1988] but the PVC casing tended towards the organic contamination discussed earlier [Averner, et. al., 1987]. Other materials tested included porous polyethylene tubes [Dreschel, et al., 1988; Dreschel, 1988; Dreschel, et al., 1990a] and extruded polypropylene tubes [Orbisphere Corporation, 1988]. Exploded views of various generations of this tubular design are reprinted in Figures 5.3 to 5.5.

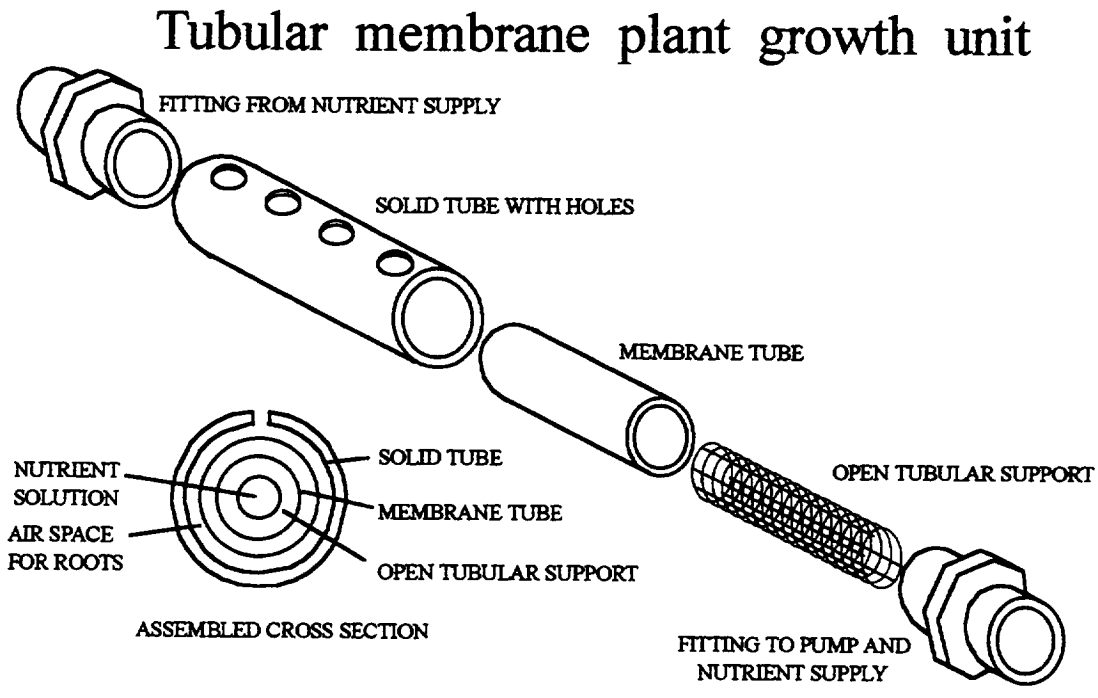

Figure 5.3 Reprint from Dreschel, et al., 1988: Schematic Diagram of the Tubular Membrane Plant Growth Unit (Original Design)

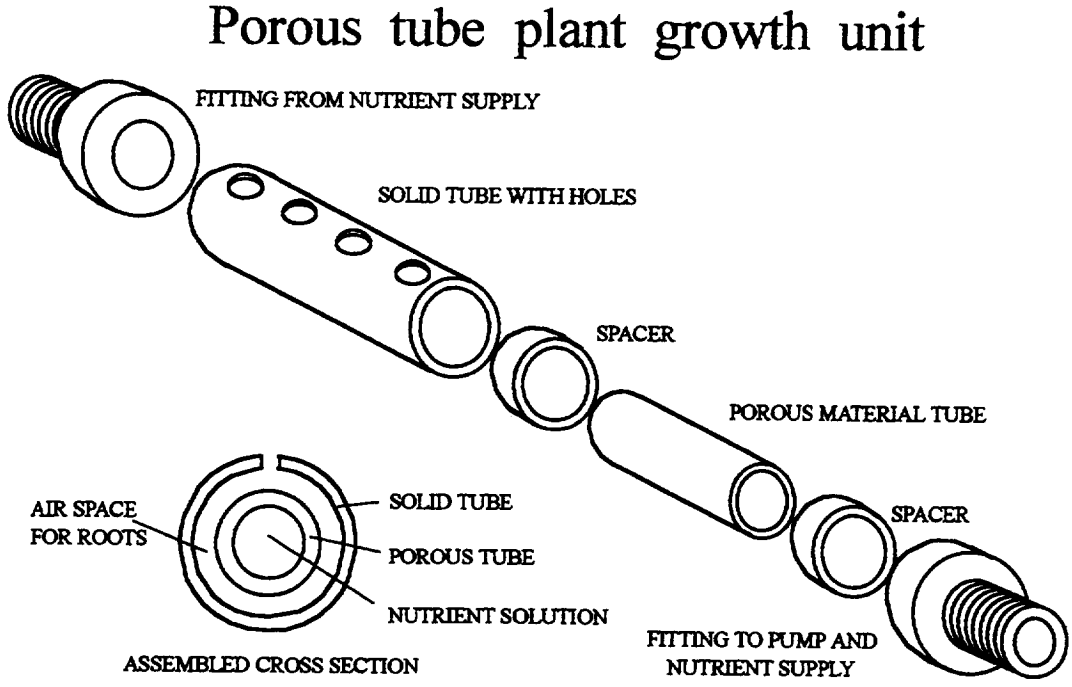

Figure 5.4 Reprint from Dreschel, et al., 1988: Schematic Diagram of the First Design of the Porous Tube Plant Growth Unit

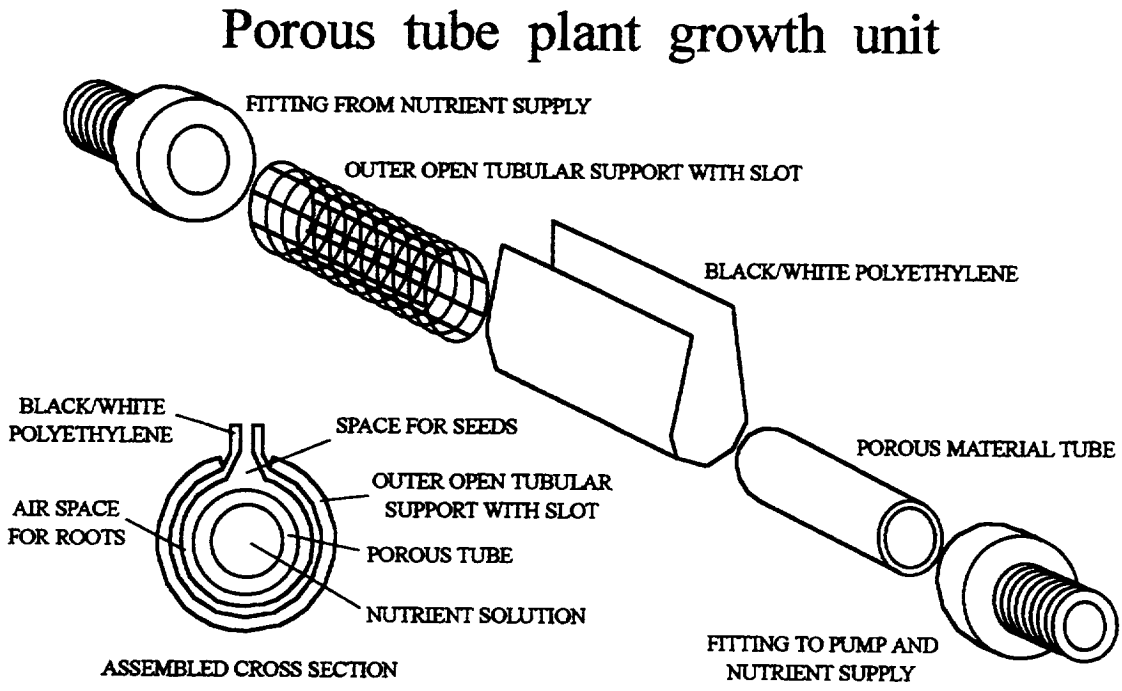

Figure 5.5 Reprint from Dreschel, et al., 1988: Schematic Diagram of the Second Design of the Porous Tube Plant Growth Unit

In addition to the problems involving PVC, further problems arose due to the leaching of toxic substances particularly from black polyethylene. These tubes can release copper and zinc into the nutrient solution [Averner, et al, 1987] and although they are plant nutrients, their concentrations may reach toxic levels. A problem that arose with the polypropylene tubes was that they are naturally hydrophobic. In order to wet these tubes, a surfactant treatment must be performed which can cause complications if done improperly. Of the more recent porous materials tested in this tubular configuration, porous stainless steel (type 316) and ceramic tubes have proven quite successful.

At the Wisconsin Center for Space Automation and Robotics (WCSAR), the stainless steel tubes (30 micron pore size) have been examined in conjunction with a non-organic rooting medium such as arcillite (Montmorillonite clay) which is maintained in direct contact with the tubes [Morrow, et al., 1992]. In this nutrient delivery system, the stainless steel tubes compensate for the fluid handling problems present in a mirogravity environment while the non-organic medium provides a simulated soil environment for the roots. The basic concept behind the external medium is that simultaneous contact of the plant roots with nutrient solution and air can be maintained. In particular, capillary action through the stainless steel tubes and into the soil-like medium will fill the smaller pores while the larger pore will remain open. Thus, the plant roots will obtain the necessary root aeration. The advantages of this system include a rigid, durable tubular construction, an even distribution of liquid, and a root environment similar to soil. The disadvantages are that the extraction of the roots from the medium at harvest may be difficult and time consuming. In addition, the stainless steel which is inherently hydrophobic can introduce possible toxic elements such as chromium and nickel [Koontz, et al., 1990]. Although initial tests with this material revealed only very low levels of these elements, long term or continuous plant growth may cause these levels to reach more deleterious concentrations.

The Porous Ceramic Tube - Nutrient Delivery System (PCT-NDS) which is currently being tested at Kennedy Space Center (KSC) is configured in the same manner as the tubular design given in Figure 5.4. The materials used in the construction of these ceramic tubes are listed as highly purified inorganic oxides and high temperature fluxing

agents [Osmonics, Inc., 1988]. They come in various tube lengths, diameters, and pore sizes (0.30 to 25 microns) which allows for a wide variation in applications. Other advantages include extreme rigidity and durability as well as being hydrophilic in nature [Dreschel, et al., 1988; Dreschel, et al., 1990b]. In addition, plants can be grown with their roots in direct contact with the ceramic tube and do not require an external rooting medium. Thus, the extraction of the plant roots is considerably simplified as compared to the system utilized at WCSAR. As for the release of toxic substances or the interaction with certain nutrients, no definite results have been obtained for this ceramic material.

5.2 Modeling the Porous Ceramic Tube - Nutrient Delivery System

The development of the mathematical model describing the Porous Ceramic Tube - Nutrient Delivery System was accomplished as a separate, yet necessary, portion of this thesis. The results of this development are provided as a background to the development of the nutrient uptake models for plants cultivated on this system. In order to construct the model, a physical description of the "wetness" on the surface of the ceramic tubes was developed [Tsao, et al., 1992]. This was accomplished using empirical observations obtained from a microscope visualizing the surface of the ceramic tubes while water was flowed within. The results of these observations provided a means to diagram the porous material in relation to the water contained inside. This diagram is presented in Figure 5.6, adapted from the original source. Once this physical model of the system was accomplished, the tubular ceramic material was characterized using physical parameters typically used to describe porous media. This lead to the development of the mathematical model based on a force balance describing the interactions between the applied pressure, gravity, and surface tension acting on the water [Tsao, et al., 1992]. Verification of this model was obtained through a series of experiments which subjected the system to static [Tsao, 1993a] and steady state flow conditions [Tsao, 1993b]. These ground based experiments also served as the precursors (controls) for the non-standard gravitational experiments conducted later.

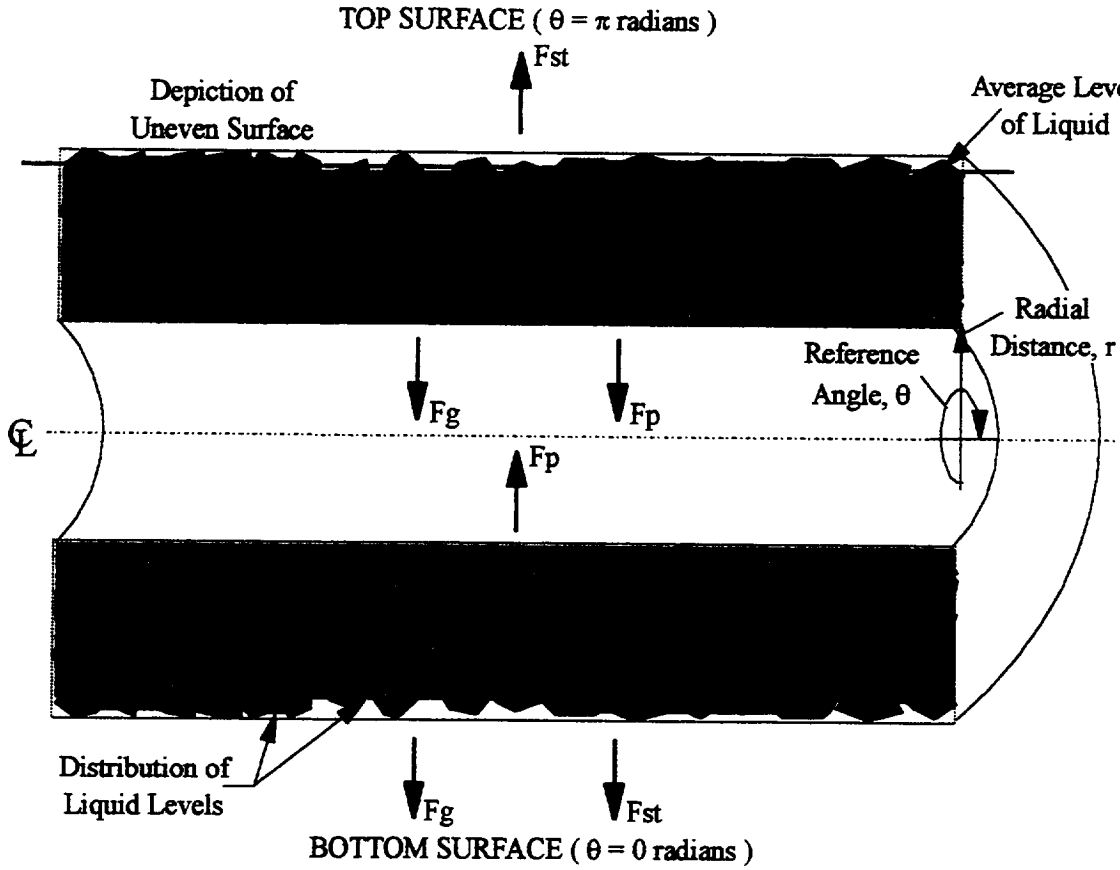

Figure 5.6 Adapted from Tsao, et al., 1992: Developed Physical Model of the Porous Ceramic Tube - Nutrient Delivery System (PCT-NDS)

5.2.1 Characterization of the Porous Ceramic Media

The physical dimensions of the ceramic tubes were measured for each individual tube and are reported in Table 5.1. These include the internal diameter, D_i, external diameter, D_o, length, L, average pore diameter, d, and porosity, ε. On average, each ceramic tube contained internal and external diameters of 1.2 and 1.6 cm, respectively, while the overall lengths averaged 12.7 cm. As for the average pore diameters, these were reported to be 0.30, 0.70, 1.5, and 2.2 microns (= $x10^{-4}$ cm) [Osmonics, Inc., 1988]. Although a pore size distribution was not known for these ceramic tubes, the deviations

listed in Table 5.1 were assumed based on the reported number of significant digits for the average pore diameters. These deviations are utilized in subsequent error propagation.

In order to determine the porosities of these ceramic tubes, the dry weights were compared to the weights of the tubes when completely saturated with water ($\rho = 1$ g/cm^3). This lead to the following average porosities, ε, provided in Table 5.1 for each different pore sized ceramic tube. Included in this table are the standard deviations for the various physical dimensions determined from the entire population of measurements of the individual tubes (5 to 7 tubes per pore size).

Another physical dimension that can be used to characterize the ceramic tubes is the effective diameter, D_e, that liquid can flow within. This parameter is calculated from the total wettable cross-sectional area, A_{wet}, which includes the interior portion of the ceramic tubes as well as the porous spaces in a cross section of the matricies. In order to calculate this total wettable area, the total wettable volume, V_{wet}, divided by the average length of the tubes can be utilized. This quantity is determined from Equation (5.1).

$$A_{wet} = V_{wet} / L = \left[\frac{\pi D_i^2}{4} L + \varepsilon \frac{\pi (D_o^2 - D_i^2)}{4} L\right] / L \qquad (5.1)$$

By defining the wettable cross-section as, $A_{wet} = \pi D_e^2 / 4$, then the effective diameter can be calculated from Equation (5.1). These values are also reported in Table 5.1 along with the propagated errors.

Table 5.1 Average Physical Dimensions of the Ceramic Tubes with Standard Deviations

d (μm)	L (cm)	D_i (cm)	D_o (cm)	D_e (cm)	ε (Unitless)
0.30 ± 0.005	12.74 ± 0.02	1.00 ± 0.10	1.60 ± 0.01	1.29 ± 0.05	0.422 ± 0.012
0.70 ± 0.005	12.71 ± 0.03	1.17 ± 0.06	1.63 ± 0.01	1.40 ± 0.03	0.454 ± 0.018
1.5 ± 0.05	12.75 ± 0.01	1.25 ± 0.04	1.63 ± 0.01	1.47 ± 0.02	0.538 ± 0.016
2.2 ± 0.05	12.74 ± 0.02	1.16 ± 0.06	1.63 ± 0.02	1.45 ± 0.03	0.580 ± 0.020
Averages	12.73	1.16	1.62	———	———

5.2.2 Affecting Forces

Three main forces affect the availability of solution from the PCT-NDS [Tsao, et al., 1992]. These are the surface tension of the solution in the matricies, F_{st}, the applied suction pressure, F_p, and the uni-directional gravity, F_g. The magnitude of the surface tension of water in the radial direction, $\gamma\cos\phi$, is given in units of force per unit length where γ is the surface tension of water (72.75 dyne/cm at 20°C) and ϕ is the contact angle between the liquid and the pore walls [Bromberg, 1984]. These two parameters, respectively, represent the cohesive molecular attraction that water has for itself and the adhesive interaction between the water and the walls of the ceramic pores. Furthermore, this term applies to the contact length between the water and the circumference of the pore spaces in the ceramic material. However, this force is controlled by the regional characteristics of the matrix leading to an average value taken over the entire tube surface and liquid level distributions. Since surface tension pulls the liquid radially outwards, then this force is always positive in terms of a cylindrical coordinate system. As for the magnitude of the force exerted by the applied negative pressure, P_s, this represents the radial pressure differential between the internal and external (atmospheric) pressures. Therefore, this force can be positive or negative depending on whether the pressure causes liquid to move into the center of the ceramic tube (negative) or outwards (positive). The units of this term are measured on a per unit area basis and would be applied to the surface area of the air-liquid interface. Again, this would depend upon the local characteristics of the porous surface. As for the magnitude of the specific gravity, $\rho g\cos\theta$, the total liquid volume within the tube must be used since this term is given in a force per unit volume measure where ρ is the liquid density, g is the gravitational constant (980.6 cm/s^2), and θ is the reference angle to the vertical, established for the uni-directional effects of g. At the top surface of the ceramic tube, gravity causes the liquid to move inward attaining a overall negative value for this force while at the bottom of the tubes, gravity exerts its force outwards leading to a positive force contribution. Therefore, the vertical reference angle, θ, is taken to be 0 radians in the direction of the gravitational vector.

In order to relate all of these forces together, a balance can be performed which would describe the PCT-NDS under static conditions. Before this can be accomplished, the appropriate unit factors must be derived. The volume of liquid contained in the porous ceramic matrix, $V_{void,filled}$, can be expressed as shown in Equation (5.2).

$$V_{void,filled} = \varepsilon(\pi/4)[(D_i + 2h)^2 - D_i^2]L \qquad (5.2)$$

In this Equation (5.2), ε is the porosity, D_i is the internal diameter of the tube, L is the length, and h is the average height of liquid in the porous matricies above the internal diameter. Therefore, if the average height of liquid is at the outer surface, then $(D_i + 2h) = D_o$, the external diameter of the ceramic tubes. Another method which can be used to estimate this parameter utilizes a theoretical number of pores, n_p, and the average diameter of the pores, d. At a given average liquid level in the ceramic tube, $V_{void,filled}$ can be written as follows in Equation (5.3).

$$V_{void,filled} = n_p\pi d^2 h/4 \qquad (5.3)$$

Similarly, the total circumference of all of the pore spaces, $C_{void,filled}$, as well as the total interfacial surface area, $A_{void,filled}$, at this liquid level, h, can be expressed and related to the volume. These are represented in Equations (5.4) and (5.5), respectively.

$$C_{void,filled} = n_p\pi d = 4V_{void,filled} / hd \qquad (5.4)$$

$$A_{void,filled} = n_p\pi d^2/4 = V_{void,filled} / h \qquad (5.5)$$

Under steady state conditions, the sum of the three affecting forces of surface tension, F_{st}, radial pressure differential, F_p, and gravity, F_g, should be equivalent to zero. Therefore, the mathematical model describing this system can be developed from the combination of Equations (5.3), (5.4), and (5.5) with the magnitudes of each force. The simplified results of this model development are presented below in Equation (5.6).

$$[(4\gamma\cos\phi)/hd + P_s/h + \rho g\cos\theta]\varepsilon[(D_i+2h)^2 - D_i^2] + \rho g D_i^2\cos\theta = 0 \qquad (5.6)$$

In this Equation (5.6), D_i is the internal tube diameter, d is the average pore diameter, and ε is the tube porosity. For the properties of water, ρ is the density (1.0 g/cm^3) and γ is the surface tension (72.75 dyne/cm). Furthermore, $4\gamma\cos\phi$ equals the surface tension of water within the porous matricies, P_s is the applied suction pressure, and $\rho g\cos\theta$ represents the gravitational force where θ is the vertical reference angle. Each of these forces contributes to a steady state value for the average height of liquid in the matricies, h, as well as the contact angle between the liquid and the porous material, ϕ.

During the derivation of Equations (5.3) and (5.5), used in the model equation, the air-liquid interface was taken as perpendicular to the pore walls. This surface is actually a curved meniscus with a contact angle, ϕ. Therefore, the surface area of the air-liquid interface, $A_{void,filled}$, and filled matrix volume, $V_{void,filled}$, should be larger than indicated in these equations. However, since the ceramic tubes that are used in this hydroponic system are originally designed for ultrafiltration [Osmonics, Inc., 1988], the reported average pore diameters, d, actually represents the maximum pore size. Therefore, the use of the maximum pore diameter in these two equations can compensate for the under-predictions used in the derivations. This leads to rough estimates of these two quantities. Similarly for the circumference of wetted pore spaces, $C_{void,filled}$, derived in Equation (5.4), this quantity was taken as a two dimensional measure where in reality, it depends upon the contours of the local matricies. Therefore, this quantity also represents a rough estimate since the maximum pore diameter partially compensates for this assumption.

Under micro-gravitational conditions, the magnitude of this force becomes negligible compared to the applied suction pressure and surface tension forces. Therefore, the model equation can be reduced to a direct relationship between P_s and $\gamma\cos\phi$. Furthermore, under constant gravitational situations such as here on Earth, the model equation directly relates pressure and surface tension but with a constant term. Therefore, assuming either of these conditions, the shape and height of the meniscus (ϕ and h) are only dependent upon the radial pressure differential and the properties of the liquid in the matricies. An example of this dependency is the analogous situation that occurs when liquid is drawn into and out of a syringe changing the shape and height of the meniscus.

5.3 Verification of the Model Equation

The verification of the model equation presented earlier in Equation (5.6) was accomplished through two sets of experiments involving static (no flow) and steady state flow conditions. In the static experiments, the operational limits of weeping and cavitation were defined theoretically from the model equation with only the weeping limit verified experimentally. This particular operational limit is of more interest in terms of the standard operation of the PCT-NDS as well as for the cultivation of plants. As for the steady state flow experiments, the effect of pressure drop and the frictional losses through the ceramic tubes were examined. This was accomplished by comparing mechanical energy balances taken at specific points along the fluid circuit and determining the inlet and outlet pressures with the resulting heights and contact angles obtained from the model equation.

5.3.1 Operational Limits - Static Experiments

The first type of experiment that were conducted to verify the model equation for the PCT-NDS were performed under static conditions [Tsao, 1993a]. These experiments were utilized to verify the operational limits for the system based on the theoretical limits derived from the model equation. Specifically, these conditions are known as weeping and cavitation and can be quantified through the applied suction pressure, P_s. The basic theory behind the operational limits for this system is illustrated in Figure 5.7 where idealized pores are experiencing different applied suction pressures.

The variations in pressures shown in Figure 5.7 include the theoretical operational limit of weeping where the applied pressure differential, $P_s = P_w$, is not large enough to contain the liquid in the porous matricies. This is depicted at the far left of Figure 5.7. Under this condition, liquid is about to exit the matricies; thus, the height of liquid, h, is at the outer surface of the ceramic tubes where $h \geq (D_o - D_i)/2$ and the contact angle, ϕ, is just equal to or slightly greater than $\pi/2$ radians or $\cos\phi \leq 0$. In order to quantify the weeping pressure, P_w, the two equivalent values for h and ϕ can be substituted into the model equation. Solving for the internally applied pressure yields Equation (5.7).

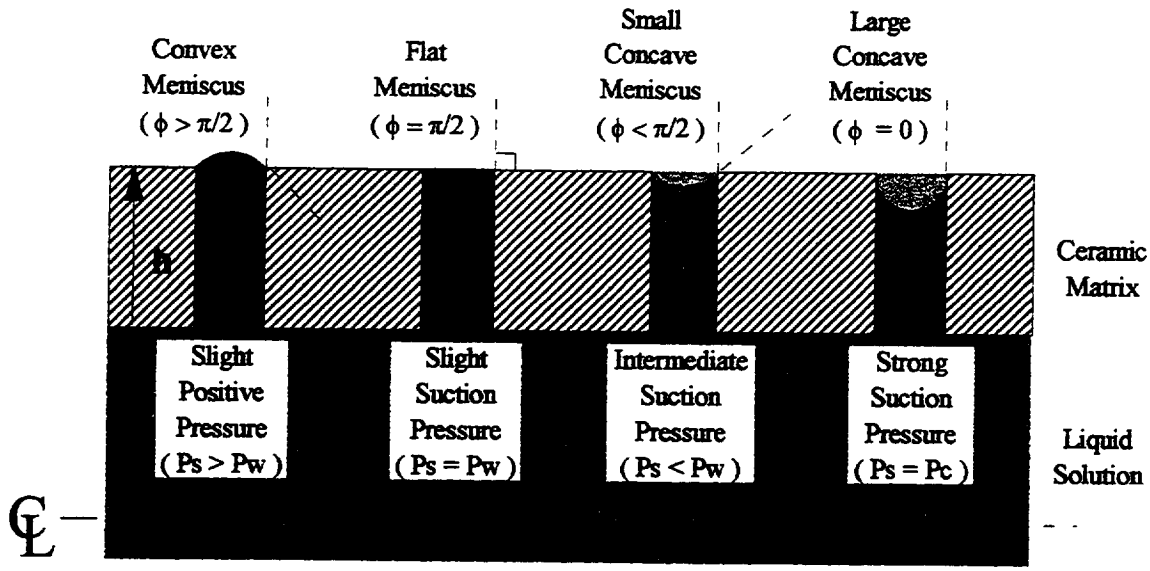

Figure 5.7 Average Height of Liquid (h) and Contact Angle (ϕ) within Idealized Ceramic Pores of Diameter, d, Experiencing Various Internally Applied Pressures (P_s = Applied Pressure, P_w = Weeping Pressure, P_c = Cavitation Pressure)

$$P_w = \frac{-\rho g(D_o - D_i)}{2}\left\{\frac{D_i^2}{\varepsilon[D_o^2 - D_i^2]} + 1\right\} \qquad (5.7)$$

During the derivation of Equation (5.7), the reference angle to the vertical was taken to be 0 radians ($\cos\theta = +1$) since the weeping of liquid would first occur out of the bottom of the ceramic tubes, in the same direction as the gravitational vector. It should be noted that the values for the weeping pressure limits are negative as indicated in Equation (5.7).

Similarly, the other theoretical operational limit of cavitation is shown on the far right of Figure 5.7 where the suction pressure in the interior, $P_s = P_c$, is so great that air is pulled into the matricies and eventually into the interior of the ceramic tube. Under this condition, the contact angle is equal to 0 radians ($\cos\phi = 1$) and the height is equal to or less than $(D_o - D_i - d)/2$ where d/2 represents the radius of curvature of a perfect air bubble forming in the matricies. Substituting these values into the model equation and solving for the applied pressure gives the following result. Furthermore, since the average diameter of the pores, d, is relatively small compared to the internal and external diameters, $D_o > D_i$

>>> d, then the first term in Equation (5.8) can be approximated with the weeping pressure, P_w. This approximation is shown as well.

$$P_c = \frac{-\rho g[(D_o-D_i)-d]}{2}\left\{\frac{D_i^2}{\varepsilon[(D_o-d)^2-D_i^2]} + 1\right\} - \frac{4\gamma}{d} \cong P_w - 4\gamma/d \qquad (5.8)$$

During the derivation of Equation (5.8), the reference angle to the vertical was taken to be π radians ($\cos\theta = -1$) since the cavitation of air into the liquid would first occur at the top of the ceramic tubes. It should be noted that the values for P_c are also negative.

Since both of these conditions depend upon the physical dimensions of the ceramic tubes (D_o, D_i, d, ε), the average values presented earlier in Table 5.1 were utilized. Substituting the values from this table into Equations (5.7) and (5.8), along with the gravitational constant, $g = 980.6$ cm/s^2, and the surface tension of water, $\gamma = 72.75$ dyne/cm (at 20 °C), yields the following theoretical weeping and cavitation pressures presented in Table 5.2 along with the associated the propagated errors.

Table 5.2 Theoretical Weeping and Cavitation Pressures Determined from the Average Physical Dimensions of the Ceramic Tubes and the Model Equation

d (μm)	$P_s = P_w$ (cm.H_2O)	$P_s = P_c$ (atm)
0.30 ± 0.005	-0.76 ± 0.03	-9.6 ± 0.16
0.70 ± 0.005	-0.77 ± 0.02	-4.1 ± 0.03
1.5 ± 0.05	-0.69 ± 0.02	-1.9 ± 0.06
2.2 ± 0.05	-0.65 ± 0.02	-1.3 ± 0.03

Since the radial pressure differentials required to cause cavitation could only be achieved using an external pressure greater than one atmosphere, these values were not verified experimentally. Furthermore, the pressure at which dissolved air would be pulled out of water ranges from -0.07 to -0.1 MPa (depending on altitude) which occurs prior to the cavitation pressures. Since the optimum cultivation of plants on the PCT-NDS would require the least amount of resistance to nutrient and water transport, only the operational

limit of weeping was verified experimentally. This was accomplished under static conditions by loading the ceramic tubes with water, sealing both ends, and allowing the liquid to weep while a gauge measured the pressure changes internally. When equilibrium was achieved between the various forces, the internal pressure was measured representing the limit for which the tubes could be operated while preventing liquid from weeping out of the matricies. The results of these experiments, conducted only on 0.30, 0.70, and 2.2 micron tubes, are presented in Table 5.3 along with the standard deviations calculated from 3 replicated results per ceramic tube (2 or 3 tubes per pore size).

Table 5.3 Comparison of Experimental ($P_{w,\,expt}$) and Theoretical ($P_{w,\,theo}$) Weeping Pressure Limits for Various Pore Sized Ceramic Tubes

d (cm)	$P_{w,\,theo}$ (cm.H_2O)	$P_{w,\,expt}$ (cm.H_2O)
0.00003	-0.76 ± 0.03	-0.62 ± 0.11
0.00007	-0.77 ± 0.02	-0.67 ± 0.10
0.00022	-0.65 ± 0.02	-1.02 ± 0.11

5.3.2 Pressure Drop Effects - Steady State Flow Experiments

Since the values of the critical operational limits for the various pore sized ceramic tubes presented in Table 5.3 are relatively small in magnitude, maintaining an operational pressure which is slightly smaller than -1 cm.H_2O should be sufficient for the standard operation of the PCT-NDS. In order for the optimum growth of plants on the system yielding the least amount of resistance to nutrient transport, the system should be operated as close to weeping conditions as possible. However, when nutrient solution is circulated through the ceramic tubes by connecting to a fluid circuit, a pressure drop will occur along the length of the tubes. This pressure drop dictates that only one point along the tube length can be maintained at the operational limit of weeping (i.e. at the tube entrance).

In order to quantify the pressure drop that occurs during the flow of solution through the ceramic tubes, steady state flow experiments were conducted [Tsao, 1993b].

Each ceramic tube was connected to a fluid circuit using modified rubber connectors attached to 16-gauge Norprene tubing (internal diameter, D_s = 0.312 cm). Within this fluid circuit contained a stoppered 500 ml graduated cylinder as a reservoir, a variable speed suction pump (Cole-Parmer L-07553-20) with a standard 16-gauge Masterflex pump head (Cole-Parmer L-07016-20) located downstream of the ceramic tube, and two pressure gauges (Dwyer Instruments 2003C and 2015C). These gauges measured the pressures upstream and downstream of the ceramic tubes and were located at a know distance, L_s = 6.4 cm, from the tube entrance and exit. By measuring the pressures at these reference locations (upstream, P_1, and downstream, P_2) at a set volumetric flow rate, Q_z, the pressures at the ends of the ceramic tubes (entrance, P_0, and exit, P_L) could be determined through a trial and error calculation procedure. This determination had to take into account the frictional losses that existed within the system between the respective pressure points (between P_1 and P_0 and between P_L and P_2). These pressure points are illustrated in Figure 5.8 along with the definitions of the relevant parameters. Once the pressures, P_0 and P_L, were determined, friction factors for the ceramic tubes, f(c), were determined.

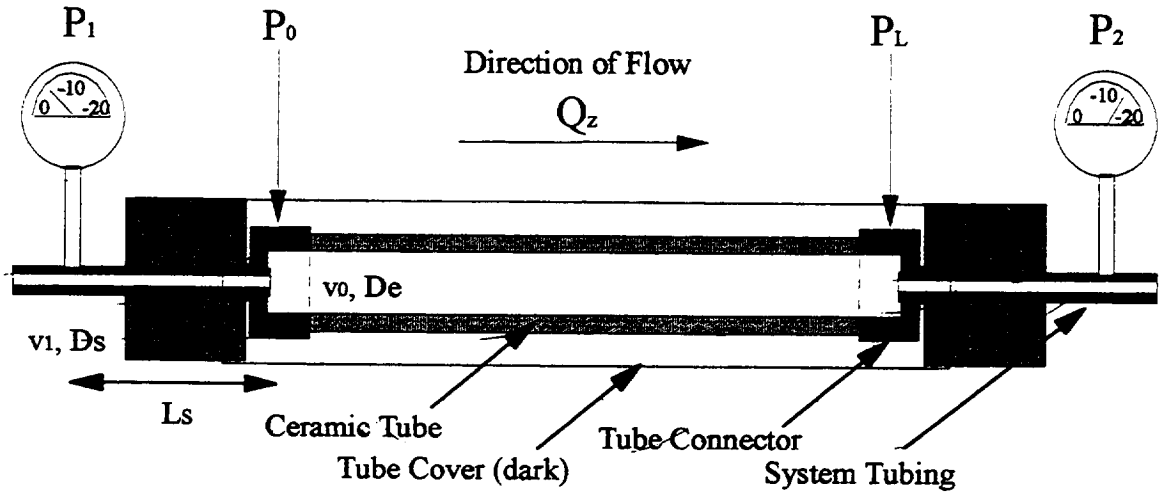

Figure 5.8 Measured (P_1 and P_2) and Calculated (P_0 and P_L) Pressures for the Ceramic Tubes Connected to a Fluid Circuit

For the upstream end of the ceramic tubes (subscripts: A = 1 and B = 0), the frictional losses, ΣF, that were taken into account included the flow through the system tubing of length, L_s, and diameter, D_s, at a flow velocity of $v_{1,av}$, and the sudden expansion between the system tubing and the wetted portion of the ceramic tube entrance. Similarly, for the downstream end of the ceramic tube (subscripts: A = 2 and B = L), the frictional losses also included the flow through the system tubing at a flow velocity of $v_{2,av}$ (= $v_{1,av}$) but contained a sudden contraction instead of an expansion in the flow conduit between the wetted ceramic exit and system tube. Using the general mechanical energy balance shown in Equation (5.9), the pressures at the ceramic tube ends, P_0 and P_L, were determined in terms of the volumetric flow rate, Q_z, and the reference pressures, P_1 and P_2, respectively. During these calculations, the flow velocities within the ceramic tube, $v_{0,av}$ and $v_{L,av}$, respectively, as well as within the system tubing, $v_{1,av}$ and $v_{2,av}$, were converted into volumetric terms. These were accomplished using the effective tube diameters, D_{e0} and D_{eL}, respectively, and the diameter of the system tubing, D_s.

$$\frac{1}{2\alpha}(v_{B,av}^2 - v_{A,av}^2) + g(h_B - h_A) + \frac{P_B - P_A}{\rho} + \Sigma F + W_{pump} = 0 \qquad (5.9)$$

For these steady state flow experiments, the ceramic tubes were oriented horizontally indicating that the gravity term, $g(h_B - h_A)$, equaled zero and since no pump was located between the pressure points, then the work term, W_{pump}, equaled zero as well. The range of volumetric flow rates, Q_z, used during these experiments were from 2.4 to 3.4 ml/s (Reynold's numbers, N_{Re}, for the system tubing of diameter, D_s, and length, L_s, from 980 to 1390). Therefore, for the friction factors, $F_f(s)$, for the flow through the sections of system tubing, the laminar flow equation of Hagen-Poiseuille was utilized [Geankoplis, 1983]. This is shown in Equation (5.10) below where the density, ρ, and viscosity, μ, of the fluid were taken for water (1.0 g/cm^3 and 0.01 g/cm.s, respectively).

$$F_f(s) = \Delta P/\rho = 128\frac{\mu L_s Q_z}{\rho \pi D_s^4} \qquad (5.10)$$

As for the sudden expansion, $F_f(ex)$, and contraction, $F_f(cn)$, in the flow conduit, the following frictional losses based on Fanning friction factors were used [Geankoplis, 1983]. Since laminar flow conditions existed, then the flow characteristic term, α, was set equal to 1/2 ($\alpha = 1$ for turbulent flow) in both Equations (5.11) and (5.12).

$$F_f(ex) = (1 - D_s^2/D_{e0}^2)^2 \frac{8Q_z^2}{\alpha\pi^2 D_s^4} \tag{5.11}$$

$$F_f(cn) = 0.55(1 - D_s^2/D_{eL}^2) \frac{8Q_z^2}{\alpha\pi^2 D_s^4} \tag{5.12}$$

Substituting Equations (5.10) and (5.11) into the general mechanical energy balance yields a relationship between the measured upstream pressure, P_1, and the pressure at the ceramic tube entrance, P_0. Similarly, combining Equations (5.10) and (5.12) with Equation (5.9) gives a relationship between the measured downstream pressure, P_2, and the pressure at the ceramic tube exit, P_L. The resulting Equations (5.13) and (5.14) are presented below where all parameters are as defined earlier.

$$P_0 = P_1 - \left[\frac{16Q_z^2}{\alpha\pi^2 D_{e0}^2}\left(\frac{1}{D_{e0}^2} - \frac{1}{D_s^2}\right) + \frac{128\mu L_s Q_z}{\rho\pi D_s^4}\right]\rho \tag{5.13}$$

$$P_L = P_2 + \left[\frac{8Q_z^2}{\alpha\pi^2}\left(\frac{1}{D_s^2} - \frac{1}{D_{eL}^2}\right)\left(\frac{1.55}{D_s^2} + \frac{1}{D_{eL}^2}\right) + \frac{128\mu L_s Q_z}{\rho\pi D_s^4}\right]\rho \tag{5.14}$$

Since the effective diameters, D_{e0} and D_{eL}, depend upon the wetted cross-sectional area within the matricies, then these parameters depend on the average heights of liquid in the ceramic matricies at their respective locations, denoted as h_0 and h_L, respectively. In order to calculate the corresponding effective diameters, Equation (5.1) was modified by replacing D_o with $(D_i + 2h)$ where $h = h_0$ or h_L as shown in Equations (5.15) and (5.16).

$$D_{e0} = \{D_i^2 + \varepsilon[(D_i + 2h_0)^2 - D_i^2]\}^{1/2} \tag{5.15}$$

$$D_{eL} = \{D_i^2 + \varepsilon[(D_i + 2h_L)^2 - D_i^2]\}^{1/2} \quad (5.16)$$

In order to calculate h_0 and h_L, Equation (5.6) was utilized. Since this model equation also depends upon the applied suction pressures at the respective ceramic tube ends, then the calculations of P_0 and P_L became trial and error procedures. During these calculations, the assumption that the cosine of the contact angle, $\cos\phi$, is linearly related to the applied suction pressures was used. This is shown in Equation (5.17) where it has been previously assumed that $\cos\phi = 0$ when $P_s = P_w$ and $\cos\phi = 1$ when $P_s = P_c$.

$$\cos\phi = \frac{P_s - P_w}{P_c - P_w} \quad (5.17)$$

Therefore, initial pressures were guessed for P_0 and P_L and substituted into the model equation, combined with Equation (5.17), in order to calculate h_0 and h_L, respectively. Once these values were obtained, D_{e0} and D_{eL} were determined from Equations (5.15) and (5.16). Substituting these diameters into Equations (5.13) and (5.14), respectively, yielded values for P_0 and P_L. Upon comparing these calculated results with the initial guesses, convergences were determined using the accuracy of the pressure measurements (P_1 and P_2) as criterion. When convergence was not satisfied, the average values between the guessed and calculated pressures were used as the initial guesses for the next iterations.

The measured pressures and corresponding pressures calculated through trial and error for the ceramic tube entrance and exit are presented in Table 5.4 for the volumetric flow rates tested and average pore diameters of 0.30, 0.70, and 2.2 microns. For the measured pressures, the standard deviations (convergence criteria) are reported for 12 replicated results for each ceramic tube while the propagated errors are presented for the calculated pressures. The standard deviations for the measured volumetric flow rates used in the propagated errors were determined to be $\pm$ 0.04 for Q_z = 2.4 ml/s and $\pm$ 0.01 for Q_z = 3.4 ml/s. From the propagated errors, it can be seen that the deviations in the measured pressures are the major contribution. Therefore, the assumption that α, μ, ρ, L_s, and D_s were constant in these calculations was reasonable.

Table 5.4 Measured (P_1 and P_2) and Calculated (P_0 and P_L) Pressures at Various Volumetric Flow Rates, Q_z, for Different Pore Sized Tubes

Pore Size (μm)	Flow Rate Q_z (ml/s)	Measured P_1 (cm.H_2O)	Calculated P_0 (cm.H_2O)	Calculated P_L (cm.H_2O)	Measured P_2 (cm.H_2O)
0.30	2.4	-1.46 ± 0.33	-2.02 ± 0.33	-6.76 ± 2.48	-8.96 ± 2.48
	3.4	-14.3 ± 2.2	-15.0 ± 2.2	-28.8 ± 4.9	-32.8 ± 4.9
0.70	2.4	-1.11 ± 0.62	-1.69 ± 0.62	-4.56 ± 1.39	-6.76 ± 1.39
	3.4	-16.8 ± 1.5	-17.6 ± 1.5	-29.0 ± 2.0	-33.0 ± 2.0
2.2	2.4	-1.67 ± 0.27	-2.25 ± 0.27	-4.65 ± 0.62	-6.85 ± 0.61
	3.4	-18.2 ± 0.9	-19.0 ± 0.9	-29.4 ± 1.7	-33.4 ± 1.7

Using the differences between the experimental values for P_0 and P_L, representing the pressure losses associated with the flow through the ceramic tubes, allows for the determination of friction factors, f(c). These factors, defined as the shear stress at the surface (pressure drop times cross sectional area per wetted surface area) divided by density times velocity head, can be determined from Equation (5.18) [Geankoplis, 1983]. The results of these calculations are presented in Figure 5.9 along with the results obtained for flow rates of 7.1 ± 0.21 and 8.1 ± 0.24 ml/s. These two latter flow rates are within the transition range between laminar and turbulent flows ($2900 < N_{Re} < 3300$ for $D_s = 0.312$ cm) and are, therefore, presented with some skepticism. The error bars presented in this figure represent the propagated errors for f(c).

$$f(c) = \frac{\Delta P_f \pi R_e^2}{2\pi R_e \Delta L} \Big/ \frac{\rho v^2}{2} = \frac{(P_0 - P_L)\pi^2 D_e^5}{32 \rho L Q_z^2} \qquad (5.18)$$

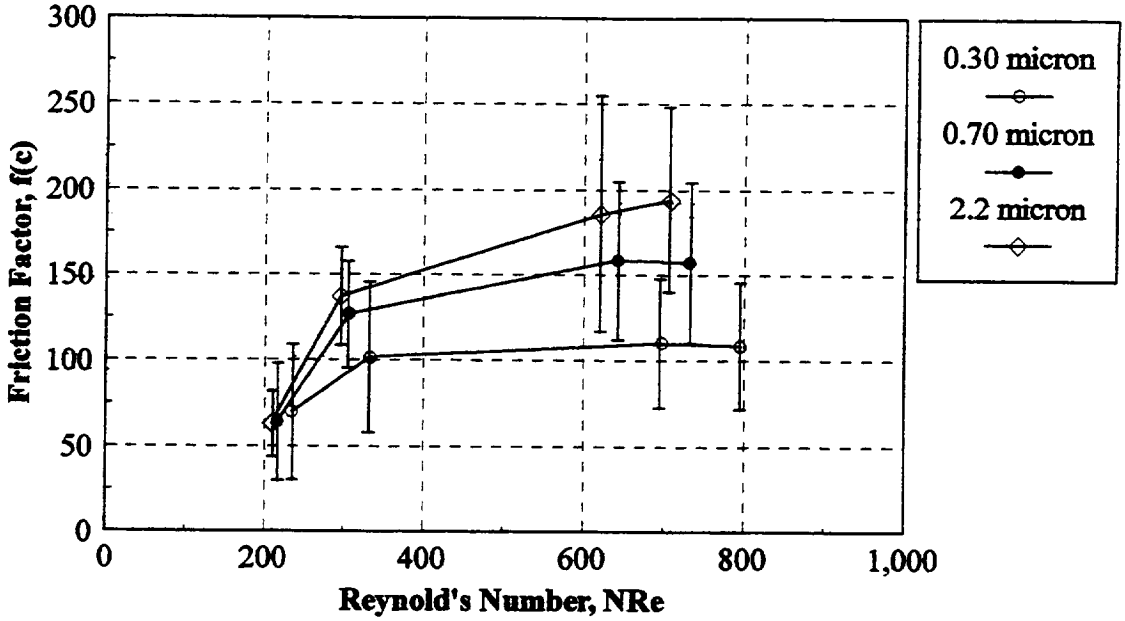

Figure 5.9 Friction Factors, f(c), as a Function of Reynold's Number, N_{Re}, Characterizing the Various Pore Sized Ceramic Tubes

5.4 System Control

With the model verification complete, a suitable control equation was developed based on the mechanical energy balance taken at the ceramic tube entrance. This was presented in Equation (5.13). In order to verify the applicability of this control equation, the PCT-NDS was subjected to dynamic gravitational conditions using NASA's KC-135 flight facilities [Dreschel, et al., 1993; Tsao, 1994]. This specially modified cargo plane produced a parabolic flight path which simulated gravities ranging from near-zero to twice standard gravity. Furthermore, this control equation was implemented under hyper-gravitational situations upto 10 g's using a small scale centrifuge to impart an artificial gravitational field [Tsao, et al., 1996]. Verification of the control equation was obtained from the results of both sets of experiments.

5.4.1 Theoretical Development

Theoretical control of the moisture availability at the outer ceramic tube surface was illustrated in Figure 5.7 where different applied suction pressures altered the average height of liquid, h, and the contact angle, ϕ, between the liquid and the porous matricies. The variations in pressures shown included the theoretical operational limit of weeping (second from left) where the applied pressure differential from atmospheric, $P_s = P_w$, is just enough to contain the liquid in the porous matricies. During the cultivation of plants on the PCT-NDS, the least amount of resistance to nutrient transport from the system into the plant roots will be desired [Dreschel and Sager, 1989; Tsao, et al., 1994]. In order to obtain optimum water availability at the tube outer surface for plant growth, the applied pressure should be maintained as close to weeping conditions as possible. This operational limit was previously derived in Equation (5.7).

Since the flow of liquid down the length of the ceramic tubes requires a pressure drop, then only one point can theoretically be controlled at this near weeping condition. Specifically, this point can only exist at the entrance of the ceramic tube; thus, the pressure at the ceramic tube entrance, P_0, should be maintained at the weeping pressure, P_w. In order to develop a control equation for this condition, the mechanical energy balance obtained for the ceramic tube entrance derived earlier in Equation (5.13) can be combined with the weeping pressure limit. By setting P_0 in Equation (5.13) to P_w of Equation (5.7) and solving for P_1, a control equation for the optimum operation of the PCT-NDS can be derived which is based on controlled flow rate, Q_z, and the effective gravitational force, g. Therefore, as g changes, the flow rate can be used to maintain a constant upstream pressure with optimum (near-weeping) conditions existing at the ceramic tube entrance. This control equation is shown in Equation (5.19) below.

$$P_1 = \frac{-\rho g(D_o - D_i)}{2}\left\{\frac{D_i^2}{\varepsilon[D_o^2 - D_i^2]} + 1\right\} + \left\{\frac{16Q_z^2}{\alpha\pi^2 D_{e0}^2}\left(\frac{1}{D_{e0}^2} - \frac{1}{D_s^2}\right) + \frac{128\mu L_s Q_z}{\rho\pi D_s^4}\right\}\rho \qquad (5.19)$$

5.4.2 Dynamic Control - KC-135 Parabolic Flight Experiments

Since the PCT-NDS was conceived to circumvent the problems of fluid handling under non-standard gravitational situations [Dreschel, et al., 1988], this system was tested by NASA using the KC-135 parabolic flight facilities at Johnson Space Center, TX. on 20-21 October, 1992 [Dreschel, et al., 1993]. A typical parabolic profile subjected the system to gravities ranging from near-zero to twice standard as illustrated in Figure 5.10.

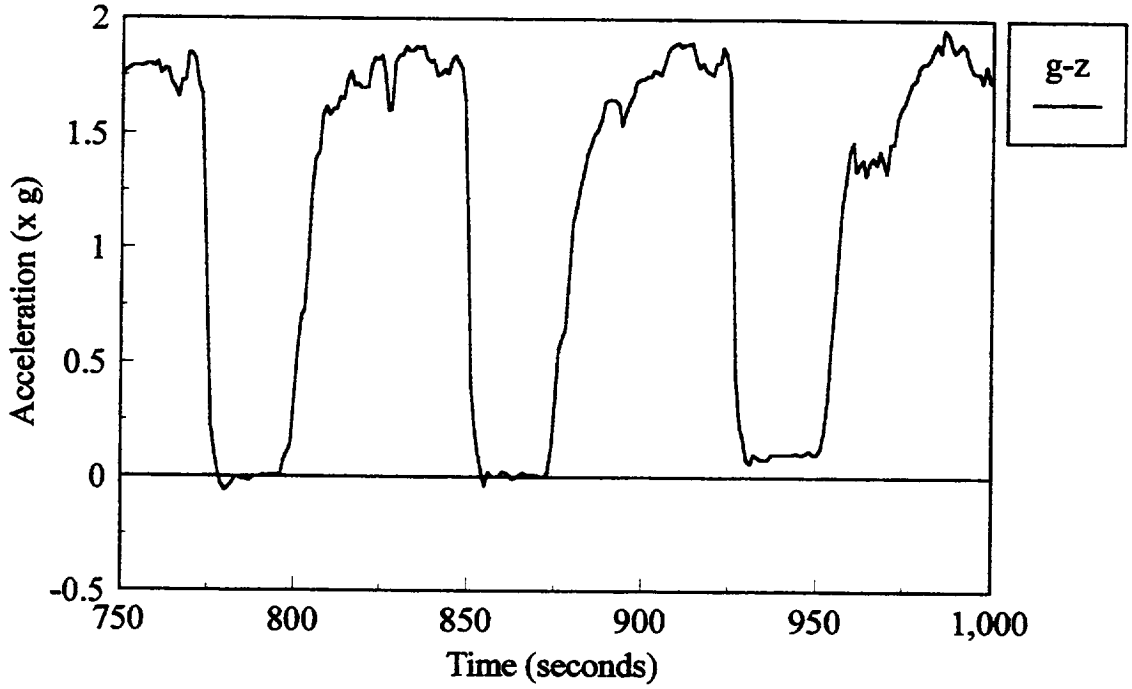

Figure 5.10 Effective Gravitational Accelerations, g_z, during a KC-135 Parabolic Flight

A schematic outline of the Test Bed Units (TBU) used during these experiments is reprinted in Figure 5.11 [Dreschel, et al., 1993]. Specifically, each TBU consisted of a pump (Q_z = 100 to 150 ml/min), ceramic tube (pore size, d = 0.30, 0.70, or 2.2 μm), Water Availability Sensor (WAS), upstream and downstream pressure transducers, flow meter, manual flow control valve, and a Water Delivery System (WDS) each bolted to an aluminum base plate. These components were connected in a fluid circuit attached through 1/4" stainless steel tubing (D_s = 0.46 cm) and fittings. Surrounding the ceramic tubes were Plexiglas shrouds which insured the containment of any liquid weeped from the surfaces.

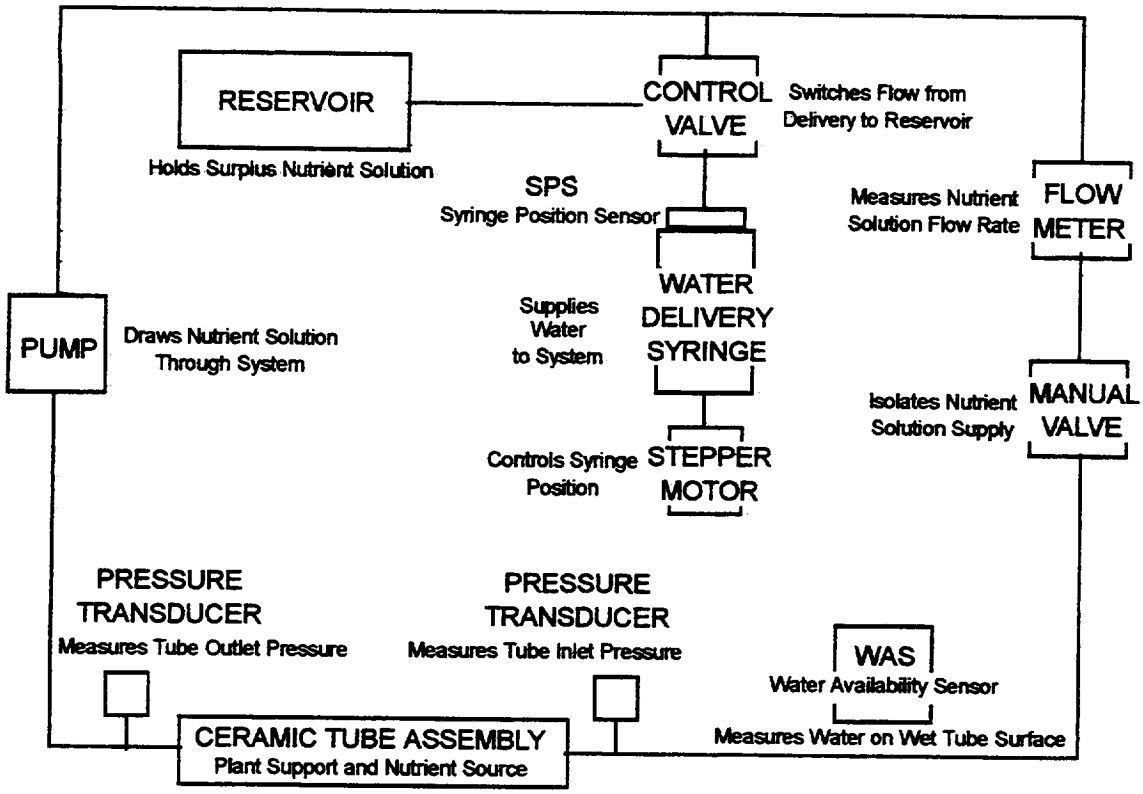

Figure 5.11 Reprint from Dreschel, et al., 1993: Schematic Diagram of One of the Porous Tube Plant Nutrient Delivery System Test Bed Units (TBU)

The three TBU's used during these flight missions were continually monitored through a data acquisition system which measured time, temperature, WAS voltages (1 channel per TBU), upstream and downstream pressures, and the effective vertical (z-direction) gravitational force during each of the three sorties flown. For the total quantity of liquid within the entire system, the WDS for these experiments contained a water delivery syringe attached to a stepper motor with a potentiometer (POT) used to monitor the relative position of the syringe piston. As the POT voltage changed, water was injected or withdrawn from the system, changing the height of liquid in the porous matricies. Three additional data acquisition channels were used to measure the POT voltages for each of the TBU's. The total amount of data acquired consisted of the three TBU's flown during three sorties which consisted of four parabolic sets of 12 to 13 parabolas each (a total of 147 parabolas).

Although this mission was not explicitly flown to test the control equation but to examine the capabilities of the ceramic tube system itself [Dreschel, et al., 1993], the data acquired during this mission was used for verification purposes. Specifically, the inlet pressure readings as illustrated in Figure 5.12 were entered into Equation (5.19) as P_1 along with the appropriate values for D_{e0}, D_s, L_s, Q_z, α, μ, and ρ to calculate corresponding values for the pressure at the ceramic tube entrance, P_0. These pressures (P_0) were then compared to the gravity dependent weeping pressures (P_w) as defined in Equation (5.7). When the values for P_0 from Equation (5.19) were smaller in magnitude (i.e. less negative) than P_w of Equation (5.7) then weeping occurred as predicted by the control equation. Therefore, confirmation of weeping would verify the control equation for the PCT-NDS subjected to dynamic gravity changes between near-zero and 2 g's from a KC-135 parabolic flight mission.

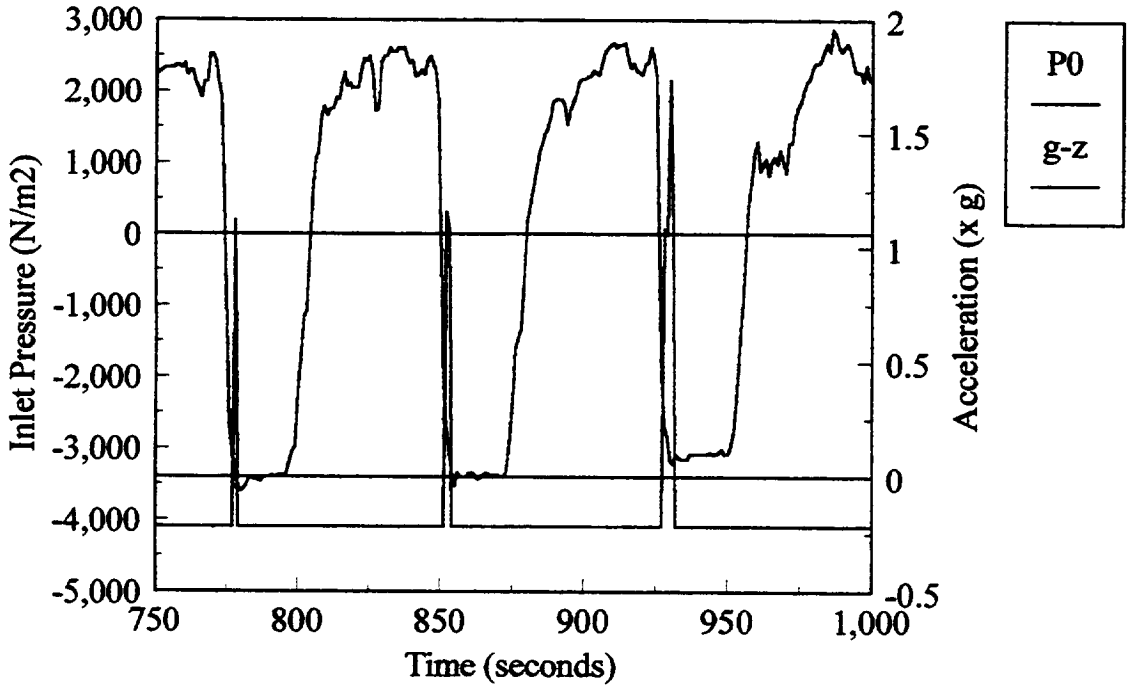

Figure 5.12 Inlet Pressure Measurements during a KC-135 Parabolic Flight

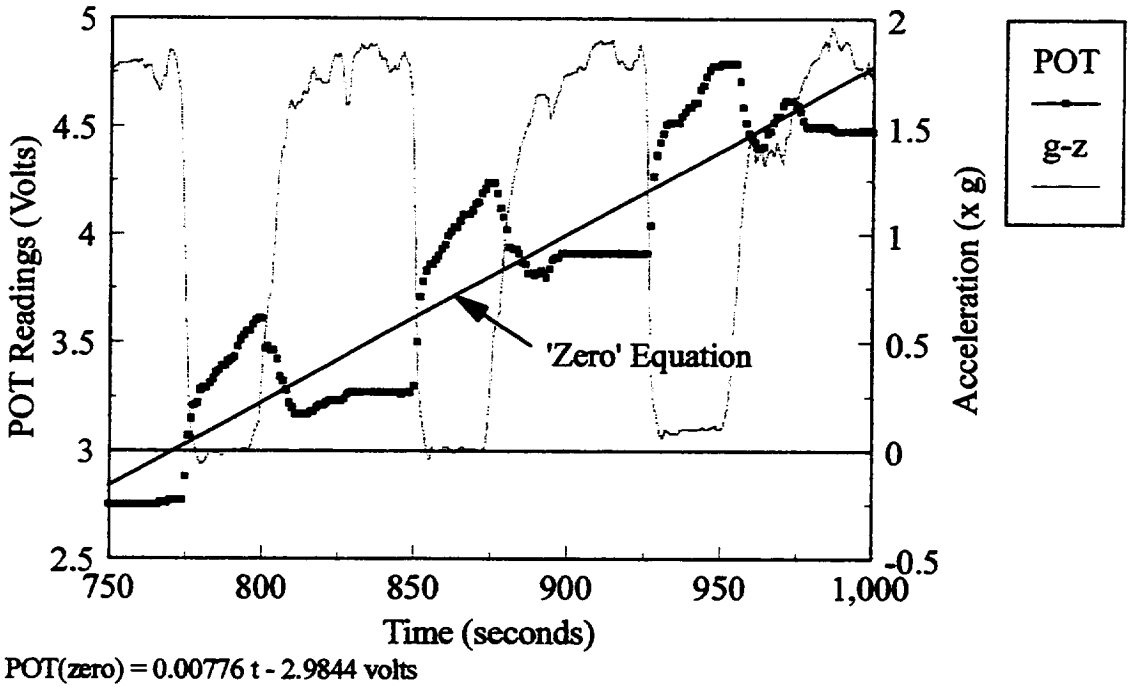

Figure 5.13 Potentiometer (POT) Readings during a KC-135 Parabolic Flight with 'Zero' Equation Used for Standardization

This confirmation was obtained using the POT readings as illustrated in Figure 5.13 which shows an increasing trend in POT readings illustrating that water was continuously injected into the system in order to replace the weeped water. After these POT readings were standardized using 'zero' equations derived from the average values determined over the entire set of parabolas, they were used to determine the experimental heights of liquid in the porous matricies, h_{expt}. Changes above or below the 'zero' equation indicated respective increases or decreases in the total volume within the system, V_{tot}, which is defined by the physical parameters of the ceramic tubes (D_o, D_i, L, ε). In order to calculate h_{expt} from the standardized POT readings, the actual volume of water, V*, at a specific time, t, needs to be determined. This is shown in Equation (5.20) where $V^* = V_{tot} \pm \Delta Vol$.

$$V^* = (\pi/4)[D_i^2 L + \varepsilon(D_o^2 - D_i^2)L] \pm \frac{11.56\ \mu l}{0.01\ V}(POT_{std}) \qquad (5.20)$$

The 11.56 μl per 0.01 volts used in the ΔVol term of Equation (5.20) indicates that a 0.01 voltage change in the potentiometer readings caused the corresponding volumetric changes in the system volume [Dreschel, et al., 1993]. Since the changes in actual volume affect the height of liquid in the matricies, then these quantities were related as shown in Equation (5.21).

$$h_{exptl} = \frac{-D_i}{2} + \frac{1}{2}\left\{D_i^2 + \frac{1}{\varepsilon}\left[\frac{4V^*}{\pi L} - D_i^2\right]\right\}^{1/2} \qquad (5.21)$$

By combining Equations (5.20) and (5.21), the experimental liquid heights, h_{exptl}, were calculated and compared to $h = (D_o - D_i)/2$. When h_{exptl} was greater than h, then it was confirmed that weeping occurred due to the changes in effective gravity, g_z. When comparing Figures 5.12 and 5.13, the spikes in the inlet pressure readings leading to values of P_0 greater than P_w (when weeping occurs) corresponded to the POT readings appearing above the 'zero' equation. Therefore, the control equation for the PCT-NDS was verified for the dynamic changes in gravity during a KC-135 parabolic flight.

5.4.3 Sustained Hyper-Gravitational Control - Centrifuge Experiments

A small-scale centrifuge was constructed from a variable speed pump with rotational speeds, ω, ranging from 6 to 600 rpm. In order to attach radial arms to the pump drive, a standard pump head consisting of a rotor but with only half of the tube containment casing was bolted to the drive unit. On the rotor of the pump head, three T-shaped radial arms (r_{arm} = 19 cm) were attached by bolting them through holes present on the rotor. Two clamps were then attached to each of the radial T arms in order to support the ceramic tubes. The tubes are oriented perpendicular to the radial arms. The top view of this configuration is shown schematically in Figure 5.14.

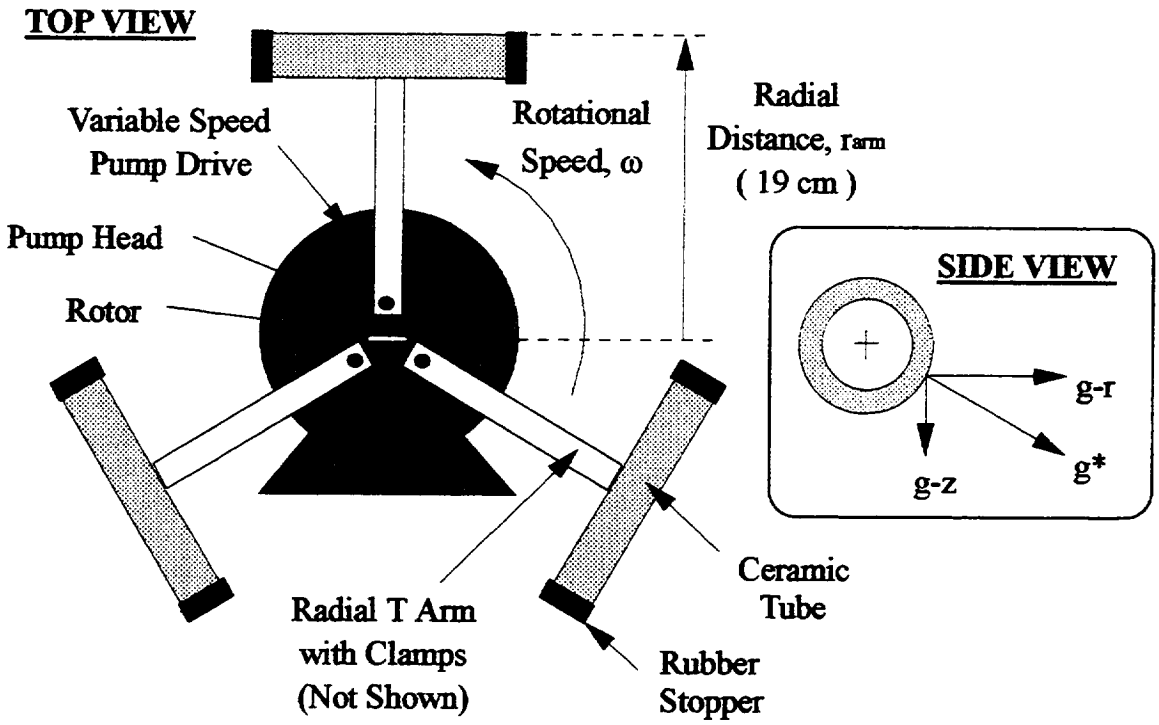

Figure 5.14 Schematic Diagram of the Centrifuge with the Ceramic Tube (Side View Included)

The rotational speeds were measured for each of the settings on the pump controller (marked from 1 to 10). Plotting these rotational speeds versus the drive settings, a calibration curve for the pump was obtained. This curve was then used to obtain the desired rotational speeds in order to subject the ceramic tubes to different effective gravitational accelerations in the radial direction. Since these experiments were conducted under standard gravity in the z-direction, then this influence was taken into account. As shown on the side view on Figure 5.14, since the ceramic tubes are cylindrical, then the radial gravitational accelerations set up by the centrifuge was added vectorially to the gravity in the z-direction. The resultant gravitational acceleration that the ceramic tubes were subjected to was determined from Equation (5.22) where g_z = the z-component and g_r = the radial component of the effective gravity, g*. Furthermore, $(\omega^2 r_{arm})$ was substituted in for the radial component as follows.

$$g^* = [g_z^2 + g_r^2]^{1/2} = [g_z^2 + (\omega^2 r_{arm})^2]^{1/2} \qquad (5.22)$$

Using Equation (5.7) defining the weeping pressure, P_w, except replacing the standard gravitational constant, g, with g* for non-standard gravities, the minimum pressure, $P_w = P_{min}$, required to contain the liquid in the matricies can be calculated with Equation (5.23).

$$P_{min} = \frac{-\rho g^*(D_o - D_i)}{2}\left\{\frac{D_i^2}{\varepsilon[D_o^2 - D_i^2]} + 1\right\} \qquad (5.23)$$

Substituting in Equation (5.22) for g* gave Equation (5.24) for the minimum pressure in terms of the rotational speed, ω, and the physical dimensions of the system. This relationship between P_{min} and ω is plotted for various pore sized ceramic tubes in Figure 5.15 with effective gravitational accelerations of 2, 3, 5, and 10 g's delineated..

$$P_{min} = \frac{-\rho[g_z^2 + (\omega^2 r_{arm})^2]^{1/2}(D_o - D_i)}{2}\left\{\frac{D_i^2}{\varepsilon[D_o^2 - D_i^2]} + 1\right\} \qquad (5.24)$$

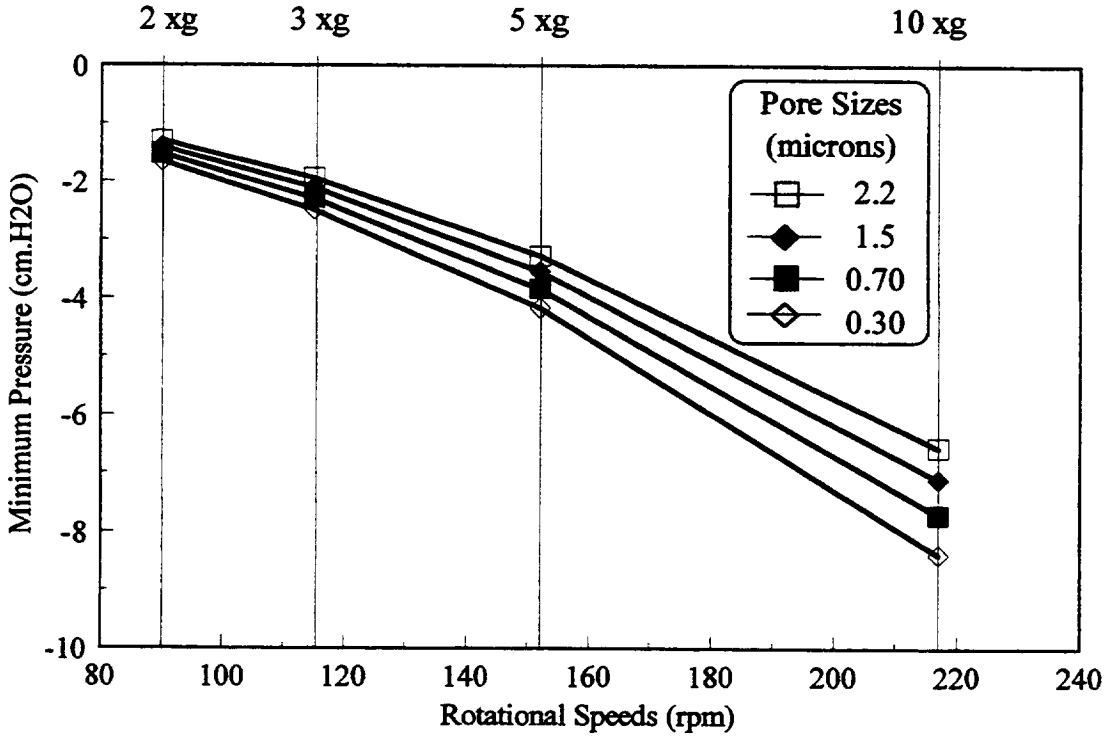

Figure 5.15 Minimum Pressures (P_{min}) as a Function of the Rotational Speeds (ω)

In order to verify Equation (5.24), the different pore sized ceramic tubes were centrifuged after the desired negative pressures were obtained. These pressures were obtained by completely loading each ceramic tube (of known dry weight) with water and capping with rubber stoppers (also of known dry weight) while still submerged. By allowing the water on the surfaces of the tubes to evaporate, the average height in the porous matricies, h, decreased corresponding to an increase in suction internal pressure, P_s, according to Equation (5.6). Therefore, the desired weight which measures the total quantity of water contained in the tube interior as well as the matricies was obtained as measured to the nearest 0.0001 grams after the rubber stoppers were dried thoroughly. Once the desired weight was obtained, the ceramic tubes were removed and clamped into place onto one of the radial T arms on the centrifuge (see Figure 5.14). Each of the different pore sized ceramic tubes were tested at 2, 3, 5, and 10 xg by setting the appropriate Pump Drive Setting as dictated by the calibration curve. While the ceramic tubes were centrifuging, a visual inspection for water droplets appearing on the absorbant material located peripherally around the centrifuge was made. When weeping did not occur (i.e. no water droplets appeared on the paper towels), then Equation (5.24) was verified; thus, proving that the applied suction pressure can be utilized to contain the liquid within the ceramic tubes subjected to sustained hyper-gravitational conditions. This satisfied the objective of maintaining and controlling the water availability within the ceramic tubes using the applied internal pressure under hyper-gravitational conditions induced by a small-scale centrifuge.

5.4.4 Future Implementations of the Control Equation

The research conducted on verifying the control equation subjected the PCT-NDS to variable gravity ranging from near-zero to 2 g's using a KC-135 parabolic flight facility and to sustained hyper-gravitational conditions of 2, 3, 5, and 10 g's using a small-scale centrifuge. Although these experiments provided evidence that the upstream pressure and flow rate through the system can be used to control the moisture content at the outer

surface of the ceramic tubes, additional experiments would be required for other operational conditions of interest. Specifically, sustained hyper-gravities under steady-state flow conditions as opposed to the static conditions used in this research should be examined. This could be accomplished using the Test Bed Units within a large-scale centrifuge. With liquid flowing through the system, a desired upstream pressure can be set according to the control equation, taking into account the sustained hyper-gravities. Furthermore, a dynamic experiment utilizing the KC-135 facility to explicitly test the control equation would give more conclusive evidence for verification purposes. Current inlet pressure data (see Figure 5.12) indicated that the pressure transducers were too insensitive and could not meter small fluctuations in pressure caused by the changes in gravity. Only during the drastic change from twice standard to near-zero did pressure transducers measure any appreciable change. Finally, the control equation for the PCT-NDS should be tested under sustained micro-gravity conditions such as on the space shuttle. This operational condition will be of particular importance if the PCT-NDS is to be included on the upcoming international space station.

CHAPTER 6 - RATIONALE AND SIGNIFICANCE

This chapter provides the rationale and significance of modeling the nutrient uptake kinetics into plants. In Section 6.1, the current state of the research methods used to investigate the effects of water potential on the nutrient uptake into plants is discussed. This will be particularly geared towards some of the inherent problems with these methods and how the Porous Ceramic Tube - Nutrient Delivery System (PCT-NDS) used in this research can alleviate these short-comings. In Section 6.2, a detailed overview of the overall hypothesis of this research is provided. This includes a description of the mechanistic reaction chain used to breakdown the various nutrient uptake theories as well as the specific objectives used to prove this hypothesis. Included in this section will be a discussion of the problems associated with the two main styles of nutrient uptake models, the Nye and Tinker and the Barber-Cushman models. It will be further discussed how the models produced in this research will be an improvement upon these predecessors. Furthermore, in Section 6.3, other applications besides the basic scientific research methods will be discussed. These include the application of the nutrient uptake models towards fertilization and irrigation schemes used in conventional field agriculture as well as the standard methods of producing crops hydroponically. This section will also include a discussion of how the uptake models developed in this research can be applied towards the needs of the National Aeronautics and Space Administration (NASA) in their endeavors to produce plants in space environments. Finally, this section will conclude with a discussion of possible applications in other areas of research such as phytoremediation and plant cell and tissue culture technologies.

6.1 Current State of Research

The current state of the research methods used to maintain water potentials in the root-zone of plants is overviewed in this section. Typically, these types of experiments are conducted in order to determine the effects of water deficits on the growth and production in agriculturally viable crops and other plant derived products. Furthermore, other experiments which directly affect the water potential that do not explicitly examine the water potential effects are the nutrient uptake studies. Specifically, when changing the composition of a nutrient solution for the purposes of measuring uptake rates, there exists an inherent change in the osmotic component, π, of the water potential, Ψ (see Section 2.3.4). This inherent change in Ψ typically cannot be separated from the effects of the changes in nutrient solution composition.

6.1.1 Maintaining Constant Root-Zone Water Potentials

Current methods of research on the effects of water deficits on plant growth and development utilize several means of changing the root-zone Ψ. The first is the use of various soil media characterized by different water holding capacities [Cox and Barber, 1992]. This method is based on the principle that soils with differing characteristics (i.e. particle size, surface area, microporous spaces, degree of compaction) are capable of holding different quantities of water when completely saturated. As the soils dry out due to the natural evaporation into the atmosphere, the surface tension forces within the soil matricies becomes a dominant factor [Lafolie, et al., 1991]. This surface tension is quantified as the matric potential, $P_m = -2\gamma / r$, where γ equals the surface tension of water (7.275×10^{-8} MPa m) and r represents the radius of curvature of the meniscus. This surface tension force dictates the magnitude of the overall water potential, Ψ, by increasing the magnitude of the hydrostatic component, $P = P_m$. Another similar method involves varying the intervals between irrigations subjecting plants to various levels of non-saturating soil moisture after a certain length of time. However, maintaining a

constant Ψ under either method can be difficult as soils continue to dry out and produce a vertical stratification in moisture [Wraith and Baker, 1991; Vetterlein, et al., 1993].

Compounding this problem is that during the depletion of water from the soil solution due to evaporation, the concentration of the dissolved ions increases. This increase alters the osmotic potential of the soil according to the relationship, $\pi_{soil} = -RTC_{soil}$, where C_{soil} represents the total concentration of all solutes and R and T have their usual meanings. Therefore, in addition to water deficit conditions, saline stress conditions are also present during these types of experiments. Unless accounted for by altering the composition, these two factors are not separable. Similar to this problem is the presence of non-essential elements such as silicon, cobalt, selenium, and sodium on the surfaces of the soil colloids. Initial saturation of the soil leads to the release of these elements into the nutrient solution altering C_{soil}. Furthermore, these ions can be subsequently absorbed by the plant leading to reported changes in plant response [Mackowiak, et al., 1989; Miyage and Takahashi, 1983; Menzies, et al., 1991; Akeson and Munns, 1990; Barrachina, et al., 1994].

One method that has been widely used to modify the osmotic potential of a hydroponic solution is the addition of non-penetrating solutes such as high molecular weight polyethylene glycols (PEG) or mannitol [Hohl and Schopfer, 1991]. The PEGs that have been used as hydroponic solution osmotica range in molecular weights from 1,000 to 20,000 [Yaniv and Werker, 1983]. However, the lower molecular weight PEGs as well as the mannitol have been shown to enter the root apoplast and even the symplast which can lead to the transport of the solutes in the transpirational stream [Yaniv and Werker, 1983; Hohl and Schopfer, 1991]. Therefore, the results obtained from these experiments may be suspect due to the altered transport characteristics imposed by the supposedly non-penetrating solutes. Furthermore, it has not been excluded that the higher molecular weight PEGs may behave in the same manner during long term experiments as the lower molecular weight PEGs during short term experiments [Hohl and Schopfer, 1991]. In fact, eight different plant species including tomato were subjected to different molecular weight PEGs for 24 hrs leading to the deposition of white material on the leaves. This material

was later identified as the osmotica indicating the presence in the transpirational stream [Yaniv and Werker, 1983]. Furthermore, root morphology has been shown to be altered when subjected to these osmotica by decreasing root elongation with a simultaneous increase in diameter [Materechera, et al., 1992].

Another problem indicative of soil based experiments is that the separation of the roots from the soil particles can be difficult and can lead to possible errors during subsequent tissue analyses. For a single plant grown to maturity in soil, the separation process can achieve hours of meticulous work as root hairs tend to form intimate contact with soil particles. Furthermore, this procedure generally requires that the roots be washed with water which can substantially reduce the nutrients weakly bound to the outer root membrane. This washing reduces the nutrient concentrations at the root surface, $C_{surface}$.

6.1.2 Changing Nutrient Solution Compositions

When the composition of a nutrient solution is altered in order to investigate the effects of different levels of essential elements, one inherent change that is often overlooked is that the osmotic component of the water potential is changed as well. The influence of the water potential change can lead to the responses subsequently attributed to the change in composition. This is evident from the examples presented earlier on the effects of altering standard nutrient solutions (see Section 4.1.2). The problem with altering the composition is that the change in water potential cannot be separated. Although this problem is generally considered as negligible in soil-borne experiments where the dominant factor controlling water potential is the matric component, several experimental methods often used are subject to this occurrence.

In order to study uptake kinetics, several soilless culturing methods (see Section 4.2.3) are generally employed. This includes using various nutrient concentrations and following the depletion rate with time in order to obtain Michaelis-Menten type kinetics [Barber and Cushman, 1981]. However, as the base nutrient concentrations are altered, so are the effective water potentials of the solution. Altering the total osmotic potential of the

nutrient solution has been shown to lead to different nutrient uptake capacities anyway [Glass, 1989]. Another method subject to this condition is the split root method which utilizes a single clean root mass divided between two solutions of different concentrations [Johnson, et al., 1991]. Using radioactive tracers, the uptake can be determined as a function of time. However, altering the local water potential of some of the roots automatically changes the uptake rate in those roots. Again, the problem is not separable unless care is taken to maintain a constant osmotic potential between both solutions.

In order to maintain a constant osmotic potential, the addition of various ionic solutes such as sodium salts, typically NaCl [Knight, et al., 1992], as well as non-penetrating osmoticum such as PEG [Charles, et al., 1990] have been utilized. In addition to the problems mentioned earlier (see Section 6.1.1) for the non-penetrating osmotica, there exists other problems associated with the ionic solutes. These include interferences by the non-essential ion such as Na interactions with K [Wrona and Epstein, 1985] and the alterations in the electrical conductivity of the solution [Knight, et al., 1992]. By altering the electrical conductivity, the ability of the nutrients to pass through the root membrane is altered as well. According to Equation (2.8), the Goldman equation for the diffusion potential of a membrane, ΔE_m, passive transport of nutrients through protein channels requires that the individual Nernst potential, ΔE_{mj}, for nutrient, j, must overcome this membrane potential (see Section 2.4.1). Therefore, increasing the external concentration of, say, Na in the form of NaCl to replace the standard nutrient solution KCl in equal molar quantities alters ΔE_m since the individual permeabilities, P_j, are different for each element, j. Furthermore, the Nernst potential for other ions such as Ca and Mg remain the same even though the membrane potential has been changed. This leads to a change in the passive transport rates of these nutrients as well which are not accounted for during the changes in solution concentration of the nutrient in question.

One problem that should be mentioned even though it is impossible to avoid but sometimes overlooked is that nutrient uptake studies are undoubtedly dependent upon the particular species and cultivar studied. Furthermore, these experiments are dependent upon the growth stage of the plants when the experiments are conducted [Carpena, et al.,

1988]. For example, two cultivars of tomato (Vemone and Marglobe) were grown in identical nutrient solutions with the consumption rates measured during various stages of the growth cycle. In general, the Vemone variety consumed greater quantities of N, P, K, Ca, Mg, Fe, Mn, Zn, and B during the later stages of development (fruit ripening). However, during the initial growth stages (vegetative growth), the Marglobe variety accumulated greater quantities of some of the nutrients such as N, K, Zn, and B. During the intermediate stages (flowering and fruiting), these initial trends reversed for some nutrients and persisted for others until the later stages. Therefore, nutient uptake studies should examine the entire growth cycle of a plant, particularly when comparing species and cultivars. However, the nutrient uptake experiments discussed earlier were, generally, conducted on the short-term (2-3 weeks at most) while the entire growth cycle of a plant can be several orders of magnitude larger (months).

6.1.3 Advantages of using the PCT-NDS

The problems encountered using the current methods of research into the effects of water potential and nutrient solution composition on the uptake capacity of plants can be overcome using the Porous Ceramic Tube - Nutrient Delivery System (PCT-NDS). Specifically, this system is capable of maintaining controlled moisture levels at the surface where the plant roots are in direct contact [Dreschel, et al., 1993; Tsao, 1994; Tsao, et al., 1996]. Furthermore, this degree of control allows for the changes in osmotic potential due to solution alterations to be compensated for using the applied suction pressure. Therefore, constant water potentials can be maintained across different nutrient solution regimes, isolating the nutrient effects from the water potential effects. In order to illustrate these basic scientific applications of the PCT-NDS as compared to current research methods, the following examples are provided.

In order to test the effects of different water potentials, Ψ, on the growth or production of a plant, ceramic tubes with different pore sizes, d, can be utilized to alter the matric component, $P_m = -2\gamma / r$, of the effective water potential (see Section 2.3.4). Using

Figure 6.1, illustrating an ideal pore of diameter, d, with a liquid meniscus contacting the solid walls at an angle, ϕ, the radius of the meniscus, r, can be determined as $r = d/(2\cos\phi)$. Therefore, the matric potential becomes, $P_m = -(4\gamma\cos\phi) / d$. Since the pore diameter, d, appears in the denominator of this relationship, then decreasingly smaller values increase the magnitude of the matric potential (P_m becomes more negative). This assumes that the systems are operated identically but with different pore sized tubes. For example, if the contact angle, ϕ, is set to 85° (= 1.48 radians), then for ceramic tubes of pore sizes of 0.30 and 2.2 microns, the matric potential can be calculated to be -0.085 and -0.012 MPa, respectively. Decreasing ϕ to 75° (= 1.31 radians) changes these values to -0.251 and -0.034 MPa, respectively. For comparison, Ψ_{soil} ranges from -0.05 MPa for moist conditions to -0.5 MPa for dry soils [Lafolie, et al., 1991]. Extremely dry soils attain values of -3.0 MPa which corresponds to the permanent wilting point for most plants [Taiz and Zeiger, 1991].

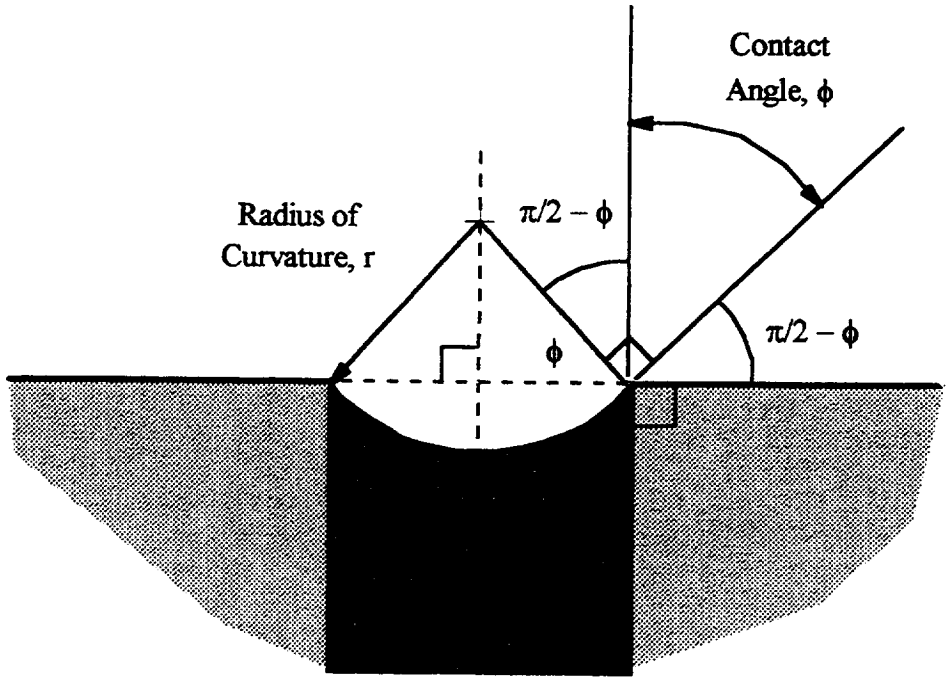

Figure 6.1 Relationship between Pore Diameter, d, and the Radius of Curvature of a Meniscus, r, on an Ideal Pore

In order to obtain these conditions, a rough estimate of the required applied suction pressure, P_s, can be calculated from Equation (5.17). This equation linearly relates $\cos\phi$ to P_s (see Section 5.3.2) using the values for the weeping, P_w, and cavitation, P_c, pressures presented in Table 5.2. For these individual conditions, P_s can be determined to be -0.084 and -0.248 MPa for the 0.30 micron tube with respective contact angles of 85° and 75° and -0.011 and -0.034 MPa for the 2.2 micron tube. Unfortunately, the system is limited to operational pressures that are greater than approximately -0.08 MPa where dissolved air is pulled out of liquid water.

Although the PCT-NDS is limited in its applications to study the effects of sustained water potentials on the growth and productivity of plants, the operational pressure range between 0 and -0.1 MPa is readily applicable to the study of nutrient uptake. Specifically, when a change in the nutrient solution concentration is imposed on a plant, the soil osmotic potential, $-\pi_{soil} = -RTC_{soil}$, changes according to the value of the osmolarity, C_{soil}, measured in moles of solute per kg water (see Section 2.3.4). This change, in turn, alters the overall water potential of the soil solution, $\Psi_{soil} = P_m - \pi_{soil}$. In order to separate the effects of the change in nutrient concentration from the change in water potential, both of which affect the growth and productivity of plants [Glass, 1989], the matric potential can be altered for compensation. For example, if the concentration of solutes in a standard Hoagland's #1 hydroponic solution (see Section 4.1.1) is decreased in magnitude from normal levels of 31.1 mmol/kg to 7.78 mmol/kg (1/4 strength), then $-\pi_{soil}$ increases from -0.078 MPa to -0.019 MPa at T = 300 K. This change can be subsequently compensated for by increasing the applied suction pressure which increases the magnitude of the matric potential. Specifically, the matric potential can be decreased by 0.059 MPa by increasing the applied suction pressure by an amount dependent upon the ceramic tube pore size and the original operating pressure.

When conducting experiments involving biological systems, it is desired to maintain as strong of a control over the perspective effectors as much as possible. The PCT-NDS offers a means to obtain control over the effective water potential at the root-zone which has been relatively lacking under current research methods.

6.2 Hypothesis and Objectives

This section provides the statement of research involving modeling the nutrient uptake kinetics into plants. This entails the mechanistic reaction chain developed in this research which describes the possible rate limiting steps in plant nutrient uptake. In order to prove this hypothesis, the specific objectives set forth for this research are described in detail including the use of the Porous Ceramic Tube - Nutrient Delivery System.

6.2.1 Research Hypothesis

The overall hypothesis of this research is: "The rate limiting step in the nutrient uptake processes of plants can be modeled either as an environmentally manipulated supply or a physiological manipulation by the plant." This rate limiting step is determined from a mechanistic reaction chain described in Figure 6.2 which takes on the form of a standard chemical reaction sequence.

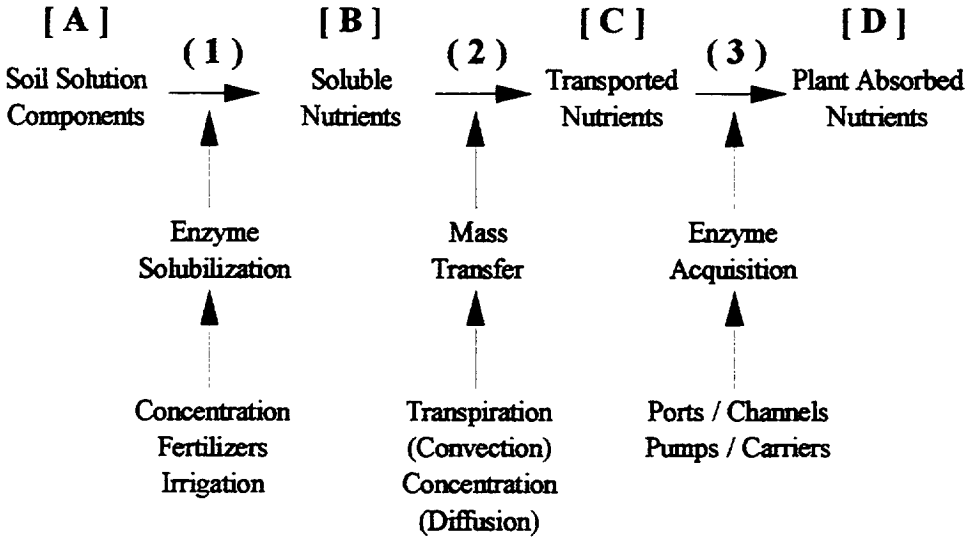

Figure 6.2 The Mechanistic Reaction Chain for Nutrient Uptake into Plants

There are four "chemical components" involved in this reaction. The initial reactant, denoted as **[A]** in Figure 6.2 consists of the nutrients existing in both the solid and liquid phases present in the soil solution. For a hydroponic system, this will, generally, only include the liquid phase; although, solid precipitates can form in a hydroponic solution as found in this research. The first "reaction intermediate" in this sequence, denoted as **[B]**, is the formation of soluble (liquid phase) nutrients in the soil solution. This reaction step, denoted as **(1)**, can be catalyzed by enzymes that are either actively released into the soil environment or concentrated as transmembrane channels or carriers. Examples of this enzyme production by the plants include released acid phosphatases [Garcia and Ascencio, 1992], bound Ca^{2+}-ATPases [Le Bot, et al., 1990], and Fe-chelate reductases [Holden, et al., 1991]. Factors affecting the rate of this reaction step include the application of fertilizers, the natural decay of organic components in the soil environment, and the weathering of the soil either through rainfall or applied irrigation. Each of these occurrences leads to a different soil environment which, in turn, leads the plant to respond accordingly. Therefore, reaction step **(1)** can be considered an enzyme based manipulation of the soil environment leading to an increase in the concentration of soluble nutrients. However, this manipulation is highly dependent upon the conditions for which the plant roots are experiencing and subsequently, forming the enzymatic response. Although the method of sensing the soil environment is not directly known, possible means can include hormonal changes such as abscisic acid produced during soil moisture sensing [Johnson, et al., 1991; Bruckler, et al., 1991; Trejo, et al., 1995].

Once the formation of the soluble nutrients has occurred, the second reaction intermediate of transported nutrients can be subsequently formed. Denoted as **[C]** in Figure 6.2, this reaction intermediate is formed through the mechanisms of mass transfer, including both convection and diffusion. This is denoted as reaction step **(2)** in Figure 6.2. The convection component is caused by the bulk flow of solution caused by the transpirational stream while the diffusional component is caused by the localized concentration gradients between the soil solution and the surface of the plant root. Typically, these are described using classical convection/diffusion equations such as those

derived by Nye and Tinker, France and Thornley, and Barber and Cushman (see Section 3.3.2).

There are several environmental factors affecting the rate of convective mass flow of nutrient solution including both terrestrial (see Sections 2.3.3, 2.3.4, and 2.4.2) and subterranean (see Sections 2.3.4 and 2.4.2). The terrestrial factors include stomatal conductance, the leaf surface boundary layer resistance, the atmospheric temperature, air water potential, leaf structure, wind speed, planting density, and canopy height [Taiz and Zeiger, 1991]. The subterranean factors include concentration, the root-zone water potential, the temperature of the soil [Taiz and Zeiger, 1991], particle size, microporous spaces, surface area, degree of compaction, and depth [Bruckler, et al., 1991; Lafolie, et al., 1991; Cox and Barber, 1992].

Similarly, there are several effectors of the rate of diffusion of the nutrients in the soil solution (see Section 2.3.4). These include the particle size, microporous spaces, surface area, degree of compaction, depth, and moisture content [Bruckler, et al., 1991; Lafolie, et al., 1991; Cox and Barber, 1992]. Furthermore, additional environmental factors such as soil pH, nutrient interactions, concentrations, compositions, and temperature (see Section 2.4.2) also greatly affect the ability of nutrients to diffuse through soil matricies. In addition to these physical and environmental factors, the concentration gradients driving this process of reaction **(2)** are dependent upon the enzymatic activity of reaction step **(1)**. For example, actively released acid phosphatases produce soluble phosphates concentrated in the soil as compared to the root surface. This concentration gradient then leads to the diffusional transport of the phosphates to the root surface in addition to the convective flow in the transpiration stream. Therefore, reaction step **(2)** leading to the formation of transported nutrients in the mechanistic reaction chain is environmentally based due to the factors affecting the rate of mass transfer.

The problem with the Nye and Tinker style models, written in the simplest form in Equation (3.50), is that it only describes the diffusional portion of step **(2)**. Although this form of mass transfer does play an important role in the transport of nutrients to the root surface, the actual uptake may not be governed by this environmentally based rate but may

be influenced by the constituents at the root surface. This will be described for step **(3)**. Furthermore, the Nye and Tinker model does not consider the sources of the soluble nutrient pools in the bulk soil solution and the possible influences that the plant may have over these concentrations such as those described for step **(1)**. Similarly, this model does not consider the changes in the plant demands for both water and the nutrients over the entire growth cycle. This model must be applied discretely to each growth stage.

Once the dissolved inorganic nutrients reach the root surface, several mechanisms of uptake become possible including symports, antiports, pumps, carriers, and channels (see Section 2.4.1). Each of these occurs through a membrane bound protein or enzyme which must be produced by the plant. Therefore, this third reaction step, denoted as **(3)** in Figure 6.2 is a plant based manipulation due to resource availability, photosynthetic production, carbon fixation, and energy production (see Sections 2.2.1 and 2.2.2). The product of this third reaction step which is the final product of the mechanistic reaction chain is the formation of plant absorbed nutrients. This is denoted as **[D]** in Figure 6.2. Furthermore, as the nutrients enter the root proper (see Figure 2.1), these enzymatic mechanisms are continually utilized in order for these nutrients to pass through the adjacent cellular membranes in the root. This nutrient transport mechanism is conducted through the transcellular and symplastic pathways (see Section 2.3.1). However, some nutrients can be carried through the apoplastic pathway through the mass transfer mechanisms of reaction step **(2)**. As the nutrients are passed from cell to cell in the root tissue, they eventually reach the endodermis and the Casparian strip surrounding the xylem tissues. Once at this location, the nutrients must be acquired through an enzyme transport mechanism leading to their transport upwards throughout the remainder of the plant through the transpirational stream (see Section 2.3.1). In terms of the mechanistic reaction chain, the rate of reaction step **(3)** is dependent upon the activities of the membrane bound enzymes and is, therefore, a plant based manipulation of the nutrient uptake process.

Although the Nye and Tinker model did not incorporate this plant based step in the nutrient uptake process, the France and Thornley and Barber-Cushman models do consider the influences of the plant. These models were presented earlier in Equation

(3.59) for the France and Thornley model and Equations (3.61) to (3.66) for the Barber-Cushman model with the associated initial and boundary conditions. One problem with these models, similar to the Nye and Tinker model, is that they do not take into account the changes in plant demand for both water and nutrients. As these rates are altered by the plant in order to meet the changing needs at the various stage of growth, these models would have to be applied at each discrete step [De Willigen and Van Noordwijk, 1994b]. Therefore, these models do not provide a complete picture of the nutrient uptake requirements of the complete plant. An improvement to these models would be to incorporate this time based consideration.

For the Barber-Cushman model, this short-coming is explicitly stated in one of the 13 assumptions used to derive the model. This assumption states that the characteristics of the root are not changed by the age [Barber and Cushman, 1981]. Although this assumption may be reasonably valid when investigating a single root under a short time frame as is the case with the Barber-Cushman model, it does not accurately describe the kinetics involved with the whole plant over the entire growth cycle. In addition, another of the 13 assumptions states that the soil moisture conditions remain at a steady state [Barber and Cushman, 1981]. This implies that the model would change due to rainfall or other irrigation. Therefore, although this model is very sound scientifically, it has very little real-world applications in that it only describes a very specific set of conditions for a short time frame. A broadening of the applicability of this model in terms of different conditions as well as the time considerations would be significant improvements to this model.

6.2.2 Research Objectives

For each of the essential nutrients present in the soil solution, the mechanistic reaction chain includes all of the possible process steps required for uptake by the plant roots. Furthermore, each of the steps in this chain can serve as the rate limiting step depending upon the specific requirements of the nutrient. Therefore, the overall hypothesis of, "The rate limiting step in the nutrient uptake processes of plants can be modeled either

as an environmentally manipulated supply or a physiological manipulation by the plant" inherently includes determining the mechanistic steps required for a particular nutrient. Once the required steps are known, the possible rate limiting step in the uptake of the nutrient can be determined (see Chapter 7). In order to prove this hypothesis and validate the mechanistic reaction chain, several objectives have been set forth in this research.

(1) Use the PCT-NDS to produce plants under controlled environmental conditions.
(2) Vary the controlled environmental conditions in order to determine whether a particular nutrient is directly influenced by these changes or due to some "other" (plant) factor.
(3) If the nutrient is controlled directly by the environment, then model using convection and diffusion equations with the incorporation of the water potential gradients.
(4) If the nutrient is controlled by the manipulations required by the plant, then model using enzyme based kinetics (i.e. Michaelis-Menten kinetics).

Objective (1) consists of two parts. The first is to show that a select plant species can be cultivated on the PCT-NDS through its normal developmental cycle comparable to conventional growth methods (i.e. field and/or hydroponic grown). The plant species chosen is *Lycopersicon esculentum* cv. Cherry Elite tomatoes. The results and environmental conditions of these experiments can be entered into established growth and transpiration models for comparison to the results reported for conventional methods in the literature. The second portion of this objective is to show that the root-zone environment of constant water potential and constant nutrient solution concentrations can be maintained in the system throughout the life cycle of the plant. These environmental conditions can be set using a standard (1x) Hoagland's #1 hydroponic solution (see Table 4.1) and minimal applied suction pressures (i.e. near weeping conditions; see Section 5.3.1). The results from these experiments can subsequently be used as the control condition for future experiments.

For Objective (2) of this research, the different controlled root-zone environmental conditions are dictated by the operation and set-up of the PCT-NDS. Different pore sized ceramic tubes ranging from 0.30 to 2.2 microns (i.e. different P_m) can be attached to the circulation loop and can be used in conjunction with different nutrient solution concentrations (i.e. different π_{soil}). Each of these solutions differ in overall concentrations as a fraction (i.e. 1/4x, 1/2x) of the standard (1x) solution. The tomato plants can, therefore, be subjected to a wide range of root-zone environments such as different overall values of Ψ_{soil} with constant concentrations as well as different values of C_{soil} but with a maintained level of water potential. By altering these environmental conditions and examining the resulting effects on the nutrient uptake capacity of the tomato plants, a determination can be made of whether the uptake of specific essential nutrients are environmentally controlled. A strong statistical correlation between the imposed change and the nutrient uptake response indicates a rate limiting step in the mechanistic reaction chain that is an environmental manipulation. On the other hand, a lack of statistical correlation indicates a plant based influence for the specific nutrient. In order to monitor the nutrient concentrations in the solution as well as in the plant tissues, standard analytical techniques will be employed (see Section 3.3.1).

After a determination is made of which controlling process is involved in the uptake of a specific nutrient, Objective (3) or (4) will be conducted. For Objective (3), the environmentally manipulated nutrients will be modeled based on classical convection/diffusion equations. These will incorporate Fick's Law for diffusion, Darcy's Law for the bulk flow through porous media, and the principle of mass conservation (see Section 3.3.2). The effective diffusion coefficients, D_{eff}, and surface concentrations, $C_{surface}$, for each measured nutrient will be estimated statistically. As for Objective (4), the plant controlled uptake of specific nutrients will be modeled based on enzyme kinetic (Michaelis-Menten) equations. Again, the kinetic parameters, $J_{c,max}$ and $K_{c,m}$ will be estimated statistically.

6.3 Applications

In addition to the application of the PCT-NDS for basic scientific research, the models formulated in this research have several applications as well. These include conventional field agriculture, hydroponic productions, and NASA's goal of utilizing plants for maintaining human life in space. Furthermore, the models also have possible applications in the areas of phytoremediation and nutrient uptake studies involving plant cell and tissue cultures.

6.3.1 Conventional Agriculture

For conventional agricultural practices, there are several lines of applicability for the nutrient uptake models developed in this research. This includes typical field agriculture where crops are produced over acres of land area and crop rotation schemes are often employed [Oyer and Touchton, 1990]. Furthermore, specialty crops such as herbs, spices, and, even, ornamental plants are generally produced under better defined (measured) conditions [Sammis and Jerrigan, 1992]. These environmental inputs include not only the terrestrial factors such as temperature and humidity, but include the soil moisture and nutrient concentration levels as well. These last two factors are directly applicable in the models of this research. Finally, the increasing numbers of hydroponic growers can use these kinetic models in order to design a more automated system with a variable nutrient solution formulated specifically for the particular requirements of a crop.

Plants require sufficient water and inorganic nutrients in order to grow to maximum potential (i.e. harvest value). Furthermore, the nutrient requirements change with the particular stage of growth of the plant. Therefore, standard agricultural practices employ the use of irrigation and fertilization schemes which can be based on mathematical models developed from various environmental factors (see Chapter 3). One of the influencial factors in the growth, development, reproduction, daily maintenance, and yield of plants (see Chapter 2) is the water potential of the soil [Glass, 1989]. Furthermore, this factor is closely linked to the soil nutrient concentrations and their effects on these growth

parameters. Specifically, when soil moisture levels change, the dissolved inorganic nutrient concentrations change accordingly. These can lead to nutrient deficiencies or toxicities which have the effect of decreasing the overall yield of the crop (see Section 2.4.3).

For the typical field farmer, these types of models can be used as a tool to aid in the scheduling of the irrigations and fertilizations. Specifically, since crop species require different levels of nutrients at different stages of growth, then knowledge based on the models of this research can be applied in order to determine the timing of these applicants. For example, if a specific nutrient is required at a specific stage of growth of a crop species, then the nutrient uptake kinetics developed in this research can be used to model these requirements. If these models are known, then the farmer can insure the proper levels of the nutrient at the correct time in the life cycle of the crop. Although nature generally has the ability to supply most of these requirements, these artificial supplementations are still often required. With accurate kinetic data, the timely application of the inorganic nutrient and/or water can be optimized thus reducing the quantity of resources required. Since typical fertilizers are broadcast as a liquid mixture containing the inorganic nutrients, then, for a particular crop, the nutrient concentrations in these mixtures can be specifically designed. Again, these will depend upon kinetic data for the nutrient uptake capacity of the crop species.

Similar to conventional field agriculture, the goal of the increasing numbers of hydroponic growers is to produce the maximum harvest for the least amount of time, energy, and resources (see Section 4.2.1). In order to accomplish this goal, accurate models of the water and inorganic nutrient requirements for the plants are required. Furthermore, implementing the supply scheduling for these essential nutrients can be based on uptake models developed specifically for the crop species cultivated. This will aid in the reduction of resources as well as predict the spent solution concentrations which can be recycled for the next production sequence. Furthermore, continuous hydroponic production systems such as those currently in operation [Field, 1988], may be made more efficient by having the nutrient supplies meet the demands more closely; thus, reducing the replenishment process.

6.3.2 Applications to Space Agriculture

Since the plants produced in this research are cultivated on the PCT-NDS established by NASA (see Chapter 5), then the models and procedures used in this research have direct applications for space agriculture. The current endeavors of the National Aeronautics and Space Administration (NASA) to sustain humans in a space environment are based upon the concepts of the Controlled Ecological Life Support System (CELSS). The CELSS concept utilizes minimal inputs carried on-board with a complete recycle all of the wastes produced into useful resources [Averner, 1989]. One component of the CELSS is the hydroponic production of plants to supply water and food for the crew as well as regenerate oxygen from human respiratory CO_2 and other wastes [Wright and Bausch, 1984]. In order to produce plants in space environments under this CELSS concept, the quantity of inorganic nutrients and water will have to be accurately quantified. This will require water for dilution of some of the nutrients and supplementation to bring others to the desired levels. Therefore, substantial knowledge of the uptake requirements of the candidate species grown as well as accurate kinetic models for the efficient connectivity to the rest of the systems contained in a CELSS are needed. Therefore, the results of the models developed in this thesis as well as the methodology used to determine the kinetic constants is directly applicable to NASA's desires.

The candiate crop species currently being investigated for inclusion in the space program include wheat, brassica, beans, rice, potatoes, and salad vegetables such as lettuce, radishes, and tomatoes [Dreschel, et al., 1988; Dreschel and Sager, 1989; Tsao, et al., 1994]. Preliminary experiments involving these crops have shown growth and yield results on the PCT-NDS comparable to conventional plant growth methods. One criteria used for selecting candidate crop species is plant size. Due to the limited volume of a space capsule, the growth chambers used to produce these plants will be severely limited as well. Therefore, plants with a high productivity to growth volume ratio are selected. One such species which can possibly meet this requirement is the Cherry Elite tomatoes used in this research.

6.3.3 Other Applications

In addition to the aforementioned applications, the research developed in this thesis can be applied to other areas of research such as phytoremediation and nutrient studies in plant cell and tissue cultures. For the former application, soils are often contaminated with non-essential elements such as selenium, cobalt, nickel, arsenic, lead, silicon, cobalt, aluminum, and sodium as well as toxic levels of essential nutrients such as zinc (see Section 2.4.2). In order to render these soils "environmentally friendly," plants have been looked at as possible means of clarifying these soils [Rouhi, 1997]. Since the uptake mechanisms of many of the contaminating elements are similar or identical to the mechanisms involved in the uptake of essential nutrients, then the application of the mechanistic reaction chain can be used to determine the rate limiting step. Furthermore, the methodology used to develop the kinetic models in this research can be directly applied in order to determine the uptake capabilities of plants for these unwanted elements.

The other possible application of this research in the area of nutrient uptake studies in plant cell and tissue cultures is actually a simplified version of the whole plant uptake process. Specifically, since there is no transpirational driving force in cellular cultures as there is in whole plants, the convection term used to describe the environmentally manipulated nutrients can be eliminated. This leaves a purely diffusional mass transport term while the nutrients that undergo plant based manipulations can be modeled similarly to whole plants. Specifically, the plant cells produce the same specific enzymes which are either membrane bound or excreted into the surrounding medium which facilitate the uptake of the nutrient into the plant cell. With the advent of adequate bioreactors for the growth and secondary production of plant cellular cultures [MacElvey, et al., 1993], the need for nutrient uptake models into plants becomes more important as commercialization and scale-up of these processes begins to reach fruition [Kossen, 1992].

CHAPTER 7 - MATERIALS AND METHODS

This chapter details the experimental materials and methods used in order to satisfy the objectives set forth in order to prove the research hypothesis presented in the previous chapter. These objectives are reprinted below along with the overall hypothesis of the research.

HYPOTHESIS:

"The rate limiting step in the nutrient uptake processes of plants can be modeled either as an environmentally manipulated supply or a physiological manipulation by the plant."

OBJECTIVES:

(1) Use the PCT-NDS to produce plants under controlled environmental conditions.
(2) Vary the controlled environmental conditions in order to determine whether a particular nutrient is directly influenced by these changes or due to some "other" (plant) factor.
(3) If the nutrient is controlled directly by the environment, then model using convection and diffusion equations with the incorporation of the water potential gradients.
(4) If the nutrient is controlled by the manipulations required by the plant, then model using enzyme based kinetics (i.e. Michaelis-Menten kinetics).

In order to conduct the experiments required for Objective (1) of producing plants on the Porous Ceramic Tube - Nutrient Delivery System (PCT-NDS) under controlled environmental conditions, the design and construction of the experimental apparatus is provided in Section 7.1. This will include the conversion of a standard laboratory chemical hood into the plant growth chamber used in this research as well as the construction of the test bed units (TBU) on which the plants are produced. In Section 7.2, the formulation of the standard hydroponic solution as well as the alterations in concentrations used in this research are provided. Furthermore, the methods used to compensate for the changes in the osmotic potentials, π_{soil}, for these different nutrient solutions are detailed as well. This will involve the use of the PCT-NDS with various pore sized ceramic tubes under controlled suction pressures. Finally, this section will outline the overall water potentials, Ψ_{soil}, in combination with the nutrient concentrations that will be examined in order to determine the environmental influences on the nutrient uptake capabilities of plants. This design of experiments will satisfy Objective (2). Finally, in Section 7.3 of this chapter, the methodologies used in analyzing the results obtained from these experiments are provided. This includes the analyses of the various plant tissues and nutrient solutions as well as the statistical methods used to determine whether a nutrient is environmentally manipulated or controlled by the enzymes produced in the plant roots. Once this discrimination is made of the rate limiting step in the mechanistic reaction chain, the model parameters for either case will be estimated statistically. Specifically, the bulk flow rate will be determined directly from water uptake measurements while the diffusion coefficient will be estimated through regression. As for the enzyme kinetic constants, these will be determined from the results applied to a linearized version of the Michaelis-Menten equation. The data used for this estimation will be obtained from the experiments conducted with differing nutrient concentrations but constant water potentials. This will satisfy Objectives (3) and (4).

7.1 Experimental Apparatus

The experimental apparatus used in this research consists of two distinct portions based on the environmental requirements of plants. For the terrestrial environment, a plant growth chamber was constructed from a standard laboratory chemical hood which supplies the plants with the required temperature, humidity, lighting, and atmospheric constituents. The construction of this growth chamber is provided in this section along with the degree of control that is maintained on these various environmental conditions. Similarly, this section also provides the design and construction of the PCT-NDS test bed units used to provide the controlled root-zone environments for the plants grown.

7.1.1 Growth Chamber

Although a complete environmentally controlled growth chamber was not available for this research, a chamber for the production of plants on the PCT-NDS was constructed from a standard laboratory chemical hood (1.3 m wide by 0.6 m deep by 0.8 m high). This was accomplished by accounting for all of the necessary terrestrial environmental conditions including lighting, temperature, humidity, and atmospheric gas composition. The standard hood lamp and air vents were shut off. This chamber can accommodate four Test Bed Units (TBU) as described below (see Section 7.1.2).

In order to supply plants with adequate lighting, three fluorescent light banks (2 bulbs each) were mounted at the top of the hood interior using standard chemical stands, clamps, and cross beams. The light bulbs used in these banks were 3 standard 40 watt bulbs plus 3-40 watt wide spectrum bulbs specifically designed for plant growth (Gro-Lux Wide Spectrum Light Bulbs). In order to increase the amount of light incident on the plants produced within the chamber, aluminum foil and mirrors were used to line all interior surfaces of the hood including the front safety glass. This shield was partially closed leaving 0.15 m (by 1.3 m wide) of space for access into the chamber. The total photosynthetically active radiation (400-700 nm) supplied averaged 50 $\mu E\ m^{-2}\ s^{-1}$ at the level of the ceramic tubes and increased to 70 and 90 $\mu E\ m^{-2}\ s^{-1}$ at 25 and 50 cm canopy

heights, respectively. This lighting system was connected to a common electrical wire which was subsequently attached to a 24 hour timer set to a 16 hour light / 8 hour dark cycle. During the experiments of this research, these light levels were assumed constant over time.

The access gap also allowed for the temperature and humidity to remain under the control of the surrounding laboratory. For the temperature of the growth chamber, although specific control systems were not installed, the building housing the chamber maintains atmospheric temperature, T_a, at $\pm$ 1.7 °C although the absolute temperature varies with the time of year between an average of 20 (winter) to 29 (summer) °C. Time courses of the temperatures during the individual experiments are provided in Appendix A (see Figures A.1 to A.8). Furthermore, the temperature during the light cycle was slightly higher than during the dark due to the heat generated by the light bulbs. There was also a slight temperature gradient between the top of the hood (nearer to the lights) and the bottom where the ceramic tube systems were placed. During the experiments, all temperature measurements were obtained from the bottom center of the hood.

Similarly, the building also provides a relative humidity, RH, of approximately 50 $\pm$ 10% year-round. These values were measured directly inside of the growth chamber with and without plants. Time courses of the relative humidities are also presented in Appendix A (see Figures A.1 to A.8) along with a table summarizing the averages and standard deviations for both the temperature and relative humidities during each experiment (see Table A.1). As for the atmospheric constituents, again, no direct control was maintained. Therefore, O_2, N_2, and CO_2 concentrations were assumed equal to the standard atmospheric levels of 21%, 79% and 0.035%, respectively [Galtier, et al., 1995].

Although the temperature and RH varied considerably during the experiments of this research, their effects on the growth, solution uptake, and transpiration will be left as a recommendation for further investigation (see Section 10.2.1). For the purposes of this research, only general rate equations for these processes are required for the nutrient uptake studies. However, since the temperature can affect the solution osmolarity as dictated in Equation (2.2), this factor will be examined in detail later (see Section 7.2.1).

7.1.2 Porous Ceramic Tube - Nutrient Delivery System Test Bed Units

In order to accomplish the experiments for this research, Test Bed Units (TBU) consisting of four ceramic tubes connected in parallel were constructed. A schematic drawing of a TBU is provided in Figure 7.1. The main components of this unit are the individual ceramic tube assemblies mounted to a plastic plate. The nutrient delivery components also shown in Figure 7.1 consist of a variable speed pump (Cole-Parmer L-07553-20) with a 16-gauge pump head, a flow meter, and a metering valve. Each of these are connected in the fluid circuit by system tubing (16-gauge Norprene tubing; internal diameter, D_s = 0.312 cm). Within this fluid circuit is a 500 ml graduated cylinder capped with a 2-holed #10 stopper. This cylinder which serves as a nutrient reservoir is wrapped in aluminum foil in order to reduce the occurrence of algal growth. In order to measure the upstream and downstream pressures, various sized vacuum gauges (Dwyer Instruments 2003C and 2015C; Cole-Parmer L-07380-62) located at a distance, L_s = 5.5 cm from the ceramic tubes were attached according to the required pressure ranges. Finally, as shown in Figure 7.1, the TBU is connected to the nutrient delivery system forming the entire PCT-NDS.

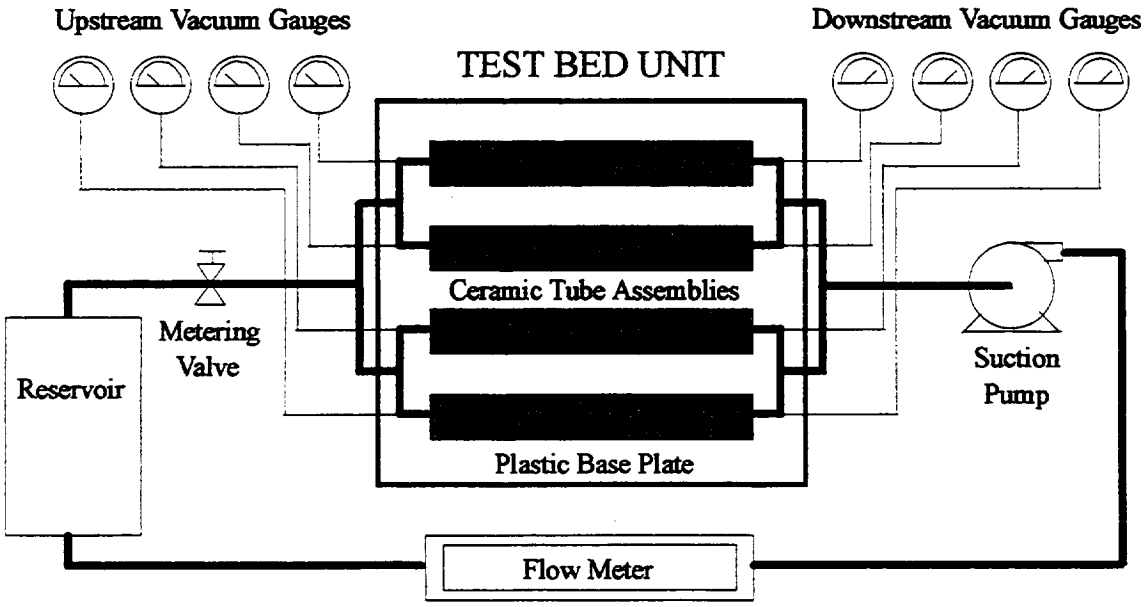

Figure 7.1 Schematic Drawing of an Experimental Test Bed Unit (TBU) Connected to the Nutrient Delivery System

One component not fully depicted in Figure 7.1 are the individual ceramic tube assemblies which are represented by the gray rectangles. These assemblies, as detailed in the exploded view of Figure 7.2, consist of a ceramic tube connected to the system tubing through rubber connectors. Prior to connecting these ceramic tubes to the fluid circuit, the ends are wrapped with Teflon tape to insure a leak-proof connection (leaks appear as air bubbles in the circulating solution). Surrounding these tubes are opaque covers which provide root-zone darkness but have a 1/4" hole cut into the top side of them in order to accommodate an emerging plant. These covers are attached to the ceramic tube through rubber connectors which fit over the ceramic tube connectors but inside of the tube covers. Each of these connectors are modified test tube stoppers containing a hole penetrated by the system tubing. As for the physical dimensions and porosities of the ceramic tubes that can be attached to this system (Osmonics, Inc. Controlled Porosity Ceramic Microfilters 46824, 5, 6, and 8), the average values were presented earlier in Table 5.1.

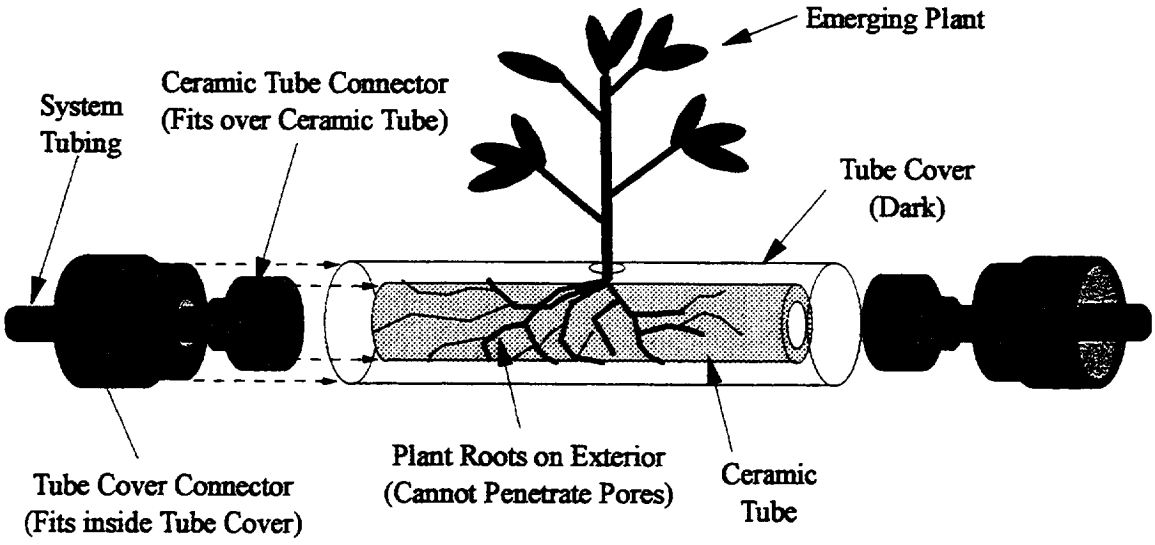

Figure 7.2 Exploded View of the Porous Ceramic Tube Assembly with Plant Orientation

7.2 Experimental Design

This section details the experimental design that is used in order to determine the effects of the root-zone environment on the nutrient uptake capacity of a test species. This test species was chosen to be *Lycopersicon esculentum* cv. Cherry Elite tomatoes (see Section 6.3.2 for reasoning). Since different nutrient solution concentrations will be utilized in this research, the standard formulation will be presented along with the protocols used to produce the various solutions. Furthermore, these different nutrient concentrations will be described in terms of the effective osmotic potentials contributing to the overall root-zone water potential that the tomatoes will be subjected. In order to compensate for these variations in π_{soil}, the methods used to alter the matric component, P_m, will be provided as well. This will include the various pore sized ceramic tubes used with the system described in terms of the effective matric potentials, P_m, achieved using the applied suction pressure, P_s. Finally, the specific environmental conditions in terms of the range of root-zone water potentials, Ψ_{soil}, that will be examined are provided.

7.2.1 Hydroponic Solution Formulations

The formulation of the inorganic nutrient solution used in this research follows the standard Hoagland's #1 hydroponic solution (see Table 4.1). This solution is prepared from 1 M stock solutions of KH_2PO_4, KNO_3, $Ca(NO_3)_2{\cdot}4H_2O$, and $MgSO_4$ (Aldrich Chemical Company). In addition to these macro-nutrient solutions, iron is added from a Sequestrene 330 Fe Stock solution prepared by adding 5 g of chelated iron (Ciba-Geigy; 10% chelated iron from sodium ferric DTPA) into 1 L of distilled water. For the remaining micro-nutrients, these are combined in a 10x Stock Solution by adding 28.6 g H_3BO_3, 18.1 g $MnCl_2.4H_2O$, 2.2 g $ZnSO_4.7H_2O$, 0.8 g $CuSO_4.5H_2O$, and 0.2 g $H_2MoO_4.H_2O$ (Aldrich) to 1 L of distilled water. Once these stock solutions are prepared, 10 L of the standard (1x) strength hydroponic solution can be formulated using the following recipe:

Recipe for the Hoagland's #1 Hydroponic Solution used in this research:

1) In 9 L of distilled water, the following quantities of Stock Solutions are added:
2) 10 mls of 1 M Potassium Phosphate - KH_2PO_4 - Stock Solution
3) 50 mls 1 M Potassium Nitrate - KNO_3 - Stock Solution
4) 50 mls 1 M Calcium Nitrate - $Ca(NO_3)_2 \cdot 4H_2O$ - Stock Solution
5) 20 mls 1 M Magnesium Sulfate - $MgSO_4$ - Stock Solution
6) 100 mls Sequestrene 330 Fe Stock Solution
7) 1 ml 10x Micronutrient Stock Solution
8) Measure the pH of the solution and adjust using 1 M NaOH to 5.9 $\pm$0.1
9) Add distilled water to make up the remaining volume to 10 L

This standard (1x) solution can be calculated to have an osmolarity of 31.1 mmol/kg. At an atmospheric temperature of 27 °C (300 K), the osmotic potential, π, can be calculated from Equation (2.2) to be -0.078 MPa. During the experiments of this research, the concentration levels that were also examined were 1/2x and 1/4x strength solutions prepared by diluting the standard mixture. Therefore, the corresponding osmotic potentials can be determined to be -0.039 and -0.019 MPa, respectively. Again, since there exists a temperature fluctuation over the course of a year, this factor can be taken into account during the calculation of the uptake results. However, since the average temperature, $T_{a,avg}$, during the experiments only varied from 20 to 29 °C (see Appendix Table A.1 for seasonal averages), then according to Equation (2.4), the osmotic potential, π_{soil}, only varies by $\pm$0.001 MPa. Therefore, the temperatures experienced during this research do not significantly alter the osmotic potential of the solutions. For the calculations, an osmotic potential of π_{soil} = -0.078 MPa will be used for the 1x solution. As the nutrient concentrations are altered from full to 1/2x or 1/4x strength solutions, the change in osmotic potential will be calculated as the fractions of this value.

7.2.2 System Operation

With these values for the osmotic potentials, the matric potentials required to compensate for the change in π while maintaining a constant overall water potential need to be determined. The first step is to calculate the desired matric potential, P_m. This value of P_m is dictated by the average pore size, d, according to Equation (7.1) (see Section 6.1.3 for derivation).

$$P_m = -(4\gamma\cos\phi) / d \tag{7.1}$$

For the ceramic tubes used in this research, the pore sizes are 0.30, 0.70, 1.5, and 2.2 microns as shown in Table 5.1. In addition to the pore size, the matric potential is also dependent upon the contact angle, ϕ, that the liquid makes with ceramic material. Furthermore, this contact angle is dependent upon the applied suction pressure, P_s, according to Equation (5.17). This equation is reprinted below where the theoretical weeping and cavitation pressures, P_w and P_c, respectively, are presented in Table 5.2.

$$\cos\phi = \frac{P_s - P_w}{P_c - P_w} \tag{5.17}$$

Combining Equations (7.1) and (5.17) allows for the matric potential to be determined in terms of d and P_s as shown in Equation (7.2).

$$P_m = -(4\gamma/d)[(P_s - P_w)/(P_c - P_w)] \tag{7.2}$$

Since the amount of suction pressure that can be applied to the system is limited by the pressure at which dissolved air is pulled out of aqueous solution (approximately -0.08 $\pm$ 0.01 MPa), then the limitations in the effective matric potentials for each pore sized ceramic tube can be determined. These are presented in Table 7.1 along with the propagated errors using a value of $\Delta\gamma = \pm 0.001 \times 10^{-8}$ MPa·m. As can be seen in the last column of this table, the limiting matric potentials that can be achieved are equal at this level of significant digits to the limiting pressure at which dissolved air is pulled out of

aqueous solution. This result makes sense since according to Equation (5.8), $P_c \cong P_w - 4\gamma/d$. When substituted into Equation (7.2) along with the assumption that limiting suction pressure (P_s = -0.08 MPa) is considerably larger in magnitude than the weeping pressure, P_w, then P_m is approximately equal to this value of P_s. Therefore, if the range of pressure applied to the system is relatively far away from the weeping condition, then the matric potential can be estimated using the applied suction pressure.

Table 7.1 Limiting Matric Potentials that can be Achieved on the Porous Ceramic Tube - Nutrient Delivery System

Pore Size, d (μm)	Weeping, P_w ($cm.H_2O$)	Cavitation, P_c (MPa)	Matric, P_m (MPa)
0.30 ± 0.005	-0.76 ± 0.03	-0.96 ± 0.016	-0.08 ± 0.01
0.70 ± 0.005	-0.77 ± 0.02	-0.41 ± 0.003	-0.08 ± 0.01
1.5 ± 0.05	-0.69 ± 0.02	-0.19 ± 0.006	-0.08 ± 0.01
2.2 ± 0.05	-0.65 ± 0.02	-0.13 ± 0.003	-0.08 ± 0.01

In order to acquire this control pressure, the pump speed can be increased causing a decrease in the applied suction pressure. This was illustrated in Table 5.4 for various pump speeds. Again, since there exists a pressure drop along the length of the ceramic tubes when solution is flowed within, then an average suction pressure, P_s, can be used since the plant roots grow over the entire tube surface. Another method that can be used in conjunction with altering the flow rate is partially closing the Metering Valve located upstream of the tubes as shown in Figure 7.1. This constriction also causes a decrease in the applied suction pressure allowing for the desired matric potential to be achieved.

As an example of this operational procedure, the PCT-NDS containing a 0.30 micron tube with a 1x strength solution flowing within at near weeping pressures, has an overall water potential, Ψ_{soil}, which can be calculated from the following contributions. With a 1x solution, the osmotic potential can be calculated (assuming T_a = 27 °C) to be π_{soil} = -0.078 MPa. For the 0.30 micron tube at near weeping pressure, the matric potential is negligible in comparison; therefore, $P_m \cong 0$ MPa. Therefore, Ψ_{soil} can be calculated as ($P_m - \pi_{soil}$) = -0.078 MPa. In order to examine the effects of a 1/2x solution

on the growth and nutrient uptake kinetics into tomato plants, π_{soil} of this solution is first determined to be, -0.039 MPa. Taking the difference between the Ψ_{soil} and this new osmotic potential, results in a pressure difference of -0.039 MPa. In order to determine the operating pressure required to achieve this compensating matric potential, this value is entered into Equation (7.2) along with the appropriate weeping and cavitation pressures. Upon doing so, the applied suction pressure, P_s, can be determined to be -0.039 MPa as well. This average value for the operation of the PCT-NDS can be achieved by measuring the upstream and downstream pressures, P_1 and P_2, respectively, while altering the flow rate, Q_z, and/or manipulating the Metering Valve. These pressure and flow rate measurements will be carried out daily in order to maintain the conditions as constant as possible.

In order to determine the effects of nutrient concentrations and water potentials on the nutrient uptake kinetics into tomato plants, several different root-zone environmental conditions will be examined. A manipulation of these conditions allows for a determination of whether the uptake of a specific nutrient is controlled by this factor or by some other (i.e. plant-based) mechanism. The specific experimental conditions are presented in Table 7.2. For the overall water potentials, these range from relatively dry to relatively moist conditions. Dry root-zone conditions are dictated by a high salt content and a low water level while a moist condition is indicated by a low salt concentration and a high water level. In this table and throughout the text, the matric potential level of -0.000 refers to near weeping conditions where the pressures are on the slightly negative side but approximately zero for the number of signficant digits.

Table 7.2 Experimental Conditions of Different Osmotic, Matric, and Root-Zone Water Potentials (in MPa)

Ψ_{soil} = -0.019		Ψ_{soil} = -0.058		Ψ_{soil} = -0.078		Ψ_{soil} = -0.117		Ψ_{soil} = -0.137	
π_{soil}	P_m	π_{soil}	P_m	π_{soil}	P_m	π_{soil}	P_m	π_{soil}	P_m
-0.019	-0.000	-0.019	-0.039	-0.019	-0.059	-0.078	-0.039	-0.078	-0.059
				-0.039	-0.039				
				-0.078	-0.000				

In order to obtain the various levels of water potentials listed on the top row of Table 7.2, different combinations of osmotic and matric potentials will be set in the system. For the different osmotic levels of -0.078, -0.039, and -0.019 MPa, these are equivalent to the nutrient solution concentrations of 1x, 1/2x, and 1/4x, respectively. As for the matric potentials, these levels represent the relative range of applied matric pressures for which the system is operated. Specifically, the -0.000 MPa level corresponds to the operation of the system at near weeping conditions (i.e. the least amount of applied suction pressure). In this case, the matric potential can be calculated using Equation (7.2). On the other end, the -0.059 MPa level for the matric potential represents the system operation at high suction pressure. In this case, the P_m can be approximated as P_s.

7.3 Analytical Methods

This section reviews the methods used in order to monitor the growth and development of the tomato plants as well as to analyze the tissues and solution samples for the concentrations of nutrients present. This will include measurements of the masses of the various tissues, plant height, leaf development, daily solution usage, solution pH changes, and solution replenishment. During these experiments, solution and tissue samples are produced and prepared for analysis in an Inductively Coupled Plasma - Atomic Emissions Spectrometer (ICP-AES). The procedures used for this preparation are described in this section. Furthermore, the results obtained in this research will be analyzed statistically for growth rates, nutrient uptake rates, and rate controlling mechanisms.

One condition to consider is that since the nutrient uptake rates change with the plant growth stage, then different harvest times will be utilized with these various conditions. The specific times will be based on the different stages of leaf development between the 7th and 15th true leaves (main vegetative growth stage). The last leaf stage examined is just prior to the development of fruit meaning that the vegetation produced up to this stage is the critical indicator for the production of adequate photosynthates required for fruit production.

7.3.1 Growth Measurements

During the experiments of this research, several factors will be measured on a daily basis. These include the height of the plant, leaf stage development, and the volume of solution taken up. At the end of the experiment, the wet and dry tissue masses of the leaves, branches, and roots will be measured as well.

In order to measure the growth rate of the tomato plants, the number of days, t_{DAE}, required to reach specific leaf stages, LS, after the plants have emerged will be counted. Producing a regression equation for this relationship between t_{DAE} and LS which takes into account the various test conditions (π_{soil} and P_m) allows for the plants to be measured on a leaf stage basis. This time scale is more desirable than an absolute scale since the experiments conducted in this research are performed during the various yearly seasons. Although environmental conditions were relatively stable within a single experiment, the results from experiments conducted during different seasons produce faster or slower growing plants based on the terrestrial conditions (mainly temperature). Therefore, the leaf stage scale consolidates the results onto a scale that is relative to the plant development.

Once this relationship is established, the daily plant heights, h_{plant}, corresponding to the occurrence of the various leaf stages will be regressed as well. These statistical analyses will also take into consideration the effects of the osmotic and matric potentials used to produce each plant. Since both the height and dry weight of the plant tissues, $W_{tissue,d}$, represent physiological characteristics that increase during the development, then these factors will be statistically regressed for each tissue type as well as the whole plant. Once adequate correlations are established for the entire plant as well as the individual tissue types, then the daily height measurements obtained throughout the experiments can be used to estimate the dry mass of the plant tissues without the actual destructive harvest. It is expected that the final correlations for the growth equations will attain an exponential form. Therefore, the mass of the plant tissues at different growth (leaf) stages and times during the experiments can be estimated at each occurrence instead of only after the final harvest for the plants produced under the different test conditions.

This method of measuring growth through the height of the plant is acceptable since as the plant increases in height, the entire mass of the individual tissues should increase as well. Specifically, in order to produce the photosynthetic components required for the main stem, an increased number of leaves will be required for this production. In order to support the leaves and reduce shading, a more extensive branching system is required. Finally, as the plant increases in height and leaf surface area, the rooting system needs to become more extensive in order to provide physical support.

Once the daily growth of the plants in terms of dry weight is estimated using this procedure, the water status for these plants will be evaluated as well. Initially, the growth in terms of wet tissue weights, $W_{tissue,w}$, will be determined using a procedure identical to the one used to produce the dry weight growth equations. The difference between these corresponding growth equations for the various tissues will then be used to produce a model for the plant hydration or water retention in the tissues, $H_{w,tissue}$ (in ml). Since the growth equations are expected to be exponential functions of leaf stage, then the plant hydration is expected to be exponential as well. These absolute measures of the plant hydration can then be used to determine the rate of solution retention, Q_r.

The quantities of water retained in the tissues are included in the total amount of solution taken up by the plants during the course of the experiments. This rate of solution uptake, Q_u (in ml solution per day) can be calculated from the total sum of the daily solution uptake measurements, V_u, plotted versus the average leaf stage of development, LS. Furthermore, the effects of the different osmotic and matric components need to be shown not to contribute significantly to V_u for a constant overall water potential. However, when the effects of different levels of water potential on the solution uptake are compared, then this factor, Ψ_{soil}, needs to be shown to be significant. The combination of these two provisions produces the evidence for satisfying Objective (1) of controlling the root-zone environment using the PCT-DNS.

Once the rate of solution uptake and hydration are determined, then the transpirational rate, E_t^* (in ml day^{-1}), can be determined. Under normal field conditions, the uptake of water follows the transpiration occurring mainly during the day [Van

Ieperen and Madery, 1994]. Since the uptake minus hydration equals the quantity of water released into the atmosphere through transpiration, then the rate of transpiration can be determined by taking the derivatives of V_u and $H_{w,tissue}$. The difference between these derivatives produces the relationship for the rate of transpiration from the tomato plants. This is shown in Equation (7.3).

$$E_t^* = dV_u/dt - dH_{w,tissue}/dt = Q_u - Q_r \qquad (7.3)$$

7.3.2 Tissue and Solution Concentration Analyses

In addition to the daily measurements for the growth and transpiration of the tomato plants, daily measurements will also be made of the solution pH. This is due to the solubility of the nutrient being highly dependent upon this factor. In addition to the pH, the nutrient solution will be analyzed for the concentration of the dissolved inorganic nutrients on roughly a weekly basis. This will be accomplished using the ICP-AES. The solution samples are prepared by withdrawing a 19.6 ml sample of the solution from the reservoir and replacing with an equal volume of fresh Hoagland's solution. This sample is acidified with nitric acid and sent to the Department of Food Sciences, School of Agriculture, Purdue University for analysis.

The analytical procedure for this spectroscopic technique involves energizing the elements in the sample by injecting them, in aerosol form, into an argon plasma [Boss and Fredeen, 1989]. This plasma is created by stripping electrons off an argon gas stream and energizing these electrons in a magnetic field. This high temperature plasma, known as Inductively Coupled Plasma, ranges from 6,000 to 10,000 K depending upon location in the discharge. Once the sample is introduced into this plasma, the droplets are desolvated to form microscopic salt particles. Then, the solid particles are vaporized into a gas which is then atomized. The next two steps are conducted in order to cause the characteristic radiation emission by the atoms. The first is the ionization of these atoms which leads to a more general radiation emission while the second step of excitation produces a more specific release of energy characteristic to the element. The combination of these two

atomic emissions can be measured spectroscopically (AES). Furthermore, the intensity of the emissions produces a measure of the concentration of the element in the sample.

In addition to the solution samples, the plant tissues can be analyzed using this spectrometer. In order to prepare the plants for this analysis, the following procedure is used. First, the plants are harvested from the system by clipping and collecting the leaves of the tomato plant leaving only the main stem, branches, and the root mat attached to the ceramic tube, still connected to the PCT-NDS. These leaves are collected in a weighing boat of known tare weight and the wet mass is determined. Next, the branches and main stem are separated from the root mat where the main stem emerges from the hole cut in the tube cover (see Figure 7.2). All portions of the plant above the tube cover are considered the terrestrial portion while the root system consists of the bio-material inside. Again, these tissues are collected in a weighing boat for the measurement of the wet mass. After the terrestrial portion of the tomato plants are removed, the system is drained of solution by disconnecting the outlet tube from the reservoir. Then, the ceramic tube assembly, as shown in Figure 7.2, is removed from the fluid circuit and dismantled. When the tube cover is removed from the ceramic tube, the root mat covering the entire surface of the ceramic tube is exposed to the outside air. Due to the delicate nature of the root system, particularly the root hairs, these tissues tend to dry out fairly rapidly. Root tips have been seen to dry out within minutes. In order to obtain accurate wet measurements of these tissues, the root mat is quickly trimmed from the ceramic tube by cutting the mat down the length of the ceramic tube. Once this cut is made, the root mat simply peels off of the ceramic tube since the pore sizes are smaller than the root hairs themselves. A measurement of the root fresh weight is generally made within minutes of the removal of the tube cover. In order to harvest several plants from a single experiment, this entire procedure is conducted to completion and started again on the next plant.

After the fresh tissues are weighed, the separate samples are dried in an oven at 70 °C for two days. After this time, the tissue samples are removed, allowed to cool, and then the dry masses are measured. Once complete, the tissues are ground to pass through a 40-mesh screen where they are subsequently collected and set for analysis in the ICP-AES. At

this point, an addition procedure is required to analyze these samples which begins with an acid digestion using nitric or perchloric acid. This digestion procedure is generally complete; although, some samples containing high levels of silicon are only partially digested. This contamination can be introduced from the glassware used in the digestion procedure as well as from other sources [personal communication]. At this stage, the tissue samples are treated the same as soluton samples in terms of the ICP-AES analysis. The results from these measurements will be used to complete the inorganic nutrient mass balances as well as to calculate the uptake rates, J_i.

7.3.3 Statistical Analyses

The production of the various models used to describe the development, growth, solution uptake, and inorganic nutrient uptake processes in the tomato plants will be conducted using statistical regressions. The methodology used to determine the statistically adequate regression models begins with the formulation of a possible model equation such as a linear or exponential equation. These models may contain terms for each of the possible influences such as leaf stage, osmotic potential, matric potential, overall water potential, and concentration. In some cases, the data used to formulate these regressions will be transformed by taking the natural logarithms and determining whether a significant linearized correlation exists from these results. If this is the case, then the linearized regression can be transformed back into the specific non-linear functions.

Once the form of a model is decided upon, possibly through some external means such as the established exponential model for plant growth, the model parameters are estimated using the method of least squares reduction of the sum of squares of the residual. In order to determine whether the particular model is at least adequate and should not contain any additional terms, an analysis of the variances (ANOVA) associated with model and the left-out terms can be performed. This analysis is based on the null hypothesis which assumes that the variance in the experimental data is only due to the random error of the experiment instead of some imposed condition. In order to refute this

hypothesis, this analysis utilizes the F-statistic which is the ratio of these variances to the error variance associated with the experimental measurements. A model term is deemed a significant contribution if the calculated F-statistic is greater than a critical value based on the risk of wrongly including the model term when, in fact, it does not belong. The risk used in this analysis is denoted as the α_{risk} and is dependent upon the degrees of freedom of both the model or left-out terms and the residual (or error). If the calculated F-statistic for this model is greater than this critical value, then the null hypothesis can be safely rejected and the model terms significantly contribute to describing the results. However, in order to establish an adequate model, the calculated F-statistic for the left-out terms must be shown to be less than the critical value. In this case, the null hypothesis cannot be rejected and the remaining error can be attributed to simple random error. Therefore, an adequate model is formulated when both of these criteria are met.

This type of statistical analysis will be conducted during the formulation of a general growth equations. The growth rates of higher plants are generally considered as exponential functions based on the dry weight of the tissues (see Section 7.1.1). These are empirical or semi-empirical equations based on the growth response of the plants over time. Therefore, during the formulation of the growth rates for these tomato plants, an exponential function will be developed. This will be obtained from a combination of the empirical models developed between t_{DAE} and LS, h_{plant} and LS, and $W_{tissue,d}$ and h_{plant}.

Similarly, this general statistical model building procedure will be used during the development of the solution uptake rates, Q_n. These uptake rates will be subsequently correlated to the root-zone water potentials achieved in this research in order to show that the environmental conditions are under the degree of control predicted by the conditions set in the experiments. Once this is achieved, the different nutrient concentrations can be evaluated for their effects on the nutrient uptake capacity of the tomato plants.

By altering the nutrient concentrations in these experiments, the nutrient mass transport rates that are based on the environmental manipulation can be examined separately from the influences of the plant enzyme or protein activities. First, the nutrient uptake rates, J_i, will be determined from the experimental data for each nutrient, i. These

rates will be calculated from the tissue concentrations, dry weights, and the number of days after emergence for each individual plant. These rates will then be modeled based on the various factors possibly affecting the nutrient uptake rate including the leaf stage, osmotic potential, matric potential, and solution concentration.

Once these experimental rates are determined, they will be compared to the rates of convection, $J_{conv,i}$, calculated using Equation (7.4) below. The concentration terms in Equation (7.4) attain the values for each individual nutrient present in the particular solution used to cultivate the plant. As for the solution uptake rates, these will be determined from the time derivatives of the regression models of V_u as a function of LS.

$$J_{conv,i} = Q_u C_{soln,i} \tag{7.4}$$

This comparison will be accomplished by using a statistical t-test where the average difference between J_i and $J_{conv,i}$ will be hypothesized to be equal to zero. The calculated t-statistic, t_{calc}, for these comparisons can be determined from Equation (7.5).

$$t_{calc} = \frac{\bar{d} - \delta}{s_d / \sqrt{n}} \tag{7.5}$$

In Equation (7.5), $\bar{d}$ represents the average difference between the experimental and convective rates, $J_i - J_{conv,i}$, while δ is the hypothesized value for this difference of zero. Furthermore, s_d represents the standard deviation calculated for the n number of samples. At a specific α_{risk} level, these differences will either be strongly rejected as being included or be within a normal distibution around the average of zero. This normal distibution is based on a critical t-statistic determined from the risk level and the degrees of freedom.

Three possibilities exist for this comparison. If t_{calc} is statistically equal to t_{crit}, then this indicates a convective mass transfer limitation. In other words, the rate at which the nutrients are absorbed by the root is equal to the rate at which they reach the root surface. However, if t_{calc} is a positive value greater than positive t_{crit}, then this indicates that the rate of supply is greater than the rate for which convection transport can account for alone. Furthermore, this indicates that the enzymatic activity at the root surface is greater

than the convective supply and is, in fact, causing a substantial concentration gradient leading to an additional diffusion of nutrients. In this case, there exists a diffusion mass transfer limitation which is also an environmentally based influence. Finally, the last possibility is if t_{calc} is a negative value less than negative t_{crit}. Under this condition, the nutrient supply rate to the root surface is greater than the rate of acquisition. This indicates a limitation caused by the saturation of the active sites on the transport proteins. The distinction between these three possibilities satisfies Objective (2).

In terms of the mechanistic reaction chain, only two of the three contributing mechanisms are accounted for during this type of analysis. However, for the PCT-NDS, the occurrence of nutrient solubilization by actively released enzymes (see the first reaction step, [1], in Figure 6.2 is assumed negligible since these usually operate on organic matter normally present in a soil. This is not present in this case. Alternatively, these enzymes can be membrane bound and act to solubilize nutrients that are precipitated or bound to soil colloids in contact with the root surface. However, for this system, the inert chemical nature of the ceramic and microporous channels would restrict this contact.

Once the rate limiting step during the uptake of the particular nutrient is determined, the classical convection/diffusion model and the Michaelis-Menten equation will be tested to determine whether these adequately describe the results. For the mass transfer limited nutrients, these can be further divided into convection limited or diffusion limited. For the diffusion limited nutrients, this portion of the mass transfer rate is described by Fick's Law. As for the convection limited nutrients, the model presented in Equation (7.4) is the standard convection equation. Incidentally, Equation (7.4) would have already been shown to be an adequate description of the convection limited nutrients through the t-test. As for the other possibilities of diffusion limitation or enzyme saturation, the adequacy of the respective models will be tested by performing an analysis of variance on the linearized forms of these models. An adequate model will result in each of the model terms being significant without the requirement for additional (left-out) terms. The derivation of these linearized models as well as the specific statistical analyses are presented in Chapter 9. These analyses would satisfy Objectives (3) and (4).

CHAPTER 8 - EXPERIMENTAL RESULTS

This chapter presents the growth, solution uptake, and mass balances obtained for tomato plants (*Lycopersicon esculentum* cv. Cherry Elite) grown on the Porous Ceramic Tube - Nutrient Delivery System (PCT-NDS). Section 8.1 presents the growth results for the plants subjected to the various root-zone environments maintained in this research. Furthermore, included in this section are the results for the overall development of the tomato plants in terms of leaf stage development as well as the mass accumulation rates based on daily plant height measurements. This is followed with Section 8.2 on the water status results for the plants including the plant hydration, solution uptake rates, and transpirational capacities. Once the solution uptake and water retention rates are determined, the transpirational rates can be estimated based on the differences between these rates. Finally, this chapter concludes with Section 8.3 on the development of the inorganic nutrient mass balances. Initially, the equation for the nutrient content measured in the plant tissues will be derived followed by the quantities found in the system. This includes the solution supplied, the amounts remaining or removed from the systems, and the quantities precipitated out of the solution. A comparison of the tissue to solution levels will provide evidence of complete mass balances for the inorganic nutrients. This includes a description of the measurement and experimental errors that were encountered during the various stages of analysis. Finally, this section will conclude with a specific example of this mass balance closure using the results obtained from a single experiment. It is assumed that if the mass balances can be shown to be complete for one experiment, then it will be complete for the remainder.

Many of the equations developed in this chapter will be subsequently utilized during the development of the nutrient uptake rates. These include the rates of leaf stage development, mass accumulation, and solution uptake. Furthermore, by showing that a complete mass balance can be achieved, the concentrations measured in the tissue samples can be used to develop the nutrient uptake quantities along with the tissue weights. These quantities can further be used to determine the uptake rates. Therefore, this chapter serves as a prelude and provides justifications for the methodologies used during the development of the nutrient uptake models for this research. The actual development of these models are provided later in Chapter 9.

8.1. Growth Results

The root-zone conditions which were controlled in this research which may influence the rate of growth include the nutrient solution concentration, the ceramic tube pore size, and the applied suction pressure within the system. The specific values for the concentrations used in this research are a 1, 1/2, and a 1/4 times the standard concentration of nutrients contained in Hoagland's #1 hydroponic solution. These values represent osmotic potentials of -0.078, -0.038, and -0.019 MPa, respectively. These different levels of π_{soil} were compensated for during the plant growth experiments by altering the matric potential, P_m. This matric potential is directly dependent upon the pore sizes of the ceramic tubes, d, as well as the applied suction pressure, P_s. This was detailed in Equation (7.2). The specific values for the pore diameters are 0.30, 0.70, 1.5, and 2.2 microns. Since the different solution concentrations were circulated inside each of the different pore sized tubes, the applied pressure was manipulated as a result of these combinations. The specific magnitude of this applied pressure was dictated by the desired matric potential and the overall root-zone water potential, Ψ_{soil}, that were to be maintained. Therefore, the variables which may affect the growth of the plants produced in this research are reduced to the osmotic and matric potentials. The affects of these variables on the growth rates are examined statistically.

Although other conditions such as the atmospheric temperature, lighting, and ambient CO_2 levels have been proven to greatly affect this growth rate (see Sections 2.2.1, 2.2.2, and 2.3.3), these effectors will not be examined in this research. Under the conditions of the experiments conducted to produce the tomato plants, these variables were maintained as constant as possible. However, as will be shown in the discussion below, the growth of the plants resulted in fairly large errors. Therefore, the mean square of the residual will be used instead of the standard error during the statistical analyses to determine model significance and adequacy.

From the literature, the typical equations describing the growth of plants generally acquires an exponential form. This was shown in the discussion of the growth equations such as the Gompertz equation, the logistics model, Chanter's equation, and Richard's growth function (see Section 3.1.1). Therefore, it is desired that the growth model produced in this research will attain this form as well.

8.1.1. Overall Tomato Plant Development Rates

One unavoidable occurrence in these experiments was the genetic variations that are inherent in any biological species. This is more pronounced with higher life forms such as plants. Some seeds placed on the moist ceramic tube surface germinated immediately (within 2-3 days) while others required substantially longer times (weeks). Furthermore, the development of the tomato plants once they produced root and shoot radicles was also dictated to some degree by the genetics of the seed. Some plantlets produced the initial few true leaves within a week of germination while others required several weeks.

In order to partially compensate for these differences, the growth of these plants were measured on a time scale based on the number of days between leaf stages after full emergence. Full emergence was considered as zero time or the zeroth leaf stage. During the growth of the plants, each number of days required to reach each odd numbered leaf stage was recorded. The even numbered leaf stages were not recorded due to the inability to distinguish between the emergence of a new leaf and the small morphology of the

primordial structures of the odd leaves that just emerged (i.e. before significant expansion of the pre-existing odd leaf).

This method of measuring time is reasonable when one considers that a seed does not begin to produce photosynthates until the cotyledons have emerged. Furthermore, since the available surface area of these cotyledons dictates the initial rate of photosynthesis, then the rate of subsequent leaf development is dependent upon this area. Another factor besides the genetically defined size of the cotyledons based on the individual seed is the ability to completely shed the aria (seed coat). If partially covered, this will reduce the initial rate of photosynthesis and subsequent development.

In order to produce a model for t_{DAE}, a general equation was developed that was a linear function of LS, π_{soil}, and P_m. This represented a starting point for the model development. The results of this analysis showed that the only significant contribution to the number of days after emergence was the leaf stages. Since leaf stage development is another measure of time to a plant, then this variable should be directly related to the time after emergence. Furthermore, this equation should be origin bound since, by definition, the zeroth leaf stage is equivalent to the time of emergence from which the days are counted afterwards. The final model is presented below as Equation (8.1).

$$t_{DAE}(\text{days}) = 3.605(\text{LS}) \qquad (8.1)$$

The actual data used in order to reach this final model are presented in Appendix B (see Tables B.1 to B.7 for the different π_{soil} and P_m conditions). The values for the model parameters were determined using the method of least squares regression while the significance of each term was analyzed at an α_{risk} level of 0.05 by performing an analysis of variance (ANOVA). The ANOVA table for this final model is provided in Table 8.1 while the ANOVA table for the complete linear model is provided in Appendix B (see Table B.8). Although the sum of squares of the left-out terms is fairly large indicating a possible term which may be significant, this was not pursued in order to simplify future calculations involving Equation (8.1). Finally, this model is plotted in Figure 8.1 along with the data.

Table 8.1 Analysis of Variance Table for the Model Describing the Number of Days after Emergence (Y) as a Linear Function of Leaf Stage (X1)

	DOF	Sum Sqs.	Mean Sqs.	Fcalc		Fcrit	Signif?
Total	408	217377				$\alpha_{risk} = 0.05$	
Model	1	205283	205283	6908	>	3.867	yes
b1	1	205283	205283	6908	>	3.867	yes
Resid	407	12094	29.72				
Error	359	10629	29.61				
LOT	48	1465	30.53	1.027	<	1.394	no

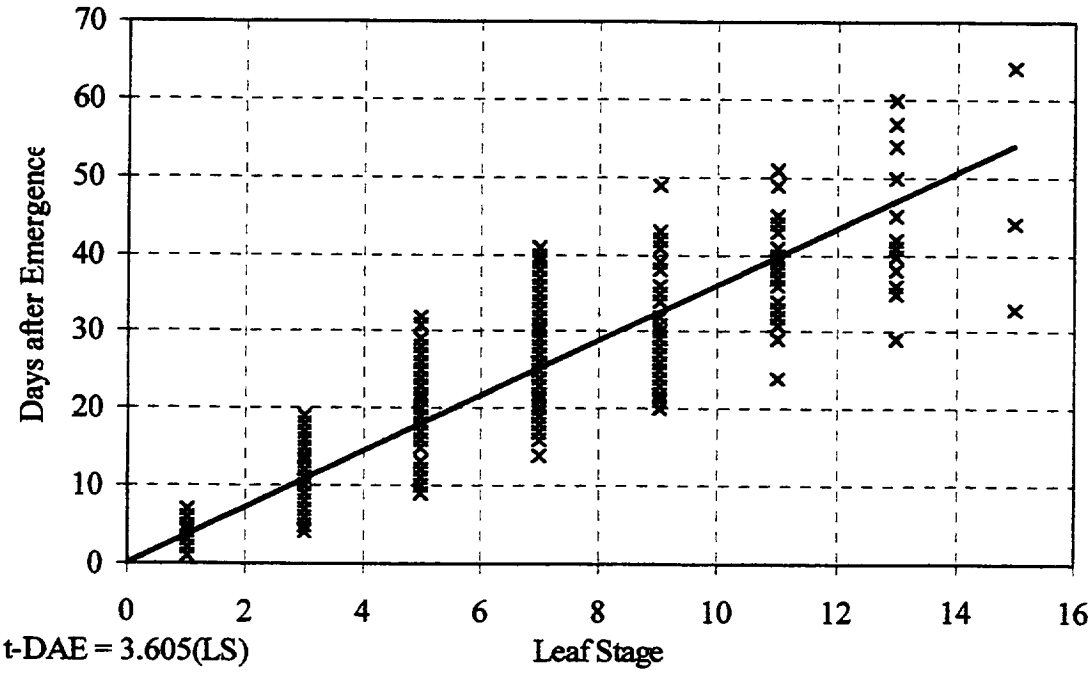

Figure 8.1 Comparison of the Model Equation and the Actual Data for the Relationship between the Number of Days after Emergence and the Leaf Stage

Similar to the development of leaf stages is the overall height of the tomato plants. Again, this characteristic is dependent upon the genetically defined potentials of the initial seed. Furthermore, the initial rate of photosynthesis affecting the rate of leaf development, also affects the overall height of the plant. During the experiments of this research, the plant heights were measured on a daily basis. Therefore, the heights corresponding to the

plants at the various leaf stages can be modeled. Furthermore, since LS is related to the number of days after emergence according to Equation (8.1), then this model describing the change in plant heights can be converted into an equation relating h_{plant} to t_{DAE}.

When plotting h_{plant} versus leaf stage (or time) for a set concentration and ceramic tube pore size, a possible relationship that becomes evident is an exponential equation. This form is desired in order to produce the final exponential growth function as will be shown later. Therefore, the form of the equation relating the two physiological characteristics of h_{plant} and LS will be modeled using an exponential function. In order to linearize the responses, the natural logarithm of the plant heights will be used in the model equation. After the final model is produced, the linearized equation can be converted back into the non-linear exponential form.

In addition to leaf stage, the effects of the solution osmolarity and the matric potential of the ceramic tubes were examined statistically as well. This was conducted in a manner identical to the previous development of Equation (8.1). In this case, the plant heights were shown to be significantly dependent on each of these factors. This is shown in Table 8.2 which provides the analysis of variances for the final model for h_{plant} at an α_{risk} level of 0.05. Furthermore, the F-statistic calculated for the left-out terms proved to be insignificant. The data used to produce this model are presented in Appendix B in matrix form (see Tables B.9 to B.15 for the different π_{soil} and P_m conditions). The values for the model parameters were determined using the method of least squares regression and are shown in linearized form in Equation (8.2). Again, the magnitude of the sum of squares for the left-out terms does warrant the investigation of additional terms; however, for simplicity, these were not pursued.

$$\ln(h_{plant}) = 0.918 + 0.231(LS) + 2.310(\pi_{soil}) + 3.891(P_m) \qquad (8.2)$$

Transforming Equation (8.2) back into the non-linear, exponential form results in Equation (8.3) where h_{plant} is a function of LS, π_{soil}, and P_m.

$$h_{plant} = 2.504 \exp[0.231(LS) + 2.310(\pi_{soil}) + 3.891(P_m)] \qquad (8.3)$$

An example of Equation (8.3) is plotted in Figure 8.2 along with the actual data for the experimental conditions where π_{soil} = -0.078 and P_m = -0.000 MPa (near weeping).

Table 8.2 Analysis of Variance Table for the Model Describing the Natural Log of the Plant Height (Y) as a Linear Function of Leaf Stage (X1), Osmotic Potential (X2), and Matric Potential (X3)

	DOF	Sum Sqs.	Mean Sqs.	Fcalc		Fcrit	Signif?
Total	499	1850				α_{risk} = 0.05	
Model	4	1771	443	2754.58	>	2.396	yes
b0	1	1392	1392	8662.75	>	3.867	yes
b1	1	374	374	2329.09	>	3.867	yes
b2	1	1.000	1.000	6.224	>	3.867	yes
b3	1	3.254	3.254	20.244	>	3.867	yes
Resid	495	79.56	0.161				
Error	371	55.56	0.150				
LOT	124	24.00	0.194	1.204	<	1.263	no

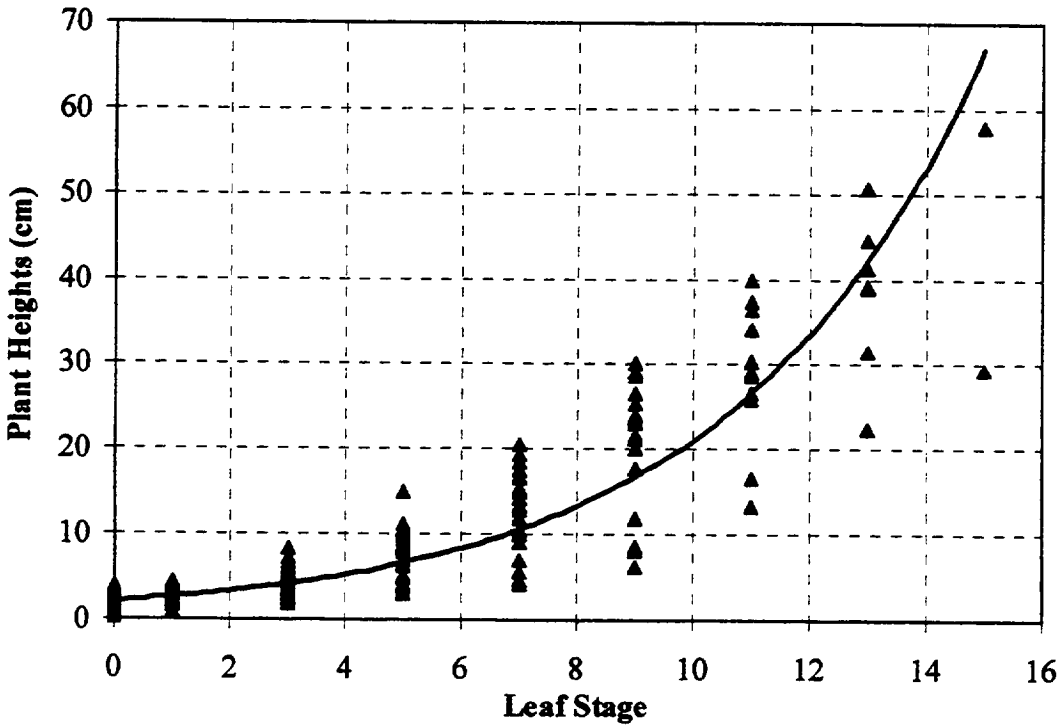

Figure 8.2 Comparison of the Model Equation and the Actual Data for the Relationship between the Plant Heights and the Leaf Stage for the Experimental Conditions where π_{soil} -0.078 = and P_m = -0.000 MPa

The functional relationship between leaf stage and plant height is fairly straight forward from a physiological stand point. As the plants increase in the number of leaf stages, the overall heights increase as well. These are general characteristics of the growth of plants. As for the effects of the osmotic and matric potentials on the heights, increasing the applied suction pressure or decreasing the pore size causes the matric potential to become more negative which, in turn, causes the plants to become stunted in height. Similarly, higher solution concentrations cause the osmotic potential to become more negative as well. In Equation (8.3), π_{soil} and P_m are negative pressure values. This reduction in height could be due to the restriction in the supply of water; although, the water potential levels maintained in this research should not cause severe water deficits. Alternatively, the roots grown in direct contact with the ceramic matrix could have reduced cell expansion as a results of the larger magnitude (more negative) water potentials. Therefore, the overall size of the root mat would be reduced. The reduction in size means that larger, taller plants cannot be supported as well. Furthermore, a continuation of this root-zone condition could cause the plant to produce more roots, diverting resources from the production of terrestrial biomass.

8.1.2. Mass Accumulation Rates

Since the mass of the plant tissues produced in this research cannot be measured during the middle of an experiment but only at the end of the experiment, then a method for calculating the intermdiate masses was desired. This was accomplished by using the measured masses of the plant tissues at the end of the experiments and regressing these values to the final heights of the plants prior to harvest. This method is reasonable since the plants were produced to various stages of the growth cycle. According to Equation (8.1), these growth (leaf) stages are related to the number of days after emergence. Furthermore, the heights were shown to be dependent upon the leaf stage according to Equation (8.3). Therefore, if a statistically adequate relationship can be developed

between the final heights and tissue weights, then a measure of the daily growth can be determined from a combination of this relationship and Equations (8.1) and (8.3).

Since the plants produced in this research were subjected to different root-zone conditions, then these factors should influence the weight of the tissues. However, since h_{plant} was already shown to significantly affected by π_{soil} and P_m, then regressing the dry weights to heights will inherently incorporate these factors. The basic assumption of this relationship is that a tomato plant at whatever height will contain approximately the same amount of dry mass even though the levels of inorganic nutrients may differ. In other words, the inorganic nutrient quantities are small enough not contribute significantly to the overall dry masses. This assumption is reasonable when considering that the dry mass of the tomato plants is primarily comprised of the products of photosynthesis (i.e. C, H, and O) with only small contributions by the inorganic nutrients (see Table 2.1). This assumption is tested by modeling the plant tissue weights as a function of height and solution concentration. Specifically, the individual tissues of leaves, branches, and roots were regressed separately as were the total plant masses determined from the sum of these portions. If the concentration terms are shown to be insignificant influences on the tissue weights, then this will validate the assumption.

In order to determine what form of model should be used for these relationships, the R^2 correlation coefficients were determined for linear, polynomial, exponential, and power functions. This was conducted for each of the different tissue types by plotting the tissue weights versus the plant heights at constant solution concentrations. An example of this comparison is provided in Figure 8.3 for the leaves of the plants produced using a 1x solution. As shown in this figure, the largest R^2 coefficients were obtained for the power functions. The plots for the all of the tissues and concentration levels are provided in Appendix B (see Figures B.1 to B.6).

The result of these model building procedures for the individual plant tissues as well as the entire plant are presented below. In order to produce regression equations for the allometric relationships, the power functions were first linearized by taking the natural logarithms of the effects and responses. Unlike the previous analyses for the models

describing t_{DAE} and h_{plant}, the relative concentration values of 1x and 1/4x were used instead of the osmotic potential equivalents. It should be noted that the tissues from the plants produced using the 1/2x solution were not included since these were combined from several plants. In contrast, all of the data used to formulate these models represent individual plants. This data is provided in Appendix B (see Tables B.16 and B.17).

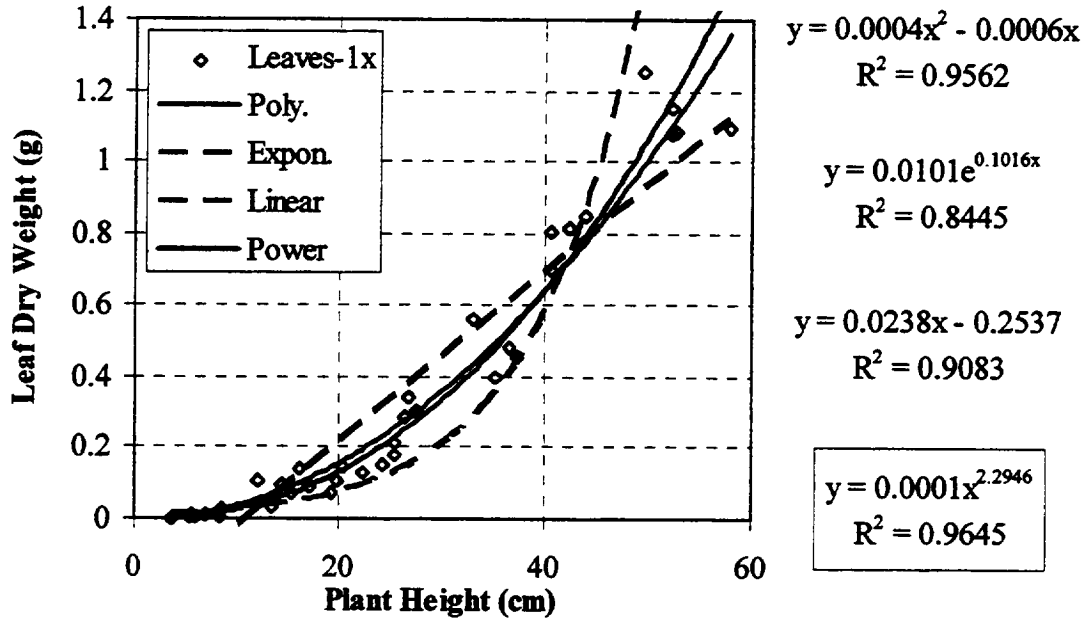

Figure 8.3 Comparison of Various Relationships between Leaf Dry Weight and Height for Tomato Plants Produced using a 1x Solution

Beginning with a complete linearized model, the significance of each individual term was determined from an analysis of variance taken at the α_{risk} level of 0.05. The results of this showed that the weights were only significantly related to the height while the concentration of the solution did not contribute significantly. Furthermore, the statistical analyses of the left-out terms showed that additional terms were not required. The ANOVA tables for the final adequate models for the individual tissues are provided in Appendix B (see Tables B.18 to B.21). Therefore, these equations were then transformed back into the power functions and are provided in Equations (8.4) to (8.7). In these equations, $W_{leaf,d}$, $W_{branch,d}$, $W_{root,d}$, and $W_{plant,d}$, represents the dry mass of the particular

tissue types and the total plant, respectively. An example of Equation (8.7) for the whole plant is provided in Figure 8.4 along with the actual data.

$$W_{leaf,d} = 1.454x10^{-4}(h_{plant})^{2.254} \quad (8.4)$$

$$W_{branch,d} = 0.461x10^{-4}(h_{plant})^{2.588} \quad (8.5)$$

$$W_{root,d} = 0.712x10^{-4}(h_{plant})^{2.204} \quad (8.6)$$

$$W_{plant,d} = 2.402x10^{-4}(h_{plant})^{2.368} \quad (8.7)$$

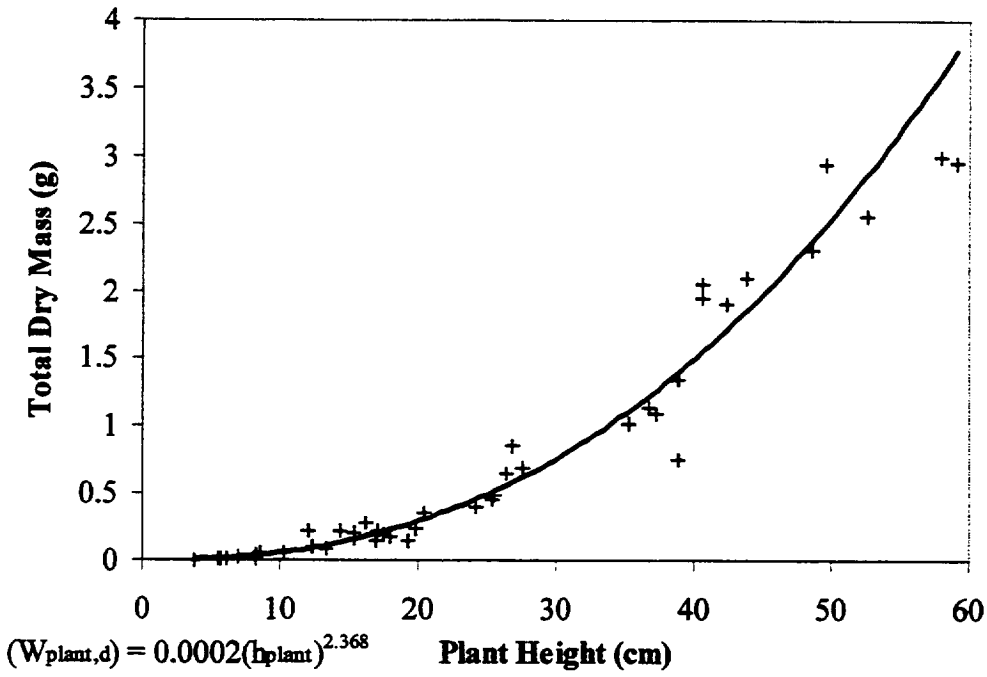

Figure 8.4 Comparison of the Model Equation and the Actual Data for the Relationship between the Dry Weight of the Whole Plant and the Plant Height

The lack of dependence of these relationships to the solution concentration at a constant water potential level provides an indication that the assumption that a plant at whatever height will contain approximately the same amount of dry mass is validated. However, the levels of the inorganic nutrients in these plants may still differ but do not alter the overall dry masses significantly. Furthermore, the rate at which the dry mass is

accumulated as opposed to the absolute values should be subject to the root-zone conditions. This is shown by combining Equations (8.1) and (8.3) with each of Equations (8.4) to (8.7) for the different plant tissues. These relationships form the standard exponential functions which are generally used to describe biological growth. However, these incorporate the effects of the components of the water potential at the root-zone on the accumulation of mass in the various plant tissues.

$$W_{leaf,d} = 1.151x10^{-3} \exp[0.144(t_{DAE}) + 5.206(\pi_{soil}) + 8.769(P_m)] \quad (8.8)$$

$$W_{branch,d} = 4.961x10^{-4} \exp[0.166(t_{DAE}) + 5.978(\pi_{soil}) + 10.069(P_m)] \quad (8.9)$$

$$W_{root,d} = 5.382x10^{-4} \exp[0.141(t_{DAE}) + 5.090(\pi_{soil}) + 8.574(P_m)] \quad (8.10)$$

$$W_{plant,d} = 2.112x10^{-3} \exp[0.152(t_{DAE}) + 5.471(\pi_{soil}) + 9.215(P_m)] \quad (8.11)$$

8.2. Plant Water Status Results

The water status of the tomato plants grown in this research includes three distinct phases consistent with the soil-plant-atmosphere continuum. Beginning with the plant itself, the quantity of water that is retained in the tissues, or hydration level, $H_{w,tissue}$, was determined from the difference between the wet and dry masses of the tissues at final harvest. Furthermore, from the models for the dry masses formulated as Equations (8.8) to (8.11) for the different respective tissues, related models were produced for the wet weights. Therefore, the differences between the wet and dry mass models for the individual tissues produced models for the hydration or water retention levels.

Once the hydration of the plants were determined, the amounts of solution absorbed by the plant roots, V_u, were determined as well. These were further shown to differentiate based on the soil water potential, Ψ_{soil}. These differences provided direct evidence that the PCT-NDS was capable of controlling the root-zone environment. Using the difference between the total solution uptake rates and the hydration of the plants resulted in a calculation method for the daily transpiration, E_t*, from the tomato plants.

8.2.1. Plant Water Retention

In order to determine the amount of water retained in the tissues of the tomato plants, the wet masses were regressed to the plant heights in a manner identical to the procedure used for the dry masses. This produces equations identical in form to Equations (8.4) to (8.7); although, the values for the parameters differ. This difference is due to the values of the dry masses used to produce Equations (8.4) to (8.7) as compared to the wet masses as presented in Appendix C (see Tables C.1 and C.2). Again, the effects of concentration were shown to be insignificant on these weights as were the left-out terms for the final model. The statistical results for the final adequate model are shown in the ANOVA tables presented in Appendix C (see Tables C.3 to C.6). The final regression equations for the various wet masses of the tissues as well as the whole plant are presented below as Equations (8.12) to (8.15), respectively. In these equations, $W_{leaf,w}$, $W_{branch,w}$, $W_{root,w}$, and $W_{plant,w}$, represents the wet mass of the particular tissue types and the total plant, respectively. An example of Equation (8.15) for the whole plant is provided in Figure 8.5 along with the actual data.

$$W_{leaf,w} = 2.177\text{x}10^{-3}(h_{plant})^{2.057} \quad (8.12)$$

$$W_{branch,w} = 1.402\text{x}10^{-3}(h_{plant})^{2.329} \quad (8.13)$$

$$W_{root,w} = 2.795\text{x}10^{-3}(h_{plant})^{1.937} \quad (8.14)$$

$$W_{plant,w} = 5.834\text{x}10^{-3}(h_{plant})^{2.141} \quad (8.15)$$

Since the plant heights were shown to be statistically affected by the leaf stage, osmotic potential, and matric potential according to Equation (8.3), then the wet weights can be shown to be influenced by these factors as well. Furthermore, since the leaf stage is directly related to the number of days after emergence according to Equation (8.1), then the models for the wet weights can be converted to this time scale as well. This combination of Equations (8.1) and (8.3) with Equations (8.12) to (8.15) produces the exponential growth equations for the wet weights of the tissues and whole plant. These are presented in Equations (8.16) to (8.19) below. These equations are identical in form to the dry mass counterparts presented as Equations (8.8) to (8.11).

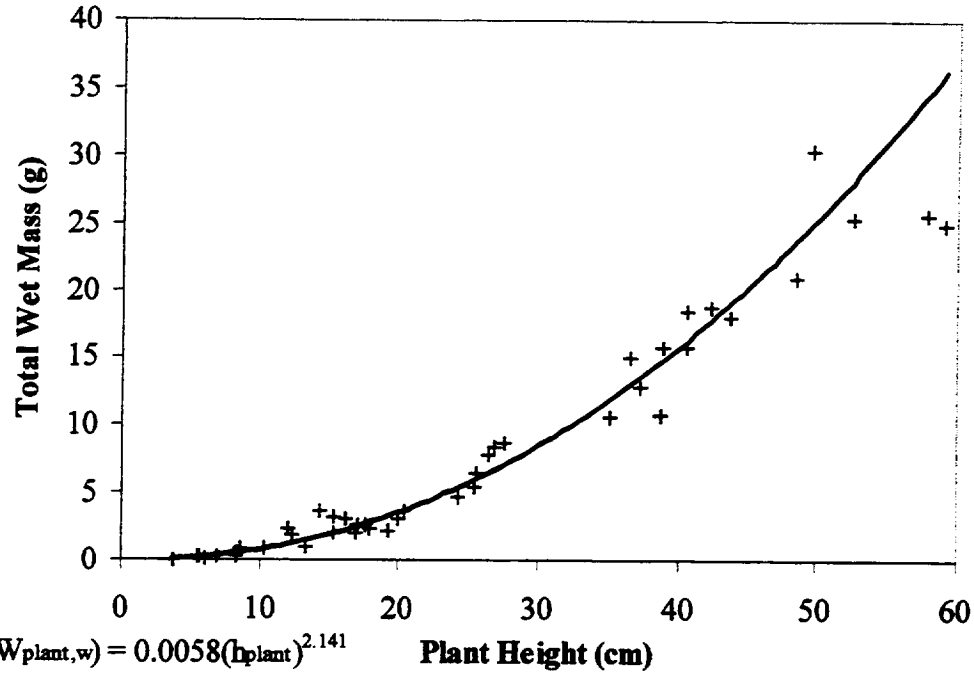

Figure 8.5 Comparison of the Model Equation and the Actual Data for the Relationship between the Wet Weight of the Whole Plant and the Plant Height

$$W_{leaf,w} = 1.438x10^{-2} \exp[0.132(t_{DAE}) + 4.752(\pi_{soil}) + 8.004(P_m)] \quad (8.16)$$

$$W_{branch,w} = 1.189x10^{-2} \exp[0.149(t_{DAE}) + 5.380(\pi_{soil}) + 9.062(P_m)] \quad (8.17)$$

$$W_{root,w} = 1.654x10^{-2} \exp[0.124(t_{DAE}) + 4.474(\pi_{soil}) + 7.537(P_m)] \quad (8.18)$$

$$W_{plant,w} = 4.163x10^{-2} \exp[0.137(t_{DAE}) + 4.946(\pi_{soil}) + 8.331(P_m)] \quad (8.19)$$

Since the wet masses includes both the water and the inorganic nutrients contained in the tissues, then Equations (8.16) to (8.19) represent the portions of the total solution taken up that is retained in the tissues. In order to determine the hydration of the tomato plants, $H_{w,tissue}$ (in ml), the difference between the corresponding wet and dry masses are calculated. The resulting quantities represent the amounts of water retained in the various tissues.

$$H_{w,tissue} = W_{tissue,w} - W_{tissue,d} \quad (8.20)$$

8.2.2. Water Uptake and Transpiration Rates

The absolute uptake of solution into the tomato plants grown on the PCT-NDS were determined by taking measurements of the change in volume in the reservoir on a daily basis. These values, $\Delta V_{res,j}$, were recorded to the nearest ml of solution on each day, j. In order to determine the rate of uptake, Q_u (in ml solution per day), the total quantity of these daily changes in solution level, $V_u = \Sigma_j \Delta V_{res,j}$, was modeled as a function of the estimated leaf stage of development. These leaf stages were determined from Equation (8.3) using the average daily measurements of the plant heights, h_{plant}. Furthermore, by incorporating the various effects of the osmotic and matric potentials tested in this research, the capabilities of the PCT-NDS to control the root-zone environment can be evaluated. This is shown in the analyses below.

One of the capabilities of the ceramic tube system is the ability to compensate for changes in the osmolarity of the solution with changes in the applied suction pressure in order to maintain a constant root-zone water potential. In order to test this, the results for the constant water potential level of Ψ_{soil} = -0.078 MPa were obtained using the three solution osmolarities of π_{soil} = -0.019, -0.039, and -0.078 MPa compensated for by the respective levels of the applied matric potential, P_m = -0.059, -0.039, and -0.000 MPa. From the initial appearance of the relationship between V_u and LS at each individual test condition, an exponential function is suggested as a possible model. These plots are provided in Appendix C (see Figures C.3 to C.5). Therefore, these relationships between V_u and LS were linearized by taking the natural logarithm of V_u. In order to determine the significance of the effects of the osmotic and matric potentials on V_u, each of these factors were included in the linearized model and subsequently analyzed. This was accomplished by comparing the calculated F-statistics for each of these terms at an α_{risk} level of 0.01 with the critical value determined using the average standard deviation from all data sets.

The risk level of 0.01 used in this analysis as compared to previous models which used an α_{risk} of 0.05 was considered acceptable when considering the sources of errors for the solution uptake measurements. First of all, the volumetric measurements were taken to the nearest ml. During the initial stages of growth, this is the same order of magnitude as

the measurements themselves. Furthermore, at these early stages, the magnitude of the evaporation of water from the ceramic surface is relatively large compared to the change in volumes caused by the plant. This initial evaporation occurs through the hole cut into the opaque tube cover (see thge description of Figure 7.2) until the plant stem fills this hole. Next, the transpirational driving force for the uptake of solution through the roots is highly dependent upon the terrestrial conditions of temperature and humidity. Although these were maintained as constant as possible, the results presented in Appendix A illustrate the degree of variability in $T_{a,ave}$ and RH between the experiments as well as during a specific experiment. And, finally, since several plants were produced on a single test bed unit with a single reservoir, then the daily volumetric measurements are the total quantities of solution taken up by all of the plants. In order to put this on a per plant basis, the average daily solution uptake quantities were determined and used in the analyses.

The results of this analysis showed that the different osmotic and matric potentials did not have a significant effect on the uptake of solution. This was based on the values of F_{calc} versus F_{crit} as shown in Table 8.3 below. The only significant term in this model is the effect of the different stages of growth on the solution uptake. Furthermore, the left-out terms from this model were shown to be insignificant even after eliminating the $b_2(\pi_{soil})$ and $b_3(P_m)$ terms from the model. This updated ANOVA table is presented in Table 8.4.

Table 8.3 Analysis of Variance Table for the Complete Model Describing the Natural Log of the Solution Uptake (Y) as Affected by the Leaf Stage (X1), Osmotic Potential (X2), and Matric Potential (X3) at a Constant Water Potential Level of -0.078 MPa

	DOF	Sum Sqs.	Mean Sqs.	Fcalc		Fcrit	Signif?
Total	418	5394				$\alpha_{risk} = 0.01$	
Model	4	5328	1332	8311	>	3.368	yes
b0	1	4493	4493	28032	>	6.701	yes
b1	1	834.32	834.32	5206	>	6.701	yes
b2	1	0.305	0.305	1.904	<	6.701	no
b3	1	0.808	0.808	5.040	<	6.701	no
Resid	414	66.349	0.160				
Error	387	59.664	0.154				
LOT	27	6.685	0.248	1.545	<	1.789	no

Table 8.4 Analysis of Variance Table Describing the Natural Log of the Solution Uptake (Y) as Affected by Only the Leaf Stage (Y) at a Constant Water Potential Level of -0.078 MPa

	DOF	Sum Sqs.	Mean Sqs.	Fcalc		Fcrit	Signif?
Total	418	5394				$\alpha_{risk} = 0.01$	
Model	2	5327	2663	16424	>	4.660	yes
b0	1	4493	4493	27703	>	6.701	yes
b1	1	834.32	834.32	5145	>	6.701	yes
Resid	416	67.462	0.162				
Error	387	59.665	0.154				
LOT	29	7.798	0.269	1.658	<	1.760	no

Since the differences in the osmotic and matric potentials for these test conditions did not affect the solution uptake significantly, then this is an indication that the water potential was maintained at a constant level. Therefore, these results are an indication that the PCT-NDS is capable of maintaining a specific root-zone water potential under different nutrient solution concentrations by altering the applied matric potential. This partially satisfies Objective (1) of this research. Additional proof would need to be shown that different root-zone water potentials change the quantity of solution taken up.

In addition to testing this system at a constant water potential, different combinations of π_{soil} and P_m were examined in order to maintain different root-zone environmental conditions. This was desired in order to study the effects of these conditions on the growth and nutrient uptake into plants as compared to the manipulations conducted by the plants themselves. The specific levels of Ψ_{soil} tested were presented in Table 7.2. Again, linearized exponential equations were determined for these relationships containing terms for the leaf stage and the overall root-zone water potential. The individual exponential plots for the different test conditions are provided in Appendix C (see Figures C.1 to C.7). The data presented in these appendix figures were used to model the solution uptake into the plants grown on the PCT-NDS. For these situations, the different π_{soil} and P_m values should result in significant effects since these dictate the

overall water potential levels. More specifically, the conglomeration of these two factors into their usual form, $(P_m - \pi_{soil})$, which is equivalent to Ψ_{soil} according to Equation (2.4), should result in a significant contribution to the solution uptake. This is shown in the following ANOVA table presented in Table 8.5. The final adequate regression model for the solution uptake is presented in Equation (8.21).

$$\ln(V_u) = 1.551 + 0.400(LS) + 8.605(\Psi_{soil}) \qquad (8.21)$$

Substituting Equation (2.4) into Equation (8.21) for Ψ_{soil} allows for the solution uptake to become a function of not only the leaf stage, but the osmotic and matric potentials as well.

$$\ln(V_u) = 1.551 + 0.400(LS) + 8.605(P_m - \pi_{soil}) \qquad (8.22)$$

Transforming Equation (8.22) back into the non-linear exponential form results in Equation (8.23) shown below. Equation (8.23) represents the final model of the solution uptake which incorporates the time dependence as well as the various root-zone conditions that were used to produce the plants on the PCT-NDS.

$$V_u = 4.716 \exp[0.400(LS) + 8.605(P_m - \pi_{soil})] \qquad (8.23)$$

Table 8.5 Analysis of Variance Table for the Final Model Describing the Natural Log of the Solution Uptake (Y) as a Linear Function of the Leaf Stage (X1) at All Water Potential Levels (X2)

	DOF	Sum Sqs.	Mean Sqs.	Fcalc		Fcrit	Signif?
Total	724	9570				$\alpha_{risk} = 0.01$	
Model	3	9417	3139	14813	>	3.812	yes
b0	1	7993	7993	37718	>	6.674	yes
b1	1	1383	1383	6528	>	6.674	yes
b2	1	40.700	40.700	192.05	>	6.674	yes
Resid	721	152.79	0.212				
Error	654	137.35	0.210				
LOT	67	15.445	0.231	1.088	<	1.480	no

Since the present results provide proof that the root-zone conditions and the corresponding solution uptake can be controlled using this system, then these results in conjunction with the previous results for the constant water potential level satisfy Objective (1). Again, since π_{soil} and P_m are negative pressure values, then more negative values decrease the solution uptake. This makes sense conceptually since the water potential gradient between the root-zone and the root, (Ψ_{soil} - Ψ_{root}), which is a positive value, would be reduced as Ψ_{soil} is decreased (the root water potential is more negative than the soil).

Using Equation (8.1) relating the leaf stage to the number of days after emergence, the model for the solution uptake can be transformed from the leaf stage time scale to the number of days after emergence. This is shown in Equation (8.24) below.

$$V_u = 4.716 \exp[0.111(t_{DAE}) + 8.605(P_m - \pi_{soil})] \qquad (8.24)$$

Since both the plant hydration and solution uptake quantities have been modeled as a function of t_{DAE}, the rate of transpiration from the tomato plants can be determined as well. This is accomplished by first combining Equations (8.19) and (8.11) describing the wet and dry plant masses, respectively, with Equation (8.20) for the hydration. Taking the derivative of this resulting equation with respect to t_{DAE} results in an expression for rate of water retention, $Q_r = dH_{w,tissue}/dt$. Subtracting this rate from the rate of solution uptake, $Q_u = dV_u/dt$, results in a model equation for the transpiration rate, E_t^*. This was presented earlier in Equation (7.3). Substituting the exponential models for both $H_{w,tissue}$ and V_u, into Equation (7.3) leads to a model equation describing the relationships between E_t^* and the leaf stage, osmotic potential, and matric potential. This is presented in Equation (8.25).

$$\begin{aligned} E_t^* &= dV_u / dt_{DAE} - dH_{w,tissue} / dt_{DAE} \\ E_t^* &= 5.235\text{x}10^{-1} \exp[0.111(t_{DAE}) + 8.605(P_m - \pi_{soil})] \\ &\quad - 5.716\text{x}10^{-3} \exp[0.137(t_{DAE}) + 4.946(\pi_{soil}) + 8.331(P_m)] \\ &\quad + 3.210\text{x}10^{-4} \exp[0.152(t_{DAE}) + 5.471(\pi_{soil}) + 9.215(P_m)] \end{aligned} \qquad (8.25)$$

8.3. Inorganic Nutrient Mass Balances

In addition to showing that the root-zone water potential can be controlled to specific levels using the PCT-NDS, it was also required to maintain a constant Ψ_{soil} while subjecting the tomato plants to different solution concentrations. This was in order to obtain the kinetic data independent of the effects of different solution uptake rates. For this situation, the different osmotic and matric potentials (in MPa) were controlled, respectively, to the experimental levels of (π_{soil} / P_m) of (-0.019/-0.059), (-0.039/-0.039), and (-0.078/-0.000) shown in Table 7.2. The tomato plants produced under these conditions were harvested and analyzed for the inorganic nutrient contents using the method described earlier (see Section 7.3.2).

The inorganic nutrients that were examined in this research include the essential nutrients, P, K, Mg, Ca, Fe, B, Cu, Mo, Mn, and Zn, and the non-essential Na. The Inductively Coupled Plasma - Atomic Emission Spectroscopy (ICP-AES) used to analyze for these various nutrients was conducted in three distinct phases or passes through the spectrometer. During one pass, the spectroscopic emissions from P, Mg, and Ca were detected while during another, K and Na were analyzed. Finally, for the micronutrients, these spectral readings were measured during the third pass. The characteristic wavelengths for each of these elements are presented in Table 8.6 below along with the background equivalents, detection limits, and interfering elements. The results from this analytical system were generated as a computer output and presented on a part per million (ppm) basis. These data were automatically corrected for any dilutions that were required during sample preparation as well as any changes in background noise (compared to calibration samples). These nutrient concentrations were obtained for both solution and tissue samples and were used to produce mass balances confirming the analytical technique used in this research. Once the inorganic balances were closed, the nutrient uptake rates into the tomato plants produced on the PCT-NDS could be determined. These rates are calculated in Chapter 9.

Table 8.6 Characteristic Wavelengths, Background Equivalents, Detection Limits, and Interfering Elements for the Analysis of the Plant Nutrients in the ICP-AES System

Element	Wavelength (nm)	Background Equivalent (ppm)	Detection Limit (ppm)	Interfering Elements
P	214.914	2.56	0.08	
Mg	202.582	0.01	0.02	
Ca	213.933	0.02	0.01	
Na	589.592	0.99	0.03	
K	766.491	7.10	0.50	
Mo	202.030	0.26	0.008	
Zn	213.856	0.06	0.002	Cu
B	249.678	0.16	0.006	Fe
Mn	257.610	0.05	0.002	
Fe	259.940	0.42	0.007	Mn
Cu	324.754	0.18	0.006	

For the macro-nutrient elements, the concentrations obtained from both the liquid and tissue samples are well above the detection limits listed in Table 8.6. Therefore, the values provided in the computer outputs can be used with reasonable assurance for quantification purposes. As for the micro-nutrients, some of the elemental concentrations reported are on the same order of magnitude as the detection limits. In order for reasonable quantifications to be made, the concentrations in the samples should be at least 5 times the detection limit [Boss and Fredeen, 1986]. Below this multiple is only a qualitative assessment that the nutrient is present in the sample. This is true for the liquid sample quantities of most of the micro-nutrients including Mo, Zn, B, Mn, and Cu. Therefore, accurate mass balances cannot be confirmed for these nutrients. However, the tissue samples resulted in concentrations for these micro-nutrients that were several orders of magnitude greater than the detection limit and can, therefore, be utilized to determine the mass transport and kinetic models (see Chapter 9).

8.3.1. Plant Measurements

The mass balances produced for the various inorganic nutrients compared the amount measured in the plant tissues to the calculated amount depleted from the PCT-NDS. The quantities in the plant tissues were determined by multiplying the concentrations (in ppm or $\mu g\ g^{-1}$ dry weight) reported on the ICP-AES output by the respective dry mass of the tissues analyzed. This included the leaves ($q_{leaf,i} = C_{leaf,i} \times W_{leaf,d}$), branches ($q_{branch,i} = C_{branch,i} \times W_{branch,d}$), and roots ($q_{root,i} = C_{root,i} \times W_{root,d}$) where i represents a specific element. The sum of these quantities produces one side of the mass balance, $q_{plant,i}$, as shown in Equation (8.26).

$$q_{plant,i} = q_{leaf,i} + q_{branch,i} + q_{root,i} = \sum_{plant} (C_{leaf,i}W_{leaf,d} + C_{branch,i}W_{branch,d} + C_{root,i}W_{root,d}) \quad (8.26)$$

Associated with these measurements are several experimental errors including the collection of the tissues, weighing of the samples, incomplete digestion of the tissues, and spectroscopic variances. For the first two sources of error, the dry weight measurements were estimated to have a standard deviation of, $\sigma_{Wtissue,d} = \pm 0.001$ g, regardless of the tissue type. The reasons for these sources of error are due to both the experimenter and the weighing balance. When collecting tissues as described earlier (see Section 7.3.2), the harvesting and separation of the leaves from the branches and the main stem from the root mass is dependent upon the actual location of the cut. Although care was taken to conduct this procedure in a consistent manner, there are undoubtably differences which can be considered during the mass balance calculations. The magnitude of this error was approximated based on a ± 0.05 cm difference in the cut location. Comparing this ± 0.05 cm difference in location to an identical difference in the plant height measurements (i.e. both vision based) allows for the error associated with the weights to be propagated using Equations (8.4) to (8.6) relating the tissue dry weights to the plant heights. Assuming a change in plant height from 2 to 65 cm leads to the average error in the weights of ± 0.001 g. This analysis is provided in Appendix D. As for the the precision of the balance used, repeated weight measurements of identical samples lead to an average error of only

$\pm$0.0005 g. Therefore, the error associated with the cut location encompasses the error in weight measurement.

As for the magnitude of the errors associated with analyzing tissues in the ICP system, these were determined by submitting tissue samples obtained from identical sources and comparing the results. Unfortunately, this procedure could not be repeated for each tissue sample collected due to the sample size requirements as compared to total tissue quantities available as well as the cost of each individual analysis. Multiple samples of leaves, branches, and roots were analyzed with the resulting estimates of the standard deviations averaged over the different tissues and sample numbers. This analysis, presented entirely in Appendix D (see Tables D.1 to D.3), resulted in the average standard deviations listed in Table 8.7 below for the concentrations of the different inorganic nutrients. These values will be used in the subsequent error propagation calculations of the mass balances. Included on this table are the average percentages of the ratio of the standard deviation estimates for the different tissues, $\sigma_{Ctissue,i}$, to the average concentration values, $C_{tissue,i,ave}$. These percentages are presented in order to give an idea of the magnitude of these errors compared to the reported results.

Table 8.7 Standard Deviations Associated with the Analysis of Plant Tissues in the Inductively Coupled Plasma - Atomic Emissions Spectrometer

Nutrient Element	$\sigma_{Ctissue,i,ave}$ (μg/g)	% ($\sigma_{Ctissue,i}/C_{tissue,i,ave}$)
P	$\pm$ 1159.52	21.95
Mg	$\pm$ 2189.82	11.90
Ca	$\pm$ 8702.26	30.06
Na	$\pm$ 242.59	11.63
K	$\pm$ 3571.68	8.64
Mo	$\pm$ 0.67	21.42
Zn	$\pm$ 14.12	8.35
B	$\pm$ 7.32	10.92
Mn	$\pm$ 8.21	12.31
Fe	$\pm$ 206.06	28.92
Cu	$\pm$ 1.68	13.47

8.3.2. Solution Measurements

In order to balance the measured plant tissue masses, the amount of each nutrient depleted from the PCT-NDS over the course of an experiment were determined. This was accomplished by sampling the hydroponic solution used during an experiment and submitting these samples for ICP analysis. These results were also reported on a ppm basis and it was assumed that the nutrient solution had a density equivalent to water (ρ = 1.0 g ml^{-1}). This assumption is validated when considering the isotonic salt levels in the solution.

Again, associated with these measurements are errors similar to the analysis of the tissues samples. When preparing the 20 ml liquid samples (V_{sample}), 19.6 ml of solution (V_{soln}) are mixed with 0.4 ml of nitric acid. These volumetric measurements of the solution were conducted using a 50 ml storage tube graduated to the nearest ml. Therefore, an estimated standard deviation for these measurements is $\sigma_{V_{sample}} = \sigma_{V_{soln}} = \pm 0.1$ ml. As for the addition of the nitric acid, a 1 ml micro-pipetter was utilized which would not contribute significantly to any volumetric differences as compared to the solution quantity. Therefore, when determining the concentration of the nutrients in the solution, $C_{soln,i}$, from the concentrations in the acid mixture, $C_{sample,i}$, these volumetric differences can be considered through a propagation of errors. The calculation of the actual solution concentration from the sample concentration measured in the ICP system is presented in Equation (8.27).

$$C_{soln,i} = (C_{sample,i}\, V_{sample}) / V_{soln} \tag{8.27}$$

An additional source of error associated with the analysis of the solution samples is contained within the ICP system itself. In order to determine the magnitude of these errors, replicates were conducted by measuring the concentrations of the various elements using samples from identical sources. By using the fresh Hoagland's solution prepared for each individual experiment, the errors associated with the preparation of the bulk solutions between the various experiments can be incorporated as well. The individual standard deviations in the bulk solution samples obtained from each experiment were averaged over all experiments and average concentrations, $C_{sample,i,ave}$. The specific data are presented in

Appendix D (see Tables D.4 to D.9). This resulted in the following average standard deviations in sample measurements, $\sigma_{Csample,i,ave}$, for each of the individual nutrients, i, that were analyzed. These are presented in the Tables 8.8 to 8.10 for the 1x, 1/2x, and 1/4x solutions, respectively, along with the average percentage ratios of the standard deviations over the average sample concentrations for each experiment and concentrations. These values will be used in the subsequent propagation of errors during the calculations of the mass balances and nutrient uptake rates. In addition to the inorganic nutrients, the average standard deviation for the pH of the solutions is presented as well. This value will be used during the examination into the effects of pH on the solubility of the inorganic ions described below.

Table 8.8 Concentrations and Standard Deviations Associated with the Analysis of 1x Solution Samples in the Inductively Coupled Plasma - Atomic Emissions Spectrometer

Nutrient Element	1x Solution $C_{sample,i,ave}$ (μg/ml)	1x Solution $\sigma_{Csample,i,ave}$ (μg/ml)	1x Solution Percentage Error $\sigma_{Csample,i}/C_{sample,i}$ x 100%
P	29.13	± 0.380	1.90
Mg	92.53	± 1.666	2.23
Ca	203.14	± 3.725	2.29
Na	11.22	± 0.158	2.64
K	218.55	± 2.214	1.78
Mo	0.02	± 0.003	19.62
Zn	0.05	± 0.010	28.12
B	0.72	± 0.025	4.20
Mn	0.48	± 0.010	3.09
Fe	4.73	± 0.077	2.85
Cu	0.15	± 0.024	18.15
pH	5.98	± 0.086	1.52

Table 8.9 Concentrations and Standard Deviations Associated with the Analysis of 1/2x Solution Samples in the Inductively Coupled Plasma - Atomic Emissions Spectrometer

Nutrient Element	1/2x Solution $C_{sample,i,ave}$ (µg/ml)	1/2x Solution $\sigma_{Csample,i,ave}$ (µg/ml)	1/2x Solution Percentage Error $\sigma_{Csample,i}/C_{sample,i}$ x 100%
P	14.39	± 0.141	1.00
Mg	44.39	± 0.141	0.33
Ca	98.78	± 2.828	2.92
Na	6.06	± 0.078	1.31
K	111.16	± 0.283	0.26
Mo	0.01	± 0.000	0.00
Zn	0.02	± 0.000	0.00
B	0.40	± 0.000	0.00
Mn	0.20	± 0.000	0.00
Fe	2.14	± 0.000	0.00
Cu	0.20	± 0.000	0.00
pH	6.31	± 0.325	5.15

Table 8.10 Concentrations and Standard Deviations Associated with the Analysis of 1/4x Solution Samples in the Inductively Coupled Plasma - Atomic Emissions Spectrometer

Nutrient Element	1/4x Solution $C_{sample,i,ave}$ (µg/ml)	1/4x Solution $\sigma_{Csample,i,ave}$ (µg/ml)	1/4x Solution Percentage Error $\sigma_{Csample,i}/C_{sample,i}$ x 100%
P	7.20	± 0.221	3.23
Mg	24.01	± 0.632	3.00
Ca	54.00	± 1.111	2.53
Na	3.01	± 0.161	5.67
K	55.93	± 2.151	3.94
Mo	0.01	± 0.003	16.67
Zn	0.02	± 0.015	38.98
B	0.22	± 0.011	4.41
Mn	0.12	± 0.004	3.27
Fe	1.18	± 0.045	3.81
Cu	0.17	± 0.039	27.26
pH	6.04	± 0.110	1.92

When comparing the standard deviations presented for the solutions inTables 8.8 to 8.10 to the values determined for the plant tissue analyses presented in Table 8.7, several conclusions can be drawn. For the macro-nutrients, the percentage errors are an order of magnitude lower in the liquid samples as compared to the tissue counterparts. This is an indication that the major source of error associated with the tissue samples is due to the acid digestion process used in preparation. Once in liquid form, the analytical errors are reduced. As for the micro-nutrients, the standard deviations are generally within the same range for both analyses. Therefore, the digestion and actual spectroscopic analyses are relatively equal contributors to the error.

In order to determine the amount of each nutrient depleted from the PCT-NDS, the concentrations of the initial and final solutions of each experiment were analyzed. The initial concentrations obtained from the ICP analyses, $C_{soln,i,init}$ were multiplied by the total volume of fresh solution used during each experiment. In order to determine the total amount of fresh Hoagland's solution supplied to the system, the total sum of the daily quantities of solution taken up by the plants were determined. These changes in the reservoir volume, $\Delta V_{res,j}$, for each day, j, were replenished using fresh Hoagland's solution as well. Furthermore, periodic solution samples were withdrawn during the course of each experiment and replaced with an equal volume of fresh solution. Therefore, these additions to the systems due to the sampling volumes removed, V_{soln}, are considered as well. Therefore, the total amount supplied is equal to these replenishment volumes added to the initial volume of the system, V_{sys}. This initial volume is dependent upon the specific ceramic tubes attached to the system due to the different porosities and other physical dimensions. Multiplying this total volume by the concentration of the solution used in the system allows for the total supply of each nutrient, i, to be determined, $q_{input,i}$. This calculation is provided in Equation (8.28).

$$q_{input,i} = C_{soln,i,init} \times (V_{sys} + \sum_{j} \Delta V_{res,j} + \sum_{k} V_{soln}) \qquad (8.28)$$

The concentration term in Equation (8.28) can be combined with Equation (8.27) where $C_{soln,i,init} = C_{soln,i}$ and $C_{sample,i} = C_{sample,i,init}$.

In addition to the errors associated with the concentration of nutrients in solution, there exists experimental errors contributed by the measurement of the volumetric changes in the reservoir as well as the system volume. Since the reservoir used in this research was a 500 ml cylinder graduated to the nearest 5 ml, then these volumetric based measurements have an estimated standard deviation of ± 0.5 ml. This value applies to both $\sigma_{V_{sys}}$ and $\sigma_{\Delta V_{res,j}}$ and will be used in subsequent propagation of error calculations.

In order to determine the amount of each nutrient remaining in solution in the system after the experiment or removed during the experiment, $q_{rem,i}$, a similar procedure was utilized. Solution samples from the final bulk were withdrawn and submitted to the ICP analysis. These concentrations, $C_{soln,i,final}$ where i represents the individual nutrients, were first calculated using Equation (8.27) and then multiplied by the final volume of solution remaining in the system after the plants were harvested. This volume is determined as the system volume minus the change in the reservoir volume for that day, $V_{sys} - \Delta V_{res,f}$. In addition to these remaining quantities, $q_{rem,i}$ also includes the quantities of nutrients contained in the periodic solution samples. This portion can be determined as the sum of the individual products of the sampling volume, V_{soln}, and the measured concentrations, $C_{soln,i,k}$, for sample, k. Although different notations are used, $C_{soln,i,final}$ is equal to $C_{soln,i,k}$ when k is the final sample taken and $\Delta V_{res,f} = \Delta V_{res,j}$ when j is the last day. Therefore, the total quantity of nutrients either remaining in the system at the end or removed during the experiment can be calculated using Equation (8.29) below.

$$q_{rem,i} = q_{remain,i} + q_{removed,i} = C_{soln,i,final} \times (V_{sys} - \Delta V_{res,f}) + \sum_{k} (C_{soln,i,k} \times V_{soln}) \quad (8.29)$$

In addition to the quantities of nutrients dissolved in the solution, there existed visible precipitates throughout the systems. These precipitates could be found in the dead spaces of the reservoir as well as throughout the system. The formation of these solid materials were due to the effects of pH on the concentration of the various inorganic ions. As the pH changed during the course of an experiment (generally increased from 5.7 to slightly above neutral), some nutrients would begin to precipitate out of solution. When

obtaining the liquid samples from the system, these precipitates were not collected nor were they accounted for during the calculation of the depletion amount from the system. In other words, $q_{rem,i}$ would be underestimated if concentrations were larger than measured due to the precipitates not being included in the sample measurement.

In order to approximate the amounts of each nutrient precipitating out of solution due to the changes in pH, a side experiment was conducted which altered the pH of a fresh Hoagland's #1 hydroponic solution (1x strength) in a stepwise manner. As the pH was altered from the initial level of 5.7 to a maximum value of 8.0 using 10% NaOH, precipitates could be visually seen to fall out of solution. Decanting the remaining solution from these mixtures and preparing solution samples allowed for the determination of the pH dependent concentrations for the individual nutrients, $C_{soln,i}$. Statistical regressions of these relationships between $C_{soln,i}$ and the pH were produced and are presented in Equations (8.30) to (8.34) below. The corresponding regression figures, ANOVA tables, parameter significance, and model adequacy calculations are provided in Appendix D (see Figures D.1 to D.5 and Table D.10 to D.14). The only results presented are those for which accurate mass balances can be established. These include P, Mg, Ca, K, and Fe. Furthermore, the concentrations of the other micro-nutrients besides Fe remained constant during this pH experiment (see Figure D.6). Since the base used to adjust the pH was NaOH, the concentration changes for Na were not analyzed.

The results of this experiment revealed that the concentration of soluble P, Mg, Ca, and Fe decreased with increasing pH while the concentration of K remained constant.

$$C_{soln,P} = -4.865(pH)^2 + 54.394(pH) - 122.77 \quad (8.30)$$

$$C_{soln,Mg} = -3.921(pH) + 114.22 \quad (8.31)$$

$$C_{soln,Ca} = -32.299(pH) + 392.46 \quad (8.32)$$

$$C_{soln,K} = 212.98 \quad (8.33)$$

$$C_{soln,Fe} = -0.793(pH) + 9.35 \quad (8.34)$$

In order to apply these relationships to the experiments conducted with the tomato plants, the ratios of these concentrations to the standard concentration at the initial pH

level, $C_{soln,i}^{\circ}$, were determined for the precipitation experiment. Since the volumes of these samples are constant in this experiment, then these concentration ratios, $f_{sol,i}$, are also equivalent to the ratios of the quantities remaining soluble at the various pH levels to the total quantities in the initial mixture. This is shown in Equation (8.35) below.

$$f_{sol,i} = C_{soln,i}/C_{soln,i}^{\circ} = q_{remain,i}/q_{remain,i}^{\circ} \qquad (8.35)$$

Therefore, these concentration ratios were subsequently used to determine the levels of precipitates present in the system, $q_{precip,i}$, at the end of the plant experiments. This was achieved by calculating $C_{soln,i}$ using the final pH of the solution in Equations (8.30) to (8.34). Dividing these concentrations by the corresponding $C_{soln,i}^{\circ}$ from the pH experiment, calculated using the same equations but with pH = pH_0, resulted in the concentration ratios according to the first two terms in Equation (8.35). Since this ratio also defines the ratio of the quantities according to the first and third terms in Equation (8.35), then the total quantities of the nutrients present at the end of the plant experiments, $q_{remain,i}^{\circ}$, can be determined as ($q_{remain,i}$ / $f_{sol,i}$) where $f_{sol,i}$ is dependent upon the results of the pH experiment. In order to calculate the nutrient quantities present in the final solution, $q_{remain,i}$, the measured concentrations of the final solution, $C_{soln,i,final}$, are multiplied by the final volume, (V_{sys} - $\Delta V_{res,f}$). Since the total quantities are equal to the sum of the soluble and precipitated quantities, then the precipitated amount can be determined as the difference between $q_{remain,i}^{\circ}$ and $q_{remain,i}$. Furthermore, substituting the values for the quantities gives the result in Equation (8.36) in terms of the final solution concentration. It should be emphasized that $f_{sol,i}$ in this equation is calculated from the results of the pH experiment while $C_{soln,i,final}$ is the concentration from the plant experiment.

$$q_{precip,i} = q_{remain,i}^{\circ} - q_{remain,i} = \frac{1 - f_{sol,i}}{f_{sol,i}} C_{soln,i,final}(V_{sys} - \Delta V_{res,f}) \qquad (8.36)$$

This method of determining the precipitation quantities is based on the assumption that there exists a pH based equilibrium between the quantities in solution and in the solid phase. This has been similarly reported for ionic solutions contained in various soils

[Traina, et al., 1986; Reuss, et al., 1990]. For the present purposes, this method is acceptable although an addition investigation into the effects of pH on the hydroponic solution is warranted. This is discussed later as future research (see Section 10.2.2).

In addition to the errors associated with the concentration and volumetric measurements discussed earlier, there exists errors associated with the pH measurements. These errors affect the soluble concentrations which, in turn, affect the concentration ratios appearing in Equation (8.36). The values for the standard deviations in the pH measurements were presented earlier in Tables 8.8 to 8.10 and can be used to propagate the effects into the precipitation quantities.

The total quantity of nutrients removed during the experiment or remaining in the system after the tomato plants are harvested, $q_{output,i}$, can be calculated as the sum of the soluble and precipitated quantities. Furthermore, the quantity of nutrients taken up by the plants can be determined as the difference between the amount supplied, $q_{input,i}$, and the amount remaining or removed, $q_{output,i}$. This is shown in Equation (8.37) below.

$$q_{plant,i} = q_{input,i} - q_{output,i} = q_{input,i} - q_{rem,i} - q_{precip,i} \qquad (8.37)$$

The values of $q_{plant,i}$ determined from Equation (8.37) can then be compared to the values obtained from Equation (8.26). Equivalent results prove the mass balances for each nutrient, i. Although the values generally are not exactly equal, an acceptable range of results can be determined from the errors associated with these values. These are determined from the propagation of the errors associated with each individual measurement used. The derivation of the general propagation of these errors are provided in Appendix D but are discussed sequentially in the example below.

8.3.3. Example of the Completed Mass Balance

In order to illustrate the complete mass balance accounting for all of the sources of error, a specific experiment was analyzed completely with the results presented below. The values for the various error contributions are presented in Table 8.11 below and are

used in conjunction with the values presented earlier in Tables 8.7 to 8.10 for the errors in the ICP analyses. It was assumed that if it can be shown that the mass balance is complete for one experiment, then it was complete for the remainder.

Table 8.11 Standard Deviations Associated with the Inorganic Mass Balances

Variables	Associated Errors	Values
Dry Masses:	$\sigma_{Wleaf,d} = \sigma_{Wbranch,d} = \sigma_{Wroot,d} = \sigma_{Wtissue,d}$	= $\pm$0.001 g
Tissue Concs:	$\sigma_{Cleaf,i} = \sigma_{Cbranch,i} = \sigma_{Croot,i} = \sigma_{Ctissue,i,ave}$	see Table 8.7
Sample Volume:	$\sigma_{Vsample} = \sigma_{Vsoln}$	= $\pm$0.1 ml
Sample Concs:	$\sigma_{Csample,i} = \sigma_{Csample,i,ave}$	see Tables 8.8 to 8.10
Reservoir Volume:	$\sigma_{Vsys} = \sigma_{\Delta Vres,j}$	= $\pm$0.5 ml
Solution pH:	σ_{pH}	see Tables 8.8 to 8.10

The experiment used to verify the mass balance is denoted as Experiment #10 and consisted of four test bed units (TBU) each with a dedicated reservoir. The first TBU (designated 1a) consisted of three 0.30 micron tubes while the second TBU (designated 1b) consisted of two similar pore sized tubes. Both of these contained a standard strength hydroponic solution and were operated at the (-0.078/-0.039) level. The third and fourth TBU's (designated 2a and 2b) both consisted of 1.5 micron tubes where the third contained three tubes and the fourth consisted of two tubes. These TBU's were subjected to a 1/4x and 1x solutions, respectively, and were operated at the (-0.019/-0.039) and (-0.078/-0.039) levels for (π_{soil} / P_m) in MPa. These conditions were imposed during the experiment when all of the tomato plants were established in the main vegetative growth stage. At this time, the tomato plants from a single tube were harvested from System #2a (Tube #1).

During this experiment, as with all experiments, the daily change in pH was measured after the quantity of solution taken up by the plant, $\Delta V_{res,j}$, was determined on each day, j. The volumes of the reservoirs were reset to their maximum values afterwards using the respective fresh solution (i.e. 1x or 1/4x strength). The total length of this experiment lasted for 50 days from seed germination to plant harvest, during which time,

periodic samples of the solutions were removed, analyzed, and replaced with standard solution. At the end of this experiment, the tissues were harvested using the general procedure described earlier (see Section 7.3.2) in order to determine the tissue compositions. Furthermore, the remaining solutions after the tomato plants were harvested were sampled and analyzed in the ICP-AES as well.

In order to confirm the mass balances for the four test bed units, the total quantities of each inorganic nutrient measured in the plants produced on a single TBU were determined. These were calculated using Equation (8.26) where the quantities for the individual tissue types were measured as the product of the respective dry weights and concentrations for each individual plant part. The errors associated with the various measurements used in this equation can be propagated through in order to determine the error in $q_{plant,i}$ for each nutrient, i. The general equation used to calculate these errors is derived in Appendix D (see Equation D.8). These errors can range upto 36% of the absolute values depending upon the particular nutrient but average approximately 13.5% over all nutrients analyzed. The final numerical results for all of the plants produced on each test bed unit are presented in Table 8.12 below while the individual tissue results are presented in Appendix D (see Tables D.15 to D.18). It should be noted that some of the tissues were combined prior to ICP analysis.

Table 8.12 The Inorganic Nutrient Masses and Related Error Ranges as Measured in the Tissues of the Tomato Plants Grown during Experiment #10

Nutrient	$q_{plant,i}$ (μg) - 1a	$q_{plant,i}$ (μg) - 1b	$q_{plant,i}$ (μg) - 2a	$q_{plant,i}$ (μg) - 2b
P	7897 ± 1175	847 ± 183	9259 ± 1140	4485 ± 943
Mg	16115 ± 2218	3138 ± 346	17106 ± 2154	11619 ± 1780
Ca	29978 ± 8814	5225 ± 1374	34596 ± 8558	22552 ± 7074
Na	1172 ± 246	211 ± 38	2043 ± 239	834 ± 197
K	71766 ± 3618	13147 ± 567	83852 ± 3518	57657 ± 2904
Mo	6.50 ± 0.68	2.03 ± 0.11	9.49 ± 0.66	4.41 ± 0.55
Zn	143.83 ± 14.30	79.58 ± 2.34	430.77 ± 13.95	112.33 ± 11.48
B	68.49 ± 7.41	18.38 ± 1.16	105.92 ± 7.20	79.16 ± 5.95
Mn	111.43 ± 8.32	20.69 ± 1.30	78.46 ± 8.08	63.32 ± 6.68
Fe	812.96 ± 208.72	146.13 ± 32.55	572.95 ± 202.64	462.64 ± 167.50
Cu	33.02 ± 1.70	8.33 ± 0.27	38.30 ± 1.66	24.58 ± 1.37

In order to determine the quantities of nutrients supplied to each TBU during this experiment, each of the different volumes appearing in Equation (8.28) were determined. These volumes are presented in Appendix D for each unit (see Table D.19) and were multiplied by the standard nutrient concentrations of the solutions prepared for this experiment (i.e. either the 1x or 1/4x compositions). These concentrations can be found in Appendix D as well (see Table D.6). Substituting Equation (8.27) into Equation (8.28) for $C_{soln,i,init}$ results in Equation (8.38) describing the total quantity of each nutrient supplied.

$$q_{input,i} = C_{sample,i,init} \frac{V_{sample}}{V_{soln}} (V_{sys} + \sum_{j} \Delta V_{res,j} + \sum_{k} V_{soln}) \qquad (8.38)$$

The error associated with these quantities were calculated based on the errors associated with the various measurements as provided in Tables 8.8, 8.10, and 8.11. The general equation used to calculate the propagated errors is also presented in Appendix D (see Equation D.10) as are the final numerical results for each of the test bed units (see Table D.20).

In order to determine the quantities of nutrients either removed from the system during the experiment as solution samples or remaining in the system at the end, Equation (8.27) can be combined with Equation (8.29). This substitution is conducted twice, once where $C_{soln,i} = C_{soln,i,final}$ and $C_{sample,i} = C_{sample,i,final}$ and a second time where $C_{soln,i} = C_{soln,i,k}$ and $C_{sample,i} = C_{sample,i,k}$. This results in Equation (8.39) below.

$$q_{rem,i} = \frac{C_{sample,i,final} V_{sample}}{V_{soln}} (V_{sys} - \Delta V_{res,f}) + \sum_{k} (C_{sample,i,k} V_{sample}) \qquad (8.39)$$

Again, the volumetric terms for the system and reservoir can be found in Appendix D (see Table D.21) as can the solution concentrations (see Tables D.22 to D.25). Furthermore, 11 solution samples were withdrawn during this experiment with the volume of 19.6 ml each in order for the total sample volume to be 20 ml after acidification. The final results for these calculations are presented in Appendix D (see Table D.26) along with the values

for the propagated errors. These errors were determined from the errors associated with the various measurements provided in Tables 8.8, 8.10, and 8.11. The general equation used to calculate the propagated errors is also presented in Appendix D (see Equation D.12)

Finally, in order to determine the quantities of each nutrient present in the system at the end of this experiment as solid precipitates, Equation (8.36) can be adjusted using Equation (8.27). This substitution produces the Equation (8.40) in terms of the measured concentration in the sample of the final solution, $C_{sample,i,final}$.

$$q_{precip,i} = \left(\frac{1 - f_{sol,i}}{f_{sol,i}}\right)\left(\frac{C_{sample,i,final} V_{sample}}{V_{soln}}\right)(V_{sys} - \Delta V_{res,f}) \qquad (8.40)$$

The volumetric terms and final solution concentrations are identical to those found in Appendix D (see Table D.21 to D.25). Similarly, V_{sample} and V_{soln} attain their usual values of 20 and 19.6 ml, respectively. As for the values of the concentration ratios, $f_{sol,i}$, these were determined based on the pH of the final solutions as provided on the same tables as the concentrations. These values were entered into Equations (8.30) to (8.34) and divided by the concentration of the 1x standard solution used in this experiment in order to calculate $f_{sol,i}$. Substituting each of these values into Equation (8.40) allows for the quantities of precipitated inorganic nutrients to be calculated. The final results for these calculations are presented in Appendix D (see Table D.27).

The errors corresponding to these precipitation quantities were based on the errors associated with the various measurements as provided in Tables 8.8, 8.10, and 8.11. Furthermore, the errors associated with the concentration ratios, $\sigma_{fsol,i}$, can be calculated from Equations (8.30) to (8.34), evaluated at pH and pH_0 from the pH-concentration experiment. The general equation for $f_{sol,i}$ used for the propagation of the errors can be expanded from Equation (8.35) and is provided in Equation (8.41).

$$f_{sol,i} = \frac{[b_{0,i} + b_{1,i}(pH) + b_{2,i}(pH)^2]}{[b_{0,i} + b_{1,i}(pH_0) + b_{2,i}(pH_0)^2]} \qquad (8.41)$$

In this equation, the model parameter terms, $b_{0,i}$, $b_{1,i}$, and $b_{2,i}$, attain the same values as those presented in Equations (8.30) to (8.34) for the respective nutrients. The propagation equation for $\sigma_{fsol,i}$ is derived in Appendix D (see Equation D.16) as is the general equation used to calculate $\sigma_{qprecip,i}$ (see Equation D.14).

In order to determine the quantities of nutrients depleted from the systems, the results from Equations (8.28), (8.29), and (8.36) can be combined according to Equation (8.37). These are provided in Tables 8.13 to 8.16 below for the different test bed units. Furthermore, the values for $q_{plant,i}$ obtained from the tissue samples and presented earlier in Table 8.12 are provided for comparison. Since the error ranges from these two measurement methods overlap, then the mass balances for the growth of tomato plants on the PCT-NDS can be considered complete for this experiment.

Table 8.13 Comparison of the Nutrients Measured in the Plant Tissues and the Calculated Quantities Depleted from the System Solutions for TBU-1a of Experiment #10

Nutrient	$q_{plant,i}$ (μg) - Tissues	$q_{plant,i}$ (μg) - Solution
P	7897 ± 1175	12340 ± 3488
Mg	16115 ± 2218	18436 ± 19782
Ca	29978 ± 8814	36376 ± 57264
Na	1172 ± 246	
K	71766 ± 3618	87418 ± 12800
Mo	6.50 ± 0.68	
Zn	143.83 ± 14.30	
B	68.49 ± 7.41	
Mn	111.43 ± 8.32	
Fe	812.96 ± 208.72	929.36 ± 624.18
Cu	33.02 ± 1.70	

Table 8.14 Comparison of the Nutrients Measured in the Plant Tissues and the Calculated Quantities Depleted from the System Solutions for TBU-1b of Experiment #10

Nutrient	$q_{plant,i}$ (μg) - Tissues	$q_{plant,i}$ (μg) - Solution
P	847 ± 183	-3548 ± 9671
Mg	3138 ± 346	-797 ± 18344
Ca	5225 ± 1374	-26418 ± 60480
Na	211 ± 38	
K	13147 ± 567	15721 ± 11345
Mo	2.03 ± 0.11	
Zn	79.58 ± 2.34	
B	18.38 ± 1.16	
Mn	20.69 ± 1.30	
Fe	146.13 ± 32.55	-411.81 ± 727.43
Cu	8.33 ± 0.27	

Table 8.15 Comparison of the Nutrients Measured in the Plant Tissues and the Calculated Quantities Depleted from the System Solutions for TBU-2a of Experiment #10

Nutrient	$q_{plant,i}$ (μg) - Tissues	$q_{plant,i}$ (μg) - Solution
P	9259 ± 1140	11749 ± 2769
Mg	17106 ± 2154	9017 ± 16533
Ca	34596 ± 8558	5127 ± 47115
Na	2043 ± 239	
K	83852 ± 3518	97726 ± 12116
Mo	9.49 ± 0.66	
Zn	430.77 ± 13.95	
B	105.92 ± 7.20	
Mn	78.46 ± 8.08	
Fe	572.95 ± 202.64	635.76 ± 515.80
Cu	38.30 ± 1.66	

Table 8.16 Comparison of the Nutrients Measured in the Plant Tissues and the Calculated Quantities Depleted from the System Solutions for TBU-2b of Experiment #10

Nutrient	$q_{plant,i}$ (μg) - Tissues	$q_{plant,i}$ (μg) - Solution
P	4485 ± 943	8525 ± 7255
Mg	11619 ± 1780	11512 ± 20321
Ca	22552 ± 7074	28668 ± 63267
Na	834 ± 197	
K	57657 ± 2904	55515 ± 12798
Mo	4.41 ± 0.55	
Zn	112.33 ± 11.48	
B	79.16 ± 5.95	
Mn	63.32 ± 6.68	
Fe	462.64 ± 167.50	623.41 ± 736.15
Cu	24.58 ± 1.37	

Although some of the absolute values for the nutrient quantities obtained through the solution samples are negative, the corresponding ranges of error are large enough to include the values obtained from the tissue samples. This is particularly true for the results from TBU-1b. The negative results for this TBU may be explained by comparing the absolute values obtained from the tissues between the different units as well as the magnitude of the calculated errors associated with the solution sample results. This comparison shows that the tissue quantities obtained for TBU-1b are, in general, an order of magnitude smaller than the other units. However, the values of the corresponding errors are on the same order of magnitude as the other units. Thus, the accuracy of the mass balances are reduced at these lower tissue quantities. In fact, the magnitude of the errors associated with the depletion from the solution are considerably larger than the tissue counterparts. Some are an order of magnitude higher than the absolute value. Therefore, this is an indication that these results are less reliable as compared to those obtained from the tissue samples.

CHAPTER 9 - NUTRIENT UPTAKE CHARACTERISTICS

According to the mechanistic reaction chain presented in Figure 6.2, there exists three distinct steps for nutrient transport from the soil solution into the plant roots. These are the solubilization of the nutrients (step 1), the transport of these soluble nutrients in the transpiration stream (step 2), and the uptake of the nutrients at the root surface (step 3). Since the system used in this research is a hydroponic based system, then the nutrient solution used contains all of the essential nutrients in soluble form. Therefore, step (1) of this mechanistic chain can be eliminated as a possible rate limiting step leaving steps (2) and (3) as possibilities. These steps are characteristic of mass transfer through a porous medium and the enzymatic activity of the root cell wall components, respectively.

This chapter presents the methodology used to determine the rate limiting steps in the nutrient uptake processes of plants as well as the calculations of the nutrient uptake parameters. In Section 9.1, the quantities present in the tissues, $q_{plant,i}$, were modeled based on the experimental conditions for which they were produced. Differentiation of the resulting equation for each nutrient with respect to time allows for the determination of J_i. Once each of these rates are determined, these will be compared to the theoretical rates of convection, $J_{conv,i}$, in Section 9.2. The general convection equation will be based on the standard solution concentrations for the different test conditions and the solution uptake rate, $Q_u = dV_u/dt_{DAE}$. Subtracting these convection rates from the overall uptake rates and statistically determining whether these differences are significant allows for the determination of which uptake mechanism is limiting the overall rate. For nutrients that have statistically equal rates for J_i and $J_{conv,i}$, these can be considered convection limited since this transpiration driven rate of supply to the plant root dictates the rate of uptake.

For the nutrients that have a $J_{conv,i}$ that is less than J_i, these can be considered to be limited by the rate of diffusion since the uptake of the nutrient is greater than the rate of convective water uptake. This leads to a concentration gradient between the bulk solution and the surface of the root where the rapid depletion takes place. Therefore, the differences between J_i and $J_{conv,i}$ will be used to model the rate of diffusion, $J_{diff,i}$. This transport enhancing diffusion becomes the limiting step in the uptake process and is modeled in Section 9.3. Combining the equations for $J_{diff,i}$ with $J_{conv,i}$ results in the overall mass transfer equation for the nutrients limited by the environmentally determined supply.

Alternatively, if $J_{conv,i}$ is greater than J_i, then this is an indication that the rate of transport of the nutrient into the plant root is less than the rate of water transport. Therefore, some sort of resistance to the uptake is impeding the transport through the convective flow. This impedance is attributable to the saturation of the active sites on the enzyme or protein present on the root surface which is responsible for the transport through the root membranes. Therefore, these biologically based limitations on the uptake of the nutrients will be modeled in Section 9.4.

9.1. Calculation of the Nutrient Uptake Rates

This section presents the calculations of the nutrient uptake rates as determined from the tissue samples. Although the inorganic nutrients were shown to be balanced between the amount measured in the tissues as compared to the amount calculated as being supplied by the system, the results from the solution samples were less reliable than the tissue samples. This was due to the relative magnitudes of the associated errors between the two measuring methods. For the tissues, these average around 13.5% while the solution samples yielded errors upto an order of magitude higher than the absolute value. Furthermore, the low concentrations obtained for some of the nutrients in solution were only qualitative in nature. Therefore, the nutrient uptake rates, J_i, for each nutrient, i, into the tomato plants grown under the various test conditions on the Porous Ceramic Tube - Nutrient Delivery System (PCT-NDS) were calculated using the tissue results.

9.1.1. Derivation of the General Rate Equation

In order to determine the rate of nutrient uptake into the plants produced in this research, the total quantities measured in the tissues, $q_{plant,i}$, were calculated using Equation (9.1) below. These were based on the tissue concentrations, $C_{tissue,i}$, measured in the Inductively Coupled Plasma - Atomic Emissions Spectrometer (ICP-AES) and the corresponding dry weights, $W_{tissue,d}$. The data used to derive these values are presented in Appendix E (see Tables E.1 to E.6).

$$q_{plant,i} = C_{leaf,i}W_{leaf,d} + C_{branch,i}W_{branch,d} + C_{root,i}W_{root,d} \qquad (9.1)$$

These inorganic nutrient quantities were then modeled as functions of leaf stage, overall root-zone water potential, and the individual concentration of the nutrient in solution. For the leaf stage, LS, these time values were determined by taking the total weight of the dry tissues, $W_{plant,d}$, as measured in the experiments and calculating the number of days after emergence, t_{DAE}, using Equation (8.11). These time values were then converted to the more general leaf stage scale using Equations (8.1) relating t_{DAE} to LS. Since Equation (8.11) is dependent upon the osmotic and matric potentials, π_{soil} and P_m, the specific values used during the production of each plant were used in the calculation. Furthermore, since the concentration of the individual nutrient in the solution can affect the transport, then these factors were incorporated in the models as well. Each of these factors are presented in the data tables presented in Appendix E (see Tables E.1 to E.6). Therefore, by modeling $q_{plant,i}$ as a function of leaf stage, LS, and differentiating the resulting equation with respect to LS, results in the equations for J_i which were based on the developmental stage, root-zone water potential, and concentration.

The form of the model chosen for the nutrient quantities was a form based on the standard convection equation where the flow rate is multiplied by the concentration. Since the solution uptake rate in this research was shown to be an exponential function in Equation (8.23), then $q_{plant,i}$ was modeled in this form as well. However, in order to incorporate the solution concentration, $C_{soln,i}$, as a pre-exponential term, this factor was

adjusted as shown in Equation (9.2) for the general case. Furthermore, the water potential is written in terms of the osmotic and matric components according to Equation (2.4).

$$q_{plant,i} = \exp[c_{0,i} + c_{1,i}(LS) + c_{2,i}(P_m - \pi_{soil}) + c_{3,i}\ln(C_{soln,i})] \quad (9.2)$$

In this equation, the model parameters, $c_{0,i}$, $c_{1,i}$, $c_{2,i}$, and $c_{3,i}$ were determined for each nutrient, i, using statistical regressions. In order to accomplish this, Equation (9.2) was linearized by taking the natural logarithm. This resulted in Equation (9.3).

$$\ln(q_{plant,i}) = c_{0,i} + c_{1,i}(LS) + c_{2,i}(P_m - \pi_{soil}) + c_{3,i}\ln(C_{soln,i}) \quad (9.3)$$

By performing an analysis of variance (ANOVA) for each model, the significant terms for each specific nutrient were determined. This was accomplished by comparing the calculated F-statistic for each term with the critical value determined at an α_{risk} level of 0.05. This was conducted on the complete linear model containing each term presented in Equation (9.3) and eliminating the insignificant contributions from the model. Furthermore, as these terms were eliminated, the significance of the possible left-out terms was determined by the F-statistic as well. This procedure was conducted until an adequate model was produced for each nutrient without the presence of any left-out terms.

Once these exponential equations are developed, the models for the uptake rates can be determined from the quantities measured in the plants. This is shown in Equation (9.4) below where $c_{1,i}$ represents the model parameter for nutrient, i, obtained from the exponential relationship between $q_{plant,i}$ and LS.

$$J_i = d(q_{plant,i}) / d(LS) = c_{1,i}\, q_{plant,i} \quad (9.4)$$

Combining Equations (9.2) and (9.4) and rearranging leads to the general model for the rate of nutrient uptake into plants grown on this system. This is shown in Equation (9.5).

$$J_i = c_{1,i}\,(C_{soln,i})^{c3,i} \exp[c_{0,i} + c_{1,i}(LS) + c_{2,i}(P_m - \pi_{soil})] \quad (9.5)$$

Therefore, using Equation (9.5), the uptake rates for each nutrient at the different stages of development can be determined based on the conditions for which they were produced.

9.1.2. Calculation of the Uptake Rates

The results of the model building procedure described in the previous section are shown in Table 9.1 which presents the values of the model parameters for P, Mg, Ca, Na, K, Mo, Zn, B, Mn, Fe, and Cu, respectively. In each case, the leaf stage was shown to be the only consistently significant contribution to the quantities in the tissues, regardless of the nutrient. Conceptually, this make sense since as the plants become older, more nutrients would be continually absorbed as long as they were available. As for the effects of the osmotic potential, matric potential, and solution concentration, the significance of these contributions were dependent on the particular nutrient. These can be seen in the final ANOVA tables for each nutrient presented in Appendix E (see Tables E.7 to E.17).

Table 9.1 Parameters for the Linearized Model of the Natural Log of the Plant Inorganic Nutrient Quantities (Y) as a Function of Leaf Stage (X1), Root-Zone Water Potential (X2), and Solution Concentration (X3)

Nutrient	$c_{0,i}$ (unitless)	$c_{1,i}$ (unitless)	$c_{2,i}$ (MPa^{-1})	$c_{3,i}$ (unitless)
P	2.726	0.470	13.959	0.378
Mg	3.539	0.423	10.240	0.355
Ca	4.401	0.373	11.027	0.401
Na	3.263	0.315		
K	5.141	0.470		
Mo	-2.164	0.258		
Zn	1.264	0.360	6.003	
B	-1.680	0.469		
Mn	-0.615	0.384		0.977
Fe	0.767	0.415		0.053
Cu	-1.796	0.424	4.622	

In order to determine the nutrient uptake rates, the parameters presented in Table 9.1 can be entered into Equation (9.5) defining J_i. However, this equation is a purely empirically based equation. In order to produce more mechanismtic models of the nutrient uptake rates into plants, the rates from the experimental data can be determined from the quantities measured in the plants. According to Equation (9.4), the uptake rates can also

be determined by multiplying the quantities calculated in the plant tissues by the exponential parameter for the leaf stage, $c_{1,i}$. Therefore, the experimental values for J_i were determined by combining Equations (9.1) and (9.4). This results in Equation (9.6) shown below.

$$J_i = c_{1,i} [C_{leaf,i}W_{leaf,d} + C_{branch,i}W_{branch,d} + C_{root,i}W_{root,d}] \qquad (9.6)$$

These resulting experimentally determined uptake rates were then used to model the nutrient kinetics limited by either the environmental mass transfer or the plant based absorption mechanisms.

9.2. Modeling Convection Limitations

This section presents the methodology used to determine the rate limiting step in the nutrient uptake process into plants. Using a statistical approach, the experimental nutrient uptake rates, J_i, can be compared to the convective rate of supply, $J_{conv,i}$, based on the solution uptake rate, Q_u, and the concentration of the bulk standard solution, $C_{soln,i}$. The method of comparison that is used in this research is the t-test which determines whether a particular sample belongs to the normal distribution of a specific set of data. If the experimental J_i can be shown to be statistically within the normal distribution of the convection rate, then convection can be considered the rate limiting step. In other words, the rate of nutrient transport to the root surface is limiting the rate at which the nutrients are taken up by the plant. If this convection rate is decreased such as caused by a smaller water potential gradient, then the uptake rate should decrease accordingly. If the experimental uptake rates are shown to be statistically different from the convective supply rate, then this indicates that a different mechanism is limiting the transport of the nutrients.

Two additional possibilities exist from this statistical analysis. The second possibility is that the $J_{conv,i}$ is less than J_i. In this case, in addition to convective transport, there must exist a substantial diffusive flux since the rate of uptake is faster than the

convective supply. This occurs when the transport of the nutrient through the plant root membrane is faster than the rate of water uptake. This possibility exists when the membrane proteins or enzymes remain active while water uptake is not favored. The nutrients which are limited by this type of mechanism will be modeled in Section 9.3.

The third possibility is when $J_{conv,i}$ is greater than the actual J_i. This occurrence indicates a saturation of the active sites on the protein or enzyme used by the plant to cause the transfer of the nutrient from the surrounding solution into the root itself. This is due to a high supply of nutrients to a limited number of active sites causing the experimental uptake rates to be lower than the convective supply. The nutrients which undergo this type of nutrient uptake limitation will be modeled in Section 9.4.

9.2.1. Derivation of the General Convection Equation

In order to determine the rate limiting step in the uptake of inorganic nutrients into plants, a general equation describing the rate of convection of the nutrients was derived. In order to calculate the convective component, $J_{conv,i}$, the solution uptake rate, Q_u, is multiplied by the solution concentration, $C_{soln,i}$. This was shown in Equation (7.4). This flow rate can be determined by differentiating V_u defined in Equation (8.23) with respect to LS. The results of this derivation are shown in Equation (9.7).

$$Q_u = dV_u/d(LS) = 1.886 \exp[0.400(LS) + 8.605(P_m - \pi_{soil})] \qquad (9.7)$$

Multiplying this rate by the concentration of each nutrient present in the solution leads to Equation (9.8) defining the convective supply rate, $J_{conv,i}$.

$$J_{conv,i} = 1.886(C_{soln,i}) \exp[0.400(LS) + 8.605(P_m - \pi_{soil})] \qquad (9.8)$$

Using the data presented in Appendix E (Tables E.1 to E.6) for the conditions used to produce the plants (i.e. LS, π_{soil}, and P_m) and the solution concentrations presented in Tables 8.8 to 8.10, the convection rates corresponding to each experimental uptake rate, J_i, were determined.

9.2.2. Determining the Rate Limiting Steps

In order to determine the rate limiting step in the nutrient uptake process for each individual nutrient, the convective rate of supply, $J_{conv,i}$, was subtracted from the overall nutrient uptake rate determined from the experimental data, J_i. Since each of these are determined for specific values of leaf stage and overall root-zone water potential, then it is hypothesized that if the convective supply is the rate limiting step, then $J_i - J_{conv,i}$ should be equal to zero ($\delta = 0$). Using the t-test at an α_{risk} level of 0.05 ($n = 61$), the average of the differences between J_i and $J_{conv,i}$ can be examined as to whether they are statistically equal to the hypothesized zero value. Rejection of this hypothesis is achieved when the calculated t-statistic is greater in magnitude than the critical value. For this two-sided test, the values of the differences can be either positive or negative. Therefore, the value of the critical t-statistic should be the same sign as the calculated value.

The results of this analysis for the different nutrients are presented in Table 9.2. In this table, it can be seen that none of the actual experimental nutrient uptake rates are statistically equal to the convection rates. This would have occurred if the values for t_{calc} were between -2.000 and +2.000 ($t_{crit,0.05,60}$). Therefore, none of the nutrient were limited by the convective supply. However, K and Zn were shown to be mass transfer limited by the rate of diffusion while the remainder of the nutrients were shown to be limited by the saturation of the active sites on the proteins or enzymes present on the root cell walls. These were indicated by the positive and negative values for t_{calc}, respectively.

Table 9.2 Comparison of the Calculated t-Statistics for the Differences between the Experimental Uptake Rates and the Convective Supply Rates and the Critical Value, $t_{crit,0.05,60} = \pm 2.000$

Macro-Nutrients	t_{calc}		Micro-Nutrients	t_{calc}
P	-81.41		Mo	-7.76
Mg	-374.13		Zn	+61.11
Ca	-639.03		B	-44.31
Na	-165.00		Mn	-41.33
K	+317.12		Fe	-112.08
			Cu	-24.83

9.3. Modeling Diffusion Limitations

According to the results of the previous section, only two nutrients were limited by the rate of diffusion. These were K and Zn. In order to model the kinetics for these nutrients, the rates of diffusion, $J_{diff,i}$, were determined as the difference between the total rate, J_i, and the convective component, $J_{conv,i}$. Since this rate is independent of the conditions of the plants but dependent on the root-zone environmental conditions (i.e. π_{soil}, P_m, and $C_{soln,i}$), then these differences were divided by the exponent of the leaf stage used to evaluate the rate of convection, $e^{u1(LS)}$. The parameter for this exponent, u_1, can be found in Equation (9.8) to be equal to 0.400. This eliminated the effects of the different convection rates caused by the variations in the developmental stage of the plants. This procedure basically assumes that the rate of formation of the concentration gradient between the bulk solution and the root surface increases with the growth of the plant. These resulting diffusion rates, $J_{diff,i}$, were modeled according to the classical equation containing an effective diffusion coefficient, $D_{eff,i}$, and a concentration gradient, $\Delta C/\Delta r$.

9.3.1. Derivation of the General Diffusion Equation

In order to determine the magnitude of the diffusional contribution to the mass transfer of nutrients to the plant roots, the convection rate, $J_{conv,i}$, is subtracted from the overall rate, J_i. This is shown in Equation (9.9) below which includes the parameter, $c_{1,i}$, for the exponential term in Equation (9.2) relating $q_{plant,i}$ to the leaf stage.

$$J_{diff,i} = J_i - J_{conv,i} = c_{1,i}\, q_{plant,i} - Q_u C_{soln,i} \qquad (9.9)$$

For the nutrients that were shown to be limited by diffusion, the values for $c_{1,i}$ can be found in Table 9.1. Again, $q_{plant,i}$ is determined from Equation (9.1) while Q_u is calculated as the derivative of Equation (8.24) with respect to time.

After these diffusion rates are determined, they were entered into Equation (9.10) shown below which defines the rate of diffusion independent of the developmental stage of the plant since these exponential terms also appear in $q_{plant,i}$ and Q_u, respectively. In this

equation, u_1 represents the parameter for the exponential relationship between Q_u and LS and is found in Equation (9.8) to have a value of 0.400.

$$J_{diff,i} = (c_{1,i}\, q_{plant,i} - Q_u C_{soln,i}) / e^{u1(LS)} \qquad (9.10)$$

These resulting rates are then entered into Equation (9.11) defining the diffusion between the bulk solution flowing through the interior of the ceramic tubes and the exterior surface where the plant roots are in direct contact. The respective concentrations at these points are designated as $C_{soln,i}$ and $C_{surface,i}$ while the distance between these points is measured as $(D_o - D_i)/2$ where D_o and D_i are the external and internal diameters, respectively.

$$J_{diff,i} = -D_{eff,i} \frac{C_{surface,i} - C_{soln,i}}{(D_o - D_i)/2} \qquad (9.11)$$

Assuming that the diameters of the ceramic tubes are relatively consistent between the different tubes, then Equation (9.11) can be modeled as a linear equation relating $J_{diff,i}$ to $C_{soln,i}$. This equation is rewritten in Equation (9.12) below in a statistical model form where $d_{0,i}$ and $d_{1,i}$ represent the model parameters for the diffusion equation for nutrient, i.

$$J_{diff,i} = d_{0,i} + d_{1,i}\, C_{soln,i} = \frac{-D_{eff,i} C_{surface,i}}{(D_o - D_i)/2} + \frac{D_{eff,i}}{(D_o - D_i)/2} C_{soln,i} \qquad (9.12)$$

Since values for $d_{0,i}$ and $d_{1,i}$ can be determined from regression, then $D_{eff,i}$ can be determined from $d_{1,i}$ and the average tube diameters. Furthermore, $C_{surface,i}$ can be estimated from the value of $d_{0,i}$, the diameters, and the resulting $D_{eff,i}$.

This procedure assumes that the analysis of variance of this linear model results in significant model terms without any significant left-out terms. These will be examined at an α_{risk} level of 0.05. If significant left-out terms do exist, then this would indicate that the standard diffusion model is inadequate to describe the results of the diffusion limited nutrients in this research. In these cases, the general empirical model presented as Equation (9.5) remains the best model of the rate of uptake of these specific nutrients.

9.3.2. Estimating the Diffusion Parameters

The two nutrients that were shown in Table 9.2 to be diffusion limited were K and Zn. Each of these were modeled according to the procedure described above. In the case of K, the terms of the diffusion models were shown to be significant without any required additional terms. As for zinc, the model term, $d_{0,Zn}$, was shown to be the only significant contribution. The ANOVA tables corresponding to these statistical results are provided in Appendix E (see Tables E.18 to E.19, respectively for K and Zn). As for the values and 95% confidence limits (CI) of the significant model parameters, these were determined from the linear regressions and are presented below in Table 9.3. Furthermore, the effective diffusion coefficients for these nutrients, $D_{eff,i}$, and surface concentration, $C_{surface,i}$, were calculated using Equation (9.12) and are presented on Table 9.3 as well along with the propagated errors for these parameters. The average tube diameters were taken to be 1.62 and 1.16 cm according to Table 5.1. Unfortunately, the Michaelis-Menten kinetics for these nutrients cannot be developed from the data acquired in this research since the biological mechanisms of these nutrient uptake processes were shown not to be limiting under the present test conditions.

Table 9.3 Model Parameters for the Linear Regressions and the Diffusion Equations for the Diffusion Limited Nutrients

Nutrient	$d_{0,i}$ (μg/LS)	$d_{1,i}$ (ml/LS)	$D_{eff,i}$ (ml·cm/LS)	$C_{surface,i}$ (μg/ml)
K	-34.885 ± 18.509	0.608 ± 0.102	0.140 ± 0.023	57.377 ± 31.928
Zn	-0.827 ± 0.082			

Since these rates of diffusion are in addition to the rates of convection, then the final model equations describing the mass transfer limitations for the nutrient uptake rates of these nutrients can be written as sum of Equations (9.8) and (9.12) with the parametric values presented in Table 9.3. For K this is written in Equation (9.13) in terms of the experimental conditions, π_{soil}, P_m, $C_{soln,i}$, D_o, and D_i and the leaf stage of the plants.

$$J_K = 1.886(C_{soln,K}) \exp[0.400(LS) + 8.605(P_m - \pi_{soil})] + 0.140\frac{C_{soln,K} - 57.377}{(D_o - D_i)/2} \quad (9.13)$$

Since the concentration term in the model for Zn was shown to be an insignificant contribution to describing the rate of diffusion to the root surface, then the diffusion parameters, D_{eff} and $C_{surface,Zn}$, for this nutrient cannot be determined individually. However, the lumped value of ($D_{eff}C_{surface,Zn}$) can be determined from the regression parameter, $d_{0,Zn}$, and the average diameters of the ceramic tubes. The value of this quantity is shown in the final model presented in Equation (9.14) describing the rate of zinc transport to the root surface. This rate of transport is equivalent to the subsequent uptake.

$$J_{Zn} = 1.886(C_{soln,Zn}) \exp[0.400(LS) + 8.605(P_m - \pi_{soil})] + \frac{0.213}{(D_o - D_i)/2} \quad (9.14)$$

This discrepancy between the classical diffusion model described by Fick's Law and Equation (9.14) is possibly due to the magnitude of the error associated with the solution sample measurements. According to Tables 8.8 to 8.10, the percentage ratio of the errors to the actual concentrations, ($\sigma_{Csample,Zn}/C_{sample,Zn}$ x 100%), were between 30 and 40%. In comparison, this ratio for the macro-nutrient, K, was at a maximum of 4%. Therefore, the average concentrations used in the analysis of the Zn diffusion equation were rather inaccurate and may have resulted in the concentration term being insignificant.

9.4. Modeling Biological Limitations

In order to model the nutrient uptake rates limited by the activity of the enzymatic carriers at the root surface, $J_{c,i}$, the experimental uptake rates, J_i, were divided by the exponents of the leaf stage, $e^{c1,i(LS)}$. These exponential terms appear in Equation (9.2) describing the nutrient quantities, $q_{plant,i}$, which is subsequently used to determine J_i in Equation (9.4). This was conducted in order to place all of the rates on the same time scale since the actual catalytic rates of the individual proteins or enzymes would be

independent of the whole plant development. In others words, the overall rates may increase with the leaf stage due to the increased number of roots but the individual proteins or enzymes conduct the transport at the same rate.

Once these rates were determined, the kinetic parameters describing these rates were determined as well. This was accomplished by modeling these rates according to the Lineweaver-Burke equation of $1/J_{c,i}$ versus $1/C_{soln,i}$. Furthermore, since the PCT-NDS was capable of separating the effects of concentration from the water uptake effects, only the results at a constant water potential were used. This water potential level was maintained at Ψ_{soil} = -0.078 MPa and was coded for the individual levels of (π_{soil} / P_m) as (-0.019/-0.059), (-0.039/-0.039), and (-0.078/-0.000). The nutrients that were determined to be limited by the enzymatic actions at the root cell membranes according to the t-test included P, Mg, Ca, Na, Mo, B, Mn, Fe, and Cu. Each of these are described below in order.

9.4.1. Derivation of the General Enzymatic Equation

In order to determine the nutrient uptake rates limited by the enzymatic activity at the root surface, the experimental uptake rates, J_i are converted to a form independent of the leaf stage of development. This is accomplished by using Equation (9.15) which eliminates this dependency by dividing J_i by the exponent of the leaf stage using the parameter determined from the model of $q_{plant,i}$.

$$J_{c,i} = J_i / e^{c1,i(LS)} = c_{1,i}\, q_{plant,i} / e^{c1,i(LS)} \qquad (9.15)$$

After these rates are converted, they can be modeled according to the Michaelis-Menten equation shown as Equation (9.16).

$$J_{c,i} = \frac{J_{c,max,i}\, C_{soln,i}}{K_{m,i} + C_{soln,i}} \qquad (9.16)$$

This equation relates the rate of nutrient uptake, $J_{c,i}$, to the concentration present in solution, $C_{soln,i}$, based on a maximum rate of uptake, $J_{c,max,i}$. Furthermore, the constant, $K_{m,i}$, represents the concentration of nutrient, i, required for 1/2 $J_{c,max,i}$. In order to model this equation, the inverse is taken resulting in Equation (9.17). Furthermore, this equation is also written in statistical form where $e_{0,i}$ and $e_{1,i}$ represents the regression parameters. Since both kinetic parameters are positive values, then the regression parameters should be positive as well.

$$\frac{1}{J_{c,i}} = e_{0,i} + e_{1,i}\frac{1}{C_{soln,i}} = \frac{1}{J_{c,max,i}} + \frac{K_{m,i}}{J_{c,max,i}}\frac{1}{C_{soln,i}} \qquad (9.17)$$

Since values for $e_{0,i}$ and $e_{1,i}$ can be determined from regression, then $J_{c,max,i}$ can be determined from $e_{0,i}$ and $K_{m,i}$ can be estimated from the values of $e_{1,i}$ and the resulting $J_{c,max,i}$.

This procedure assumes that the analysis of variance of this linear model results in significant model terms without any significant left-out terms. These will be examined at an α_{risk} level of 0.05. If significant left-out terms do exist, then this would indicate that the standard Michaelis-Menten model is inadequate to describe the results of the enzyme limited nutrients in this research. In these cases, the general empirical model presented as Equation (9.5) remains the best model of the rate of uptake of these specific nutrients.

9.4.2. Estimating the Michaelis-Menten Constants

All of the nutrients except K and Zn were shown in Table 9.2 to be limited by the biological apparatus at the root surface. Each of these were modeled according to the procedure described above. In the cases of P, Mg, Ca, Na, Fe, and Cu, the terms of the Michaelis-Menten model were shown to be significant without any required additional terms. As for Mo, B, and Mn, the model terms for these nutrients, $e_{0,i}$, were shown to be the only significant contributions. The ANOVA tables corresponding to these statistical results are provided in Appendix E (see Tables E.20 and E.28, respectively). As for the

value of the model parameters, these were determined from the linear regressions and are presented below in Table 9.4 along with the 95% CI on the regression parameters. Furthermore, the values for the maximum rate of nutrient uptake, $J_{c,max,i}$, and the constant, $K_{m,i}$, were calculated using Equation (9.17) and are presented on Table 9.4 as well.

Table 9.4 Model Parameters for the Linear Regressions and the Michaelis-Menten Equations for the Enzyme Limited Nutrients

Nutrient	$e_{0,i}$ (LS/μg)	$e_{1,i}$ (LS/ml)	$J_{c,max,i}$ (μg/LS)	$K_{m,i}$ (μg/ml)
P	0.098 ± 0.032	0.895 ± 0.558	10.204 ± 3.332	9.133 ± 6.428
Mg	0.028 ± 0.007	0.449 ± 0.396	35.714 ± 8.929	16.036 ± 14.700
Ca	0.0079 ± 0.0025	0.426 ± 0.306	126.58 ± 40.058	53.924 ± 42.327
Na	0.091 ± 0.024	0.187 ± 0.169	10.989 ± 2.898	2.055 ± 1.935
Mo	40.322 ± 13.023		0.025 ± 0.008	
B	12.387 ± 1.165		0.081 ± 0.008	
Mn	2.805 ± 0.368		0.357 ± 0.047	
Fe	0.702 ± 0.150	0.560 ± 0.416	1.425 ± 0.304	0.798 ± 0.617
Cu	-1.441 ± 21.281	3.694 ± 3.335		

From the results presented in Table 9.4, several conclusions can be drawn. For the macro-nutrients, P, Mg, Ca, and Na, and the micro-nutrient, Fe, the concentrations tested in this research at the constant water potential level were, in some cases, sufficient to cause the saturation of the active sites while lower concentrations were not adequate. This can be seen by comparing the concentrations of these nutrients in solution presented in Tables 8.8 to 8.10 to the concentrations required for half of the maximum rate, $K_{m,i}$, presented in Table 9.4. In terms of producing models describing the enzyme kinetics, these situations for the concentrations are desired. This is unlike the situations for the micro-nutrients, Mo, B, and Mn. In these cases, the concentrations used in this research were all higher than the saturation concentration since the concentration terms in the models were shown to be insignificant contributions. In other words, the levels of nutrients required to saturate the active sites on the enzymes or proteins responsible for the acquisition of these nutrients are below the levels present in the 1/4x solution used in this research. Therefore, the $K_{m,i}$ parameters for the Michaelis-Menten equation for these nutrients cannot be

determined; although, it can be said that they are below the concentrations present in the 1/4x solution.

One peculiar situation arose for copper. In this case, the analysis of variance showed that both of the linear model terms were significant contributions. However, the value of the $e_{0,Cu}$ term resulted in a negative value as shown in Table 9.4. This is an impossible situation since the maximum uptake rate which is the inverse of this regression parameter cannot be a negative value. Therefore, this model is inadequate in describing the uptake of copper by the plants produced on the PCT-NDS.

This discrepancy for copper as well as the lack of significance of the concentration term for molybdenum may be due to the inaccuracies of the solution sample measurements. As seen in Tables 8.8 to 8.10, the percentage ratios of the errors to the actual concentrations for these nutrients are between 15 and 30% which indicates that the concentration terms in the respective models may be suspect. Furthermore, the levels of these nutrients present in the different test solutions were two of the three nutrients which did not follow the trend of 1x, 1/2x, and 1/4x. Incidentally, the other nutrient which does not follow this trend is Zn (see discussion in Section 9.3.2 concerning the uptake of this element). Therefore, another possible explanation for these results could be due to an unforeseen interaction between the concentrations of these particular nutrients and the osmotic potential of the overall solution. This may be due to electrochemical gradients across the root membranes which would be dependent upon both the concentrations and the osmotic potentials (as a contributor to the water potential gradient).

Since the rates of supply of these nutrients to the root surface through convection are greater than the actual biological uptake, then there should exist substantial rates of back diffusion due to the build-up of nutrients restricted from entering the roots. This rate of back diffusion can be determined using the same procedure used to develop the diffusion limited nutrients presented earlier (see Section 9.3). The results of the calculations of the regression parameters as well as the coefficients for the general diffusion model presented in Equation (9.12) are presented in Table 9.5. This also includes the 95% confidence limits on these parameters. Furthermore, the ANOVA tables for these

enzyme limited nutrients are presented in Appendix E (see Tables E.29 to E.37). For P, Mg, Ca, B, Fe, and Cu, both of the model terms were shown to be significant. However, the values for the parameters for copper resulted in an impossible situation where the concentration at the root surface would attain a negative value. The reasons behind this peculiarity were discussed earlier and are based on the errors associated with the measurements of the solution concentrations. Furthermore, for Na and Mn, the intercept terms, $d_{o,i}$, resulted in insignificant contributions to the models. However, these were not removed from the final linear models since the concentration term proved to be significant. Finally, for Mo, the concentration term resulted in a lower calculated F-statistic as compared to the critical value. Therefore, this model of the back diffusion of Mo is similar to the diffusion limitations of Zn discussed earlier. Furthermore, the explanation of large measurement errors used to describe this discrepancy in Zn may be used in this case for Mo as well.

Table 9.5 Model Parameters for the Linear Regressions and the Diffusion Equations for the Enzyme Limited Nutrients

Nutrient	$d_{0,i}$ (μg/LS)	$d_{1,i}$ (ml/LS)	$D_{eff,i}$ (ml·cm/LS)	$C_{surface,i}$ (μg/ml)
P	3.025 ± 2.968	-0.763 ± 0.113	-0.175 ± 0.026	3.965 ± 3.934
Mg	18.719 ± 11.983	-0.801 ± 0.144	-0.184 ± 0.042	23.370 ± 15.539
Ca	55.180 ± 56.416	-0.674 ± 0.309	-0.155 ± 0.036	81.869 ± 91.733
Na	6.178 ± 3.429	-0.611 ± 0.339	-0.141 ± 0.032	10.111 ± 7.935
Mo	0.017 ± 0.005			
B	0.065 ± 0.037	-0.928 ± 0.056	-0.213 ± 0.049	0.070 ± 0.040
Mn	0.327 ± 0.153	-0.780 ± 0.358	-0.179 ± 0.041	0.419 ± 0.275
Fe	0.777 ± 0.366	-0.850 ± 0.086	-0.196 ± 0.045	0.914 ± 0.440
Cu	-0.008 ± 0.045	-0.607 ± 0.279		

In order to produce the final models for the uptake rates of the enzyme limited nutrients, the convective supply rate, $J_{conv,i}$, minus the back diffusion of the nutrients from the root surface, $J_{diff,i}$, can be considered equivalent to the uptake by the biological apparatus in the root membranes, $J_{c,i}$. Therefore, the Michaelis-Menten model presented in

Equation (9.16) can be combined with the convection and diffusion models presented in Equations (9.8) and (9.12), respectively. This combination is shown in a general form in Equation (9.18) below where the parameters for the diffusion model, $D_{eff,i}$ and $C_{surfacce,i}$, are found in Table 9.5 and the Michaelis-Menten constants, $J_{c,max,i}$ and $K_{m,i}$, are found in Table 9.4. This final model describing the biologically limited nutrient uptake is directly applicable to the macro-nutrients, P, Mg, Ca, and Na, as well as the micro-nutrient, Fe.

$$J_{conv,i} + J_{diff,i} = J_{c,i} \tag{9.18}$$

$$1.886(C_{soln,i}) \exp[0.400(LS) + 8.605(P_m - \pi_{soil})] + D_{eff,i}\frac{C_{soln,.i} - C_{surface,i}}{(D_o - D_i)/2} = \frac{J_{c,max,i}\, C_{soln,i}}{K_{m,i} + C_{soln,i}}$$

It should be noted that the concentrations at the root surface, $C_{surface,i}$, presented in Table 9.5 are the levels that build up due to the restriction by the limited number of available active sites on the proteins or enzymes responsible for the uptake of the biologically limited nutrients. These levels are in addition to the continuous supply by the convective flow. This is in contrast to the nutrients that are diffusion limited where the levels of the nutrients at the root surface presented in Table 9.3 are the result of the increase in the supply rate by diffusion from the bulk solution.

CHAPTER 10 - CONCLUSIONS AND RECOMMENDATIONS

From the results of the previous two chapters concerning the modeling of the development, growth, solution uptake, and inorganic nutrient uptake into the plants produced on the Porous Ceramic Tube - Nutrient Delivery System (PCT-NDS), several conclusions and recommendations for further research can be made. Furthermore, the techniques and analytical methods described in this research provide advancements to the current state of the field of research in plant physiology, growth, and nutrient uptake. Finally, evidence from the analysis of the mass balances shows that several alterations to the procedures and methods used in this research could be made in order to improve upon the results and models. These conclusions and suggestions are presented in this chapter.

In Section 10.1, a discussion of the results is provided emphasizing the high points of this research. This will include an overview of the uses of the PCT-NDS for conducting research on the effects of water potential and nutrient concentrations on the growth, development, and nutrient uptake characteristics in plants. Furthermore, several conclusions concerning both the methodology as well as the actual models produced to describe the nutrient uptake into plants will be provided. This is followed in Section 10.2 which provides several recommendations for future research including alterations to the current methods as well as brief descriptions of other possible research applications for the system and modeling techniques.

10.1 Contributions to Current Field of Research

There are two main points of this thesis which provide considerable advancements to the current state of the field of research conducted in the area of plant physiology, growth, and nutrient uptake. The first of these is the development of a system which is capable of providing a high degree of control of the root-zone environment. In particular, the PCT-NDS provides a method of separating the effects of differing water potentials due to changes in the osmotic component from the effects of the nutrient concentrations themselves. This separation has, up until now, not been achieved to the same degree of control with current research methods as compared to the use of the system of this research. In addition to this contribution, this research provides a method of discriminating the rate limiting steps in the inorganic nutrient uptake processes utilized by plants. The resulting models produced to describe these critical steps are geared towards explaining the growth, development, and nutrient uptake for the whole plant as well as over the entire growth cycle. Furthermore, the effects of water potential and nutrient concentrations are contained within each of the models produced providing several practical applications of these results. These developments are different from previous nutrient uptake models as will be discussed below.

10.1.1 System Exploitation

One problem with the current methods of research into the effects of water potentials, nutrient concentrations, or both on the growth, development, and nutrient uptake characteristics in plants is the inability to separate the differences in water potential caused by alterations in the nutrient solution composition. According to Equation (2.2) which is a general equation relating the overall water potential, Ψ, to the osmotic component, π, and the hydrostatic component, P, changing the concentration of the solutes, C_s, in the nutrient solution automatically changes π. This change in π alters Ψ unless P is controlled as a compensation. The current methods used to make these changes, if at all, include using soils with different water holding characteristics, the

addition of supposedly non-penetrating solutes, and the use of different salt compositions [Cox and Barber, 1992; Yaniv and Werker, 1983; Hohl and Schopfer, 1991; Qasem and Hill, 1993]. The particular problems with each of these methods are provided in some detail in Sections 4.1.2, 6.1.1, and 6.1.2.

From the development of the PCT-NDS provided in this research, substantial evidence was provided which showed that a constant water potential level could be maintained while simultaneously altering the concentration of the nutrients in solution. This was shown during the development of the solution uptake model presented in Equation (8.23). Specifically, using the applied suction pressure in the system, the matric potential could be changed to a level which compensated for the changes in the solution concentrations. By increasing or decreasing the suction based on the differences in the osmotic potential, a constant water potential was shown to be maintained. The evidence for this was provided statistically in the analysis of the effects of the individual osmotic and matric potentials on the solution uptake rates. The analysis of variances presented in Table 8.3 showed that the contributions to the solution uptake by the osmotic and matric potentials were insignificant at the constant water potential level of -0.078 MPa. Furthermore, different water potential levels obtained through various combinations of π_{soil} and P_m did result in different solution uptake rates. This indicated that the system was capable of being controlled at distinct levels of Ψ_{soil}.

There are also other additional advantages to the use of the PCT-NDS for these types of plant studies. This includes the uniformity of the root-zone water potential to the roots grown in direct contact. Under current methods of using different soils or variations in irrigations [Wraith and Baker, 1991; Vetterlein, et al., 1993], there exists the problem of vertical stratification of the soil moisture. This leads to roots closer to the top surface of the soil experiencing drier conditions as compared to the roots nearer to the settled soil water. Another advantage involves the ease at which the roots can be removed from the system as compared to entwined within a soil matrix. Since the pore sizes of the ceramic tubes are smaller than the diameters of the root hairs, then the removal of the roots can be accomplished within minutes as opposed to the hours required to separate them from soil.

10.1.2 Modeling of Plant Nutrient Uptake

In addition to the problems of maintaining a constant water potential under variable solution concentrations, the typical methods used in nutrient uptake experiments are usually only applicable to specific time frames. This includes the split root method, the use of radioactive tracers, and depletion experiments [Barber and Cushman, 1981; Johnson, et al., 1991; Warncke and Barber, 1972; Wrona and Epstein., 1985; Petersen and Jensen, 1988; Tremblay, et al., 1988; Bowen, 1987; Heuwinkel, et al., 1992]. During each of these methods of studying the nutrient uptake kinetics into plants, the plants are grown to a specific stage of development and then transferred into a test solution which contains a different solution composition. Therefore, the resulting kinetics are only conditional for the particular stage of growth and the imposed root-zone conditions. Furthermore, the time frame for which these methods can be implemented are relatively short within that specific growth stage. For example, as the nutrients are depleted from a test solution, the change in osmotic potential becomes more significant over time unless this solution is replenished frequently. As the osmotic potential changes, so does the rate at which the nutrient solution reaches the root surface. For the depletion experiments, this replenishment is a contradiction to the methodology. For the split root method, these types of changes in the root-zone environment are only measurable in the roots since the terrestrial portion would be supplied through both sections of roots. As for the radioactive tracers, their continued use is expensive and requires special handling of the materials.

The nutrient uptake models that have been development such as the Nye and Tinker model, the Barber-Cushman model, and the France and Thornley model are also based on these short time frames. Specifically, contained in the 13 assumptions used in the development of the Barber-Cushman model presented in Equations (3.61) to (3.66) is that the characteristics of the root are not changed with time [Barber and Cushman, 1981]. In other words, this assumption basically states that the root growth is independent of time. When applied to a specific developmental stage, this pseudo steady state assumption is fairly reasonable since the plant tissues do grow relatively slowly. However, the results of the experiments conducted in this research showed that the characteristics of the roots are

changed between leaf stages. This was shown in the models of the dry and wet masses as a function of leaf stage and root-zone conditions provided in Equations (8.10) and (8.18), respectively. This is not addressed in the Barber-Cushman model.

Similarly, the Nye and Tinker style models presented as Equation (3.50) and the France and Thornley model presented as Equation (3.59) utilize mass transfer terms which are not explicitly altered by time. Specifically, the convective mass transport term, v, leading to the diffusional gradients is considered constant with time [Wheeler, et al., 1994; France and Thornley, 1984]. In terms of this research, the rate of solution uptake which is directly related to the mass flux term was shown in be dependent on the leaf stage of development as well. This was shown during the development of the model for the solution uptake, Equation (8.23). Therefore, the Nye and Tinker and France and Thornley models are limited to specific time frames as well.

An additional problem with the Nye and Tinker model is that it fails to take into account the influences of the biological mechanisms responsible for the actual acquisition of the inorganic nutrients. Although some adjustments to the standard form of this model do account for root growth and developmental characteristics [Nye and Tinker, 1969; Willits, et al., 1992; Bhat, et al., 1979a; Bhat, et al., 1979b], they do not address the specific rate limiting steps in the nutrient uptake processes making these models highly empirical. A similar model to these improved Nye and Tinker models is the William's Equation presented in Equation (3.52) [Silberbush and Gbur, 1994]. However, this equation is subject to the same criticisms as the Nye and Tinker models.

Since the rate of nutrient uptake should be dependent upon both the biological growth rate and the environmental supply rate and both of these rates are dependent on development, then these inorganic nutrient uptake models should contain this dependency as well. However, they are only applicable to a single growth stage. Therefore, in order to acquire a complete description of the nutrient uptake characteristics using these models, their application at several discrete times throughout the growth cycle would be required [De Willigen and Van Noordwijk, 1994b].

One of the advantages of the models that are produced in this research is that the leaf stage of development is included in the statistical analyses. This includes the models for the growth, solution uptake, and individual nutrient uptake rates. Furthermore, this factor was shown to be consistently significant for each of the nutrients analyzed. This was shown in Table 9.1 and Appendix E (see Tables E.7 to E.17 for the ANOVA tables for the various nutrients). Therefore, these models can be applied to the entire growth of the plant instead of individual growth stages as with previous models.

In addition to the incorporation of a more applicable time scale to the various models, the models produced in this research explicitly describe the effects of the root-zone conditions on the growth, solution uptake, and inorganic uptake. Although the Nye and Tinker, France and Thornley, and Barber-Cushman models do contain these environmentally based terms, they are not explicit but only implicit. Since the bulk flow term, v, leading to the convective mass transport of nutrients to the root surface is based on the rate of transport caused by the transpirational stream and this process is driven by the water potential gradients in the soil-plant-atmosphere continuum, then these models would be more applicable to real world situations with this inclusion. In fact, another one of the assumptions used in the Barber-Cushman model is that the root-zone conditions are in a steady state [Barber and Cushman, 1981]. In other words, the soil moisture level or soil water potential remains constant. This assumption does not take into account the effects of rainfall or applied irrigations. Furthermore, the bulk flow term, v, used in this and the Nye and Tinker and France and Thornley models are empirically derived from water flow rates, not on the conditions driving the flow. These conditions are the moisture level and the solute concentrations or, in other words, the matric and osmotic potentials.

One of the objectives in this research was to develop inorganic nutrient uptake models which were based on the environmental influences of the root-zone. This included both the osmotic and matric components of the root-zone water potential. By incorporating terms for π_{soil} and P_m into the models developed in this research, the effects of these factors are explicitly described. This is an advantage over the current models. Furthermore, the models developed in this research also incorporate the leaf stage

developmental rate, LS. Therefore, the present model does not refute the Barber-Cushman, Nye and Tinker, and France and Thornley models, but incorporates each of them into a single model and expands their applicability to different leaf stages and root-zone environmental conditions.

In addition to these advantages of the models over predecessors, the methodology developed in this research for discriminating the rate limiting step in the various nutrient uptake processes used by plants allows for the determination of the critical environmental or biological factor. In terms of the applicability of these models to real world situations, the determination of the rate limiting step is an important step in the formulation of a scheme to produce crops optimally. For example, if using this method reveals that the uptake of a particular nutrient into a specific plant species leads to diffusion limitations, then fertilization may be a key determinant to the success of the crop. Furthermore, the timing of the fertilizer application can be determined from the visually based measuremenets such as the plant heights and the leaf stage of development.

10.2 Future Recommendations

There are several recommendations for future research which include changes to the methods used in this current research as well as the development of additional experiments for the further investigation into the nutrient uptake kinetics into plants. The two major problems that arose during the experiments of this research were based on the environmental factors of the growth chamber and the nutrient solution. Specific changes in these conditions are proposed with a discussion of the effects that these changes would have on the current results obtained in this research. Furthermore, in order to produce better models for the growth, development, and nutrient uptake characteristics of plants, several additional experiments are proposed. These include the use of different overall solution concentrations as well as individual nutrient concentrations. These can be applied to other tomato cultivars as well as other plant species. This would produce more generalized models of the nutrient uptake processes conducted by all plants.

10.2.1 Temperature and Relative Humidity Effects

During the experiments of this research, the terrestrial environmental conditions of temperature, T_a, and relative humidity, RH, were only under the control of the building that housed the growth chamber. This lead to uncontrolled variations in these factors that were dependent upon the season (winter versus summer) as well as the daily fluctuations. The specific values for these factors are presented in Appendix A (see Tables A.1 to A.8) along with the averages values obtained during each of the experiments conducted in this research (see Table A.1). These variations lead to several effects which should be eliminated in order to obtain more conclusive results.

Although the effects that the changes in temperature have on the osmotic potentials of the solutions are relatively small ($\pm$0.001 MPa), the effect on the overall rate of growth of the plants could be substantial. This is due to the effect of temperature on the production of organic biomass from the photosynthetic machinery [Gent, 1986]. The effects of temperature on the specific growth rate was shown in Equation (3.3) while the effects on photosynthesis, P_n, were shown in Equations (3.20) to (3.23). Furthermore, both temperature and relative humidity are significant factors affecting the rate of transpiration, E_t. This is due to the rate of transpiration being dependent upon the water potential gradients throughout the soil-plant-atmosphere continuum and the water potential of the air being dependent upon T_a and RH according to Equation (2.7). Since the relative humidity varied by $\pm$7% on average (see Table A.1), then this can translate into changes in the air water potential of approximately $\pm$25 MPa (assuming a constant T_a = 293 K). This change in the water potential or humidity of the air directly affects the rate of transpiration. This is exemplified in several transpiration models such as the Stanghellini model, the Penman-Monteith equation, and the model developed by Sammis and Jernigan [Stanghellini, 1987; Johnson, et al., 1991; Jolliet, 1994; Sammis and Jernigan, 1992]. These were presented as Equations (3.42), (3.44), and (3.45), respectively.

As the temperature and relative humdities changed during the course of the experiments in this research, the rates of development, growth, and solution uptake were significantly subjected to these changes. This is evident from the large range in results

obtained for the number of days after emergence, t_{DAE}, in order for each plant to reach specific leaf stages, LS. The specific data used to derive the model, presented in Equation (8.1), describing t_{DAE} as a function of LS, are provided in Appendix B for the different test conditions (see Tables B.1 to B.7). Similarly, the corresponding plant heights, h_{plant}, also resulted in wide ranging values as shown in the data tables of Appendix B (see Tables B.9 to B.15). Finally, the measurements of the quantities of solution taken up, V_u, also resulted in highly variable results. These are shown in Appendix C for the different test conditions (see Figures C.1 to C.7). Although these data sets are presented as a single collection in these Appendicies, these were derived from individual experiments conducted under different average temperatures and humidities. The variations experienced between plants for the individual experiments are less than the results for all of the experiments taken as a whole. This is shown in Figures 10.1 to 10.3 which present samples of the averages for t_{DAE}, h_{plant}, and V_u, respectively, for two experiments differentiated by the symbols in these figures. Specifically, the closed circles represent a set of data obtained during the summer months while the open triangles represent a set of data from the winter. These results were all obtained when the test conditions of (π_{soil} / P_m) were maintained at (-0.078/-0.000). The differences between the sets of symbols can be attributed to the effects of temperature and humidity while the differences within a set of symbols can be attributed to the inherent genetic differences between plants.

As can be seen in Figure 10.1, the number of days required to reach each leaf stage for the plants produced in the summer is less than those in the winter. Therefore, the developmental rates of the summer plants are faster. Similarly, the overall heights of the summer plants are larger than the winter counterparts as shown in Figure 10.2. These results are indications that the growth of the tomato plants is faster during the warmer temperatures of the summer as compared to the colder winter. As for the solution uptake, the summer months proved to be more humid as listed in Table A.1 leading to a slower rate of solution uptake as shown in Figure 10.3.

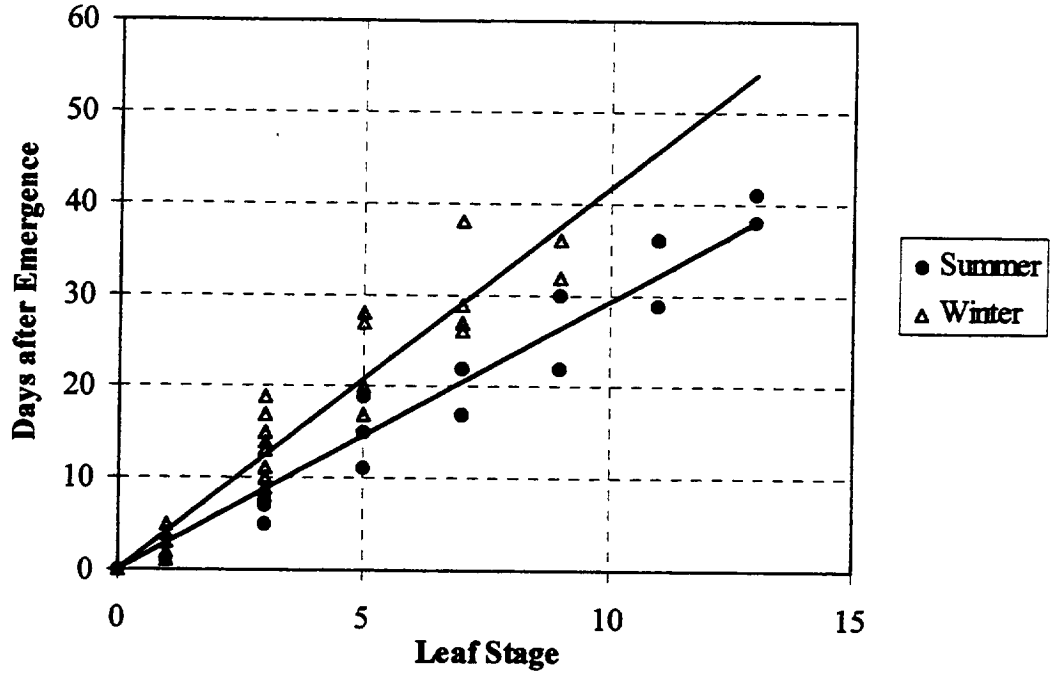

Figure 10.1 Comparison of Results for the Number of Days After Emergence for Tomato Plants Produced during the Summer and Winter

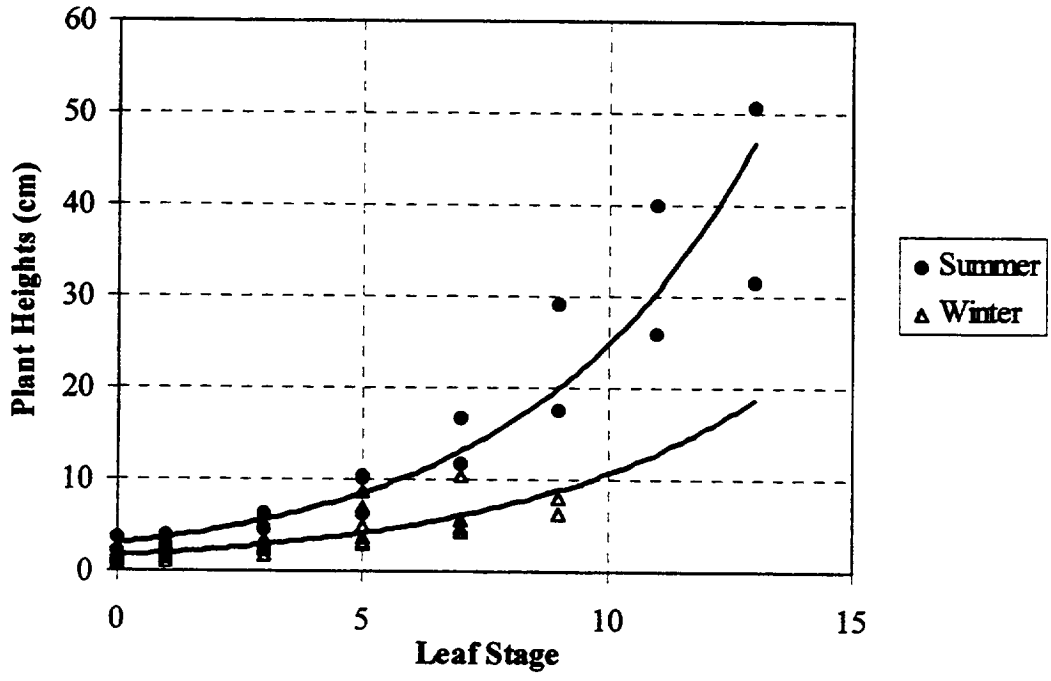

Figure 10.2 Comparison of Results for the Measured Heights of the Tomato Plants Produced during the Summer and Winter

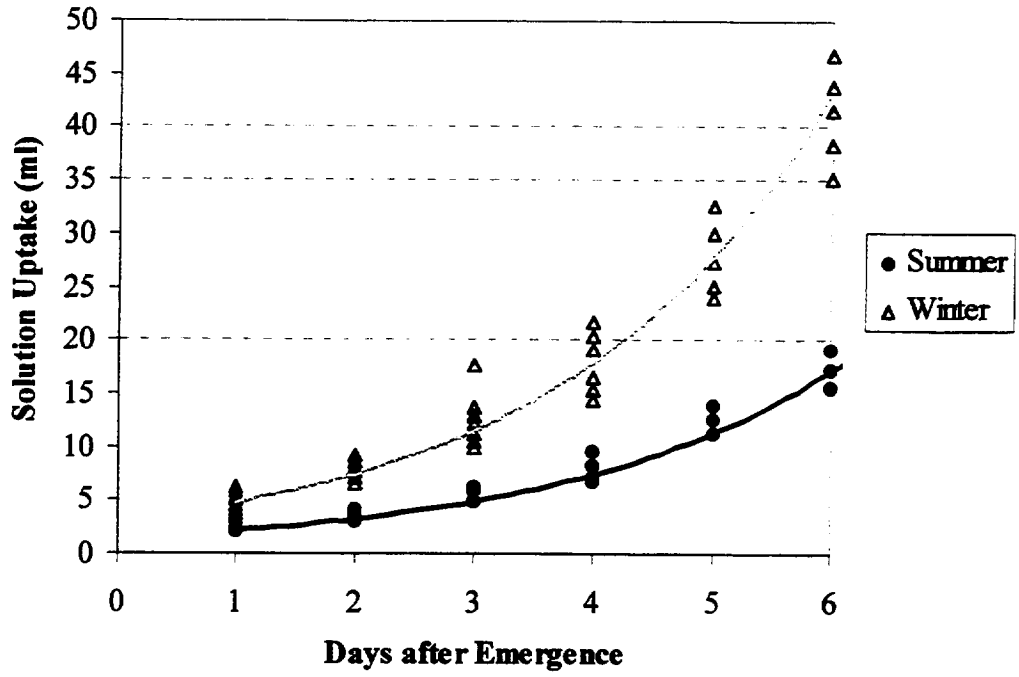

Figure 10.3 Comparison of Results for the Quantities of Solution Taken Up by Tomato Plants Produced during the Summer and Winter

In order to correct for these effects of T_a and RH on the growth, development, solution uptake, and subsequent inorganic nutrient uptake, a better control of these environmental conditions would be desirable. This can be accomplished in several ways. For the growth chamber used in this research, since the warmer temperatures resulted in faster growing plants which developed more rapidly, then a small space heater could have been installed for the winter months. As for the upper levels, the temperature never reached above 32.5 °C which is approximately at the upper threshold for the optimum temperature range for tomato plants [IPM Manual Group, 1982]. Therefore, an air cooling system should not be required. In order to control the humidity, a humidifier and a de-humidifier could be placed into the growth chamber. One problem with this solution is that the area available for the production of plants is already limited meaning that the addition of a heater, humidifier, and de-humidifier would severely restrict this area.

One alternative method is to conduct the plant experiments at approximately the same time over several years. However, this severely restricts the number of experiments

that can be conducted as well as subject these experiments to the daily differences in temperature and humidity that occur even during the particular season. Optimally, a controlled environment growth chamber specific for the production of plants could be utilized. These chambers are available and have been designed such that the environmental conditions are within $\pm 1\%$ of the set values [Averner, et al., 1987; Edeen and Henninger, 1991]. However, the set-up and operation of these advanced growth chambers are expensive and in high demand.

Whatever methods are utilized to control the temperature and relative humidity, the probable effects that this would have would be to reduce the variations in the results of these experiments. In terms of the models for the growth and development of the plants, this would change the values of the regression parameters for the models of t_{DAE}, h_{plant}, and $W_{tissue,d}$. Furthermore, this could lead to additional terms being required, particularly, for the number of days after emergence which was shown in Equation (8.1) not to be dependent upon the root-zone conditions. However, from the analysis of variances presented in Table 8.1, the sum of squares for the left-out terms was a fairly large value indicating a possible significant term.

A substantial effect that a more constant humidity would have on the results of this research is in the water status of the plants. In particular, the solution uptake model, presented in Equation (8.23) was shown in Table 8.5 to be dependent upon the leaf stage and the root-zone water potential. Although the calculated F-statistic for the left-out terms is close to a value of one indicating the remaining sum of squares is probably due to the measurement errors, the reduction of these errors due to the higher control of T_a and RH could lead to an increase in F_{calc} for the left-out terms. One possible term which may contribute significantly under these optimized terrestrial environments would be the effects of the matric potential on the solution uptake. This is particularly true since the different pore sized ceramic tubes used in the production of the plants directly affect the matric potential according to Equation (7.2). Furthermore the applied suction pressure itself was based on an average between the ceramic tube ends. Therefore, an additional dependency on P_m may become evident if the experimental errors for T_a and RH are reduced.

10.2.2 Solubilities, pH, and Precipitates

During the calculation of the desired suction pressure used in the PCT-NDS, the osmotic potential of the solution was used as a basis. This was conducted since it was desired to compensate for the changes in π_{soil} using the matric potential of the ceramic tubes. Theoretically, the 1x, 1/2x, and 1/4x concentrations should yield osmolarities of 31.1, 15.6, and 7.8 mmol/kg, respectively. However, in reality, these values can vary depending upon several factors. First, the level of contaminants in the water used to produce the solutions can be significant. Furthermore, other impurities can also be introduced into the solution from the salts originally used to make-up the stock solutions [Resh, 1978; Schwarz, 1995]. Finally, the acidity of the water which dictates the amount of NaOH added to obtain the desired pH level for the solution can also lead to significant Na concentrations. Similarly, since the number of protons present in the solution represents an additional solute contributing to the osmolarity, then this factor also contributes to the osmotic potential ($pH = -\log_{10}[H^+]$). However, this contribution is at a relatively low level of approximately 0.002 mmol/kg for the applicable range.

During the calculations of the required applied suction pressure dictating the matric potential according to Equation (7.2), all solutes were assumed to remain as ionic species throughout the course of an experiment. Therefore, the values for the osmotic potential were assumed to be equivalent to the standard solution. However, these solutions contain a mixture a dissociated ions which can reassociated into various compounds. For example, Ca^{2+}, initially formed from the dissolution of $Ca(NO_3)_2 \cdot 4H_2O$, can produce $CaSO_4$, $Ca(H_2PO_4)_2$, and $CaCl_2$ from the other constituents in the solution depending upon the equilibrium constants for these reactions. Furthermore, some of these compounds can form precipitates, depending upon the degree of hydration and the solution pH, leaving these nutrients unavailable to the plant. Therefore, the effects of solution pH on the nutrient solubilities should have been taken into consideration as well.

To some degree, this was accomplished during the analysis of the mass balances presented for P, Mg, Ca, Na, and Fe (see Section 8.3). Using a side experiment where the pH of the standard solution was altered incrementally from 5.7 to 8.0 using the addition of

NaOH, the soluble concentrations of the analyzed nutrients were shown to be dependent upon the pH level. Specifically, these dependencies were shown in Equation (8.30) to (8.34), respectively (also see Figures D.1 to D.5).

In terms of the results obtained in this research for the inorganic nutrient uptake rates, the solution pH, which was shown to continually increase from the initial level of 5.8 to near neutral conditions, caused several of the nutrients to precipitate out of the experimental solutions. An example of this trend in the pH levels is presented in Figure 10.4 below. According to the pH experiment, the major precipitated nutrients were phosphorus, calcium, and iron with a slight decrease occurring in magnesium. In other studies, both P and Fe have been shown to be highly dependent on the solution pH [Hoagland and Arnon, 1950; Resh, 1978]. Furthermore, since P, Mg, and Ca are present in relatively large quantities in the hydroponic solution, then the majority of the probable precipitates formed include calcium phosphates and magnesium phosphates.

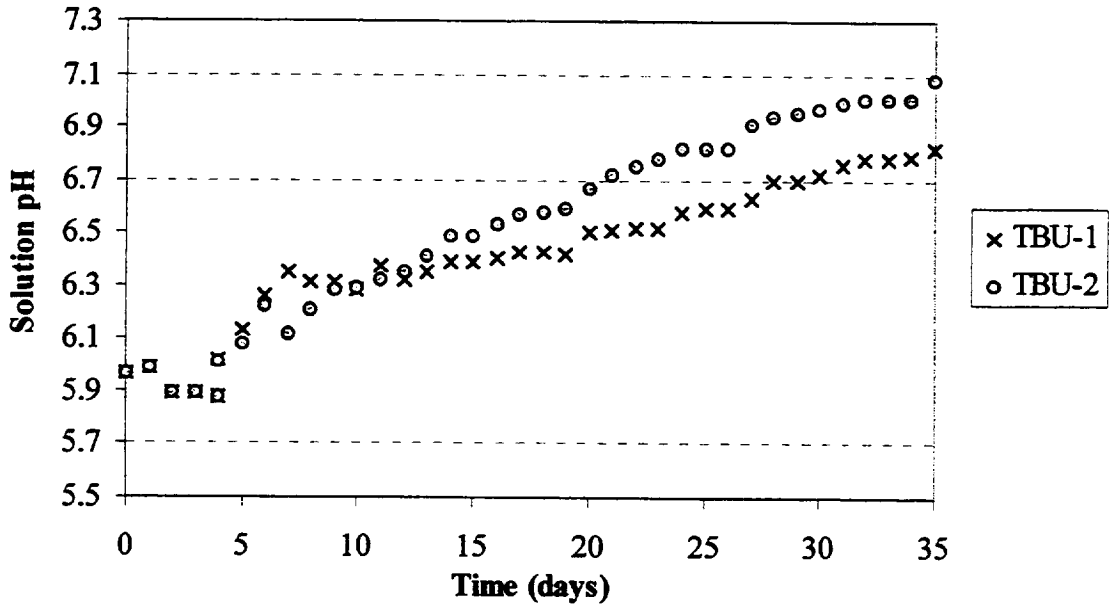

Figure 10.4 Typical Profile of the the Change in pH During the Course of an Experiment

Since most of the nutrients that precipitate out are the macro-nutrients, then this loss of total solutes would have effectively reduced the osmotic potential of the solution as well as the individual nutrient concentrations. Therefore, the levels of the osmotic, π_{soil}, or

overall water potentials, Ψ_{soil}, used in the development of the growth, development, solution uptake, and inorganic nutrient uptake models were, in reality, incorrect. Since these potentials are negative values and a reduction in the soluble concentration would have decreased their magnitudes, then the regression parameters for the various models showing a significant contribution by these factors would have been larger in value. This is also true for the values of the constants in the diffusion and enzyme kinetic models which utilize the solution concentration, $C_{soln,i}$.

In addition to these changes in the results of this research, the effects that the pH has on the concentrations would alter the determination of the rate limiting steps in the nutrient uptake processes. Specifically, the experimental uptake rates, J_i, were compared to the convection model, $J_{conv,i}$, using the t-test. This comparison resulted in the three possibilities where $J_i = J_{conv,i}$, $J_i < J_{conv,i}$ or $J_i > J_{conv,i}$. However, the solution concentrations, $C_{soln,i}$, utilized in the convection model, presented in Equation (9.8), were based on the standard concentrations of the initial solutions. These concentrations were presented in Tables 8.8 to 8.10 for the 1x, 1/2x, and 1/4x solutions, respectively. If these concentrations were, in reality, smaller than those listed in these tables due to the precipitation at higher pH levels, then the nutrients found to be biologically limited (i.e. $J_i < J_{conv,i}$) may actually be shifted towards a result leading to convection limitations (i.e. $J_i = J_{conv,i}$). This shift may be an outright shift from the onset since the pH continually increases or it could be a gradual transition between the rate limiting mechanisms as the pH levels changed slowly during the experiments. Without a further examination into the effects of pH on the nutrient uptake characteristics, this possibility will remain unknown.

In order to control the pH levels to the standard level or to other specific values in order to examine these effects, several possible changes to the solution could be made. One method is to simply change the entire solution on a periodic basis. The problem with this method is that the solution would have to be changed fairly often since the pH levels changed almost immediately (see Figure 10.4). Another method of maintaining the pH during the course of an experiment is the addition of an acid using a pH controller. In using this method, it is important to determine a form of acid which is neither toxic to

plants nor contains an essential nutrient since this could lead to a change in the uptake characteristics. One possible solution to this is the use of plant derived organic acids such as citric or oxalic acid [Goldstein, et al., 1988a]. Finally, buffering the hydroponic solution with a commercially available agent provides an economical means of compensating for the changes in the solution during the growth of the plants on the PCT-NDS.

Since the pH does have such a large impact on the concentration of the nutrients, then this factor can be specifically examined. Using the buffered or pH adjusted solutions, the plants grown can be subjected to a range in pH levels with the concentrations of the nutrient analyzed as a result. This would allow for equations similar to Equations (8.30) to (8.34) describing the pH dependencies of the nutrients to be derived. However, these results would be obtained from the actual plant experiments instead of as a side experiment without the biological influences as performed in this research. This would not only provide stronger support for the nutrient uptake models but reduce the discrepancies in the inorganic mass balances.

10.2.3 Additional Experiments

Using the PCT-NDS, several experiments could be conducted which would not only strengthen the nutrient uptake models produced during this research, but increase the applicability of the models to a more general description of plant nutrition. These experiments include producing the tomato plants used in this research (*Lycopersicon esculentum* cv. Cherry Elite) under the revised methods (i.e. T_a, RH, and pH controlled), testing the effects of maintained levels of pH on the nutrient uptake, and examining different concentration levels for various nutrients. Furthermore, the experimental and analytical methods developed to discriminate the rate limiting step in the nutrient uptake processes can be applied to other tomato cultivars as well as other plant species. This would allow the development of more generalized nutrient uptake models.

Using the revised methodology discussed previously (see Section 10.2.1 and 10.2.2), the nutrient uptake models produced in this research can be improved and

expanded. Specifically, the diffusion limited nutrients, K and Zn, can be tested at higher concentrations in order to determine the levels at which these specific enzymes become saturated. This would allow for the production of the general nutrient uptake models for these elements which would be similar in form to Equation (9.18). However, in order to test these increased concentrations while maintaining a constant water potential, two possible directions can be taken. First, the individual concentrations of these nutrients can be increased in the base solutions. However, since these nutrients are added as the salts, KNO_3 and $ZnSO_4.7H_2O$, respectively, then the anionic counterparts for these nutrients would be increased in concentration as well. The effects that these increases would have on the nutrient uptake characteristics would not be separable from the effects of the increased K or Zn levels. Although this method may be reasonable for Zn since this nutrient is present in micro-quantities and the increase in sulfate would be relatively small compared to the total sulfate concentration, the results would still be a little suspect. Alternatively, the entire solution concentration can be increased to greater than the 1x levels used in this research. However, since the osmotic potential of the 1x solution is equal to -0.078 MPa and increasing the overall concentration would decrease this value, then the constant water potential results presented in this thesis could not be used as a comparison. This is due to the matric potential also being a negative pressure. However, the results at the water potential levels of -0.117 and -0.137 MPa can be used as long as the osmtotic potentials do not exceed these limits.

In addition to these experiments, the models for the micro-nutrients, Mo, B, and Mn, can be improved since the concentrations tested in this research all resulted in saturated active sites on the biological transporter responsible for the uptake. This lead to an inability to determine the Michaelis-Menten constant, $K_{m,i}$, which is the concentration required for half of the maximal uptake rate. This was shown during the development of the results presented in Table 9.4. In order for the concentrations of these individual nutrients to be lowered to non-saturating levels, the individual salts can be decreased or the entire solution concentration can be lowered to below the 1/4x solution levels used in this research. This is similar to the discussion above concerning the increases in nutrient

concentrations. Since each of these are micro-nutrients, then changing the individual salts may not cause substantial changes in the remaining nutrients. In fact, Mo and B are introduced as molybdic and boric acids which, in a buffered solution, would not alter the concentration of the other nutrients or the pH level substantially. As for the Mn, the chloride present in the salt that is used can be replaced using NaCl. Since sodium is present in macro-quantities, then the slight increase in Na may not represent a major change in the concentration as compared to the absolute levels.

One issue which should be addressed for these and the other micro-nutrients is that the method of analysis of using the Inductively Coupled Plasma - Atomic Emission Spectrometer (ICP-AES) provided results which contained large errors. These errors need to be reduced in order for more conclusive nutrient uptake models to be produced. A possible solution to this problem is to evaporate the water solvent from the solution samples, thus, increasing the concentration of all of the nutrients in the sample. This would require larger quantities of solution since a minimum volume is required in the ICP system.

In addition to conducting these complementary experiments on the tomato cultivar used in this research, all of the (revised) experiments described in this research can be applied to other tomatoes as well as different plant species. This would provide evidence of whether the mechanisms involved in the uptake of the nutrients is standard for all higher plants or simply the individual results of the evolution of the species or cultivar. For example, if other tomato cultivars provided results which were similar to the present cultivar under the same conditions as the experiments in this research, then this would be an indication that the mechanisms of uptake in tomatoes were similar as well. Expanding this to other plant species, generalizations of the mechanisms can be made depending upon whether the same nutrients were enzyme limited or mass transfer limited and at what root-zone conditions these occurred. These generalizations would be particularly true if the Michaelis-Menten kinetic constants were statistically equal indicating the possibility of an identical enzyme or protein in the root membranes. The formulation of these generalizations are possible using the experimental and analytical techniques developed in this research.

LIST OF REFERENCES

LIST OF REFERENCES

Acock, B.A., Charles-Edwards, D.A., and Hand, D.W. (1976): An Analysis of Some Effects of Humidity on Photosynthesis by a Tomato Canopy Under Winter Light Conditions and a Range of CO_2 Concentrations. J. Exp. Bot. 37, pp. 933-941.

Adams, P. (1986): Mineral Nutrition. In: "The Tomato Crop.", J.G. Atherton and J. Rudich (eds.), Chapman and Hall, London.

Adams, P. and Holder, R. (1992): Effects of Humidity, Ca, and Salinity on the Accumulation of Dry Matter and Ca by the Leaves and Fruit of Tomato. J. Hort. Sci. 67, pp. 137-142.

Akeson, M. and Munns, D.N. (1990): Uptake of Aluminum into Root Cytoplasm: Predicted Rates for Important Solution Complexes. J. Plant Nutr. 13, pp. 467-484.

Al-Harbi, A.R. (1995): Growth and Nutrient Composition of Tomato and Cucumber Seedlings as Affected by Sodium Chloride Salinity and Supplemental Calcium. J. Plant Nutr. 18, pp. 1403-1416.

Atherton, J.G. and Harris, G.P. (1986): Flowering. In: "The Tomato Crop", J.G. Atherton and J. Rudich (eds.), Chapman and Hall, London.

Averner, M.M. (1989): Closed Ecological Life Support System. In: "Lunar Based Agriculture: Soils for Plant Growth.", D.W. Ming and D.L. Henninger (eds.), ASA-CSSA-SSSA, Madison, WI.

Averner, M.M., MacElroy, R.D., and Smernoff, D.T. (1987): Controlled Ecological Life Support Systems: Development of a Plant Growth Module. In: "Controlled Ecological Life Support System." NASA Conference Publication 2479, Ames Research Center, Moffett Field, CA.

Awada, S., Campbell, W.F., Dudley, L.M., and Jurinak, J.J. (1995): Interactive Effects of Sodium Chloride, Sodium Sulphate, Calcium Sulphate, and Calcium Chloride on Snapbean Growth, Photosynthesis, and Ion Uptake. J. Plant Nutr. 18, pp. 889-900.

Baker, D.E., Gorsline, G.W., Smith, C.B., Thomas, W.I., Grube, W.E., and Ragland, J.L. (1963): Technique for Rapid Analyses of Corn Leaves for Eleven Elements. Agron. J. 55 , pp. 133-136.

Barber, S.A. and Cushman, J.H. (1981): Nitrogen Uptake Model for Agronomic Crops. In: "Modeling Wastewater Renovation by Land Application.", I.K. Iskandar (ed.), John Wiley, New York.

Barker, A.V. and Corey, K.A. (1990): Ethylene Evolution by Tomato Plants Receiving Nitrogen Nutrition from Urea. HortScience 25, pp. 420-421.

Barrachina, A.C., Carbonell, F.B., and Beneyto, J.M. (1994): Effect of Arsenite on the Concentrations of Micro-Nutrients in Tomato Plants Grown in Hydroponic Culture. J. Plant Nutr. 17, pp. 1887-1903.

Barta, D.J., Edeen, M.A., and Eckhardt, B.D. (1992): Regenerative Life Support Systems Test Bed Performance: Lettuce Crop Characterization. SAE Technical Paper Series, Paper No. 921391.

Bar-Tal, A., Bar-Yosef, B., and Kafkafi, U. (1993): Modeling Pepper Seedling Growth and Nutrient Uptake as a Function of Cultural Conditions. Agron. J. 85, pp. 718-724.

Bausch, W.C. and Wright, B.D. (1985): The Design of a Plant Support System Suitable for Long-Term Plant Investigations in Micro-Gravity. B.D. Wright Thesis Submitted to the Agricultural and Chemical Engineering Department at Colorado State University, Fort Collins, CO.

Berard, R.G. and Thurtell, G.W. (1991): The Interactive Effects of Increased Evaporative Demand and Soil Water on Photosynthesis in Maize. Can. J. Plant Sci. 71, pp. 31-39.

Beinfait, H.F. (1988): Mechanisms in Fe-Efficiency Reactions of Higher Plants. J. Plant Nutr. 11, pp. 605-629.

Bellaloui, N. and Pilbeam, D.J. (1990): Reduction of Nitrate in Leaves of Tomato During Vegetative Growth. J. Plant Nutr. 13, pp. 39-55.

Bellaloui, N. and Pilbeam, D.J. (1991): Effects of Nitrate Withdrawal and Resupply on the Assimilation of Nitrate in Leaves of Tomato. J. Exp. Bot. 42, pp. 81-88.

Bestman, A.R. (1992a): Global Models for the Biomechanics of Green Plants. Part 1. Intl. J. Energy Research 16, pp. 677-684.

Bestman, A.R. (1992b): Global Models for the Biomechanics of Green Plants. Part 2. Intl. J. Energy Research 16, pp. 685-689.

Bestman, A.R. (1992c): Global Models for the Biomechanics of Green Plants. Part 3. Intl. J. Energy Research 16, pp. 691-696.

Bhat, K.K.S., Brereton, A.J., and Nye P.H. (1979a): The Possibility of Predicting Solute Uptake and Plant Growth Response from Independently Measured Soil and Plant Characteristics. VI. The Growth and Uptake of Rape in Solutions of Constant Nitrate Concentration. Plant and Soil 53, pp. 137-167.

Bhat, K.K.S., Nye, P.H., and Brereton A.J. (1979b): The Possibility of Predicting Solute Uptake and Plant Growth Response from Independently Measured Soil and Plant Characteristics. VIII. A Comparison of the Growth and Nitrate Uptake of Rape Grown in Similar Nitrate Concentration in Solution or in Soil Solution. Plant and Soil 53, pp. 193-201.

Blanchar, R.W., Rehm, G., and Caldwell, A.C. (1965): Sulfur in Plant Materials by Digestion with Nitric and Perchloric Acid. Soil Sci. Soc. Proc. 29, pp. 71-72.

Boss, C.B. and Fredeen, K.J. (1989): Concepts, Instrumentation, and Techniques in Inductively Coupled Plasma Atomic Emission Spectrometry. Perken-Elmer Corporation.

Bould, C., Bradfield, E.G., and Clarke, G.M. (1960): Leaf Analysis as a Guide to the Nutrition of Fruit Crops. I. General Principles, Sampling Techniques and Analytical Methods. J. Sci. Food Agric. 11, pp. 229-242.

Bowen, J.F. (1987): Physiology of Genotypic Differences in Zinc and Copper Uptake in Rice and Tomato. Plant and Soil 99, pp. 115-125.

Boyer, J.S. (1985): Water Transport. Ann. Rev. Plant Physiol. 36, pp. 473-516.

Brauer, D. (1994): Potassium Inhibition of Calcium and Magnesium Accumulation in Roots of Intact Maize Seedlings. J. Plant Nutr. 17, pp. 709-716.

Breace, B.C. and Kohl, H.C. (1970): Measuring Osmotic Pressure of Sap within Live Cells by Means of a Visual Melting Point Apparatus. Plant Physiol. 46, pp. 515-519.

Bromberg, J.P. (1984): Physical Chemistry. 2nd edition. Allyn and Bacon, Inc., Boston, MA.

Brown, J.C. (1978): Mechanisms of Iron Uptake by Plants. Plant, Cell, and Environ. 1, pp. 249-257.

Bruckler, L., Lafolie, F., and Tardieu, F. (1991): Modeling Root Water Potential and Soil-Root Water Transport: II. Field Comparisons. Soil Sci. Soc. Am. J. 55, pp. 1213-1220.

Brugge, R. and Thornley, J.H.M. (1985): A Growth Model of Root Mass and Vertical Distribution, Dependent on Carbon Substrate from Photosynthesis and with Non-Limiting Soil Conditions. Ann. Bot. 55, pp. 563-577.

Bugbee, B. and Salisbury, F.B. (1988): Studies on Maximum Yield of Wheat for the Controlled Environments of Space. NASA-Ames Cooperative Agreement No. NCC 2-139, Utah State University, Logan, UT.

Busman, L.M., Dick, R.P., and Tabatabai, M.A. (1983): Determination of Total Sulfur and Chlorine in Plant Materials by Ion Chromatography. Soil Sci. Soc. Am. J. 47, pp. 1167-1170.

Campbell, G.S. (1977): An Introduction to Environmental Biophysics. Springer-Verlag, New York.

Carpena, O., Masaguer, A., and Sarro, M.J. (1988): Nutrient Uptake by Two Cultivars of Tomato Plants. Plant and Soil, 105, pp. 294-296.

Carpenter, T.D. (1985): United States of America: Current Research and Developments. In: "Hydroponics Worldwide: State of the Art in Soilless Crop Production." A.J. Savage (ed.), International Center for Special Studies, Inc., Honolulu, HA.

Chanter, D.O. (1976): Mathematical Models in Mushroom Research and Production. D.Phil. Thesis, University of Sussex.

Charles, D.J., Joly, R.J., and Simon, J.E. (1990): Effects of Osmotic Stress on the Essential Oil Content and Composition of Peppermint. Phytochemistry 29, pp. 2837-2840.

Classen, N. and Barber, S.A. (1974): A Method for Characterizing the Relation between Nutrient Concentration and Flux into Roots of Intact Plants. Plant Physiol. 54, pp. 564-568.

Claasen, N. and Barber, S.A. (1976): Simulation Model for Nutrient Uptake from Soil by a Growing Plant Root System. Agron. J. 68, pp. 961-964.

Cohen, Y., Fuchs, M., Falkenflug, V., and Moreshet, S. (1988): Calibrated Heat Pulse Method for Determining Water Uptake in Cotton. Agron. J. 80, pp. 398-402.

Cohen, Y., Huck, M.G., Hesketh, J.D., and Frederick, J.R. (1990): Sap Flow in the Stem of Water Stressed Soybean and Maize Plants. Irrig. Sci. 11, pp. 45-50.

Coltman, R.R. (1987): Tolerance of Tomato Strains to Phosphorus Deficiency in Root Culture. HortScience 22, pp. 1305-1307.

Cooper, A. (1979): The ABC of NFT. Grower Books, London.

Cortes, P.M. (1992): Analysis of the Electrical Coupling of Root Cells: Implications for Ion Transport and the Existence of an Osmotic Pump. Plant, Cell, and Environ. 15, pp. 351-363.

Cox, M.S. and Barber, S.A. (1992): Soil Phosphorus Levels Needed for Equal P Uptake from Four Soils with Different Water Contents at the Same Water Potential. Plant and Soil 143, pp. 93-98.

Csizinszky, A.A. (1994): Yield Response of Bell Pepper and Tomato to Controlled-Released Fertilizers on Sand. J. Plant Nutr. 17, pp. 1535-1549.

Cushman, J.H. (1979): An Analytical Solution to Solute Transport Near Root Surfaces for Low Initial Concentration: I. Equations Development. Soil Sci. Soc. Am. J. 43, pp. 1087-1090.

De Kreij, C., Janse, J., Van Goor, B.J., and Van Doesburg, J.D.J. (1992): The Incidence of Calcium Oxalate Crystals in Fruit Walls of Tomato (*Lycopersicon esculentum* Mill.) as Affected by Humidity, Phosphate, and Calcium Supply. J. Hort. Sci. 67, pp. 45-50.

De Willigen, P. and Van Noordwijk, M. (1994a): Mass Flow and Diffusion of Nutrients to a Root with Constant or Zero-Sink Uptake. I. Constant Uptake. Soil Science 157, pp. 162-170.

De Willigen, P. and Van Noordwijk, M. (1994b): Mass Flow and Diffusion of Nutrients to a Root with Constant or Zero-Sink Uptake. II. Zero-Sink Uptake. Soil Science 157, pp. 171-175.

Dreschel, T.W. (1988): The Results of Porous Tube Plant Growth Unit Experiment T6B. NASA Technical Memorandum #100988, John F. Kennedy Space Center, FL.

Dreschel, T.W., Brown, C.S., Hinkle, C.R., Sager, J.C., and Knott, W.M. (1990b): Developing Future Plant Experiments for Spaceflight. ASAE Paper No. 90-4533, Chicago, IL., Dec. 18-21.

Dreschel, T.W., Carlson, C.W., Wells, H.W., Anderson, K.F., Knott, W.M., and Munsey, W. (1993): Physical Testing for the Microgravity Plant Nutrient Experiment. ASAE/CSAE Paper No. 93-4007, Spokane, WA., June 20-23.

Dreschel, T.W., Prince, R.P., Hinkle, C.R., and Knott, W.M. (1987): Porous Membrane Utilization in Plant Nutrient Delivery. ASAE Paper No. 87-4025, Baltimore, MD., June 28 -July 1.

Dreschel, T.W. and Sager, J.C. (1989): Control of Water and Nutrients Using a Porous Tube: A Method for Growing Plants in Space. HortScience 24, pp. 944-947.

Dreschel, T.W., Sager, J.C., and Wheeler, R.M. (1988): Status of Porous Tube Plant Growth Unit Research: Development of a Plant Nutrient Delivery System for Space. ASAE Paper No. 88-4524, Chicago, IL., Dec. 13-16.

Dreschel, T.W., Wheeler, R.M., Sager, J.C., and Knott, W.M. (1990a): Factors Affecting Plant Growth in Membrane Nutrient Delivery. In: "Controlled Ecological Life Support Systems: CELSS '89 Workshop." R.D. MacElroy (ed.), Ames Research Center, Moffett Field, CA.

Edeen, M. and Henninger, D. (1991): Regenerative Life Support Systems (RLSS) Test Bed Performance: Characterization of Plant Performance in a Controlled Atmosphere. In: "Regenerative Life Support Systems and Processes.", SP-873, Soc. of Automotive Engineers, Warrendale, PA.

Estaban, R.M., Collado, J.G., Lopez-Andreu, F.J., and Herrera, M.F. (1985): Effect of Boron on Soluble Protein and Sugar Contents of Tomato Roots. Plant and Soil 88, pp. 149-151.

Feddes, R.A., Kowalik, P.J., Malinka, K.K., and Zaradny, H. (1978): Simulation of Field Water Use and Crop Yield. Centre for Agricultural Publishing and Documentation. Wageningen, the Netherlands.

Field, R. (1988): Old MacDonald has a Factory. Discover 9, Vol. 12, pp. 46-51.

France, J. and Thornley, J.H.M. (1984): Mathematical Models in Agriculture. Butterworths and Co. (Publishers), Inc., London.

Galtier, N., Foyer, C.H., Murchie, E., Alred, R., Quick, P., Voelker, T.A., Thepenier, C., Lasceve, G., and Betsche, T. (1995): Effects of Light and Atmospheric Carbon Dioxide Enrichment on Photosynthesis and Carbon Partitioning in the Leaves of Tomato (*Lycopersicon esculentum* L.) Plants Over-Expressing Sucrose Phosphate Synthase. J. Exp. Bot. 46, pp. 1335-1344.

Garcia, M. and Ascencio, J. (1992): Root Morphology and Acid Phosphatase Activity in Tomato Plants During Development of and Recovery from Phosphorus Stress. J. Plant Nutr. 15, pp. 2491-2503.

Geankoplis, C.J. (1983): Transport Processes and Unit Operations. 2nd edition. Allyn and Bacon, Inc., Boston, MA.

Geisenberg, C. and Stewart, K. (1986): Field Crop Management. In: "The Tomato Crop.", J.G. Atherton and J. Rudich (eds.), Chapman and Hall, London.

Gent, M.P.N. (1984): Carbohydrate Level and Growth of Tomato Plants: I. The Effect of Carbon Dioxide Enrichment and Diurnally Fluctuating Temperatures. Plant Physiol. 76, pp. 694-699.

Gent, M.P.N. (1986): Carbohydrate Level and Growth of Tomato Plants: II. The Effect of Irradiance and Temperature. Plant Physiol. 81, pp. 1075-1079.

Glass, A.D.M. (1989): Environmental Influences on Ion Absorption. In: "Plant Nutrition." Jones and Bartlett Publishers, Boston, MA.

Goldstein, A.H., Baertlein, D.A., and McDaniel, R.G. (1988a): Phosphate Starvation Inducible Metabolism in *Lycopersicon esculentum*. I. Excretion of Acid Phosphatase by Tomato Plants and Suspension-Cultured Cells. Plant Physiol. 87, pp. 711-715.

Goldstein, A.H., Danon, A., Baertlein, D.A., and McDaniel, R.G. (1988b): Phosphate Starvation Inducible Metabolism in *Lycopersicon esculentum*. II. Characterization of the Phosphate Starvation Inducible-Excreted Acid Phosphatase. Plant Physiol. 87, pp. 716-720.

Goudriaan, J. and Monteith, J.L. (1990): A Mathematical Function for Crop Growth Based on Light Interception and Leaf Area Expansion. Ann. Bot. 66, pp. 695-701.

Hafez, A.A., Goyal, S.S., and Rains, D.W. (1991): Quantitative Determination of Total Sulfur in Plant Tissues using Acid Digestion and Ion-Chromatography. Agron. J. 83, pp. 148-153.

Heath, R.L., Hurd, R.M.S., and Madore, M.A. (1990): A Generalized Photosynthetic Model for Plant Growth Within a Closed Artificial Environment. SAE Technical Paper Series, Paper No. 901331.

Herkelrath, W.N., Miller, E.E., and Gardner, W.R. (1977): Water Uptake by Plants 2: The Root Contact Model. Soil Sci. Soc. Am. J. 41, pp. 1039-1043.

Heuwinkel, H., Kirkby, E.A., LeBot, J., and Marschner, H. (1992): Phosphorus Deficiency Enhances Molybdenum Uptake by Tomato Plants. J. Plant Nutr. 15, pp. 549-568.

Hewitt, E.J. and Smith, T.A. (1974): Plant Mineral Nutrition. The English Universities Press, Ltd., London.

Higinbotham, N., Etherton, B., and Foster, R.J. (1967): Mineral Ion Contents and Cell Transmembrane Electropotentials of Pea and Oat Seedling Tissue. Plant Physiol. 42, pp. 37-46.

Ho, L.C. and Hewitt, J.D. (1986): Fruit Development. In: "The Tomato Crop.", J.G. Atherton and J. Rudich (eds.), Chapman and Hall, London.

Hoagland, D.R. and Arnon, D.I. (1950): The Water-Culture Method for Growing Plants Without Soil. California Agricultural Experiment Station Circular 347, Berkeley, CA.

Hohl, M. and Schopfer, P. (1991): Water Relations of Growing Maize Coleoptiles. Plant Physiol. 95, pp. 716-722.

Holden, M.J., Luster, D.G., Chaney, R.L., Buckhout, T.J., and Robinson, C. (1991): Fe^{3+}-Chelate Reductase Activity of Plasma Membranes Isolated from Tomato (*Lycopersicon esculentum* Mill.) Roots. Plant Physiol. 97, pp. 537-544.

Holden, M.J., Crimmins, T.J. Jr., and Chaney, R.L. (1995): Cu^{2+} Reduction by Tomato Root Plasma Membrane Vesicles. Plant Physiol. 108, pp. 1093-1098.

Hurd, R.G. and Thornley, J.H.M. (1974): An Analysis of the Growth of Young Tomato Plants in Water Culture at Different Light Integrals and CO_2 Concentrations. I. Physiological Aspects. Ann. Bot. 38, pp. 375-388.

Ikeda, M., Mizoguchi, K., and Yamakawa, T. (1992): Stimulation of Dark Carbon Fixation in Rice and Tomato Roots by Application of Ammonium Nitrogen. Soil Sci. Plant Nutr. 38, pp. 315-322.

IPM Manual Group - M.L. Flint, Director (1982): Integrated Pest Management for Tomatoes. The Regents of the University of California, Publication 3274, Berkeley, CA.

Jackson, M.B., Davies, W.J., and Else, M.A. (1996): Pressure-Flow Relationships, Xylem Solutes and Root Hydraulic Conductance in Flooded Tomato Plants. Ann. Bot. 77, pp. 17-24.

Janes, H.W., Chin, C.-K., and Bachmansky, J. (1988): Growth and Metabolism of Tomato Roots Grown in Tissue Cultures Held at Various Temperatures. HortScience 23, pp. 773.

Johnson, I.R. and Thornley, J.H.M. (1987): A Model of Shoot:Root Partitioning with Optimal Growth. Ann. Bot. 60, pp. 133-142.

Johnson, I.R., Melkonian, J.J., Thornley, J.H.M., and Riha, S.J. (1991): A Model of Water Flow Through Plants Incorporating Shoot/Root 'Message' Control of Stomatal Conductance. Plant, Cell, and Environ. 14, pp. 531-544.

Jolliet, O. (1994): HORTITRANS, a Model for Predicting and Optimizing Humidity and Transpiration on Greenhouses. J. Agric. Eng. Res. 57, pp. 23-37.

Joly, R.J. (1989): Effects of Sodium Chloride on the Hydraulic Conductivity of Soybean Root Systems. Plant Physiol. 91, pp. 1262-1265.

Jungk, A. and Barber, S.A. (1975): Plant Age and the Phosphorus Uptake Characteristics of Trimmed and Untrimmed Corn Root Systems. Plant and Soil 42, pp. 227-239.

Kauss, H. (1987): Some Aspects of Calcium-Dependent Regulation in Plant Metabolism. Annu. Rev. Plant Physiol. 38, pp. 47-72.

Kiss, F., Wu, M.-X., Wong, J.H., Balogh, A., and Buchanan, B.B. (1991): Redox Active Sulfhydryls are Required for Fructose 2,6-Bisphosphate Activation of Plant Pyrophosphate Fructose-6-Phosphate 1-Phosphotransferase. Arch. Biochem. Biophys. 287, pp. 337-340.

Koontz, H.V., Prince, R.P., and Berry, W.L. (1990): A Porous Stainless Steel Membrane system for Extraterrestrial Crop Production. HortScience 25, p. 707.

Kossen, N.W.F. (1992): Scale-Up in Biotechnology. In: "Recent Advances in Biotechnology." (F.Vardar-Sukan and S.S. Sukan, eds.), pp. 183-208.

Knight, S.L., Rogers, R.B., Smith, M.A.L., and Spomer, L.A. (1992): Effects of NaCl Salinity on Miniature Dwarf Tomato 'Micro-Tom': I. Growth Analyses and Nutrient Composition. J. Plant Nutr. 15, pp. 2315-2327.

Lafolie, F., Bruckler, L., and Tardieu, F. (1991): Modeling Root Water Potential and Soil-Root Water Transport: I. Model Presentation. Soil Sci. Soc. Am. J. 55, pp. 1203-1212.

Landa, F.M. and Nokes, S.E. (1994): Modeling Water Uptake in Plants. ASAE Paper No. 94-7503, Atlanta, GA., Dec. 13-16.

LeBot, J., Kirby, E.A., and Van Beusichem, M.L. (1990): Manganese Toxicity in Tomato Plants: Effects on Cation Uptake and Distribution. J. Plant Nutr. 13, pp. 513-525.

MacElroy, R.D. (1991): Draft Permeable Membrane Plant Nutrient Experiment Statement of Work. Ames Research Center, Moffett Field, CA.

Mackowiak, C.L., Owens, L.P., Hinkle, C.R., and Prince, R.P. (1989): Continuous Hydroponic Wheat Production Using a Recirculating System. NASA Technical Memorandum #102784, John F. Kennedy Space Center, FL.

Macler, B.A., Janik, D.S., and Bensen, B.L. (1990): Quality Assessment of Plant Transpiration Water. SAE Technical Paper Series, Paper No. 901230.

Magalhaes, J.R. (1991): Kinetics of $^{15}NH_4^+$ Assimilation in Tomato Plants: Evidence for $^{15}NH_4^+$ Assimilation via GDH in Tomato Roots. J. Plant Nutr. 14, pp. 1341-1353.

Maggio, A. and Joly, R.J. (1995): Effects of Mercuric Chloride on the Hydraulic Conductivity of Tomato Roo Systems. Plant Physiol. 109, pp. 331-335.

Martin, B. and Thorstenson, Y.R. (1988): Stable Carbon Isotope Composition ($\delta^{13}C$), Water Use Efficiency, and Biomass Productivity of *Lycopersicon esculentum*, *Lycopersicon pennellii*, and the F_1 Hybrid. Plant Physiol. 88, pp. 213-217.

Materechera, S.A., Dexter, A.R., Alston, A.M., and Kirby, J.M. (1992): Growth of Seedling Roots in Response to External Osmotic Stress by Polyethylene Glycol 20,000. Plant and Soil 143, pp. 85-91.

Matsui, T., Eguchi, H., and Soejima, Y. (1981): Evaluation of Artificial Light for Plants on the Basis of Transpiration Model. Environ. Control Biology 19, pp. 25-34.

McKelvey, S.A., J.A. Gehrig, K.A. Hollar, and W.R. Curtis (1993): Growth of Plant Root Cultures in Liquid- and Gas-Dispersed Reactor Environments. Biotech. Prog. 9, pp. 317-322.

Menzies, J.G., Ehret, D.L., Glass, A.D.M., Helmer, T., Koch, C., and Seyward, F. (1991): Effects of Soluble Silicon on the Parasitic Fitness of Sphaerotheca fuliginea on Cucumis sativus. Phytopathology 81, pp. 84-88.

Miyaki, Y. and Takahashi, E. (1983): Effect of Silicon on the Growth of Solution-Cultured Cucumber Plants. Soil Sci. Plant Nutr. 29, pp. 71-83.

Molz, F.J. (1981a): Models of Water Transport in the Soil-Plant System. Water Resources Research 17, pp. 1245-1260.

Molz, F.J. (1981b): Simulation of Plant Water Uptake. In: "Modeling Wastewater Renovation by Land Application.", I.K. Iskandar (ed.), John Wiley, New York.

Molz, F.J., and Remson, I. (1970): Extraction Term Models of Soil Moisture Use by Transpiring Plants. Water Resourses Research 6, pp. 1346-1356.

Morrow, R.C., Bula, R.J., Tibbitts, T.W., and Dinauer, W.R. (1992): A Matrix-Based Porous Tube Water and Nutrient Delivery System. SAE Technical Paper Series, Paper No. 921390.

Nederhoff, E.M., De Koning, A.N.M., and Rijsdijk, A.A. (1992): Leaf Deformation and Fruit Production of Greenhouse Grown Tomato (*Lycopersicon esculentum* Mill.) as Affected by CO_2, Plant Density, and Pruning. J. Hort. Sci. 67, pp. 411-420.

Nederhoff, E.M. and Vegter, J.G. (1994a): Canopy Photosynthesis of Tomato, Cucumber and Sweet Pepper in Greenhouses: Measurements Compared to Models. Ann. Bot. 73, pp. 421-427.

Nederhoff, E.M. and Vegter, J.G. (1994b): Photosynthesis of Stands of Tomato, Cucumber and Sweet Pepper Measured in Greenhouses under Various CO_2 Concentrations. Ann. Bot. 73, pp. 353-361.

Nelson, D.W. and Sommers, L.E. (1973): Determination of Total Nitrogen in Plant Material. Agron. J. 65, pp. 109-112.

Newman, E. I. (1966): A Method of Estimating the Total Length of Root in a Sample. J. Appl. Ecol. 3, pp. 139-145.

Nielsen, N.N. (1972): A Transport Kinetic Concept of Ion Uptake from Soil by Plants. Plant and Soil 37, pp. 561-576.

Nkansah, G.O. and Ito, T. (1995): Comparison of Mineral Absorption and Nutrient Composition of Heat-Tolerant and Non Heat-Tolerant Tomato Plants at Different Root-Zone Temperatures. J. Hort. Sci. 70, pp. 453-460.

Nye, P.H. and Marriott, F.H.C. (1969): A Theoretical Study of the Distribution of Substances Around Roots Resulting from Simultaneous Diffusion and Mass Flow. Plant and Soil 30, pp. 459-472.

Nye, P.H. and Tinker, P.B. (1969): The Concept of a Root Demand Coefficient. J. Applied Ecology 6, pp. 293-300.

Oates, K. and Barber, S.A. (1987): Nutrient Uptake: A Microcomputer Program to Predict Nutrient Absorption from Soil by Roots. J. Agron. Educ. 16, pp. 65-68.

O'Neill, J.V. and Webb, R.A. (1970): Simultaneous Determination of Nitrogen, Phosphorus, and Potassium in Plant Material by Automatic Methods. J. Sci. Food Agric. 21, pp. 217-219.

Orbisphere Corporation (1988): Experimental Growth of Plants on Membranes. Orbiterre - A Division of Orbisphere Corporation, Switzerland.

Osmonics, Inc. Product Bulletin (1988): Controlled Porosity Ceramics. Minnetonka, MN.

Overman, A.R. (1995): Rational Basis for the Logistic Model for Forage Grasses. J. Plant Nutr. 18, pp. 995-1012.

Overman, A.R., Wilson, D.M., and Vidak, W. (1995): Extended Probability Model for Dry Matter and Nutrient Accumulation by Crops. J. Plant Nutr. 18, pp. 2609-2627.

Owens, H.R. and Miller, A.R. (1992): An Examination and Correction of Plant Tissue Culture Basal Medium Formulations. Plant Cell, Tissue, and Organ Culture 28, pp. 147-150.

Oyer, L.J. and Touchton, J.T. (1990): Utilizing Legume Cropping Systems to Reduce Nitrogen Fertilizer Requirements for Conservation-Tilled Corn. Agron. J. 82, pp. 1123-1127.

Parker, D.R., Aguilera, J.J., and Thomason, D.N. (1992): Zinc-Phosphorus Interactions in Two Cultivars of Tomato (*Lycopersicon esculentum* L.) Grown in Chelator-Buffered Nutrient Solutions. Plant and Soil 143, pp. 163-177.

Passioura, J.B. (1984): Hydraulic Resistance of Plants. I. Constant or Variable? Aust. J. Plant Physiol. 11, pp. 333-339.

Pena, J.G. (1985): Economic Considerations, Marketing and Financing of Greenhouse Vegetable Production. In: "Hydroponics Worldwide: State of the Art in Soilless Crop Production.", A.J. Savage (ed.), International Center for Special Studies, Inc., Honolulu, HA.

Penning De Vries, F.W.T., Witlage, J.M., and Kremer, D. (1979): Rates of Respiration and of Increase in Structural Dry Matter in Young Wheat, Ryegrass and Maize Plants in Relation to Temperature, to Water Stress and to Their Sugar Content. Ann. Bot 44, pp. 595-609.

Perez-Alfocea, F., Estan, M.T., Caro, M., and Guerrier, G. (1993): Osmotic Adjustment in *Lycopersicon esculentum* and *L. pennellii* under NaCl and Polyethylene Glycol 6000 Iso-Osmotic Stresses. Physiol. Plant. 87, pp. 493-498.

Peterson, R. and Jensen, P. (1988): Uptake and Transport of N, P and K in Tomato Supplied with Nettle Water and Nutrient Solution. Plant and Soil 107, pp. 189-196.

Pickens, A.J.F., Stewart, K., and Klapwijk, D. (1986): Germination and Vegetative Development. In: "The Tomato Crop.", J.G. Atherton and J. Rudich (eds.), Chapman and Hall, London.

Prager, D.J. and Bowman, R.L. (1963): Freezing-Point Depression: New Method of Measuring Ultramicro Quantities of Fluids. Science 142, pp. 237-239.

Pritchard, M.W. and Lee, J. (1984): Simultaneous Determination of Boron, Phosphorus, and Sulfur in Some Biological and Soil Materials by Inductively-Coupled Plasma Emission Spectrometry. Analytica Chimica Acta 157, pp. 313-326.

Qasem, J.R. and Hill, T.A. (1993): Effects of the Form of Nitrogen on the Growth and Nutrient Uptake of Tomato, Groundsel, and Fat-Hen. J. Hort. Sci. 68, pp. 161-170.

Resh, H.M. (1978): Hydroponic Food Production. Woodbridge Press Publishing Company, Santa Barbara, CA.

Reuss, J.O., Walthall, P.M., Roswall, E.C., and Hopper, R.W.E. (1990): Aluminum Solubility, Calcium-Aluminum Exchange, and pH in Acid Forest Soils. Soil Sci. Soc. Am. J. 54, pp. 374-380.

Romero-Aranda, R. and Longuenesse, J.J. (1995): Modelling the Effect of Air Vapour Pressure Deficit on Leaf Photosynthesis of Greenhouse Tomatoes: The Importance of Leaf Conductance to CO_2. J. Hort. Sci. 70, pp. 423-432.

Rouhi, A.M. (1997): Plants to the Rescue. C&EN 75, pp. 21-23.

Rudich, J. and Luchinsky, U. (1986): Water Economy. In: "The Tomato Crop.", J.G. Atherton and J. Rudich (eds.), Chapman and Hall, London.

Sage, R.F. (1990): A Model Describing the Regulation of Ribulose-1,5-Bisphosphate Carboxylase, Electron Transport, and Triose Phosphate Use in Response to Light Intensity and CO_2 in C3 Plants. Plant Physiol. 94, pp. 1728-1734.

Sage, R.F., Sharkey, T.D., and Seemann, J.R. (1989): Acclimation of Photosynthesis to Elevated CO_2 in Five C3 Species. Plant Physiol. 89, pp. 590-596.

Salisbury, F.B. and Ross, C.W. (1985): Plant Physiology. 3rd edition. Wadsworth Publishing Company, Belmont, CA.

Sammis, T.W. and Jernigan, D. (1992): Crop Water Stress Index of Ornamental Plants. Applied Eng. Agric. 8, pp. 191-195.

Schenk, M.K. and Barber, S.A. (1979): Root Characteristics of Corn Genotypes as Related to Phosphorus Uptake. Agron. J. 71, pp. 921-924.

Schwarz, M. (1995): Soilless Culture Management. In: "Advanced Series in Agricultural Sciences." Vol. 24. Springer-Verlag, Berlin.

Selim, H.M. and Iskandar, I.K. (1978): Nitrogen Behavior in Land Treatment of Wastewater: A Simplified Model. In: "State of Knowledge in Land Treatment of Wastewater.", Cold Regions Research and Engineering Laboratory (ed.), Hanover, NH.

Silberbush, M. and Barber, S.A. (1983): Prediction of Phosphorus and Potassium Uptake by Soybeans with a Mechanistic Mathematical Model. Soil Sci. Soc. Am. J. 47, pp. 262-265.

Silberbush, M. and Gbur, Jr., E.E. (1994): Using Williams Equation to Evaluate Nutrient Uptake Rate by Intact Plants. Agron. J. 86, pp. 107-110.

Smith, J.P. Jr. (1977): Vascular Plant Families. Mad River Press, Inc., Eureka, CA.

Smith, M.A.L., Spomer, L.A., Shibli, R.A., and Knight, S.L. (1992): Effects of NaCl Salinity on Miniature Dwarf Tomato 'Micro-Tom': II. Shoot and Root Growth Responses, Fruit Production, and Osmotic Adjustment. J. Plant Nutr. 15, pp. 2329-2341.

Stanghellini, C. (1987): Transpiration of Greenhouse Crops, an Aid to Climate Management. Ph.D. Dissertation, Agricultural University, Wageningen, The Netherlands.

Stroup, T. and Schwartzkopf, S. (1992): Crop Interaction in Polyculture and Their Implications for CELSS Design. SAE Technical Paper Series, Paper No. 921197.

Stryer, L. (1988): Biochemistry. 3rd edition. W.H. Freeman and Company, New York, NY.

Taiz, L. and Zeiger, E. (1991): Plant Physiology. The Benjamin/Cummings Publishing Company, Inc., Redwood City, CA.

Tan, C.S. and Buttery, B.R. (1995): Determination of the Water Use of Two Pairs of Soybean Isolines Differing in Stomatal Frequency Using a Heat Balance Stem Flow Gauge. Can. J. Plant Sci. 75, pp. 99-103.

Tanguilig, V.C., Yambao, E.B., O'Toole, J.C., and De Datta, S.K. (1987): Water Stress Effects on Leaf Elongation, Leaf Water Potential, Transpiration, and Nutrient Uptake of Rice, Maize, and Soybean. Plant and Soil 103, pp. 155-168.

Taylor, I.B. (1986): Biosystematics of the Tomato. In: "The Tomato Crop.", J.G. Atherton and J. Rudich (eds.), Chapman and Hall, London.

Tindall, J.A., Mills, N.A., and Radcliffe, D.E. (1990): The Effect of Root Zone Temperature on Nutrient Uptake of Tomato. J. Plant Nutr. 13, pp. 939-956.

Thornley, J.H.M. (1990): A New Formulation of the Logistic Growth Equation and Its Application to Leaf Area Growth. Ann. Bot. 66, pp. 309-311.

Thornley, J.H.M. (1991): A Model of Leaf Tissue Growth, Acclimation and Senescense. Ann. Bot. 67, pp. 219-228.

Thornley, J.H.M., Hurd, R.G., and Pooley, A. (1981): A Model of Growth of the Fifth Leaf of Tomato. Ann. Bot. 48, pp. 327-340.

Traina, S.J., Sposito, G., Hesterberg, D., and Kafkafi, U. (1986): Effects of pH and Organic Acids on Orthophosphate Solubility in an Acidic, Montmorillonitic Soil. Soil Sci. Soc. Am. J. 50, pp. 45-52.

Trejo, C.L., Clephan, A.L., and Davies, W.J. (1995): How Do Stomata Read Abscisic Acid Signals? Plant Physiol. 109, pp. 803-811.

Tremblay, N., Gasia, M.-C., Ferauge, M.-T., Gosselin, A., and Trudel, M.J. (1988): Effects of Light Spectral Quality on Nutrient Uptake by Tomato. Can. J. Plant Sci. 68, pp. 287-289.

Tsao, D.T. (1993a): Verification of the Mathematical Model for the PCTPNS. Part I: Static Conditions. Progress Report: NASA Contract NAS10-11624, John F. Kennedy Space Center, FL.

Tsao, D.T. (1993b): Verification of the Mathematical Model for the PCTPNS. Part II: Steady State Flow Conditions. Progress Report: NASA Contract NAS10-11624, John F. Kennedy Space Center, FL.

Tsao, D.T. (1994): Verification of the Mathematical Model for the PCTPNS. Part III: Dynamic Flow Conditions. Progress Report: NASA Contract NAS10-11624, John F. Kennedy Space Center, FL.

Tsao, D.T., Okos, M.R., Mitchell, C.A., Sager, J.C., and Dreschel, T.W. (1994): Modeling the Transpirational Uptake of Water into Plants Cultivated on a Ceramic Tube Hydroponic System. ASAE Paper No. 94-4580, Atlanta, GA.

Tsao, D.T., Okos, M.R., and Sager, J.C. (1996): Controlling the Water Availability from a Ceramic Tube System Subjected to Non-Standard Gravities. SAE Technical Paper Series, Paper No. 961505.

Tsao, D.T., Okos, M.R., Sager, J.C., and Dreschel, T.W. (1992): Development of Physical and Mathematical Models for the Porous Ceramic Tube Plant Nutrification System (PCTPNS). NASA Technical Memorandum #107551, John F. Kennedy Space Center, FL.

Van de Vooren, J., Welles, G.W.H., and Hayman, G. (1986): Glasshouse Crop Production. In: "The Tomato Crop.", J.G. Atherton and J. Rudich (eds.), Chapman and Hall, London.

Van Den Honert, T.H. and Hooymans, J.J.M. (1955): On the Absorption of Nitrate by Maize in Water Culture. Acta Botanica Neerlandica 4, pp. 376-384.

Van Ieperen, W. and Madery, H. (1994): A New Method to Measure Plant Water Uptake and Transpiration Simultaneously. J. Exp. Bot. 45, pp. 51-60.

Vetterlein, D., Marschner, H., and Horn, R. (1993): Microtensiometer Technique for in situ Measurement of Soil Matric Potential and Root Water Extraction from a Sandy Soil. Plant and Soil 149, pp. 263-273.

Warncke, D.D. and Barber, S.A. (1972): Diffusion of Zinc in Soil. I. The Influence of Soil Moisture. Soil Sci. Soc. Am. J. 36, pp. 39-42.

Warncke, D.D. and Barber, S.A. (1974): Root Development and Nutrient Uptake by Corn Grown in Solution Culture. Agron. J. 66, pp., 514-516.

Wheeler, R.M., Mackowiak, C.L., Dreschel, T.W., Sager, J.C., Prince, R.P., Knott, W.M., Hinkle, C.R., and Strayer, R.F. (1990): System Development and Early Biological Tests in NASA's Biomass Production Chamber. NASA Technical Memorandum #103494. John F. Kennedy Space Center, FL.

Wheeler, E.F., Albright, L.D., Walker, L.P., Spanswick, R.M., and Langhans, R.W. (1994): Plant Growth and Nitrogen Uptake Part I: Beyond the Michaelis-Menten Relationship. ASAE Paper No. 94-7506, Atlanta, GA., Dec. 13-16.

Wilkinson, R.E. and Duncan, R.R. (1993): Magnesium Influence on Calcium ($^{45}Ca^{2+}$) Absorption by Sorghum Root Tips. J. Plant Nutr. 16, pp. 1917-1920.

Willits, D.H., Nelson, P.V., Peet, M.M., Depa, M.A., and Kuehny, J.S. (1992): Modeling Nutrient Uptake in Chrysanthemum as a Function of Growth Rate. J. Am. Soc. Hort. Sci. 117, pp. 769-774.

Wraith, J.M. and Baker, J.M. (1991): High-Resolution Measurement of Root Water Uptake Using Automated Time-Domain Reflectometry. Soil Sci. Soc. Am. J. 55, pp. 928-932.

Wright, B.D. and Bausch, W.C. (1984): A Plant Growth System for Orbital Plant Experiments. ASAE Paper No. 84-2524, New Orleans, LA., Dec. 11-14.

Wrona, A.F. and Epstein, E. (1985): Potassium Transport in Two Tomato Species. Plant Physiol. 79, pp. 1068-1071.

Xu, H., Gauthier, L., and Gosselin, A. (1995): Stomatal and Cuticular Transpiration of Greenhouse Tomato Plants in Response to High Solution Electrical Conductivity and Low Soil Water Content. J. Am. Soc. Hort. Sci. 120, pp. 417-422.

Yamauchi, T., Hara, T., and Sonoda, Y. (1986): Effects of Boron Deficiency and Calcium Supply on the Calcium Metabolism in Tomato Plants. Plant and Soil 93, pp. 223-230.

Yaniv, Z. and Werker, E. (1983): Absorption and Secretion of Polyethylene Glycol by Solanaceous Plants. J. Exp. Bot. 34, pp. 1577-1584.

York, E.T., Bradfield, R., and Peech, M. (1954): Influence of Lime and Potassium on Yield and Cation Composition of Plants. Soil Science 77, pp. 53-63.

APPENDICES

APPENDIX A - TEMPERATURE AND RELATIVE HUMIDITIES

The temperature and relative humidities were only measured after the initial four experiments. Therefore, the results from these four preliminary experiments are not presented in this Appendix. Furthermore, Experiments #6 and #7 were prematurely ended due to a mold contaminating the growth chamber.

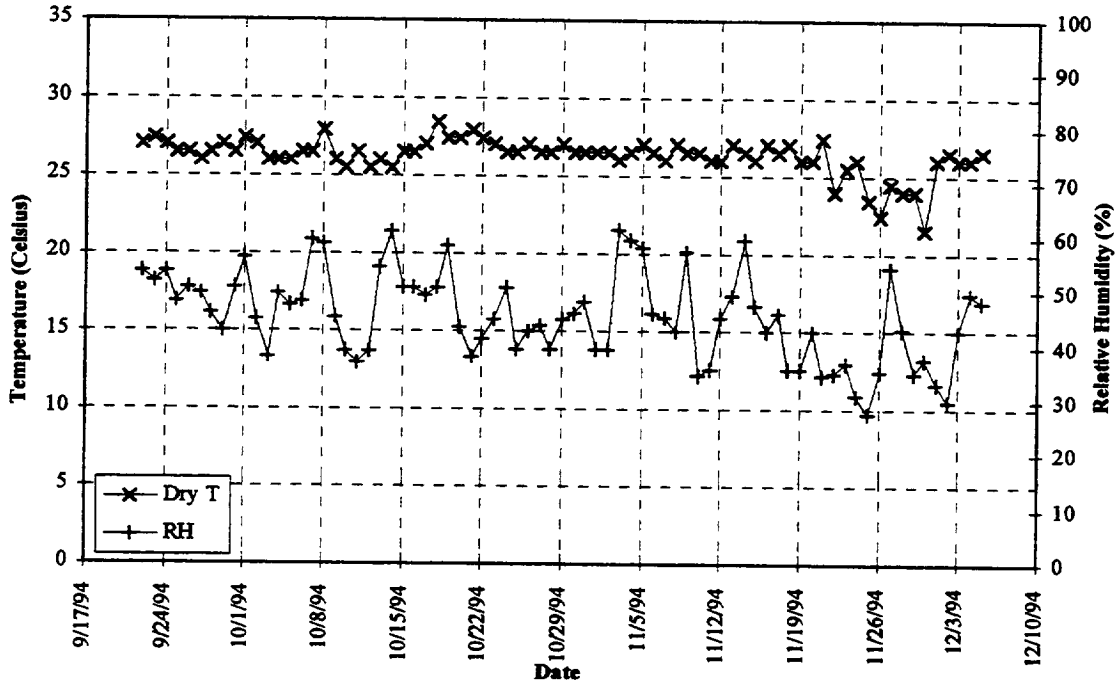

Figure A.1 Temperature and Relative Humidity Time Courses for Experiment #5 (Dates: 9/22/94 to 12/5/94)

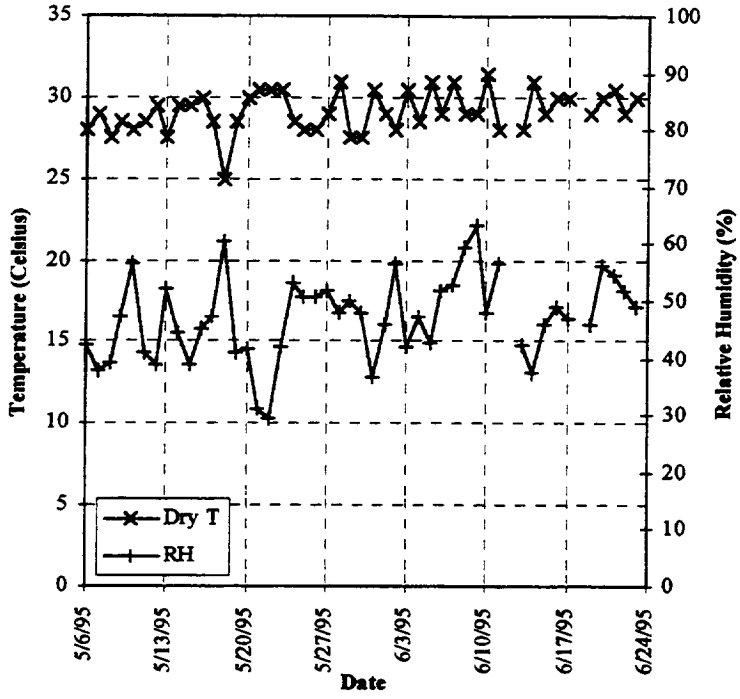

Figure A.2 Temperature and Relative Humidity Time Courses for Experiment #8 (Dates: 5/6/95 to 6/23/95)

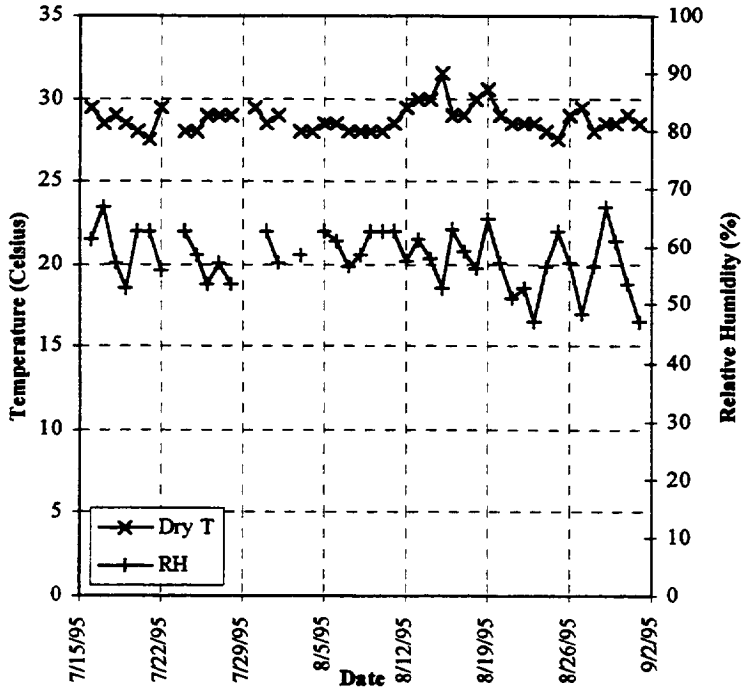

Figure A.3 Temperature and Relative Humidity Time Courses for Experiment #9 (Dates: 7/16/95 to 9/1/95)

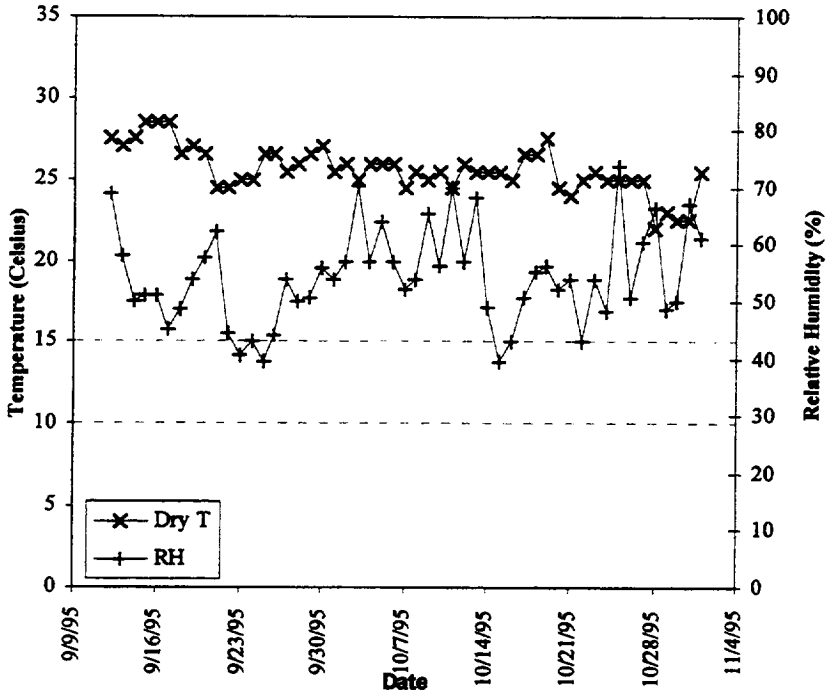

Figure A.4 Temperature and Relative Humidity Time Courses for Experiment #10 (Dates: 9/12/95 to 11/1/95)

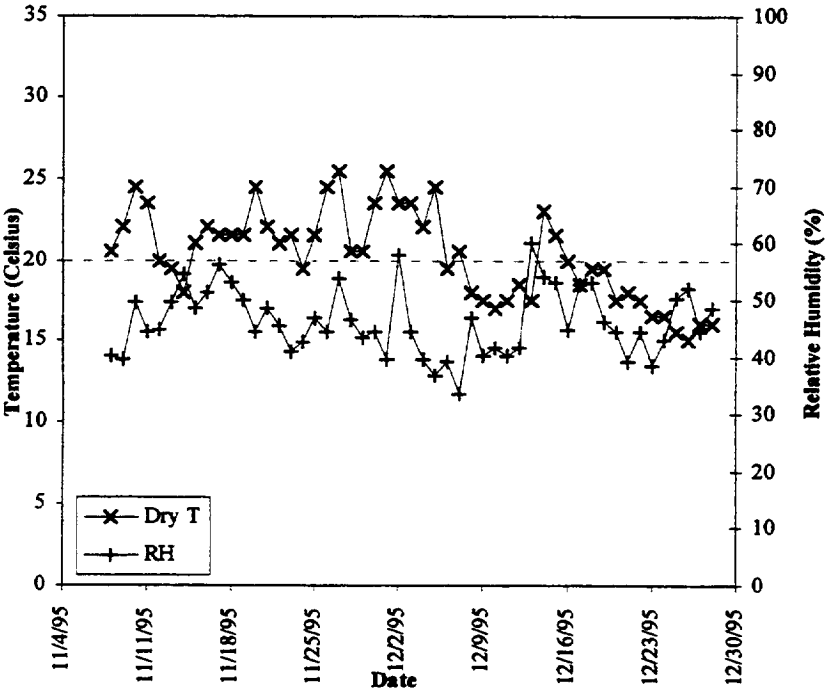

Figure A.5 Temperature and Relative Humidity Time Courses for Experiment #11 (Dates: 11/8/95 to 12/28/95)

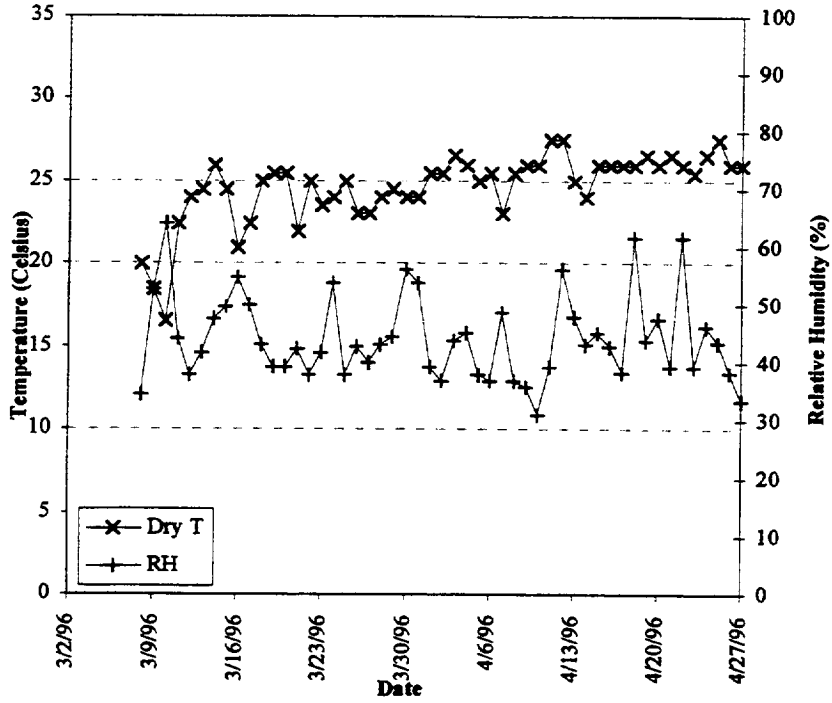

Figure A.6 Temperature and Relative Humidity Time Courses for Experiment #12 (Dates: 3/8/96 to 4/27/96)

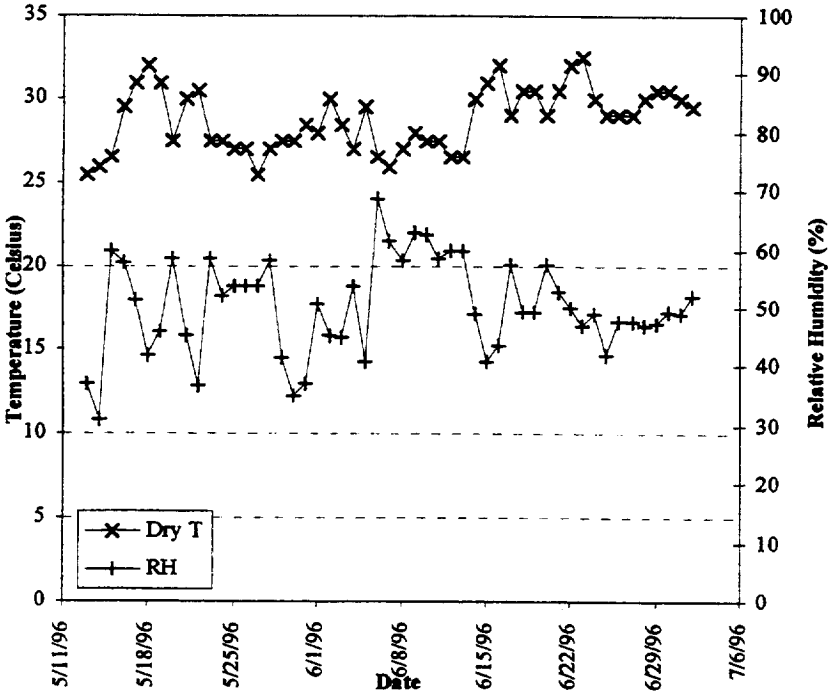

Figure A.7 Temperature and Relative Humidity Time Courses for Experiment #13 (Dates: 5/13/96 to 7/2/96)

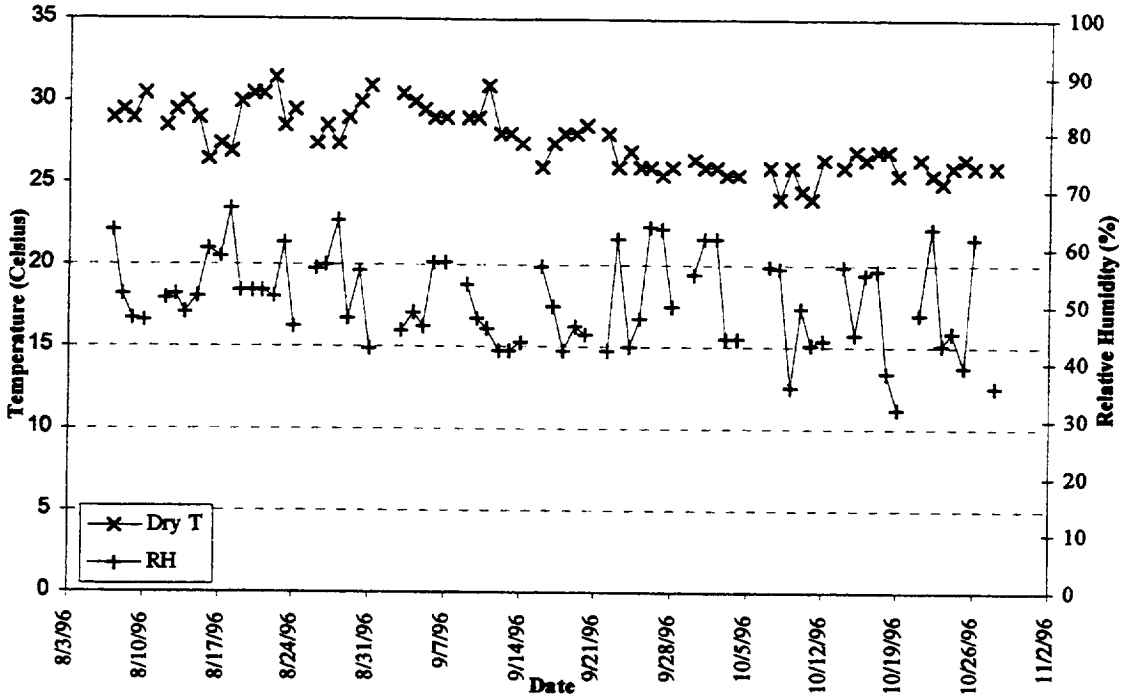

Figure A.8 Temperature and Relative Humidity Time Courses for Experiment #14 (Dates: 8/7/96 to 10/28/96)

Table A.1 Summary of Temperature and Relative Humidities during the Experiments

Expt.	Months	$T_{a,ave}$ (°C)	σ_{Ta} (°C)	RH_{ave} (%)	σ_{RH} (%)
5	Sept.-Dec.	26.28	± 1.13	45.57	± 8.11
8	May-June	29.15	± 1.28	46.99	± 7.37
9	July-Aug.	28.77	± 0.81	58.33	± 4.95
10	Sept.-Oct.	25.62	± 1.41	54.38	± 8.49
11	Nov.-Dec.	20.30	± 2.78	46.13	± 5.91
12	Mar.-Apr.	24.65	± 2.16	44.20	± 7.49
13	May-June	28.77	± 1.87	50.25	± 8.18
14	Aug.-Oct.	27.63	± 1.85	50.82	± 7.91
Ave		26.40	± 1.66	49.58	± 7.30

APPENDIX B - STATISTICAL ANALYSES - GROWTH RESULTS

The statistical analyses of the growth related functions are presented in this appendix. This includes the data for the factors, X, and the responses, Y, used to produce the various models. In addition, the analysis of variances (ANOVA) tables produced for the various steps in the development of the growth models are provided as well. These tables were generated on a Microsoft Excel v.5.0 Spreadsheet.

Initially, the statistical analyses conducted for modeling the number of days after emergence are presented. The data matricies are presented in seven groups, one for each of the different test conditions examined in this research. These correspond to the experimental levels presented in Table 7.2 as (-0.019/-0.000), (-0.019/-0.039), (-0.019/-0.059), (-0.039/-0.039), (-0.078/-0.000), (-0.078/-0.039), and (-0.078/-0.059). These are coded where the initial number represents the concentration level or osmotic potential while the second number describes the applied suction pressure or matric potential. Furthermore, the matric potentials listed as -0.000 represent near weeping conditions where the matric potentail is slightly negative but equal to zero at the number of significant digits.

Table B.1 Data for the Days After Emergence (Y) versus Leaf Stage (X1) for the Experimental Conditions where π_{soil} = -0.019 MPa (X2) and P_m = -0.000 MPa (X3)

LS	Number of Days after Emergence							
1	1	2	1	1	2	2	1	2
3	6	16	8	12	8	6	19	16
5	12	26	18	25	16	15	31	26
7	18	41	28	39	24	23		38
9	24		35		31	31		
11	29		43		37	39		
13	35				45			
15	44							

Table B.2 Data for the Days After Emergence (Y) versus Leaf Stage (X1) for the Experimental Conditions where π_{soil} = -0.019 MPa (X2) and P_m = -0.039 MPa (X3)

LS	Number of Days after Emergence								
1	4	2	4	2	1	2	1		
3	18	11	14	10	9	7	4		
5	32	22	24	21	18	13	9		
7		35	34	32	27	19	17		
9					35	27	21		
11						32			
13						36			
15									

Table B.3 Data for the Days After Emergence (Y) versus Leaf Stage (X1) for the Experimental Conditions where π_{soil} = -0.019 MPa (X2) and P_m = -0.059 MPa (X3)

LS	Number of Days after Emergence								
1	1	1							
3	7	9							
5	11	20							
7	16	32							
9	23								
11	29								
13	35								
15									

Table B.4 Data for the Days After Emergence (Y) versus Leaf Stage (X1) for the Experimental Conditions where π_{soil} = -0.039 MPa (X2) and P_m = -0.039 MPa (X3)

LS	Number of Days after Emergence								
1	2	3	2	3					
3	9	17	10	13					
5	16	28	19	25					
7	25		27	36					
9	32		36						
11	37								
13									
15									

Table B.5 Data for the Days After Emergence (Y) versus Leaf Stage (X1) for the Experimental Conditions where π_{soil} = -0.078 MPa (X2) and P_m = -0.000 MPa (X3)

LS	Number of Days after Emergence													
1	2	3	2	3	2	2	1	1	1	1	4	2	6	6
3	8	11	11	11	8	5	8	7	5	16	17	8	13	
5	15	19	21	18	15	10	15	11	19		29	13	22	
7	21	27	29	28	22	14	22	17				21	30	
9	28	34	38	35	28	20	30	22				29	38	
11	31	40		41	34	24	36	29				33	45	
13	36				40	29	41	38				42	50	
15	44					33								

LS	Number of Days after Emergence													
1	3	1	4	7	2	3	3	5	3	3	2	3	4	2
3	11	10	12	19	17	9	17	14	15	10	11	19	13	8
5	24	24	20		28	17	27		28	20			20	17
7		33	30		37	27			38	29			27	26
9			38		49	35				36				32
11			44											
13														
15														

LS	Number of Days after Emergence													
1	1	4	1	2	1	3	4	2	3	1	4	5		
3	9	13	10	10	6	10	18	10	13	13	11			
5	20		17	18	12	19	29	18	22		23			
7			26	27	18	31		27	32		34			
9			34	36	25			38						
11					33									
13														
15														

Table B.6 Data for the Days After Emergence (Y) versus Leaf Stage (X1) for the Experimental Conditions where π_{soil} = -0.078 MPa (X2) and P_m = -0.039 MPa (X3)

LS	Number of Days after Emergence													
1	1	2	2	6	2	1	1	4	1	2	3	2	3	1
3	8	8	8	18	8	9	10	13	9	13	10	8	8	13
5	17	13	12		16	22	21	22	15	23	20	21	15	
7	26	22	20			31	33	40	23	32	30	29	22	
9	32	28	26			39	42		30		38			
11	38	34							37					
13														
15														

LS	Number of Days after Emergence													
1	2	1	1	1	1	4	1	2	1	1	3	2	2	1
3	14		11	8	8	11	10	10	7	9	12	11	15	14
5			21	18	17	20	25	21	15	18	21	21	26	22
7			36		25	39			23	30	32	31	34	34
9									30		42	42	41	43
11									39		49		49	51
13											57		54	60
15											64			

Table B.7 Data for the Days After Emergence (Y) versus Leaf Stage (X1) for the Experimental Conditions where π_{soil} = -0.078 MPa (X2) and P_m = -0.059 MPa (X3)

LS	Number of Days after Emergence	
1	1	1
3	8	8
5	15	15
7	21	21
9	26	27
11		
13		
15		

The initial equation tested as a possible adequate model for the days after emergence (Y) was a linear equation containing terms for each of the possible significant factors. The ANOVA table for this model is presented in Table B.8 which shows that the model terms for the osmotic and matric potentials, b_2X2 and b_3X3, respectively, were not significant. This left only the leaf stage (X1) as a significant factor. With the removal of osmotic and matric potential terms from the model, the intercept term, b_0, should be removed as well. This is due to the definition of zeroth leaf stage being equivalent to the time that the plant emerges, or when $t_{DAE} = 0$. Therefore, an analysis of variance for the simple model of a proportional relationship between LS and t_{DAE} was conducted. This resulted in Equation (8.1) as the final adequate model with Table 8.1 as the corresponding ANOVA table.

Table B.8 Analysis of Variance Table for the Complete Linear Model for the Number of Days after Emergence (Y) as a Function of Leaf Stage (X1), Osmotic Potential (X2), and Matric Potential (X3)

	DOF	Sum Sqs.	Mean Sqs.	Fcalc		Fcrit	Signif?
Total	408	217377				$\alpha_{risk} = 0.05$	
Model	4	205360	51340	1726	>	2.397	yes
b0	1	143100	143100	4811	>	3.867	yes
b1	1	62206	62206	2091	>	3.867	yes
b2	1	49.003	49.003	1.647	<	3.867	no
b3	1	4.558	4.558	0.153	<	3.867	no
Resid	404	12017	29.745				
Error	359	10629	29.608				
LOT	45	1388	30.843	1.037	<	1.405	no

In addition to the number of days after emergence, the plant heights (Y) were modeled using the leaf stage of development (X1). The data used to produce the final linearized model presented as Equation (8.2) are presented below in Tables B.9 to B.15 for the different test conditions involving various combinations of the three osmotic (X2)

and three matric (X3) potentials. The combinations tested in this research correspond to the experimental levels presented in Table 7.2. Since the complete linear model proved to be adequate in describing this relationship without any significant left-out terms, no further modeling was conducted.

Table B.9 Data for the Plant Heights (Y) versus Leaf Stage (X1) for the Experimental Conditions where π_{soil} = -0.019 MPa (X2) and P_m = -0.000 MPa (X3)

LS	Plant Heights							
0	2.8	3.0	2.1	4.1	1.6	3.4	1.7	3.3
1	3.4	4.3	2.5	4.3	2.4	4.5	2.5	3.4
3	5.4	7.8	3.9	5.8	3.6	7.4	3.3	5.2
5	10.3	10.2	9.5	9.3	7.7	10.9	9.4	6.9
7	16.8	17.0	18.2	16.3	15.3	16.1	18.5	
9	23.0		24.7		27.2		23.9	
11	30.2		36.4		34.5		36.1	
13	41.8				48.5			
15	57.2							

Table B.10 Data for the Plant Heights (Y) versus Leaf Stage (X1) for the Experimental Conditions where π_{soil} = -0.019 MPa (X2) and P_m = -0.039 MPa (X3)

LS	Plant Heights							
0	1.4	2.7	0.9	2.5	2.5	1.8	2.4	
1	1.9	2.7	2.8	3.1	2.8	2.2	2.6	
3	2.4	3.7	4.7	5.0	5.7	2.4	3.0	
5	3.9	6.8	8.7	10.2	12.0	2.6	4.5	
7		12.3	12.9	16.0	20.6	4.3	7.3	
9					29.5	8.3	10.3	
11						11.7		
13						15.6		
15								

Table B.11 Data for the Plant Heights (Y) versus Leaf Stage (X1) for the Experimental Conditions where π_{soil} = -0.019 MPa (X2) and P_m = -0.059 MPa (X3)

LS	Plant Heights	
0	3.0	4.0
1	3.0	4.0
3	4.1	5.6
5	4.7	10.1
7	6.7	15.4
9	13.0	
11	17.9	
13	27.7	
15		

Table B.12 Data for the Plant Heights (Y) versus Leaf Stage (X1) for the Experimental Conditions where π_{soil} = -0.039 MPa (X2) and P_m = -0.039 MPa (X3)

LS	Plant Heights			
0	1.9	1.4	1.6	1.6
1	2.1	2.4	2.0	2.1
3	3.0	3.8	2.4	4.0
5	3.5	5.8	3.2	7.2
7	4.9		4.7	11.2
9	8.3		8.8	
11	10.5			
13				
15				

Table B.13 Data for the Plant Heights (Y) versus Leaf Stage (X1) for the Experimental Conditions where π_{soil} = -0.078 MPa (X2) and P_m = -0.000 MPa (X3)

LS	Plant Heights													
0	2.0	2.1	3.0	2.0	2.1	1.7	3.6	2.1	3.7	3.4	3.2	1.7	1.5	0.7
1	3.1	3.4	3.2	2.9	3.0	2.4	4.0	2.8	3.8	3.4	3.9	2.4	3.2	2.3
3	7.2	5.2	4.4	5.1	4.6	2.9	6.3	4.6	4.8	4.3	5.3	3.1	5.3	
5	15.0	9.8	8.0	8.9	8.0	4.3	10.3	6.2	10.5		6.6	5.1	9.8	
7	20.5	16.8	12.9	17.5	13.4	6.9	16.8	11.8				10.0	15.0	
9	30.0	26.5	24.0	28.8	20.1	11.8	29.2	17.7				21.3	21.4	
11	36.3	37.3		34.0	29.2	16.5	40.0	25.9				26.7	30.4	
13	44.5				38.9	22.4	50.7	31.5				41.2	39.3	
15	57.9					29.5								

LS	Plant Heights													
0	1.0	1.6	1.3	1.1	2.2	2.0	2.2	1.3	1.6	2.2	1.9	0.8	1.3	1.6
1	1.9	1.7	2.2	2.2	2.4	2.9	2.7	2.1	2.0	3.0	2.0	1.0	1.7	1.6
3	2.9	2.3	5.1	3.5	3.8	4.4	6.2	2.6	3.3	3.4	2.8	2.6	2.4	1.8
5	4.0	4.0	8.2		9.4	8.4	8.7		7.0	3.7			3.3	3.0
7		9.2	15.1		15.0	16.5			10.5	5.6			4.7	4.3
9			21.8		23.8	23.5				8.1				6.4
11			28.8											
13														
15														

LS	Plant Heights													
0	1.8	1.4	2.4	2.6	2.0	2.2	0.2	3.9	2.3	3.0	2.2	1.1		
1	2.0	2.4	3.1	3.0	2.4	2.8	1.9	4.5	3.1	4.1	3.8	3.6		
3	2.9	2.9	5.7	4.6	3.1	3.2	3.3	6.8	6.0	8.3	5.2			
5	5.0		9.7	8.0	4.1	5.1	5.2	11.3	10.8		10.8			
7			15.3	14.2	5.7	9.0		18.5	16.9		19.3			
9			23.1	21.2	8.6			25.4						
11					13.4									
13														
15														

Table B.14 Data for the Plant Heights (Y) versus Leaf Stage (X1) for the Experimental Conditions where π_{soil} = -0.078 MPa (X2) and P_m = -0.039 MPa (X3)

LS	Plant Heights													
0	2.1	3.2	1.4	0.9	2.3	2.9	1.8	0.8	2.5	2.0	1.1	1.5	2.0	1.9
1	2.2	3.4	1.6	1.0	2.3	2.9	3.0	1.9	2.7	2.2	3.0	1.7	2.2	2.0
3	3.1	3.9	2.0	2.2	2.8	3.2	4.5	3.1	3.3	2.8	4.5	2.3	2.7	2.7
5	7.1	5.6	2.1		3.4	3.8	7.0	7.6	4.0	5.3	7.2	4.1	4.0	
7	14.4	9.5	3.9			5.8	11.7	15.2	5.6	8.2	12.0	6.1	6.3	
9	21.1	14.5	5.7			7.6	15.0		8.2		15.4			
11	28.4	19.2							11.6					
13														
15														
LS	Plant Heights													
0	2.0	1.7	3.7	3.9	2.9	0.9	1.8	1.9	2.3	3.3	1.0	1.8	2.2	2.5
1	2.2	1.9	4.1	4.1	3.5	1.2	1.8	2.1	2.4	3.5	1.8	2.5	2.9	2.6
3	3.1		5.1	5.7	5.1	2.2	2.0	2.8	3.9	4.5	2.7	4.2	4.9	3.8
5			8.0	9.8	9.6	4.1	3.5	3.3	7.8	7.9	6.0	6.5	10.6	6.3
7			11.6		15.3	5.8			13.3	12.5	11.0	12.8	15.5	11.2
9									17.9		18.5	18.9	23.3	17.7
11									24.4		29.0		36.8	25.9
13											37.7		46.4	35.9
15											44.0			

Table B.15 Data for the Plant Heights (Y) versus Leaf Stage (X1) for the Experimental Conditions where π_{soil} = -0.078 MPa (X2) and P_m = -0.059 MPa (X3)

LS	Plant Heights	
0	2.5	2.1
1	2.5	2.4
3	4.7	4.7
5	8.8	8.7
7	15.2	14.7
9	21.5	20.6
11		
13		
15		

During the formulation of the models relating the tissue dry weights (Y) to the height of the plants (X1), a comparison of various forms of equations was conducted. This was accomplished by plotting the dry weights versus the corresponding heights obtained from tissues produced under identical concentrations (X2). The plots of these data are provided in Figures B.1 to B.6 for the different tissues. It should be noted that Figure B.1 is identical to Figure 8.3 presented earlier in Chapter 8 as an example of these comparisons. In these cases, the concentrations examined were the 1x and 1/4x solutions. The intermediate level was not included in this analysis since these tissues were combined whereas the other levels consisted of individual plants. The various models in this analysis including polynomials, exponential, linear and power equations were compared using the R^2 correlation coefficient. These coefficients and corresponding equations are presented on each figure. The specific data used in this analysis are provided in Tables B.16 to B.17 for the various tissues produced using either a 1x or 1/4x solution, respectively. In each case, except for the roots at 1/4x solution, the best fit equations were the power functions. Therefore, for consistency, the power functions were used throughout.

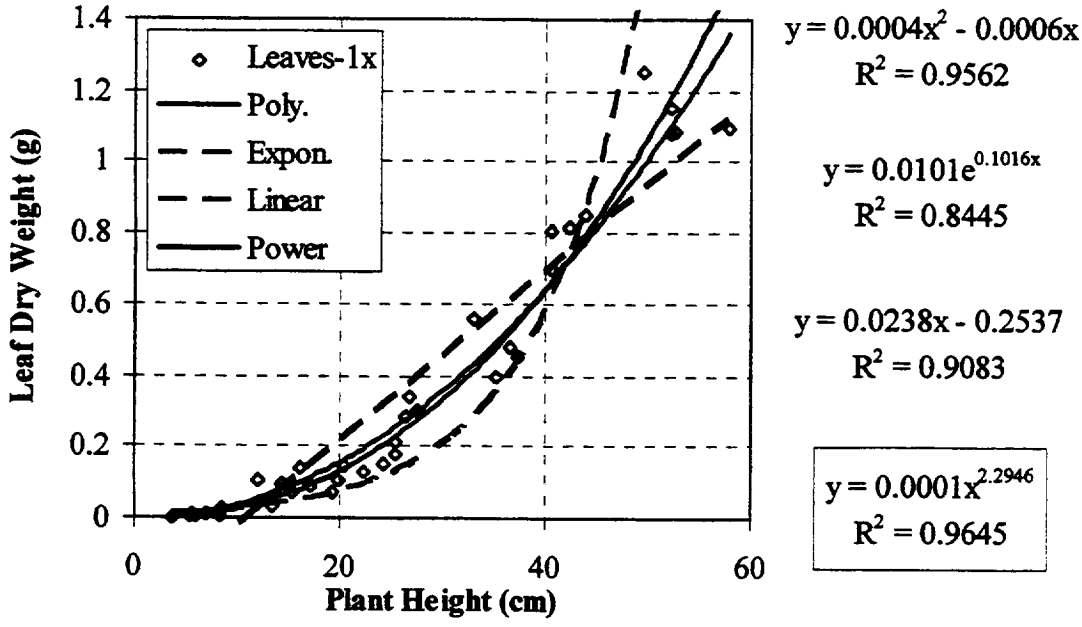

Figure B.1 Comparison of Various Relationships between Leaf Dry Weight and Height for Tomato Plants Produced using a 1x Solution

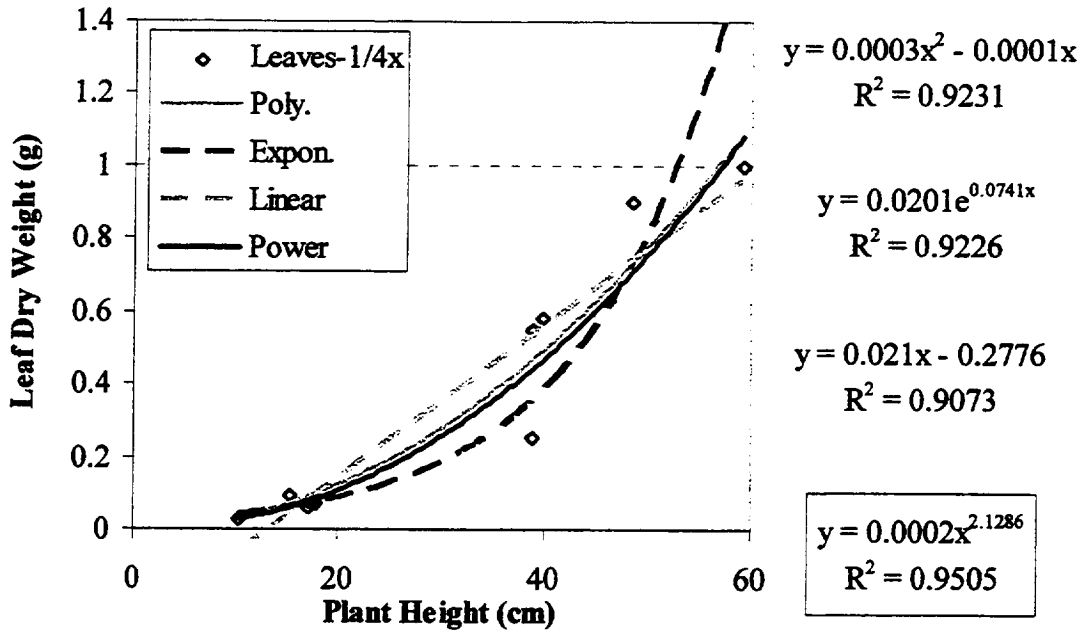

Figure B.2 Comparison of Various Relationships between Leaf Dry Weight and Height for Tomato Plants Produced using a 1/4x Solution

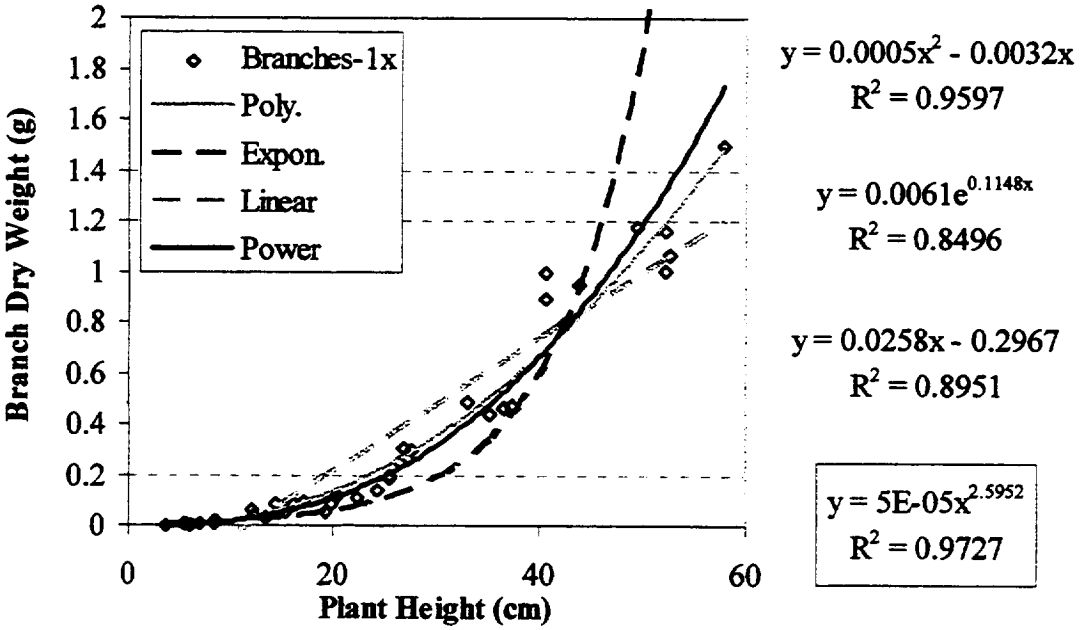

Figure B.3 Comparison of Various Relationships between Branch Dry Weight and Height for Tomato Plants Produced using a 1x Solution

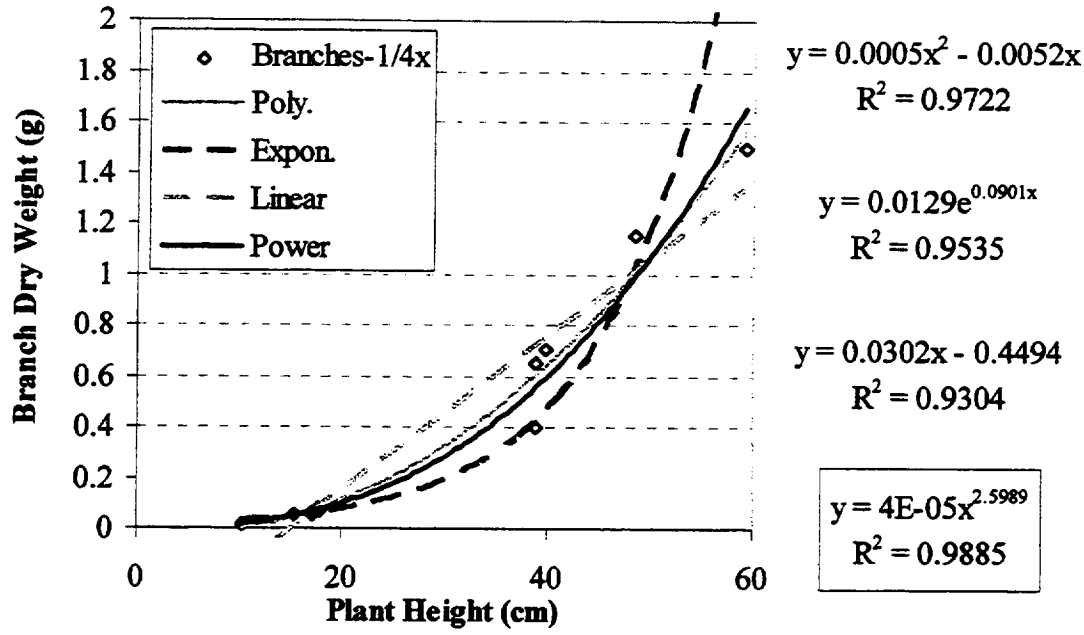

Figure B.4 Comparison of Various Relationships between Branch Dry Weight and Height for Tomato Plants Produced using a 1/4x Solution

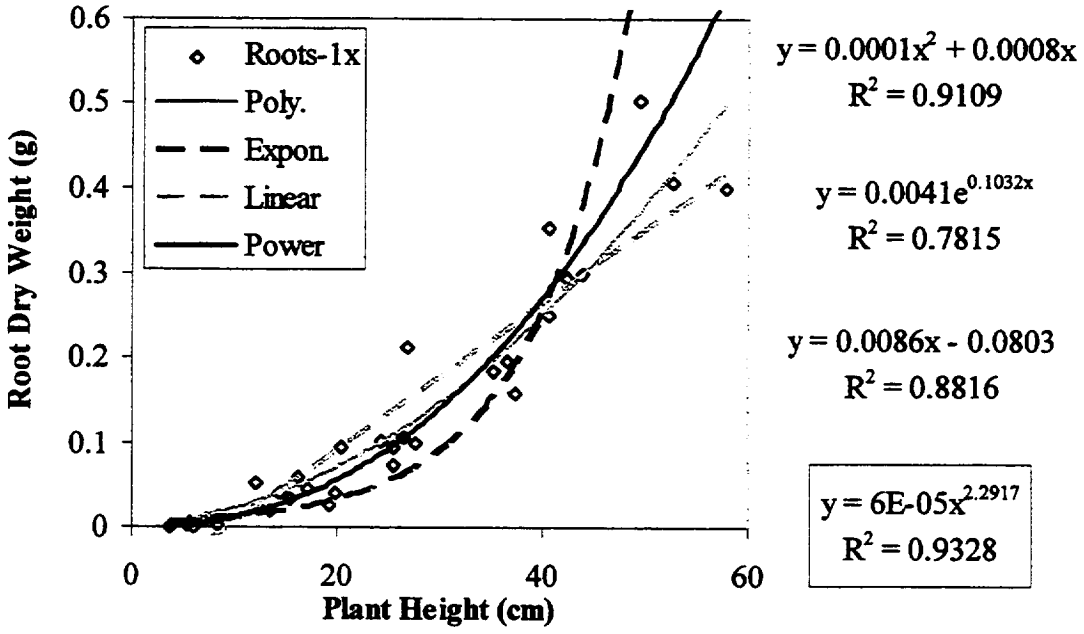

Figure B.5 Comparison of Various Relationships between Root Dry Weight and Height for Tomato Plants Produced using a 1x Solution

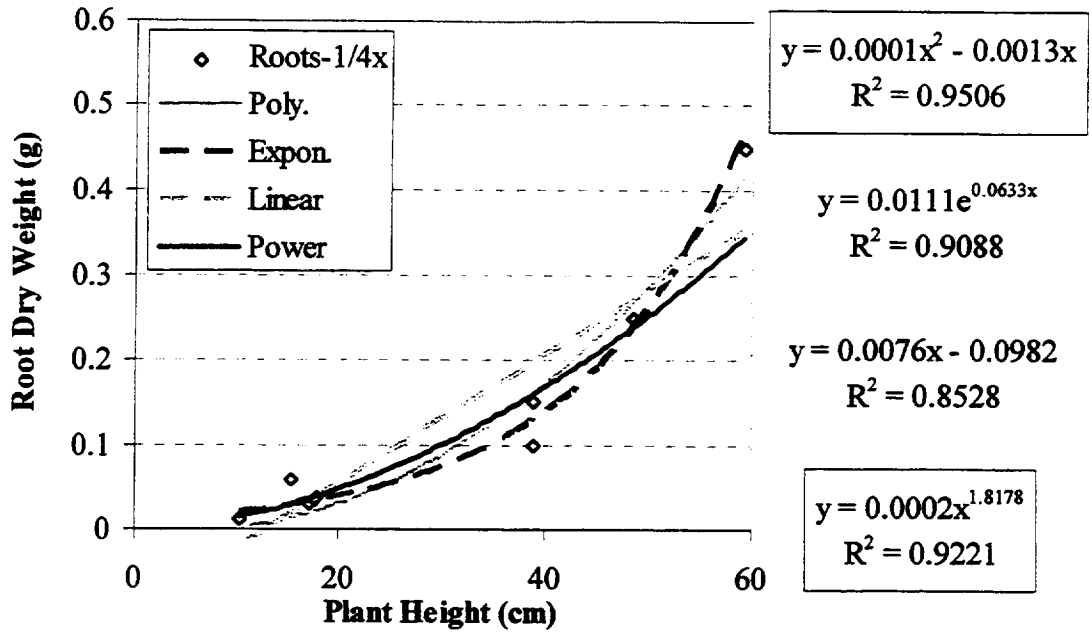

Figure B.6 Comparison of Various Relationships between Root Dry Weight and Height for Tomato Plants Produced using a 1/4x Solution

Table B.16 Tissue Dry Weights (Y) and Height (X1) Data for Tomato Plants Produced using a 1x Solution (X2)

Plant Height	Leaf DryWgt	Branch DryWgt	Root DryWgt	Plant Height	Leaf DryWgt	Branch DryWgt	Root DryWgt
3.7	0.0018	0.0011	0.0007	24.2	0.1535	0.1422	0.1022
5.5	0.008	0.0049	0.0024	25.4	0.1794	0.1859	0.0934
5.6	0.0095	0.0049	0.0043	25.5	0.2137	0.1962	0.0737
6.1	0.0048	0.0024	0.001	26.4	0.2858	0.2531	0.1055
6.9	0.0132	0.0073	0.006	26.8	0.3409	0.3041	0.2122
8.3	0.0203	0.0119	0.0125	27.5	0.3	0.3	0.1
8.3	0.0083	0.0048	0.0033	33.1	0.5606	0.4877	-----
8.6	0.0282	0.0184	0.0128	35.2	0.3956	0.44	0.1825
12.0	0.1058	0.0614	0.0513	37.3	0.4551	0.4744	0.158
12.3	0.0462	0.0391	0.0238	36.6	0.483	0.463	0.1961
13.4	0.0357	0.0335	0.0194	40.6	0.8058	0.8959	0.3525
14.3	0.0957	0.0824	0.0391	40.6	0.7	1	0.25
15.3	0.0711	0.0572	0.0322	42.3	0.8149	0.7942	0.2951
16.2	0.1375	0.0895	0.0578	43.8	0.85	0.95	0.3
17.1	0.0872	0.0907	0.0444	49.6	1.2529	1.1728	0.5047
19.3	0.0701	0.0557	0.0263	52.3	1.081	1.1619	-----
19.9	0.1069	0.084	0.0407	52.3	1.1528	1.0064	-----
20.4	0.147	0.1155	0.0935	52.6	1.0843	1.0697	0.4063
22.4	0.1282	0.1067	-----	57.9	1.1	1.5	0.4

Table B.17 Tissue Dry Weights (Y) and Height (X1) Data for Tomato Plants Produced using a 1/4x Solution (X2)

Plant Height	Leaf DryWgt	Branch DryWgt	Root DryWgt
10.3	0.0262	0.0187	0.0113
15.4	0.0958	0.0573	0.0583
17.0	0.0579	0.0612	0.031
17.0	0.0759	0.0542	-----
17.6	0.0813	0.0763	0.0354
17.9	0.0691	0.0674	0.0376
38.8	0.25	0.4	0.1
38.9	0.55	0.65	0.15
39.9	0.5797	0.7084	-----
48.5	0.9	1.15	0.25
59.2	1	1.5	0.45

Since the greatest R^2 correlation coefficients were obtained for the power equations, then the weights were modeled using this form. This was accomplished by first linearizing these equations by taking the natural logarithms of the dry weights (Y), heights (X1), and overall concentrations (X2) listed as the fraction of the standard Hoagland's solution (1 and 0.25 times). In each case, the effect of the solution concentration on the weight of the plant tissues were shown to be insignficant contributions. These were determined from the analysis of variances of the terms in the linearized model. Removing these terms from the linearized models produced adequate equations describing the allometric relationship between the tissue dry weights and plant heights. The resulting ANOVA tables are provided for the final adequate models below in Tables B.18 to B.21 for the leaves, branches, roots, and the entire plant, respectively.

Table B.18 Analysis of Variance Table for the Final Adequate Model for the Natural Log of the Leaf Dry Weights (Y) as a Linear Function of the Natural Log of the Height (X1)

	DOF	Sum Sqs.	Mean Sqs.	Fcalc		Fcrit	Signif?
Total	49	316.26				$\alpha_{risk} = 0.05$	
Model	2	310.97	155.483	1381	>	6.944	yes
b0	1	187.69	187.689	1667	>	7.709	yes
b1	1	123.28	123.277	1095	>	7.709	yes
Resid	47	5.292	0.113				
Error	4	0.449	0.112				
LOT	43	4.843	0.113	1.000	<	5.711	no

Table B.19 Analysis of Variance Table for the Final Adequate Model for the Natural Log of the Branch Dry Weights (Y) as a Linear Function of Natural Log of the Height (X1)

	DOF	Sum Sqs.	Mean Sqs.	Fcalc		Fcrit	Signif?
Total	49	379.86				$\alpha_{risk} = 0.05$	
Model	2	375.61	187.8075	2081	>	6.944	yes
b0	1	213.07	213.0747	2361	>	7.709	yes
b1	1	162.54	162.5403	1801	>	7.709	yes
Resid	47	4.241	0.090				
Error	4	0.436	0.109				
LOT	43	3.805	0.088	0.981	<	5.711	no

Table B.20 Analysis of Variance Table for the Final Adequate Model for the Natural Log of the Root Dry Weights (Y) as a Linear Function of Natural Log of the Height (X1)

	DOF	Sum Sqs.	Mean Sqs.	Fcalc		Fcrit	Signif?
Total	43	492.20				$\alpha_{risk} = 0.05$	
Model	2	483.52	241.7587	1141	>	19.000	yes
b0	1	377.59	377.5931	1783	>	18.513	yes
b1	1	105.92	105.9243	500.1	>	18.513	yes
Resid	41	8.685	0.212				
Error	2	0.946	0.473				
LOT	39	7.739	0.198	0.937	<	19.470	no

Table B.21 Analysis of Variance Table for the Final Adequate Model for the Natural Log of the Total Plant Dry Weights (Y) as a Linear Function of Natural Log of the Height (X1)

	DOF	Sum Sqs.	Mean Sqs.	Fcalc		Fcrit	Signif?
Total	43	194.74				$\alpha_{risk} = 0.05$	
Model	2	190.07	95.0342	833.5	>	19.000	yes
b0	1	67.73	67.7325	594.1	>	18.513	yes
b1	1	122.34	122.336	1073	>	18.513	yes
Resid	41	4.674	0.114				
Error	2	0.504	0.252				
LOT	39	4.170	0.107	0.938	<	19.470	no

APPENDIX C - STATISTICAL ANALYSES - WATER STATUS RESULTS

The statistical analyses of the functions describing the plant water status are presented in this appendix. This includes the data for the factors, X, and the responses, Y, used to produce the various models. In addition, the analysis of variances (ANOVA) tables produced for the various steps in the development of the water uptake models are provided as well. These tables were generated on a Microsoft Excel v.5.0 Spreadsheet.

Initially, the wet weights (Y) of the tissues and whole plant modeled as power functions of the plant heights (X1) and solution concentrations (X2) are presented. These models were produced using the same procedure as used for the dry weights presented in Appendix B except for the data used. These data are presented in Tables C.1 and C.2 for the various tissue types grown with either a 1x and 1/4x solution, respectively.

Table C.1 Tissue Wet Weights (Y) and Height (X1) Data for Tomato Plants Produced using a 1x Solution (X2)

Plant Height	Leaf WetWgt	Branch WetWgt	Root WetWgt	Plant Height	Leaf WetWgt	Branch WetWgt	Root WetWgt
3.7	0.027	0.0248	0.0117	24.2	1.1696	1.9571	1.6394
5.5	0.0718	0.0915	0.0622	25.4	1.4717	2.4063	1.5996
5.6	0.0797	0.0711	0.0725	25.5	1.8866	3.1905	1.3944
6.1	0.069	0.0619	0.0437	26.4	2.3156	3.7579	1.6856
6.9	0.1187	0.0947	0.133	26.8	2.2741	3.5679	2.567
8.3	0.1598	0.1644	0.2083	27.5	2.45	4.65	1.55
8.3	0.1075	0.111	0.0858	33.1	4.064	6.3304	-----
8.6	0.264	0.3577	0.2526	35.2	2.8992	5.3533	2.4094
12.0	0.8216	0.7813	0.7724	37.3	3.6368	6.9828	2.2545
12.3	0.4559	0.6665	0.7541	36.6	4.3792	7.5916	3.0785
13.4	0.2638	0.5441	0.2623	40.6	5.1082	9.6393	3.6829
14.3	1.1085	1.5766	0.9675	40.6	4.4	8.55	2.85
15.3	0.6294	0.8492	0.626	42.3	6.311	8.7869	3.7179
16.2	1.1404	1.2836	0.6531	43.8	5.2	8.85	4
17.1	0.7229	1.1781	0.7354	49.6	9.2554	14.4642	6.6721
19.3	0.6309	1.0074	0.5034	52.3	7.4636	11.9621	-----
19.9	0.9493	1.5629	0.6559	52.3	7.7382	10.7449	-----
20.4	1.0818	1.4511	1.0896	52.6	8.0502	12.0208	5.2924
22.4	1.0381	1.6473	-----	57.9	6.9	13.7	5.15

Table C.2 Tissue Wet Weights (Y) and Height (X1) Data for Tomato Plants Produced using a 1/4x Solution (X2)

Plant Height	Leaf WetWgt	Branch WetWgt	Root WetWgt
10.3	0.2392	0.2858	0.4212
15.4	0.8239	1.0473	1.3701
17.0	0.482	0.7453	0.8625
17.0	0.682	0.8541	-----
17.6	0.6619	0.9743	1.0199
17.9	0.5772	0.8313	0.9876
38.8	2.6	6.25	1.95
38.9	4.5	7.95	3.4
39.9	3.6709	7.5043	-----
48.5	5.65	11.1	4.2
59.2	6.75	13	5.2

In order to produce the models for the wet weights, the power equations were linearized by taking the natural logarithms of the weights (Y), heights (X1), and overall concentrations (X2) listed as the fraction of the standard Hoagland's solution (1 and 0.25 times). In each case, the contributions of the solution concentration on the wet weights of the plant tissues were shown to be insignificant. These were determined from the analysis of variances of the terms in the linearized model. Removing these terms produced adequate equations describing the allometric relationship between the tissue wet weights and plant heights. The resulting ANOVA tables are provided for the final adequate models in Tables C.3 to C.6 for the leaves, branches, roots, and the entire plant, respectively.

Table C.3 Analysis of Variance Table for the Final Adequate Model for the Natural Log of the Leaf Wet Weights (Y) as a Linear Function of the Natural Log of the Height (X1)

	DOF	Sum Sqs.	Mean Sqs.	Fcalc		Fcrit	Signif?
Total	49	107.86				$\alpha_{risk} = 0.05$	
Model	2	103.80	51.8985	599.8	>	6.944	yes
b0	1	1.10	1.09767	12.69	>	7.709	yes
b1	1	102.70	102.699	1187	>	7.709	yes
Resid	47	4.067	0.087				
Error	4	0.151	0.038				
LOT	43	3.916	0.091	1.053	<	5.711	no

Table C.4 Analysis of Variance Table for the Final Adequate Model for the Natural Log of the Branch Wet Weights (Y) as a Linear Function of the Natural Log of the Height (X1)

	DOF	Sum Sqs.	Mean Sqs.	Fcalc		Fcrit	Signif?
Total	49	149.73				$\alpha_{risk} = 0.05$	
Model	2	146.17	73.0842	965.5	>	6.944	yes
b0	1	14.47	14.4665	191.1	>	7.709	yes
b1	1	131.70	131.702	1740	>	7.709	yes
Resid	47	3.558	0.076				
Error	4	0.099	0.025				
LOT	43	3.458	0.080	1.062	<	5.711	no

Table C.5 Analysis of Variance Table for the Final Adequate Model for the Natural Log of the Root Wet Weights (Y) as a Linear Function of the Natural Log of the Height (X1)

	DOF	Sum Sqs.	Mean Sqs.	Fcalc		Fcrit	Signif?
Total	43	89.46				$\alpha_{risk} = 0.05$	
Model	2	82.22	41.1083	232.8	>	19.000	yes
b0	1	0.37	0.368177	2.085	<	18.513	no
b1	1	81.85	81.84842	463.5	>	18.513	yes
Resid	41	7.240	0.177				
Error	2	0.426	0.213				
LOT	39	6.814	0.175	0.989	<	19.470	no

Table C.6 Analysis of Variance Table for the Final Adequate Model for the Natural Log of the Total Plant Wet Weights (Y) as a Linear Function of the Natural Log of the Height (X1)

	DOF	Sum Sqs.	Mean Sqs.	Fcalc		Fcrit	Signif?
Total	43	171.21				$\alpha_{risk} = 0.05$	
Model	2	167.81	83.9042	1013	>	19.000	yes
b0	1	67.81	67.8106	818.4	>	18.513	yes
b1	1	100.00	99.9978	1207	>	18.513	yes
Resid	41	3.397	0.083				
Error	2	0.168	0.084				
LOT	39	3.229	0.083	0.999	<	19.470	no

In addition to the models for the wet weights of the plant, the total solution uptake (Y) was modeled as a function of leaf stage (X1), osmotic potential (X2), and matric potential (X3). This was conducted in two phases. First, the constant root-zone water potential level of Ψ_{soil} = -0.078, obtained using the experimental conditions of (-0.019/-0.059), (-0.039/-0.039), and (-0.078/-0.000), were tested to determine whether these different osmotic and the matric potentials affected the solution uptake. These are coded according to Table 7.2 where the initial number represents the concentration level or osmotic potential while the second number describes the applied suction pressure or matric potential. The second phase examined the effects of these levels on the solution uptake at different water potential levels. Specifically, the experimental levels examined were listed in Table 7.2 as -0.019, -0.058, -0.078, -0.117, and -0.137 MPa. An exponential equation was chosen as the form of this model based on the plots of the data shown in Figures C.1 to C.7 for the different conditions. It should be noted that these plots are not on the same scale allowing the data to be differentiated better visually.

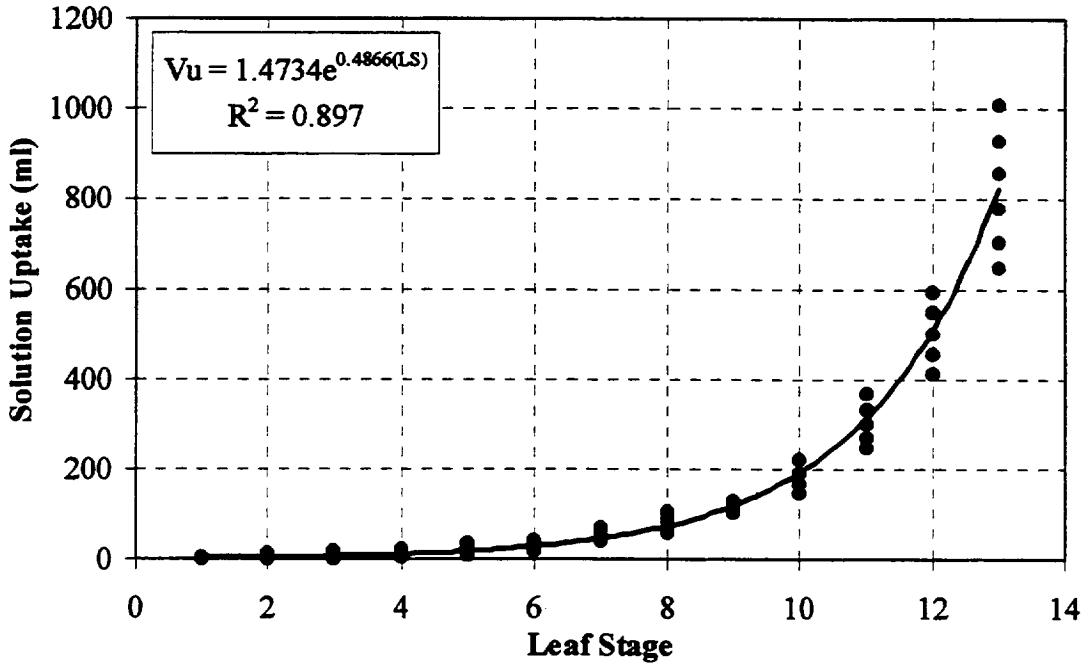

Figure C.1 Plot of the Total Solution Uptake versus the Leaf Stage for the Plants Grown at an Osmotic Potential, π_{soil} = -0.019 MPa, and a Matric Potential, P_m = -0.000 MPa. (Ψ_{soil} = -0.019 MPa)

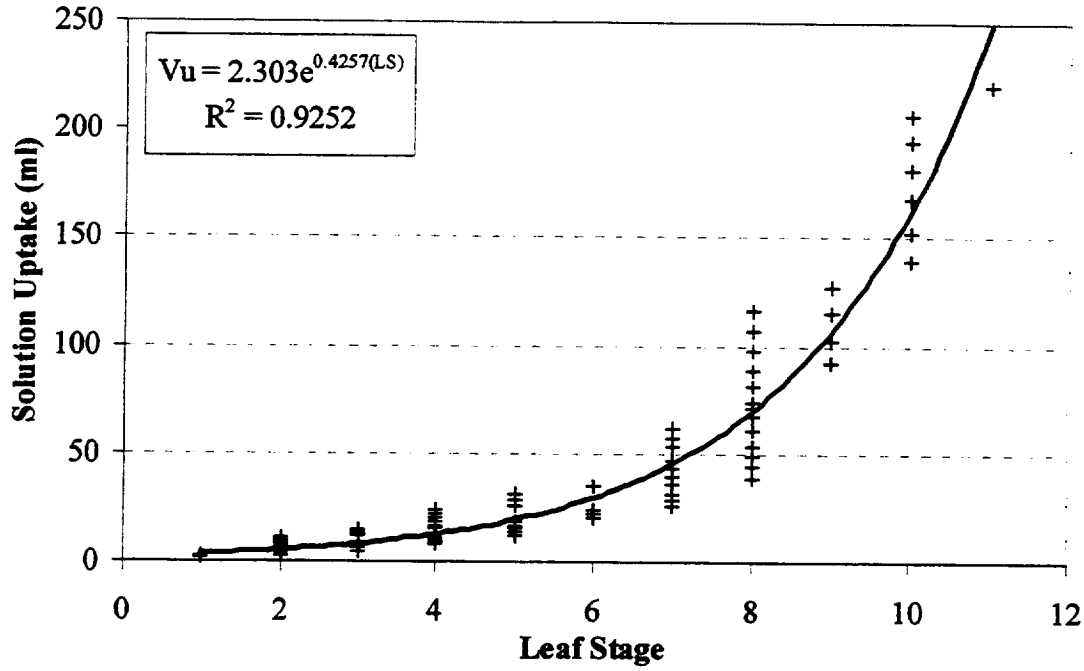

Figure C.2 Plot of the Total Solution Uptake versus the Leaf Stage for the Plants Grown at an Osmotic Potential, π_{soil} = -0.019 MPa, and a Matric Potential, P_m = -0.039 MPa. (Ψ_{soil} = -0.058 MPa)

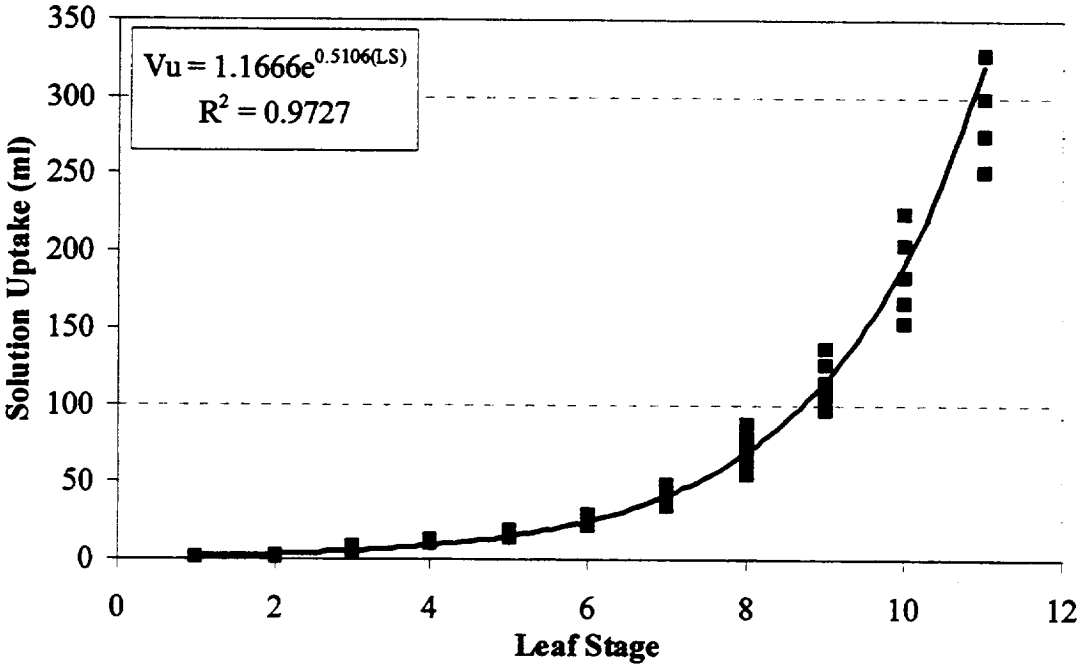

Figure C.3 Plot of the Total Solution Uptake versus the Leaf Stage for the Plants Grown at an Osmotic Potential, π_{soil} = -0.019 MPa, and a Matric Potential, P_m = -0.059 MPa. (Ψ_{soil} = -0.078 MPa)

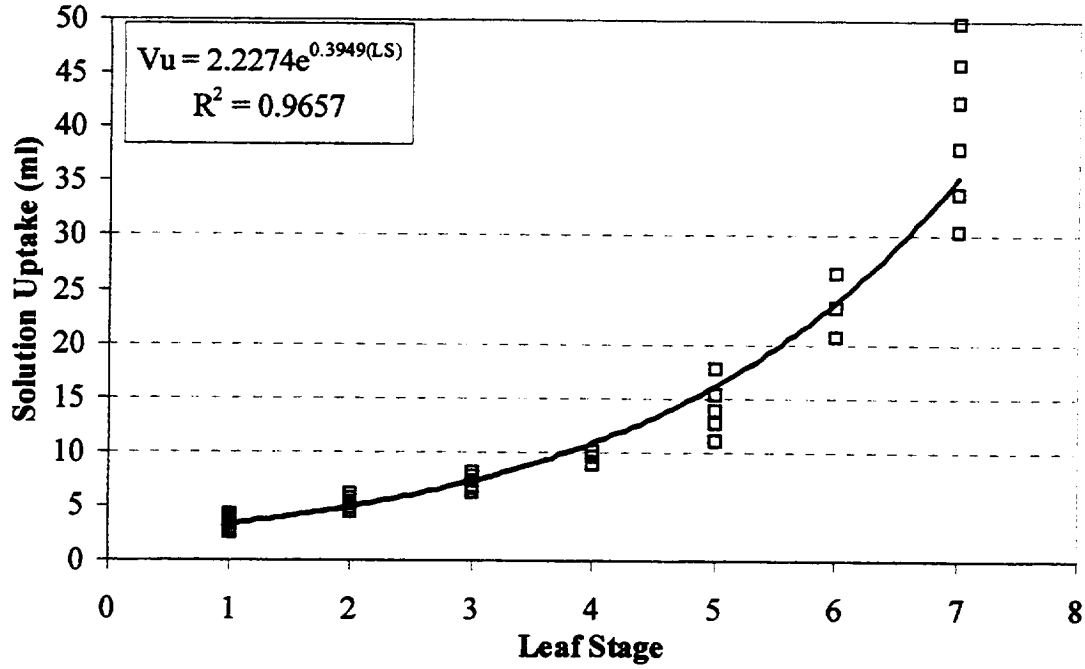

Figure C.4 Plot of the Total Solution Uptake versus the Leaf Stage for the Plants Grown at an Osmotic Potential, π_{soil} = -0.039 MPa, and a Matric Potential, P_m = -0.039 MPa. (Ψ_{soil} = -0.078 MPa)

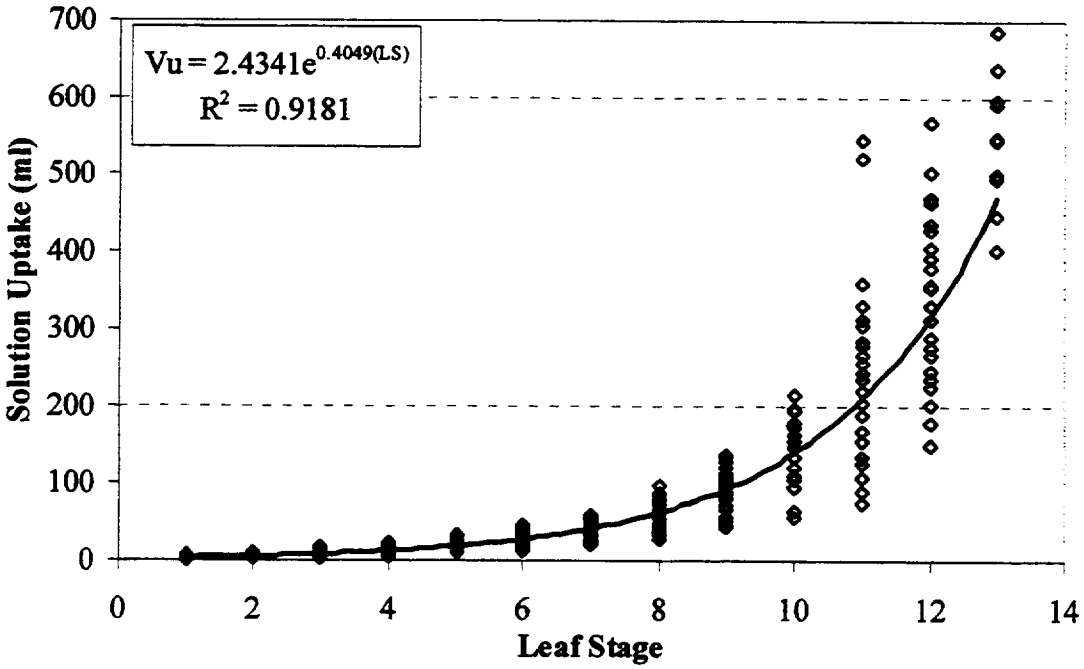

Figure C.5 Plot of the Total Solution Uptake versus the Leaf Stage for the Plants Grown at an Osmotic Potential, π_{soil} = -0.078 MPa, and a Matric Potential, P_m = -0.000 MPa. (Ψ_{soil} = -0.078 MPa)

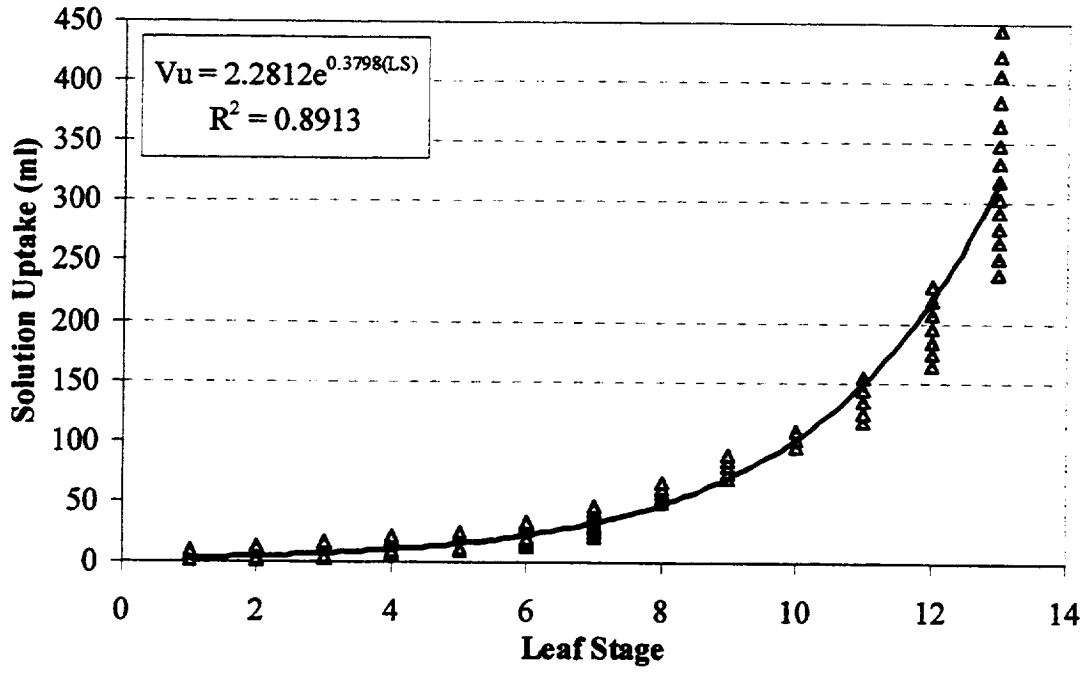

Figure C.6 Plot of the Total Solution Uptake versus the Leaf Stage for the Plants Grown at an Osmotic Potential, π_{soil} = -0.078 MPa, and a Matric Potential, P_m = -0.039 MPa. (Ψ_{soil} = -0.117 MPa)

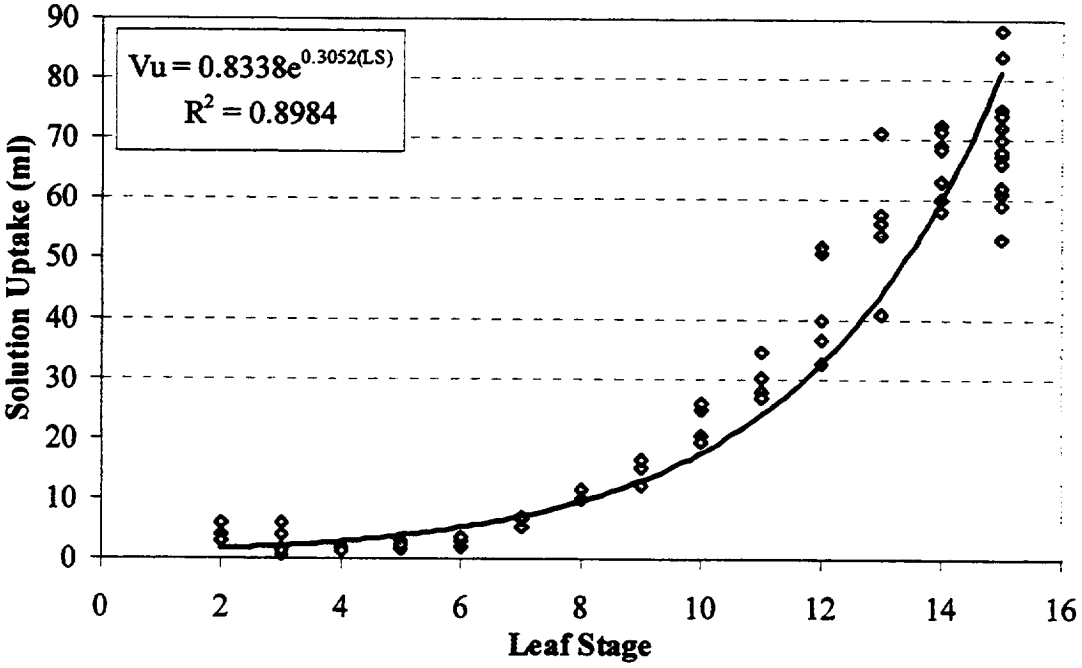

Figure C.7 Plot of the Total Solution Uptake versus the Leaf Stage for the Plants Grown at an Osmotic Potential, π_{soil} = -0.078 MPa, and a Matric Potential, P_m = -0.059 MPa. (Ψ_{soil} = -0.137 MPa)

APPENDIX D - PROPAGATED ERRORS - INORGANIC MASS BALANCES

This appendix presents the error propagation calculations concerning the inorganic mass balances. This will begin with the calculations of the errors associated with the dry weights of the plant tissues as affected by the measurement in plant heights. This error is used as an analogy to the experimental error associated with the separation of the various tissues prior to the nutrient analyses. Furthermore, the errors generated during the analysis of the tissues as well as the solution samples in the ICP-AES are presented as well. These are determined from replicate measurements of samples obtained from identical sources.

Next, the analysis of variances (ANOVA) tables produced for the correlations involving the concentrations of P, Mg, Ca, K, and Fe as a function of the solution pH are presented. These solubility experiments were conducted independently of the plant growth experiments conducted for this research. Initially, linear regression equations were examined followed by the standard model building procedure to find an adequate model with significant model parameters. These resulted in various models depending on the specific nutrient element.

With the various measurement errors determined, the errors associated with the mass balances can be propagated. The derivations of the general propagation equations are provided in this Appendix. This begins with the quantities of nutrients in the plants followed by the amounts of nutrients supplied, removed during the experiment, and precipitated from solution. Furthermore, these general equations will be applied to a specific experiment in order to show the complete mass balance for the PCT-NDS. As with all of the results in this Appendix, the tables and figures provided were generated on a Microsoft Excel v.5.0 Spreadsheet.

The propagated errors for the dry mass of the various plant tissues begins with the differentiation of Equations (8.4), (8.5), and (8.6) for the leaves, branches, and roots, respectively. These equations, reprinted below, relate the tissue weights to the overall height of the plants where the measurement error is on the order of magnitude of $\sigma_{hplant} = \pm 0.05$ cm. This visually based measurement is used as an analogy to describe the error associated with the visually based process to separate the various tissues for the dry weight measurements.

$$W_{leaf,d} = 1.454x10^{-4}(h_{plant})^{2.254} \quad (8.4)$$

$$W_{branch,d} = 0.461x10^{-4}(h_{plant})^{2.588} \quad (8.5)$$

$$W_{root,d} = 0.712x10^{-4}(h_{plant})^{2.204} \quad (8.6)$$

The error in the height measurements is propagated into the weights of the tissues using the Equation (D.1) presented below.

$$\sigma_W = [(\delta W/\delta h_{plant})^2(\sigma_{hplant})^2]^{1/2} = (dW/dh_{plant})(\sigma_{hplant}) \quad (D.1)$$

Therefore, differentiating Equations (8.4) to (8.6) with respect to h_{plant} gives the following results presented in Equations (D.2) to (D.4).

$$\sigma_{Wleaf,d} = [(2.254)(1.454x10^{-4})(h_{plant})^{1.254}][0.05 \text{ cm}] \quad (D.2)$$

$$\sigma_{Wbranch,d} = [(2.588)(0.461x10^{-4})(h_{plant})^{1.588}][0.05 \text{ cm}] \quad (D.3)$$

$$\sigma_{Wroot,d} = [(2.204)(0.712x10^{-4})(h_{plant})^{1.204}][0.05 \text{ cm}] \quad (D.4)$$

Assuming a range of plant heights from 2 to 65 cm, these errors range from $\pm 2x10^{-5}$ to ± 0.004 g with an average value of ± 0.001 g. This average error in the dry masses was then used as an estimate of the error in the weight measurements as affected by the separation of the tissues in subsequent calculations for the inorganic nutrient mass balances.

The errors generated during the analysis of the plant tissues are presented here. These were determined by submitting duplicate samples for analysis and determining the average standard deviation for all samples and tissue types. The individual estimates of the

standard deviations for each nutrient, i, and for the various tissue types, $\sigma_{Ctissue,i}$, for the n_{tissue} identical trials were calculated using Equation (D.5) where $C_{tissue,i,k}$ and $C_{tissue,i,ave}$ are the plant tissue concentrations of sample, k, and the average concentration, respectively.

$$\sigma_{Ctissue,i} = \left[\frac{\Sigma_k (C_{tissue,i,k} - C_{tissue,i,ave})^2}{n_{tissue} - 1}\right]^{1/2} \qquad (D.5)$$

For the leaves and branches, three separate samples of these tissues were obtained from a single source containing a thorough mixture of the ground tissues from four plants ($n_{leaf} = n_{branch} = 3$ each). For the root tissues, two sets of identical samples were obtained from two different plants ($n_{root} = 2$ each). The average standard deviation, $\sigma_{Ctissue,i,ave}$, for these individual data sets was determined using Equation (D.6) where $\nu_{tissue} = n_{tissue} - 1$.

$$s_{Ctissue,i,ave} = \frac{\Sigma_{tissues}\, s_{Ctissue,i}\nu_{tissue}}{\Sigma\nu_{tissue}} \qquad (D.6)$$

The values calculated for the individual standard deviations are presented in Tables D.1 to D.3 for the different tissues while $\sigma_{Ctissue,i,ave}$ is presented in Chapter 8 (see Table 8.7).

Table D.1 Standard Deviation for the Inorganic Concentrations in the Tomato Leaves Measured using the ICP-AES System

Leaves	$C_{leaf,i,1}$	$C_{leaf,i,2}$	$C_{leaf,i,3}$	$C_{leaf,i,ave}$	$\sigma_{Cleaf,i}$	%
P	2307.50	3105.83	5603.33	3672.22	1719.37	46.82
Mg	17512.50	16770.00	15036.67	16439.72	1270.53	7.73
Ca	46232.50	32516.67	23660.83	34136.67	11372.70	33.32
Na	1731.67	1662.50	1228.33	1540.83	272.84	17.71
K	35395.00	38840.83	40818.33	38351.39	2744.59	7.16
Mo	2.50	3.33	2.50	2.78	0.48	17.26
Zn	70.00	67.50	46.67	61.39	12.81	20.87
B	178.33	180.00	149.17	169.17	17.34	10.25
Mn	95.83	91.67	84.17	90.56	5.91	6.53
Fe	400.00	527.60	514.17	480.59	70.12	14.59
Cu	9.17	8.33	9.17	8.89	0.48	5.46

Table D.2 Standard Deviation for the Inorganic Concentrations in the Tomato Branches Measured using the ICP-AES System

Branches	$C_{branch,i,1}$	$C_{branch,i,2}$	$C_{branch,i,3}$	$C_{branch,i,ave}$	$\sigma_{Cbranch,i}$	%
P	3198.33	5910.83	5783.33	4964.16	1530.58	30.83
Mg	21865.83	17556.67	13050	17490.83	4408.28	25.20
Ca	15295.00	8941.67	6883.33	10373.33	4384.78	42.27
Na	2366.67	2612.50	2087.50	2355.56	262.68	11.15
K	43284.17	49502.50	52454.17	48413.61	4680.97	9.67
Mo	1.67	2.50	3.33	2.50	0.83	33.20
Zn	12.50	12.50	12.50	12.50	0.00	0.00
B	25.00	28.33	28.33	27.22	1.92	7.06
Mn	19.17	25.00	31.67	25.28	6.25	24.74
Fe	128.33	383.33	1100.00	537.22	503.78	93.78
Cu	3.33	5.00	7.50	5.28	2.10	39.77

Table D.3 Standard Deviation for the Inorganic Concentrations in the Tomato Roots Measured using the ICP-AES System

Roots	$C_{root,i,1A}$	$C_{root,i,1B}$		$C_{root,i,ave}$	$\sigma_{Croot,i}$	%
P	5454	3096		4274.86	1667.05	39.00
Mg	8582	6086		7334.08	1764.47	24.06
Ca	5543	10483		8013.11	3492.74	43.59
Na	3223	3163		3192.94	42.28	1.32
K	33796	32581		33188.57	859.19	2.59
Mo	5	3		3.98	1.44	36.11
Zn	735	690		712.51	32.22	4.52
B	22	16		19.12	4.68	24.48
Mn	40	37		38.22	2.35	6.14
Fe	456	463		459.79	5.17	1.12
Cu	47	46		46.90	0.65	1.39
Roots	$C_{root,i,2A}$	$C_{root,i,2B}$		$C_{root,i,ave}$	$\sigma_{Croot,i}$	%
P	4078	4605		4341.50	372.65	8.58
Mg	12908	14883		13895.50	1396.54	10.05
Ca	64865	35896		50380.50	20484.18	40.66
Na	1855	2339		2097.00	342.24	16.32
K	33681	41770		37725.50	5719.79	15.16
Mo	3	3		3.00	0.00	0.00
Zn	354	316		335.00	26.87	8.02
B	38	39		38.50	0.71	1.84
Mn	174	206		190.00	22.63	11.91
Fe	1290	1408		1349.00	83.44	6.19
Cu	56	62		59.00	4.24	7.19

The errors generated during the analysis of the solution samples are similar to those derived for the tissues. Specifically, equations similar to Equations (D.5) and (D.6) are used to generate the individual as well as the average standard deviation for the nutrient concentrations in the liquid samples. The individual deviations, $\sigma_{Csample,i,k}$, for each nutrient, i, were determined from the standard solutions generated for each experiment, k. This included the 1x, 1/2x, and 1/4x solutions from Experiments #8 to #13. This was conducted by calculating the average concentrations, $C_{sample,i,ave}$, from the various number of trial samples. The values calculated for the individual standard deviation estimates are presented in Tables D.4 to D.9 below. Each were averaged in order to obtain the overall standard deviation for the liquid samples, $\sigma_{Csample,i,ave}$ as presented in Tables 8.8 to 8.10.

Table D.4 Standard Deviation for the Inorganic Concentrations in the Standard Solutions (1x and 1/4x) Prepared for Experiment #8 Measured using the ICP-AES System

	Samples									
1x	**#1**	**#2**	**#3**	**#4**	**#5**	**#6**	**#7**	$C_{sample,i,ave}$	$\sigma_{Csample,i}$	**%**
P	28.44	28.74	27.74	27.47	27.91	28.22	28.35	28.12	0.440	1.56
Mg	90.86	90.97	89.15	88.56	90.60	90.34	93.67	90.59	1.631	1.80
Ca	207.46	207.88	202.62	204.09	205.01	205.88	207.98	205.85	2.061	1.00
Na	12.06	11.56	11.56	11.53	11.38	11.26	11.91	11.61	0.283	2.43
K	211.32	212.65	213.90	212.91	209.96	207.31	213.41	211.64	2.329	1.10
Mo	0.03	0.02	0.02	0.02	0.02	0.02	0.02	0.02	0.004	17.64
Zn	0.10	0.05	0.07	0.07	0.11	0.08	0.09	0.08	0.020	25.00
B	0.86	0.84	0.81	0.82	0.82	0.83	0.84	0.83	0.017	2.02
Mn	0.52	0.52	0.52	0.53	0.53	0.54	0.55	0.53	0.012	2.18
Fe	4.83	5.12	5.06	5.04	5.22	5.31	4.83	5.06	0.182	3.59
Cu	0.17	0.07	0.07	0.10	0.18	0.14	0.09	0.12	0.046	39.34
pH	5.80	5.93	5.96	6.11	5.99	5.86	5.87	5.93	0.102	1.72
1/4x	**#1**	**#2**	**#3**	**#4**	**#5**	**#6**	**#7**	$C_{sample,i,ave}$	$\sigma_{Csample,i}$	**%**
P	6.87	6.76	6.91	7.52				7.02	0.343	4.88
Mg	24.67	24.29	24.10	25.82				24.72	0.771	3.12
Ca	57.96	57.61	57.20	59.56				58.08	1.033	1.78
Na	3.17	3.18	3.21	3.19				3.19	0.017	0.54
K	52.82	53.37	55.54	54.29				54.01	1.190	2.20
Mo	0.01	0.01	0.01	0.03				0.02	0.010	66.67
Zn	0.02	0.02	0.05	0.03				0.03	0.014	47.14
B	0.37	0.37	0.39	0.38				0.38	0.010	2.54
Mn	0.14	0.14	0.14	0.13				0.14	0.005	3.64
Fe	1.31	1.31	1.36	1.36				1.34	0.029	2.16
Cu	0.10	0.10	0.16	0.11				0.12	0.029	24.44
pH	6.28	6.04	6.21	5.93				6.12	0.159	2.60

Table D.5 Standard Deviation for the Inorganic Concentrations in the Standard Solutions (1x and 1/4x) Prepared for Experiment #9 Measured using the ICP-AES System

	Samples									
1x	**#1**	**#2**	**#3**	**#4**	**#5**	**#6**	**#7**	$C_{sample,i,ave}$	$\sigma_{Csample,i}$	**%**
P	29.47	29.66	29.49	29.27	28.89			29.36	0.295	1.00
Mg	96.33	95.68	95.77	95.99	95.36			95.83	0.361	0.38
Ca	218.67	216.80	218.89	217.80	218.11			218.05	0.824	0.38
Na	10.93	10.97	11.08	11.25	11.22			11.09	0.144	1.30
K	218.09	217.21	220.41	216.16	220.32			218.44	1.887	0.86
Mo	0.03	0.02	0.02	0.02	0.01			0.02	0.007	35.36
Zn	0.05	0.07	0.07	0.09	0.07			0.07	0.014	20.20
B	0.85	0.84	0.83	0.81	0.80			0.83	0.021	2.51
Mn	0.51	0.50	0.50	0.50	0.49			0.50	0.007	1.41
Fe	4.60	4.60	4.62	4.46	4.53			4.56	0.066	1.46
Cu	0.11	0.11	0.11	0.14	0.11			0.12	0.013	11.57
pH	5.71	5.83	5.82	5.88	5.93			5.83	0.082	1.41
1/4x	**#1**	**#2**	**#3**	**#4**	**#5**	**#6**	**#7**	$C_{sample,i,ave}$	$\sigma_{Csample,i}$	**%**
P	7.23	7.18	7.28					7.23	0.050	0.69
Mg	26.01	26.39	26.03					26.14	0.214	0.82
Ca	60.69	61.67	61.21					61.19	0.490	0.80
Na	2.85	2.94	2.84					2.88	0.055	1.91
K	54.39	55.49	54.60					54.83	0.584	1.07
Mo	0.01	0.01	0.01					0.01	0.000	0.00
Zn	0.03	0.02	0.01					0.02	0.010	50.00
B	0.24	0.23	0.22					0.23	0.010	4.35
Mn	0.13	0.13	0.12					0.13	0.006	4.56
Fe	1.22	1.00	1.09					1.10	0.111	10.02
Cu	0.21	0.27	0.15					0.21	0.060	28.57
pH	5.92	6.06	5.85					5.94	0.107	1.80

Table D.6 Standard Deviation for the Inorganic Concentrations in the Standard Solutions (1x and 1/4x) Prepared for Experiment #10 Measured using the ICP-AES System

	Samples									
1x	**#1**	**#2**	**#3**	**#4**	**#5**	**#6**	**#7**	$C_{sample,i,ave}$	$\sigma_{Csample,i}$	**%**
P	28.48	28.55	29.26	26.93	26.87			28.02	1.065	3.80
Mg	94.04	94.28	96.35	78.71	78.35			88.35	9.007	10.19
Ca	208.47	210.03	214.04	186.13	158.54			195.44	23.329	11.94
Na	11.15	11.09	11.27	11.18	11.33			11.20	0.096	0.86
K	216.03	212.06	218.69	203.13	213.74			212.73	5.917	2.78
Mo	0.02	0.02	0.02	0.03	0.04			0.03	0.009	34.40
Zn	0.07	0.06	0.07	0.04	0.05			0.06	0.013	22.48
B	0.80	0.80	0.80	0.49	0.52			0.68	0.162	23.74
Mn	0.48	0.48	0.49	0.37	0.37			0.44	0.062	14.20
Fe	4.39	4.34	4.83	4.40	4.30			4.45	0.215	4.83
Cu	0.11	0.10	0.11	0.21	0.22			0.15	0.060	39.72
pH	5.92	5.92		5.93	5.99			5.94	0.034	0.57
1/4x	**#1**	**#2**	**#3**	**#4**	**#5**	**#6**	**#7**	$C_{sample,i,ave}$	$\sigma_{Csample,i}$	**%**
P	6.95	6.98	6.75	6.64				6.83	0.163	2.38
Mg	20.99	21.86	20.76	20.99				21.15	0.486	2.30
Ca	44.14	44.43	42.94	42.79				43.58	0.831	1.91
Na	2.83	3.35	2.56	2.68				2.86	0.348	12.19
K	54.01	60.67	53.01	52.33				55.01	3.839	6.98
Mo	0.02	0.02	0.02	0.02				0.02	0.000	0.00
Zn	0.07	0.06	0.01	0.04				0.05	0.026	58.79
B	0.19	0.18	0.16	0.15				0.17	0.018	10.74
Mn	0.10	0.11	0.10	0.10				0.10	0.005	4.88
Fe	1.20	1.13	1.20	1.15				1.17	0.036	3.04
Cu	0.18	0.22	0.19	0.19				0.20	0.017	8.88
pH	5.91	5.96	5.89	5.89				5.91	0.033	0.56

Table D.7 Standard Deviation for the Inorganic Concentrations in the Standard Solutions (1x, 1/2x, and 1/4x) Prepared for Experiment #11 Measured using the ICP-AES System

	Samples									
1x	**#1**	**#2**	**#3**	**#4**	**#5**	**#6**	**#7**	$C_{sample,i,ave}$	$\sigma_{Csample,i}$	**%**
P	29.00	29.10	28.60					28.90	0.265	0.92
Mg	85.30	87.00	87.10					86.47	1.012	1.17
Ca	192.80	191.70	191.00					191.83	0.907	0.47
Na	11.73	11.81	12.06					11.87	0.172	1.45
K	223.84	219.80	221.62					221.75	2.023	0.91
Mo	0.00	0.00	0.00					0.00	0.000	0.00
Zn	0.00	0.00	0.00					0.00	0.000	0.00
B	0.50	0.50	0.50					0.50	0.000	0.00
Mn	0.40	0.40	0.40					0.40	0.000	0.00
Fe	4.60	4.30	4.50					4.47	0.153	3.42
Cu	0.20	0.20	0.20					0.20	0.000	0.00
pH	5.97	6.16	6.19					6.11	0.119	1.95
1/2x	**#1**	**#2**	**#3**	**#4**	**#5**	**#6**	**#7**	$C_{sample,i,ave}$	$\sigma_{Csample,i}$	**%**
P	14.00	14.20						14.10	0.141	1.00
Mg	43.40	43.60						43.50	0.141	0.33
Ca	94.80	98.80						96.80	2.828	2.92
Na	5.99	5.88						5.94	0.078	1.31
K	109.14	108.74						108.94	0.283	0.26
Mo	0.01	0.01						0.01	0.000	0.00
Zn	0.02	0.02						0.02	0.000	0.00
B	0.40	0.40						0.40	0.000	0.00
Mn	0.20	0.20						0.20	0.000	0.00
Fe	2.10	2.10						2.10	0.000	0.00
Cu	0.20	0.20						0.20	0.000	0.00
pH	6.08	6.54						6.31	0.325	5.15
1/4x	**#1**	**#2**	**#3**	**#4**	**#5**	**#6**	**#7**	$C_{sample,i,ave}$	$\sigma_{Csample,i}$	**%**
P	6.90	7.40						7.15	0.354	4.94
Mg	21.20	23.00						22.10	1.273	5.76
Ca	46.90	50.80						48.85	2.758	5.65
Na	2.73	3.06						2.90	0.233	8.06
K	53.24	57.55						55.40	3.048	5.50
Mo	0.00	0.00						0.00	0.000	0.00
Zn	0.00	0.00						0.00	0.000	0.00
B	0.10	0.10						0.10	0.000	0.00
Mn	0.10	0.10						0.10	0.000	0.00
Fe	1.00	1.00						1.00	0.000	0.00
Cu	0.10	0.20						0.15	0.071	47.14
pH	6.08	6.32						6.20	0.170	2.74

Table D.8 Standard Deviation for the Inorganic Concentrations in the Standard Solutions (1x Macro-Nutrients Only) Prepared for Experiment #12 Measured using the ICP-AES System

	Samples									
1x	#1	#2	#3	#4	#5	#6	#7	$C_{sample,i,ave}$	$\sigma_{Csample,i}$	%
P	27.90	27.50	27.40	28.10	28.00			27.78	0.311	1.12
Mg	90.20	89.30	90.00	90.50	90.50			90.10	0.495	0.55
Ca	184.80	189.30	185.20	187.40	189.60			187.26	2.233	1.19
Na	10.10	9.90	9.70	9.80	9.80			9.86	0.152	1.54
K	209.50	209.10	209.70	208.80	208.80			209.18	0.409	0.20
pH	5.91	5.99	6.04	6.08	6.16			6.04	0.094	1.56

Table D.9 Standard Deviation for the Inorganic Concentrations in the Standard Solutions (1x and 1/4x Macro-Nutrients Only) Prepared for Experiment #13 Measured using the ICP-AES System

	Samples									
1x	#1	#2	#3	#4	#5	#6	#7	$C_{sample,i,ave}$	$\sigma_{Csample,i}$	%
P	29.00	28.70	28.60	29.70	29.50			29.10	0.485	1.67
Mg	92.90	92.40	93.20	90.70	94.40			92.72	1.348	1.45
Ca	197.20	193.30	196.30	198.70	194.70			196.04	2.109	1.08
Na	10.50	10.20	10.30	10.50	10.30			10.36	0.134	1.30
K	214.40	210.40	213.20	211.00	207.60			211.32	2.637	1.25
pH	5.97	6.01	6.03	6.08	6.07			6.03	0.045	0.75
1/4x	#1	#2	#3	#4	#5	#6	#7	$C_{sample,i,ave}$	$\sigma_{Csample,i}$	%
P	6.80	6.70	7.00	6.90	7.00			6.88	0.130	1.90
Mg	23.50	23.30	24.00	23.70	23.60			23.62	0.259	1.10
Ca	50.40	50.10	50.10	50.10	50.80			50.30	0.308	0.61
Na	2.60	2.70	2.80	2.80	2.70			2.72	0.084	3.08
K	53.00	52.00	53.90	52.30	52.20			52.68	0.779	1.48
pH	5.94	5.97	6.02	5.98	6.01			5.98	0.032	0.54

In order to determine the levels of nutrient precipitating out of solution due to the changes in pH, a side experiment which altered the pH of the standard solution from 5.7 to 8.0 was conducted. By measuring the concentration of the nutrients remaining in solution as a function of pH, the relationship between $C_{soln,i}$ and pH could be developed. This involved initially testing the model adequacy of a linear equation between these two factors by performing an analysis of variance of the model and left-out terms at an α_{risk}

level of 0.05. From these initial results, the respective models were adjusted accordingly by either adding or removing terms. The final results of these statistical analyses for P, Mg, Ca, K, and Fe are presented below in Tables D.10 to D.14 for the ANOVA tables and Figures D.1 to D.5 for the plots of the regression equations.

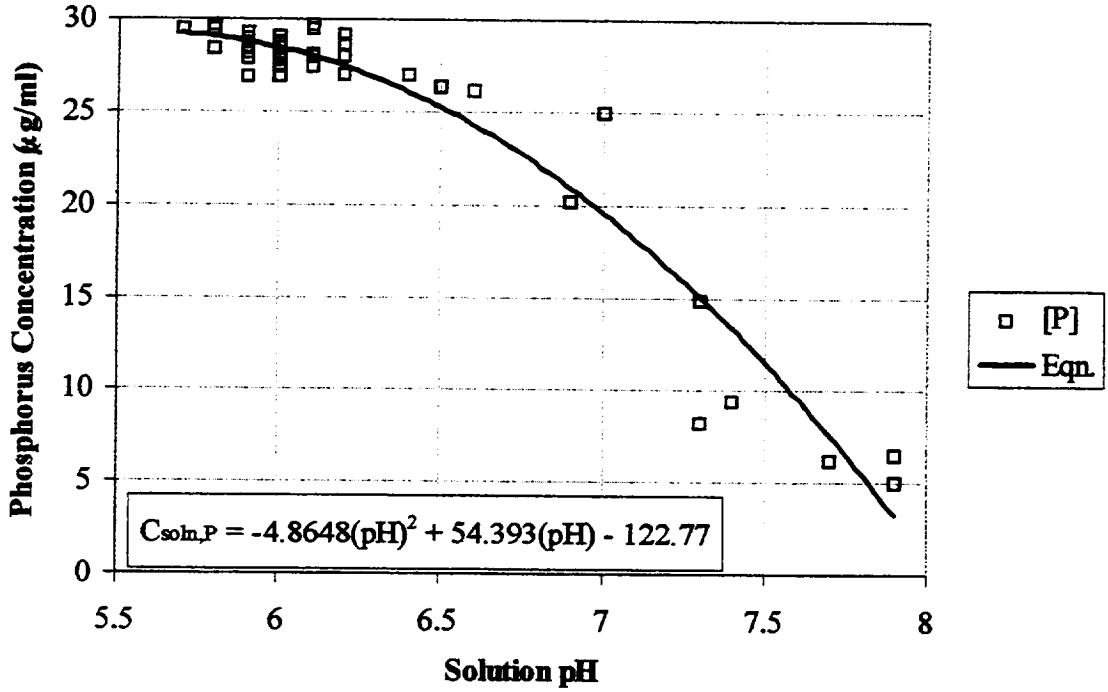

Figure D.1 Quadratic Regression of the Concentration of Soluble Phosphorus as a Function of Solution pH

Table D.10 Analysis of Variance Table for the Adequate Relationship Between the Soluble Phosphorus Concentration (Y) versus Solution pH (X1)

	DOF	Sum Sqs.	Mean Sqs.	Fcalc		Fcrit	Signif?
Total	42	28651				$\alpha_{risk} = 0.05$	
Model	3	28516	9505	2753	>	3.287	yes
b0	1	26520	26520	7680	>	4.543	yes
b1	1	1903	1903	551.19	>	4.543	yes
b2	1	93.222	93.222	26.996	>	4.543	yes
Resid	39	134.67	3.453				
Error	15	21.529	1.435				
LOT	24	113.14	4.714	1.365	<	2.288	no

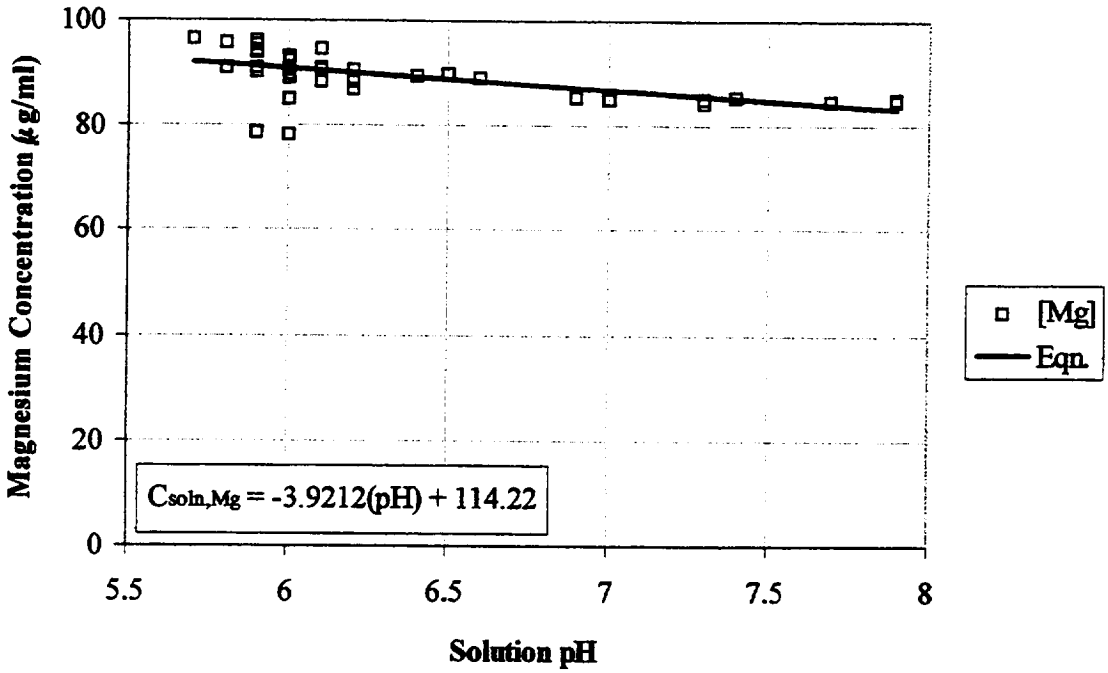

Figure D.2 Linear Regression of the Concentration of Soluble Magnesium as a Function of Solution pH

Table D.11 Analysis of Variance Table for the Adequate Relationship Between the Soluble Magnesium Concentration (Y) versus Solution pH (X1)

	DOF	Sum Sqs.	Mean Sqs.	Fcalc		Fcrit	Signif?
Total	42	337487				$\alpha_{risk} = 0.05$	
Model	2	336953	168476	12625	>	3.682	yes
b0	1	336724	336724.1	25234	>	4.543	yes
b1	1	228.78	228.78	17.145	>	4.543	yes
Resid	40	533.77	13.344				
Error	15	243.27	16.218				
LOT	25	290.50	11.620	0.871	<	2.280	no

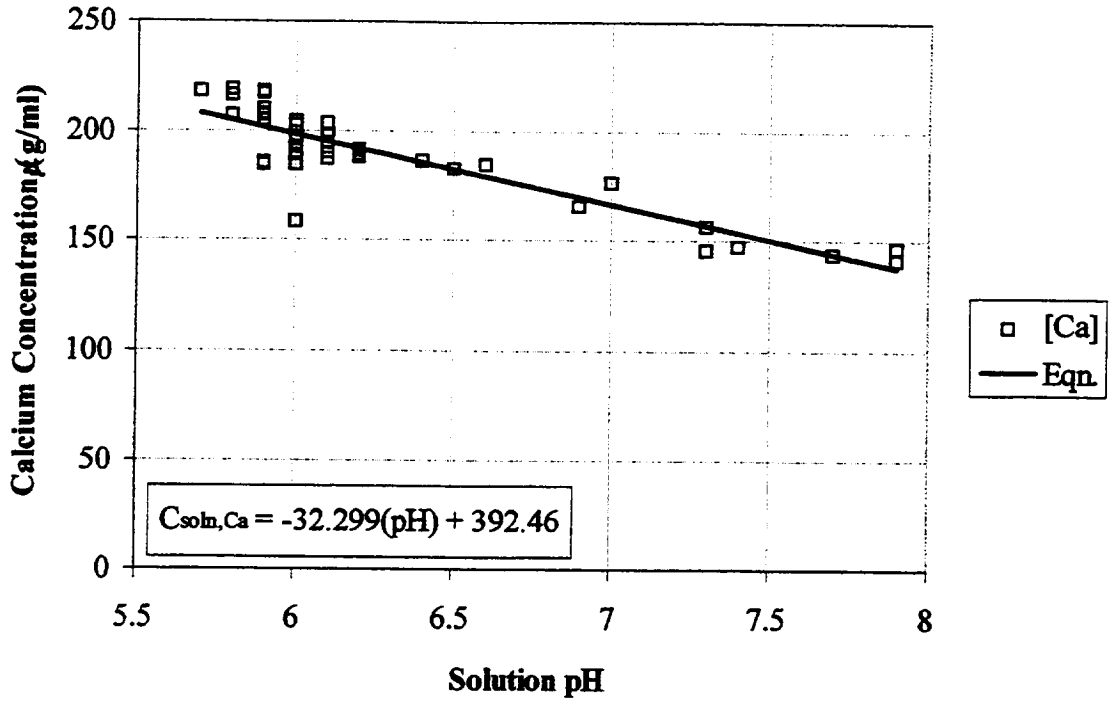

Figure D.3 Linear Regression of the Concentration of Soluble Calcium as a Function of Solution pH

Table D.12 Analysis of Variance Table for the Adequate Relationship Between the Soluble Calcium Concentration (Y) versus Solution pH (X1)

	DOF	Sum Sqs.	Mean Sqs.	Fcalc		Fcrit	Signif?
Total	42	1522114				$\alpha_{risk} = 0.05$	
Model	2	1517831	758915	7088	>	3.682	yes
b0	1	1502309	1502309	14031	>	4.543	yes
b1	1	15522	15522.21	145	>	4.543	yes
Resid	40	4283	107.07				
Error	15	1656	110.41				
LOT	25	2627	105.07	0.981	<	2.280	no

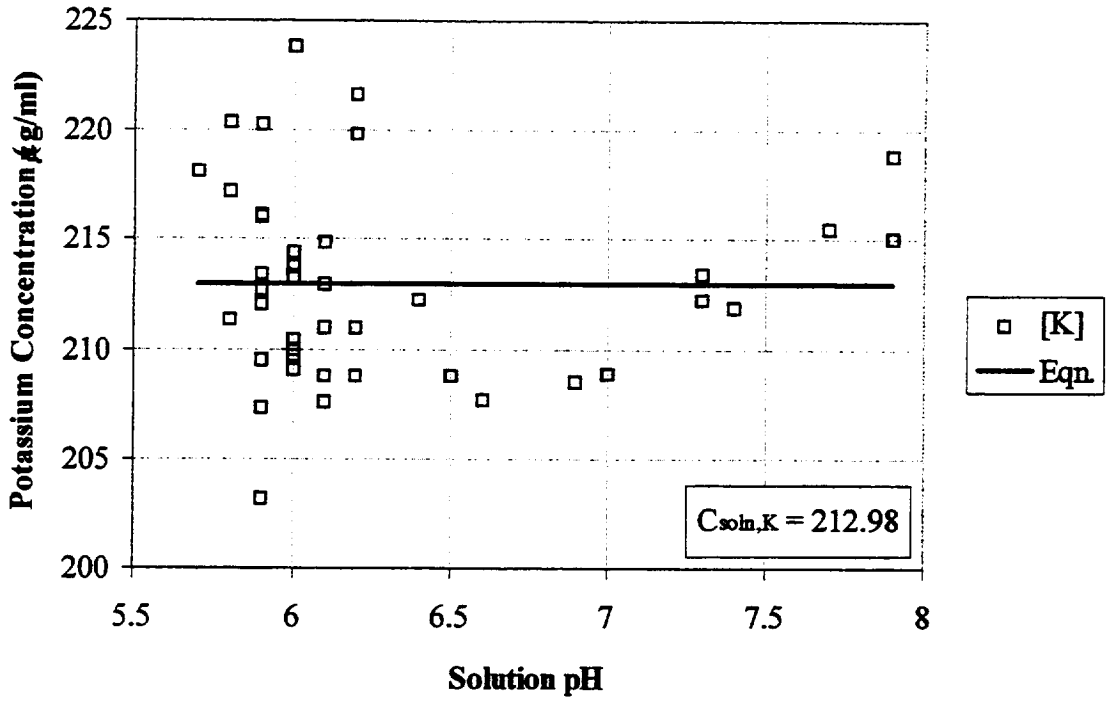

Figure D.4 Average Regression of the Concentration of Soluble Potassium as a Function of Solution pH

Table D.13 Analysis of Variance Table for the Adequate Relationship Between the Soluble Potassium Concentration (Y) versus Solution pH (X1)

	DOF	Sum Sqs.	Mean Sqs.	Fcalc		Fcrit	Signif?
Total	42	1905951				$\alpha_{risk} = 0.05$	
Model	1	1905144	1905144	96785	>	4.543	yes
b0	1	1905144	1905144	96785	>	4.543	yes
Resid	41	807.06	19.684				
Error	15	322.57	21.504				
LOT	26	484.49	18.634	0.947	<	2.272	no

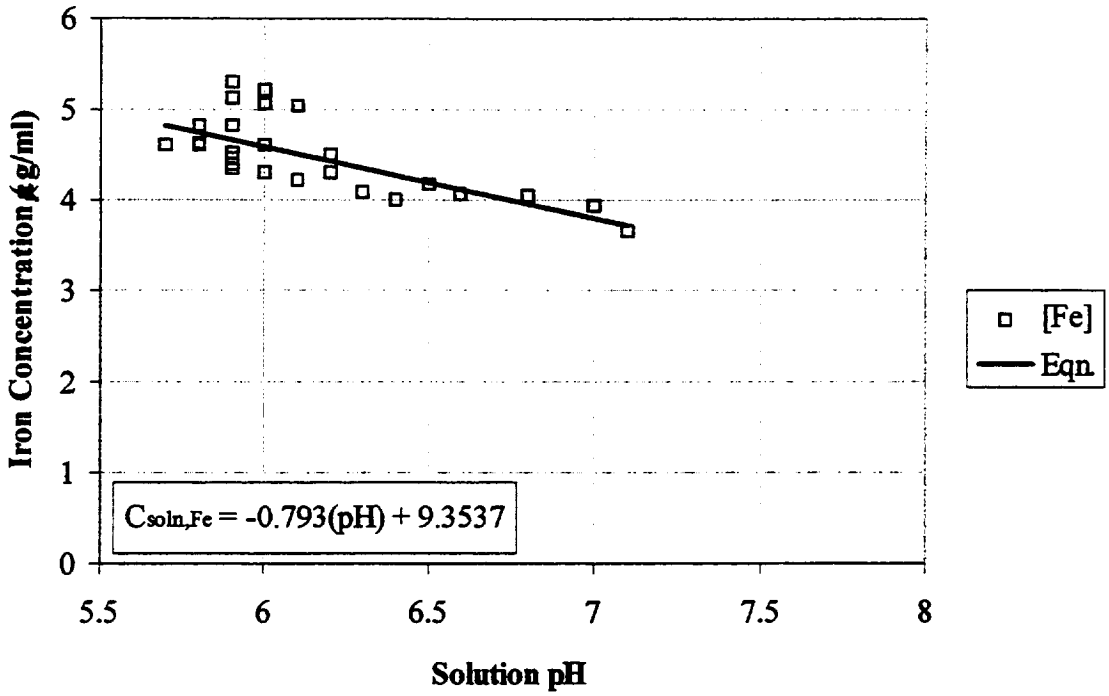

Figure D.5 Linear Regression of the Concentration of Soluble Iron as a Function of Solution pH

Table D.14 Analysis of Variance Table for the Adequate Relationship Between the Soluble Iron Concentration (Y) versus Solution pH (X1)

	DOF	Sum Sqs.	Mean Sqs.	Fcalc		Fcrit	Signif?
Total	27	548.88				$\alpha_{risk} = 0.05$	
Model	2	546.55	273.28	2938.1	>	3.806	yes
b0	1	544.28	544.28	5851.7	>	4.667	yes
b1	1	2.277	2.277	24.476	>	4.667	yes
Resid	25	2.325	0.093				
Error	13	1.757	0.135				
LOT	12	0.568	0.047	0.509	<	2.604	no

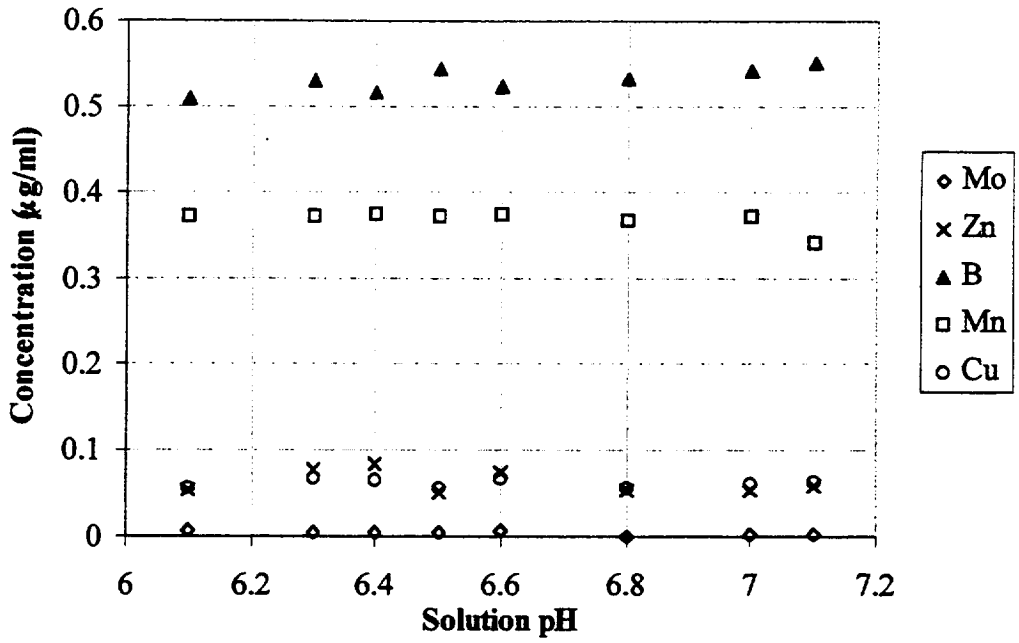

Figure D.6 Concentrations of the Other Micro-Nutrients (except Iron) as a Function of Solution pH

The mass balance for the growth of tomato plants on the PCT-NDS is divided into two portions. For the first portion, the total mass of inorganic nutrients taken up in the plants as determined from the tissue samples were calculated using the following equation.

$$q_{plant,i} = \sum_{plant} (C_{leaf,i}\, W_{leaf,d} + C_{branch,i}\, W_{branch,d} + C_{root,i}\, W_{root,d}) \qquad (8.26)$$

The error associated with these quantities, $\sigma_{qplant,i}$, were calculated using Equation (D.7).

$$\sigma_{qplant,i} = \{ \sum_{plant} [(\frac{\delta q_{plant,i}}{\delta C_{leaf,i}})^2 (\sigma_{Cleaf,i})^2 + (\frac{\delta q_{plant,i}}{\delta C_{branch,i}})^2 (\sigma_{Cbranch,i})^2 + (\frac{\delta q_{plant,i}}{\delta C_{root,i}})^2 (\sigma_{Croot,i})^2 + (\frac{\delta q_{plant,i}}{\delta W_{leaf,d}})^2 (\sigma_{Wleaf,d})^2 + (\frac{\delta q_{plant,i}}{\delta W_{branch,d}})^2 (\sigma_{Wbranch,d})^2 + (\frac{\delta q_{plant,i}}{\delta W_{root,d}})^2 (\sigma_{Wroot,d})^2] \}^{1/2} \qquad (D.7)$$

The errors associated with the tissue dry weights, $\sigma_{Wtissue,d}$, were approximated as being equal for each of the different tissue types. Similarly, the nutrient concentrations measured

using the ICP-AES contain a general error for each nutrient, $\sigma_{Ctissue,i,ave}$, as listed in Table 8.7. Therefore, Equation (D.7) can be simplified using these general errors. Furthermore, each of the partial differential terms are easily solved as shown in Equation (D.8) below.

$$\sigma_{qplant,i} = \{ \sum_{plant} [(W_{leaf,d})^2 + (W_{branch,d})^2 + (W_{root,d})^2][\sigma_{Ctissue,i,ave}]^2 + [(C_{leaf,i})^2 + (C_{branch,i})^2 + (C_{root,i})^2][\sigma_{Wtissue,d}]^2 \}^{1/2} \quad (D.8)$$

The individual tissue concentrations and dry weight values used to determine these errors for each of the different test bed units are provided in Tables D.15 to D.18 below.

Table D.15 Plant Tissue Concentrations and Dry Weight Measurements Obtained for the Tomato Plants Produced on TBU-1a during Experiment #10 (0.30 μm @ 1x Conc.)

(μg/g)	1a-L	1a-B	1a-R
DryWgt(g)	0.7348	0.6142	0.3298
P	5628.30	2740.80	6302.00
Mg	12595.00	5946.70	9726.50
Ca	27142.50	10390.00	11076.70
Na	443.33	916.67	859.66
K	24895.00	61560.00	47493.35
Mo	4.20	3.30	4.20
Zn	90.80	10.80	213.70
B	61.70	22.50	28.30
Mn	60.80	22.50	160.50
Fe	266.70	435.80	1059.20
Cu	20.00	7.50	41.60

Table D.16 Plant Tissue Concentrations and Dry Weight Measurements Obtained for the Tomato Plants Produced on TBU-1b during Experiment #10 (0.30 μm @ 1x Conc.)

(μg/g)	1b-L	1b-B	1b-R
DryWgt(g)	0.1172	0.0637	0.0845
P	3419.60	1566.00	4103.00
Mg	13734.70	10966.50	9816.30
Ca	27429.40	13633.80	13515.90
Na	437.44	1956.32	414.27
K	29007.53	83159.85	52662.10
Mo	7.10	9.30	7.20
Zn	129.40	69.70	709.70
B	108.20	46.50	32.40
Mn	119.90	32.50	54.00
Fe	552.70	627.30	489.90
Cu	37.60	13.90	36.00

Table D.17 Plant Tissue Concentrations and Dry Weight Measurements Obtained for the Tomato Plants Produced on TBU-2a during Experiment #10 (1.5 μm @ 1/4x Conc.)

(μg/g)	2a-1-L	2a-1-B	2a-1-R	2a-2-L	2a-2-B	2a-2-R
DryWgt(g)	0.0831	0.0711	0.0346	0.5797	0.7084	0.2898
P	6671.69	4333.33	10647.84	3742.93	3096.07	5333.99
Mg	11030.12	6872.34	9692.69	8338.04	6086.41	8037.55
Ca	31057.23	15379.43	17666.11	23375.46	10482.85	5240.12
Na	463.86	1393.62	1154.49	157.96	490.34	3163.04
K	31686.75	108482.3	52574.75	21073.33	43484.85	32581.03
Mo	15.06	7.09	16.61	2.49	1.67	2.96
Zn	93.37	106.38	456.81	69.84	54.11	689.72
B	69.28	49.65	66.45	86.46	25.81	15.81
Mn	84.34	21.28	282.39	35.75	13.32	36.56
Fe	358.43	301.42	539.87	141.34	170.66	463.44
Cu	15.06	7.09	16.61	13.3	6.66	46.44
	2a-3-L	2a-3-B	2a-3-R	2a-4-L	2a-4-B	2a-4-R
DryWgt(g)	0.0759	0.0542	0.0864	0.0958	0.0573	0.0583
P	3870.74	3750	5453.64	6334.29	4041.67	5369.08
Mg	10987.22	9203.59	8581.75	10260	8037.97	6406.69
Ca	31949.57	18428.27	5543.37	27317.14	16903.85	5605.85
Na	422.59	1191.98	3222.83	285.71	1292.8	564.07
K	21452.41	66861.81	33796.11	28877.14	87672.04	55954.04
Mo	7.1	10.55	4.99	8.57	8.82	13.93
Zn	88.78	79.11	735.29	60	92.75	605.85
B	88.78	36.92	22.43	68.57	43.29	27.86
Mn	53.27	26.37	39.88	57.14	23.83	62.67
Fe	372.87	458.86	456.13	245.71	380.14	480.5
Cu	21.31	15.82	47.36	17.14	11.46	20.89

Table D.18 Plant Tissue Concentrations and Dry Weight Measurements Obtained for the Tomato Plants Produced on TBU-2b during Experiment #10 (1.5 μm @ 1x Conc.)

(μg/g)	2b-L	2b-B	2b-R
DryWgt(g)	0.5534	0.4723	0.3625
P	2883.20	1261.60	6328.10
Mg	11068.00	6022.50	7308.10
Ca	19209.40	6681.00	24182.70
Na	327.39	797.49	761.63
K	20664.78	65659.33	41958.47
Mo	4.20	2.50	2.50
Zn	67.50	16.60	185.20
B	109.10	23.20	21.60
Mn	59.20	18.20	60.60
Fe	207.40	206.80	690.20
Cu	19.20	6.60	29.90

For the second portion of the mass balance, the quantities of standard solution added to the systems were compared to the soluble and precipitated quantities remaining after the plants were removed. In order to determine the total quantities of each nutrient supplied to each of the systems, Equation (8.38) was used.

$$q_{input,i} = C_{sample,i,init} \frac{V_{sample}}{V_{soln}} (V_{sys} + \sum_j \Delta V_{res,j} + \sum_k V_{soln}) \qquad (8.38)$$

The system volumes, V_{sys}, and supply quantities due to the depletion by the tomato plants, $\Sigma_j \Delta V_{res,j}$, and for sampling replenishment, $\Sigma_k V_{soln}$, are provided in Table D.19 below for the experiment used to prove the mass balances. The first number in each column on this table represents the volumes prior to the imposition of the test conditions of (+1/ 0) and (-1/ 0). As for the standard solution concentrations, these were presented in Table D.6.

Table D.19 Volumes (in ml) of Standard Solutions Supplied during Experiment #10

Test Bed Unit	V_{sys}	$\Sigma_k V_{soln}$	$\Sigma_j \Delta V_{res,j}$ (1x)	$\Sigma_j \Delta V_{res,j}$ (1/4x)
#1a (0.30)	578 + 578	156.8 + 58.8	83 + 312	0 + 0
#1b (0.30)	558 + 558	156.8 + 58.8	32 + 84	0 + 0
#2a (1.5)	590 + 568	156.8 + 58.8	198 + 0	0 + 473
#2b (1.5)	569 + 569	156.8 + 58.8	131 + 285	0 + 0

The errors associated with the various measured quantities in this equation were propagated through as shown in Equation (D.9) below in order to determine the error associated with $q_{input,i}$. This was conducted by taking the partial derivative of $q_{input,i}$ with respect to each of the terms appearing in Equation (8.38).

$$\sigma_{qinput,i} = \{\left(\frac{\delta q_{input,i}}{\delta C_{sample,i}}\right)^2 (\sigma_{Csample,i})^2 + \left(\frac{\delta q_{input,i}}{\delta V_{sample}}\right)^2 (\sigma_{Vsample})^2 + \left(\frac{\delta q_{input,i}}{\delta V_{soln}}\right)^2 (\sigma_{Vsoln})^2$$

$$+ \left(\frac{\delta q_{input,i}}{\delta V_{sys}}\right)^2 (\sigma_{Vsys})^2 + \sum_j \left[\left(\frac{\delta q_{input,i}}{\delta \Delta V_{res,j}}\right)^2 (\sigma_{\Delta Vres,j})^2\right]\}^{1/2} \qquad (D.9)$$

Since the error associated with the preparation of a liquid ICP sample is equivalent to the error associated with the measurement of the solution for the sample, then $\sigma_{V_{sample}} = \sigma_{V_{soln}}$. Furthermore, the error associated with the measurement of the system volume and the error associated with measuring the daily changes in the reservoir volume are equivalent as well. Therefore, $\sigma_{V_{sys}} = \sigma_{V_{res,j}}$. Substituting these simplifications into Equation (D.9) as well as performing the simple partial differentiations leads to Equation (D.10) used to calculate the error associated with the quantities of inorganic nutrients supplied to each unit, $\sigma_{q_{input,i}}$. These errors are presented along with the absolute values for $q_{input,i}$ in Table D.20 below for the different test bed units.

$$\sigma_{q_{input,i}} = \{\left(\frac{V_{sample}}{V_{soln}}\right)^2 (V_{sys} + \sum_j \Delta V_{res,j} + \sum_k V_{soln})^2 (\sigma_{C_{sample,i}})^2$$

$$+ \left(\frac{C_{sample,i,init}}{V_{soln}}\right)^2 [(V_{sys} + \sum_j \Delta V_{res,j} + \sum_k V_{soln})^2 + \left(\frac{-V_{sample}}{V_{soln}}\right)^2 (V_{sys} + \sum_k \Delta v_{res,j})^2] (\sigma_{V_{sample}})^2$$

$$+ (j+1)(C_{sample,i,init}\frac{V_{sample}}{V_{soln}})^2 (\sigma_{V_{sys}})^2\}^{1/2} \qquad \text{(D.10)}$$

Table D.20 The Total Quantities of Inorganic Nutrients and the Related Error Ranges as Measured in the Supply to the Tomato Plants Grown during Experiment #10

Nutrient	$q_{input,i}$ (μg) - 1a	$q_{input,i}$ (μg) - 1b	$q_{input,i}$ (μg) - 2a	$q_{input,i}$ (μg) - 2b
P	50507 ± 1387	41387 ± 1135	34677 ± 1063	50593 ± 1386
Mg	159257 ± 11541	130500 ± 9437	108908 ± 8724	159528 ± 11535
Ca	352314 ± 29874	288696 ± 24427	237324 ± 22554	352912 ± 29857
Na	20197 ± 161	16550 ± 133	14006 ± 410	20231 ± 161
K	383478 ± 7819	314233 ± 6402	266818 ± 7316	384130 ± 7814
Mo	46.87 ± 11.43	38.41 ± 9.35	47.51 ± 8.63	46.95 ± 11.43
Zn	104.55 ± 16.67	85.67 ± 13.63	106.42 ± 32.25	104.73 ± 16.66
B	1229.41 ± 207.07	1007.41 ± 169.30	848.29 ± 157.53	1231.50 ± 206.95
Mn	789.56 ± 79.62	646.99 ± 65.10	537.30 ± 60.32	790.90 ± 79.58
Fe	8025.41 ± 278.06	6576.24 ± 227.46	5606.12 ± 213.69	8039.04 ± 277.91
Cu	270.40 ± 76.17	221.57 ± 62.28	363.45 ± 60.67	270.86 ± 76.13

For the quantities of nutrients either removed or remaining in the system, $q_{rem,i}$, Equation (8.39) was used to determine these values.

$$q_{rem,i} = \frac{C_{sample,i,final} V_{sample}}{V_{soln}} (V_{sys} - \Delta V_{res,f}) + \sum_{k} (C_{sample,i,k} V_{sample}) \qquad (8.39)$$

The system volumes, V_{sys}, and final solution uptake quantities, $\sigma_{Vres,f}$, are provided in Table D.21 below for the experiment used to prove the mass balances. The first number in each column on this table represents the volumes prior to the imposition of the test conditions of (+1/ 0) and (-1/ 0). As for the nutrient concentrations in the periodic samples taken before and after the change to the test solutions, these are presented in Tables D.22 to D.29.

Table D.21 Volumes (in ml) of Solutions Remaining an the end of Experiment #10

Test Bed Unit	V_{sys}	$\Delta V_{res,f}$ (1x)	$\Delta V_{res,f}$ (1/4x)
#1a (0.30)	578 + 578	10 + 30	0 + 0
#1b (0.30)	558 + 558	2 + 8	0 + 0
#2a (1.5)	590 + 568	21 + 0	0 + 44
#2b (1.5)	569 + 569	15 + 18	0 + 0

Table D.22 Concentrations of the Periodic Solution Samples for TBU-1a Taken During Experiment #10 (k = sample designation)

Before Solution Change:

	k = 1	k = 2	k = 3	k = 4	k = 5	k = 6	k = 7	k = 8	k = f
P	27.50	27.00	26.70	26.00	25.60	24.60	22.90	21.90	20.40
Mg	104.20	103.30	103.90	103.90	104.70	107.10	109.00	111.80	102.50
Ca	205.20	204.60	203.60	203.60	206.30	207.80	211.70	214.00	218.00
Na	12.44	12.38	12.44	12.44	13.00	13.77	14.03	14.56	14.73
K	226.34	219.59	217.95	217.95	224.21	226.14	229.36	231.83	218.15
Mo	0.00	0.10	0.10	0.10	0.10	0.00	0.00	0.10	0.00
Zn	1.30	1.40	1.50	1.50	1.70	1.80	1.80	1.90	1.80
B	0.80	0.80	0.70	0.70	0.70	0.70	0.70	0.80	1.00
Mn	0.50	0.40	0.40	0.40	0.40	0.40	0.40	0.40	0.40
Fe	4.30	4.20	4.10	4.00	3.90	3.80	3.80	4.00	4.10
Cu	0.20	0.20	0.20	0.20	0.20	0.20	0.20	0.20	0.20
pH	5.94	6.04	6.19	6.26	6.31	6.44	6.52	6.62	6.77

After Solution Change:

	k = 1	k = 2	k = 3	k = f
P	26.70	25.50	24.70	24.10
Mg	88.90	95.70	104.80	95.40
Ca	185.20	203.30	217.80	178.80
Na	12.41	13.57	16.08	17.15
K	219.66	218.16	226.67	215.43
Mo	0.00	0.00	0.00	0.00
Zn	0.30	0.40	0.60	0.70
B	0.50	0.50	0.60	0.60
Mn	0.40	0.40	0.40	0.40
Fe	4.20	4.30	4.90	4.90
Cu	0.20	0.20	0.30	0.30
pH	6.08	6.32	6.48	6.74

Table D.23 Concentrations of the Periodic Solution Samples for TBU-1b Taken During Experiment #10 (k = sample designation)

Before Solution Change:

	k = 1	k = 2	k = 3	k = 4	k = 5	k = 6	k = 7	k = 8	k = f
P	26.50	25.70	25.20	23.60	19.60	16.10	14.60	11.60	9.40
Mg	101.50	102.50	102.30	101.90	101.30	103.60	105.10	105.50	94.50
Ca	202.90	204.80	200.70	200.60	197.40	191.10	198.00	193.10	191.10
Na	11.99	11.80	12.20	12.01	12.70	12.91	13.16	13.30	13.37
K	219.83	215.05	218.39	214.43	220.98	220.85	225.58	224.17	215.90
Mo	0.10	0.00	0.00	0.10	0.00	0.10	0.10	0.00	0.00
Zn	1.20	1.40	1.50	1.80	2.00	2.10	2.10	2.20	2.10
B	0.70	0.70	0.70	0.70	0.70	0.70	0.70	0.70	0.90
Mn	0.40	0.40	0.40	0.40	0.40	0.40	0.40	0.40	0.40
Fe	4.20	4.00	3.90	3.70	3.50	3.40	3.30	3.20	3.10
Cu	0.10	0.10	0.10	0.10	0.10	0.10	0.10	0.10	0.10
pH	6.15	6.28	6.42	6.50	6.79	6.93	7.12	7.39	7.63

After Solution Change:

	k = 1	k = 2	k = 3	k = f
P	26.50	22.50	12.20	7.20
Mg	87.20	92.20	91.90	82.60
Ca	188.20	190.50	176.30	140.60
Na	12.16	12.25	13.10	13.66
K	225.77	224.28	233.34	226.59
Mo	0.00	0.00	0.00	0.00
Zn	0.40	0.70	0.90	1.10
B	0.40	0.50	0.50	0.50
Mn	0.40	0.40	0.40	0.40
Fe	3.40	3.60	3.80	4.20
Cu	0.20	0.20	0.20	0.20
pH	6.69	7.05	7.65	7.82

Table D.24 Concentrations of the Periodic Solution Samples for TBU-2a Taken During Experiment #10 (k = sample designation)

Before Solution Change:

	k = 1	k = 2	k = 3	k = 4	k = 5	k = 6	k = 7	k = 8	k = f
P	26.70	25.80	27.50	28.50	26.10	25.10	23.90	21.90	20.00
Mg	102.80	101.60	106.70	113.00	113.40	120.10	121.40	129.40	110.60
Ca	204.50	201.80	217.40	229.90	228.60	240.80	238.80	249.40	227.80
Na	11.78	11.63	11.53	11.34	11.56	12.30	13.10	14.16	15.05
K	220.16	216.74	212.78	207.66	208.90	212.62	217.55	215.73	215.77
Mo	0.00	0.00	0.00	0.00	0.00	0.00	0.00	0.00	0.00
Zn	1.10	1.20	1.20	1.30	1.50	1.50	1.50	1.60	1.50
B	0.80	0.70	0.70	0.70	0.80	0.80	0.80	0.90	1.00
Mn	0.50	0.50	0.50	0.50	0.50	0.50	0.50	0.50	0.50
Fe	4.30	4.10	4.10	3.90	3.90	3.80	4.00	4.30	4.50
Cu	0.10	0.10	0.10	0.10	0.10	0.10	0.10	0.20	0.20
pH	5.94	6.05	6.18	6.33	6.48	6.63	6.69	6.78	6.78

After Solution Change:

	k = 1	k = 2	k = 3	k = f
P	7.80	7.00	4.40	3.30
Mg	28.30	28.50	24.70	22.30
Ca	64.00	65.10	55.10	47.40
Na	3.21	3.74	4.43	3.79
K	52.70	36.68	28.77	13.48
Mo	0.00	0.00	0.00	0.00
Zn	0.40	0.50	0.70	0.70
B	0.10	0.10	0.20	0.20
Mn	0.10	0.10	0.00	0.00
Fe	1.00	1.10	1.30	1.50
Cu	0.20	0.20	0.20	0.30
pH	6.14	6.67	7.2	7.26

Table D.25 Concentrations of the Periodic Solution Samples for TBU-2b Taken During Experiment #10 (k = sample designation)

Before Solution Change:

	k = 1	k = 2	k = 3	k = 4	k = 5	k = 6	k = 7	k = 8	k = f
P	26.40	22.40	18.80	15.30	13.20	11.50	11.20	11.00	10.80
Mg	100.70	98.80	100.00	101.10	102.70	100.90	100.80	116.00	105.90
Ca	204.90	192.80	193.50	181.20	177.00	173.40	171.10	195.50	197.50
Na	14.10	13.82	13.72	13.62	14.31	14.79	14.53	15.39	16.03
K	222.38	215.61	216.21	218.11	223.98	229.25	225.33	237.37	236.72
Mo	0.00	0.00	0.00	0.00	0.00	0.00	0.00	0.00	0.00
Zn	1.10	1.10	1.10	1.10	1.10	1.20	1.20	1.10	1.10
B	0.70	0.80	0.70	0.70	0.70	0.80	0.80	0.80	1.00
Mn	0.50	0.40	0.40	0.40	0.40	0.50	0.50	0.50	0.50
Fe	4.30	4.10	3.90	3.60	3.50	3.50	3.60	3.60	3.90
Cu	0.10	0.10	0.10	0.10	0.10	0.10	0.10	0.10	0.10
pH	6.31	6.87	7.17	7.43	7.46	7.53	7.55	7.74	7.73

After Solution Change:

	k = 1	k = 2	k = 3	k = f
P	23.30	20.50	17.30	14.70
Mg	90.70	104.50	109.30	100.50
Ca	193.60	202.00	197.90	168.30
Na	12.75	14.76	15.75	16.80
K	218.92	247.65	256.73	257.12
Mo	0.00	0.10	0.00	0.00
Zn	0.20	0.30	0.30	0.40
B	0.50	0.60	0.60	0.60
Mn	0.40	0.50	0.50	0.50
Fe	4.10	4.30	4.50	4.50
Cu	0.20	0.30	0.30	0.30
pH	6.42	6.88	6.99	7.05

The errors associated with the various measured quantities in this equation were propagated through as shown in Equation (D.11) below in order to determine the error associated with $q_{rem,i}$. This was conducted by taking the partial derivative of $q_{rem,i}$ with respect to each of the terms appearing in Equation (8.39).

$$\sigma_{qrem,i} = \{(\frac{\delta q_{rem,i}}{\delta C_{sample,i,final}})^2(\sigma_{Csample,i})^2 + (\frac{\delta q_{rem,i}}{\delta V_{soln}})^2(\sigma_{Vsoln})^2 + (\frac{\delta q_{rem,i}}{\delta V_{sample}})^2(\sigma_{Vsample})^2$$
$$+ (\frac{\delta q_{rem,i}}{\delta V_{sys}})^2(\sigma_{Vsys})^2 + (\frac{\delta q_{rem,i}}{\delta \Delta V_{res,j}})^2(\sigma_{\Delta Vres,j})^2 + \sum_k [(\frac{\delta q_{rem,i}}{\delta C_{sample,i,k}})^2(\sigma_{Csample,i})^2]\}^{1/2} \quad \text{(D.11)}$$

Again, $\sigma_{Vsample} = \sigma_{Vsoln}$ and $\sigma_{Vsys} = \sigma_{Vres,j}$. Therefore, substituting these simplifications into Equation (D.11) as well as performing the simple partial differentiations leads to Equation (D.12) used to calculate the error associated with the quantities of inorganic nutrients either removed or remaining in each unit, $\sigma_{qrem,i}$. These errors are presented along with the absolute values for $q_{rem,i}$ in Table D.26 below for the different test bed units.

$$\sigma_{qrem,i} = \{\{[\frac{V_{sample}}{V_{soln}}(V_{sys} - \Delta V_{res,f})]^2 + k[V_{sample}]^2\}\{\sigma_{Csample,i}\}^2$$
$$+ \{[\frac{-C_{sample,i,final}V_{sample}}{V_{soln}^2}(V_{sys} - \Delta V_{res,f})]^2$$
$$+ [\frac{C_{sample,i,final}}{V_{soln}}(V_{sys} - \Delta V_{res,f}) + \Sigma_k C_{sample,i,k}]^2\}\{\sigma_{Vsample}\}^2$$
$$+ \{2[\frac{C_{sample,i,final}V_{sample}}{V_{soln}}]^2\}\{\sigma_{Vsys}\}^2\}^{1/2} \quad \text{(D.12)}$$

Table D.26 The Total Quantities of Inorganic Nutrients and the Related Error Ranges Measured in the Solution Removed or Remaining in the System after Experiment #10

Nutrient	$q_{rem,i}$ (μg) - 1a	$q_{rem,i}$ (μg) - 1b	$q_{rem,i}$ (μg) - 2a	$q_{rem,i}$ (μg) - 2b
P	30882 ± 873	13856 ± 855	17871 ± 850	18188 ± 857
Mg	135500 ± 7306	121871 ± 7235	95937 ± 7154	138882 ± 7236
Ca	271595 ± 18896	230200 ± 18713	197516 ± 18512	247932 ± 18701
Na	21070 ± 127	18003 ± 115	12940 ± 105	21658 ± 128
K	296060 ± 4981	298511 ± 4943	169092 ± 4800	328614 ± 4983
Mo	10.00 ± 7.23	8.00 ± 7.16	0.00 ± 7.08	2.00 ± 7.16
Zn	1718.69 ± 13.86	2134.78 ± 14.97	1495.20 ± 12.85	1042.73 ± 11.77
B	1056.10 ± 130.96	931.22 ± 129.75	819.55 ± 128.35	1056.65 ± 129.65
Mn	545.51 ± 50.34	539.43 ± 49.88	374.31 ± 49.33	663.78 ± 49.87
Fe	6026.33 ± 176.16	4915.92 ± 173.82	4130.80 ± 171.82	5594.80 ± 174.13
Cu	329.67 ± 48.17	196.98 ± 47.72	306.53 ± 47.22	257.20 ± 47.69

For the quantities of nutrients precipitated in the system due to the change in pH, $q_{precip,i}$, Equation (8.40) was used to determine these values.

$$q_{precip,i} = \left(\frac{1 - f_{sol,i}}{f_{sol,i}}\right)\left(\frac{C_{sample,i,final} V_{sample}}{V_{soln}}\right)(V_{sys} - \Delta V_{res,f}) \qquad (8.40)$$

The system volumes, V_{sys}, and final solution uptake quantities, $\Delta V_{res,f}$, were provided in Table D.21 for the experiment used to prove the mass balances. As for the solution concentrations of the periodic samples, these were presented in Tables D.22 to D.25.

The errors associated with the various measured quantities in this equation were propagated through as shown in Equation (D.13) below in order to determine the error associated with $q_{precip,i}$. This was conducted by taking the partial derivative of $q_{precip,i}$ with respect to each of the terms appearing in Equation (8.40).

$$\sigma_{qprecip,i} = \left\{\left(\frac{\delta q_{precip,i}}{\delta f_{sol,i}}\right)^2(\sigma_{fsol,i})^2 + \left(\frac{\delta q_{precip,i}}{\delta C_{sample,i,final}}\right)^2(\sigma_{Csample,i})^2 + \left(\frac{\delta q_{precip,i}}{\delta V_{sample}}\right)^2(\sigma_{Vsample})^2\right.$$
$$\left. + \left(\frac{\delta q_{precip,i}}{\delta V_{soln}}\right)^2(\sigma_{Vsoln})^2 + \left(\frac{\delta q_{precip,i}}{\delta V_{sys}}\right)^2(\sigma_{Vsys})^2 + \left(\frac{\delta q_{precip,i}}{\delta \Delta V_{res,f}}\right)^2(\sigma_{\Delta Vres,f})^2\right]\}^{1/2} \qquad (D.13)$$

Again, $\sigma_{V_{sample}} = \sigma_{V_{soln}}$ and $\sigma_{V_{sys}} = \sigma_{V_{res,j}}$. Furthermore, the values for $\sigma_{C_{sample,i}}$ can be obtained from Tables 8.8 to 8.10. Therefore, substituting these simplifications into Equation (D.13) as well as performing the simple partial differentiations leads to Equation (D.14) used to calculate the error associated with the quantities of precipitated inorganic nutrients in each unit, $\sigma_{qprecip,i}$.

$$\sigma_{qprecip,i} = \{[\frac{1}{f_{sol,i}^2} \frac{C_{sample,i,final} V_{sample}}{V_{soln}} (V_{sys} - \Delta V_{res,f})]^2 [\sigma_{fsol,i}]^2 \qquad (D.14)$$

$$+ [\frac{1 - f_{sol,i}}{f_{sol,i}} \frac{V_{sample}}{V_{soln}} (V_{sys} - \Delta V_{res,f})]^2 [\sigma_{C_{sample,i}}]^2 + 2[\frac{1 - f_{sol,i}}{f_{sol,i}} \frac{C_{sample,i,final} V_{sample}}{V_{soln}}]^2 [\sigma_{V_{sys}}]^2$$

$$+ [(\frac{1 - f_{sol,i}}{f_{sol,i}})^2 (\frac{C_{sample,i,final} V_{sample}}{V_{soln}})^2 (V_{sys} - \Delta V_{res,f})^2 (1 + \frac{V_{sample}^2}{V_{soln}^2})][\sigma_{V_{sample}}]^2\}^{1/2}$$

One term which has not been solved for in this equation is the error associated with the concentration ratios, $\sigma_{fsol,i}$. These can be derived from Equation (8.41) used to calculate $f_{sol,i}$.

$$f_{sol,i} = \frac{[b_{0,i} + b_{1,i}(pH) + b_{2,i}(pH)^2]}{[b_{0,i} + b_{1,i}(pH_0) + b_{2,i}(pH_0)^2]} \qquad (8.41)$$

This was conducted by taking the partial derivative of $f_{sol,i}$ with respect to the two pH values, pH and pH_0, appearing in Equation (8.41) as shown in Equation (D.15) shown below.

$$\sigma_{fsol,i} = [(\frac{\delta f_{sol,i}}{\delta pH})^2 (\sigma_{pH})^2 + (\frac{\delta f_{sol,i}}{\delta pH_0})^2 (\sigma_{pH_0})^2]^{1/2} \qquad (D.15)$$

Using the assumption that $\sigma_{pH_0} = \sigma_{pH}$ and taking the partial derivatives in Equation (D.15) results in Equation (D.16) for the propagated errors for the concentration ratios.

$$\sigma_{fsol,i} = \{\frac{[b_{1,i} + 2b_{2,i}(pH)]^2}{[b_{0,i} + b_{1,i}(pH_0) + b_{2,i}(pH_0)^2]^2}[\sigma_{pH}]^2 + \frac{[b_{0,i} + b_{1,i}(pH) + b_{2,i}(pH)^2]^2}{[b_{0,i} + b_{1,i}(pH_0) + b_{2,i}(pH_0)^2]^4}[b_{1,i} + 2b_{2,i}(pH_0)]^2[\sigma_{pH}]^2\}^{1/2} \quad \text{(D.16)}$$

Since the regression equations describing the relationships between the concentration of the nutrients in solution and the pH vary from a constant, $b_{0,i}$, such as for K to a quadratic equation such as for P, the values for $\sigma_{fsol,i}$ are dependent upon these model parameters. The values for these parameters are identical to those found in Equations (8.30) to (8.34). Using these errors in Equation (D.14) allows for the complete propagation of the errors for the determination of $\sigma_{qprecip,i}$. These results are presented along with the absolute values for $q_{precip,i}$ in Table D.27 below for the different test bed units.

Table D.27 The Total Quantities of Inorganic Nutrients and the Related Error Ranges as Calculated for the Precipitates Formed during Experiment #10

Nutrient	$q_{precip,i}$ (µg) - 1a	$q_{precip,i}$ (µg) - 1b	$q_{precip,i}$ (µg) - 2a	$q_{precip,i}$ (µg) - 2b
P	7285 ± 1228	31079 ± 7681	5057 ± 856	23879 ± 5013
Mg	5321 ± 934	9425 ± 1672	3954 ± 655	9134 ± 1551
Ca	44343 ± 8494	84914 ± 17341	34681 ± 6049	76313 ± 14709
Na				
K	0 ± 0	0 ± 0	0 ± 0	0 ± 0
Mo				
Zn				
B				
Mn				
Fe	1069.72 ± 169.96	2072.13 ± 326.16	838.56 ± 130.29	1820.83 ± 284.12
Cu				

APPENDIX E - STATISTICAL ANALYSES - NUTRIENT UPTAKE RESULTS

The statistical analyses of the functions describing the nutrient uptake kinetics are presented in this appendix. This includes the data for the factors, X, and the responses, Y, used to produce the various models. In addition, the analysis of variances (ANOVA) tables produced for the various steps in the development of the nutrient uptake models are provided as well. These tables were generated on a Microsoft Excel v.5.0 Spreadsheet.

Initially, the total quantity of nutrients in the plants (Y) modeled as exponential functions of the leaf stage (X1), root-zone water potential (X2), and solution concentrations (X3) are presented. These models were produced using the sum of the individual tissue dry weights multiplied by the corresponding concentrations. These data are presented in Tables E.1 to E.6 for the various conditions that the plants were produced.

Table E.1 Data for the Plant Inorganic Quantities (Y) Including Total Weight and Leaf Stage (X1) for Tomato Plants Produced at a Root-Zone Water Potential (X2) of -0.117 MPa (π_{soil} = -0.078, P_m = -0.039), and a 1x Solution (X3)

		Quantities (μg)										
LS	**Wgt(g)**	**P**	**Mg**	**Ca**	**Na**	**K**	**Mo**	**Zn**	**B**	**Mn**	**Fe**	**Cu**
10	0.1888	1231	1741	4286	178	12165	2.33	31.13	11.59	18.29	69.90	2.33
13	1.3882	4485	11619	23358	834	57657	4.41	112.33	79.16	63.32	462.64	24.58
14	1.6788	7898	16115	29979	1172	71766	6.50	143.83	68.49	111.43	812.96	33.02
10	0.2654	847	3138	5225	211	13147	2.03	79.58	18.38	20.69	146.13	8.33
10	0.2994	1645	5618	8313	755	15927	1.94	73.54	21.48	34.48	168.45	9.65
12	0.64	2654	7598	19642	964	34658	2.61	124.15	59.32	94.82	412.90	12.84
10	0.2223	1132	2054	6413	417	13243	1.26	68.64	19.60	28.56	137.58	8.01
9	0.1091	546	1346	2546	235	8843	0.84	29.26	9.64	13.58	66.13	4.64
9	0.1605	531	2466	4368	481	11518	0.76	28.64	12.58	18.67	89.08	6.20
11	0.4587	2646	6124	15384	709	28164	1.62	169.35	53.00	67.46	221.82	10.15
14	2.5603	14615	30564	59454	2867	152752	7.27	250.82	150.26	199.93	843.16	63.72
14	1.9042	11910	22230	45215	2197	105458	3.83	224.48	115.43	165.72	718.05	43.90
14	2.6956	9748	38033	81594	4046	129882	3.07	336.11	182.46	154.98	1149.35	49.38
14	2.6119	10076	40741	72049	4219	124155	3.46	373.17	198.44	174.63	1316.97	50.98

Table E.2 Data for the Plant Inorganic Quantities (Y) Including Total Weight and Leaf Stage (X1) for Tomato Plants Produced at a Root-Zone Water Potential (X2) of -0.078 MPa (π_{soil} = -0.078, P_m = -0.000), and a 1x Solution (X3)

		Quantities (µg)										
LS	**Wgt(g)**	**P**	**Mg**	**Ca**	**Na**	**K**	**Mo**	**Zn**	**B**	**Mn**	**Fe**	**Cu**
14	3	14252	30148	66639	3157	128918	4.06	395.72	159.26	215.77	1441.40	28.04
13	1.95	11474	14777	35575	1401	84880	2.32	347.73	86.63	169.40	786.75	28.04
13	2.1	12487	16927	40185	1574	91423	2.73	280.48	96.71	225.53	775.38	19.61
11	0.7	4929	6143	15552	531	34994	1.33	63.86	30.21	90.20	343.52	8.13
14	2.9037	12596	17315	40710	1168	123296	3.23	574.60	123.49	126.39	1065.22	26.25
9	0.2435	1464	4621	6542	741	24452	1.46	46.06	9.48	39.82	106.58	7.81
9	0.2239	1213	5613	5138	547	17656	1.46	89.98	11.81	31.92	94.21	5.98
12	1.0875	4018	12512	23864	1678	61684	1.84	130.97	43.71	58.20	423.93	14.85
11	0.4836	2594	5064	11385	983	46521	2.82	173.45	21.18	72.50	147.58	9.48
12	1.0181	3108	12120	21287	1392	55860	1.58	122.52	44.10	52.82	381.90	13.63
13	2.0542	11944	20646	41654	1835	116246	4.08	451.18	73.18	282.56	975.85	28.94
12	0.8572	2256	9357	19646	910	43983	1.02	127.01	52.29	45.51	318.33	11.02
10	0.3979	2465	4957	10564	712	39282	2.92	172.16	20.82	81.65	132.56	9.00
10	0.2848	1513	5176	7313	654	22868	2.18	83.16	12.48	35.97	152.85	7.29
9	0.2185	964	3973	8646	713	15828	2.01	78.79	13.85	41.67	146.91	6.19
6	0.0447	397	1126	5417	238	5815	0.94	13.58	5.31	10.49	46.58	1.27
10	0.356	2164	4567	8925	781	38162	2.88	171.51	19.48	66.57	167.88	10.76
9	0.2316	1973	4852	4320	511	18358	2.32	65.48	10.00	38.82	172.02	6.87
9	0.1521	510	3462	7213	416	6852	1.84	48.19	8.11	20.48	100.82	4.05
5	0.0187	236	821	3181	186	513	0.06	10.45	2.58	7.19	27.82	0.91
5	0.0265	191	284	5132	281	1952	0.28	15.79	3.47	8.08	38.28	1.05
7	0.0594	364	3158	5168	381	4852	1.55	38.23	5.28	14.58	70.82	2.08
9	0.2172	1245	4258	8134	538	13264	2.03	86.87	8.48	34.68	150.82	5.19
11	0.6444	3588	7386	14905	649	35846	1.32	45.52	29.62	41.13	273.15	11.11
12	1.1421	4684	13648	31865	1583	76652	3.46	183.48	93.18	158.85	375.98	18.34
14	2.9304	15415	24681	70556	2816	139628	5.99	432.46	186.97	231.82	1148.46	31.82

Table E.3 Data for the Plant Inorganic Quantities (Y) Including Total Weight and Leaf Stage (X1) for Tomato Plants Produced at a Root-Zone Water Potential (X2) of -0.078 MPa (π_{soil} = -0.039, P_m = -0.039), and a 1/2x Solution (X3)

		Quantities (µg)										
LS	**Wgt(g)**	**P**	**Mg**	**Ca**	**Na**	**K**	**Mo**	**Zn**	**B**	**Mn**	**Fe**	**Cu**
7	0.0711	265	1461	3036	329	5594	0.76	31.32	6.98	20.86	64.94	4.64
9	0.1523	865	2859	7246	462	9645	0.96	58.80	10.89	24.87	91.52	5.11
10	0.2682	1245	3943	9548	678	14125	1.69	82.64	15.82	38.82	156.83	7.19
11	0.4289	2064	5643	12685	816	25052	1.44	146.46	20.56	45.85	189.78	11.84
12	0.9912	4168	9318	17649	1243	55943	2.36	158.83	49.60	95.82	359.40	26.94

Table E.4 Data for the Plant Inorganic Quantities (Y) Including Total Weight and Leaf Stage (X1) for Tomato Plants Produced at a Root-Zone Water Potential (X2) of -0.078 MPa (π_{soil} = -0.019, P_m = -0.059), and a 1/4x Solution (X3)

		Quantities (μg)										
LS	**Wgt(g)**	**P**	**Mg**	**Ca**	**Na**	**K**	**Mo**	**Zn**	**B**	**Mn**	**Fe**	**Cu**
8	0.0886	464	1765	2152	252	4418	0.73	37.37	6.88	17.64	55.48	2.91
11	0.4539	1555	4194	15356	650	12861	1.65	86.82	27.60	72.68	178.89	15.96
12	0.9928	3014	9520	18721	848	32767	2.03	221.24	37.17	91.01	357.76	29.23

Table E.5 Data for the Plant Inorganic Quantities (Y) Including Total Weight and Leaf Stage (X1) for Tomato Plants Produced at a Root-Zone Water Potential (X2) of -0.058 MPa (π_{soil} = -0.019, P_m = -0.039), and a 1/4x Solution (X3)

		Quantities (μg)										
LS	**Wgt(g)**	**P**	**Mg**	**Ca**	**Na**	**K**	**Mo**	**Zn**	**B**	**Mn**	**Fe**	**Cu**
9	0.2165	968	2074	3903	375	8172	1.54	74.56	10.68	8.92	92.58	6.57
9	0.2114	1151	1817	3912	134	11052	1.56	46.38	10.67	10.49	73.33	3.52
13	1.5779	5260	11474	22495	1356	52463	3.48	278.70	72.99	46.49	337.14	25.89
9	0.2133	1052	2264	6423	264	9513	1.04	64.48	9.82	13.90	81.97	5.19
12	1.053	3546	10894	21635	1096	35642	2.42	165.62	52.84	45.67	246.48	19.38

Table E.6 Data for the Plant Inorganic Quantities (Y) Including Total Weight and Leaf Stage (X1) for Tomato Plants Produced at a Root-Zone Water Potential (X2) of -0.019 MPa (π_{soil} = -0.019, P_m = -0.000), and a 1/4x Solution (X3)

		Quantities (μg)										
LS	**Wgt(g)**	**P**	**Mg**	**Ca**	**Na**	**K**	**Mo**	**Zn**	**B**	**Mn**	**Fe**	**Cu**
11	0.75	3279	6363	12997	764	30455	0.96	130.11	34.81	77.15	365.01	25.34
12	1.35	5712	10736	25511	936	57288	1.24	180.17	59.74	87.13	481.23	30.30
13	2.3	9418	22413	41289	3431	79620	3.94	223.52	135.53	143.20	676.32	42.23
13	2.95	8410	26728	52548	4956	68531	3.28	316.71	248.87	139.68	704.43	85.43
8	0.1501	1233	2946	7654	245	6213	0.72	39.38	7.05	6.94	59.58	3.18
8	0.1741	1435	3642	7618	319	9644	0.93	65.18	8.46	8.10	68.04	4.27
8	0.193	1764	6632	8400	418	15943	1.09	73.18	9.41	9.49	78.40	4.98
6	0.0562	905	652	4385	125	2751	0.61	28.44	4.25	4.96	20.58	1.50

In order to produce the models for the inorganic nutrient quantities, $q_{plant,i}$, the exponential equations were linearized by taking the natural logarithms of the quantities (Y) and individual nutrient concentrations (X3). This was conducted on the concentration in order to obtain this variable as a pre-exponential factor in the final models for the

nutrient quantities, $q_{plant,i}$. In each case, the effect of the leaf stage on $q_{plant,i}$ were consistently shown to be significant contributions, regardless of the nutrient. As for the other factors, their significances were dependent upon the particular nutrient. These were determined from the analysis of variances of the terms in the linearized models. The resulting ANOVA tables are provided for the final adequate models below in Tables E.7 to E.17 for the nutrients, P, Mg, Ca, Na, K, Mo, Zn, B, Mn, Fe, and Cu, respectively.

Table E.7 Analysis of Variance Table for the Final Adequate Model for the Natural Log of the Phosphorus Quantity (Y) as a Linear Function of Leaf Stage (X1), Root-Zone Water Potential (X2), and Solution Phosphorus Concentration (X3)

	DOF	Sum Sqs.	Mean Sqs.	Fcalc		Fcrit	Signif?
Total	61	3716				$\alpha_{risk} = 0.05$	
Model	4	3710	928	8826	>	2.690	yes
c0	1	3638	3638	34616	>	4.171	yes
c1	1	67.769	67.769	644.90	>	4.171	yes
c2	1	3.155	3.155	30.020	>	4.171	yes
c3	1	1.511	1.511	14.380	>	4.171	yes
Resid	57	5.990	0.105				
Error	30	2.260	0.075				
LOT	27	3.729	0.138	1.314	<	1.862	no

Table E.8 Analysis of Variance Table for the Final Adequate Model for the Natural Log of the Magnesium Quantity (Y) as a Linear Function of Leaf Stage (X1), Root-Zone Water Potential (X2), and Solution Magnesium Concentration (X3)

	DOF	Sum Sqs.	Mean Sqs.	Fcalc		Fcrit	Signif?
Total	61	4652				$\alpha_{risk} = 0.05$	
Model	4	4645	1161	9086	>	2.690	yes
c0	1	4586	4586	35882	>	4.171	yes
c1	1	56.758	56.758	444.09	>	4.171	yes
c2	1	1.169	1.169	9.149	>	4.171	yes
c3	1	1.259	1.259	9.854	>	4.171	yes
Resid	57	7.285	0.128				
Error	30	3.074	0.102				
LOT	27	4.211	0.156	1.220	<	1.862	no

Table E.9 Analysis of Variance Table for the Final Adequate Model for the Natural Log of the Calcium Quantity (Y) as a Linear Function of Leaf Stage (X1), Root-Zone Water Potential (X2), and Solution Calcium Concentration (X3)

	DOF	Sum Sqs.	Mean Sqs.	Fcalc		Fcrit	Signif?
Total	61	5500				$\alpha_{risk} = 0.05$	
Model	4	5493	1373	9935	>	2.690	yes
c0	1	5446	5446	39405	>	4.171	yes
c1	1	43.349	43.349	313.63	>	4.171	yes
c2	1	1.265	1.265	9.152	>	4.171	yes
c3	1	1.554	1.554	11.244	>	4.171	yes
Resid	57	7.878	0.138				
Error	30	2.162	0.072				
LOT	27	5.716	0.212	1.532	<	1.862	no

Table E.10 Analysis of Variance Table for the Final Adequate Model for the Natural Log of the Sodium Quantity (Y) as a Linear Function of Leaf Stage (X1)

	DOF	Sum Sqs.	Mean Sqs.	Fcalc		Fcrit	Signif?
Total	61	2695				$\alpha_{risk} = 0.05$	
Model	2	2683	1341	6376	>	3.316	yes
c0	1	2649	2649	12591	>	4.171	yes
c1	1	34.062	34.062	161.91	>	4.171	yes
Resid	59	12.412	0.210				
Error	30	4.828	0.161				
LOT	29	7.584	0.262	1.243	<	1.847	no

Table E.11 Analysis of Variance Table for the Final Adequate Model for the Natural Log of the Potassium Quantity (Y) as a Linear Function of Leaf Stage (X1)

	DOF	Sum Sqs.	Mean Sqs.	Fcalc		Fcrit	Signif?
Total	61	6310				$\alpha_{risk} = 0.05$	
Model	2	6301	3151	20994	>	3.316	yes
c0	1	6226	6226	41483	>	4.171	yes
c1	1	75.777	75.777	504.92	>	4.171	yes
Resid	59	8.855	0.150				
Error	30	3.193	0.106				
LOT	29	5.662	0.195	1.301	<	1.847	no

Table E.12 Analysis of Variance Table for the Final Adequate Model for the Natural Log of the Molybdenum Quantity (Y) as a Linear Function of Leaf Stage (X1)

	DOF	Sum Sqs.	Mean Sqs.	Fcalc		Fcrit	Signif?
Total	61	54.274				$\alpha_{risk} = 0.05$	
Model	2	41.957	20.979	100.49	>	3.316	yes
c0	1	19.120	19.120	91.587	>	4.171	yes
c1	1	22.837	22.837	109.39	>	4.171	yes
Resid	59	12.317	0.209				
Error	30	3.959	0.132				
LOT	29	8.358	0.288	1.380	<	1.847	no

Table E.13 Analysis of Variance Table for the Final Adequate Model for the Natural Log of the Zinc Quantity (Y) as a Linear Function of Leaf Stage (X1) and Root-Zone Water Potential (X2)

	DOF	Sum Sqs.	Mean Sqs.	Fcalc		Fcrit	Signif?
Total	61	1343				$\alpha_{risk} = 0.05$	
Model	3	1335	444.95	3341	>	2.922	yes
c0	1	1293	1293	9707	>	4.171	yes
c1	1	40.455	40.455	303.79	>	4.171	yes
c2	1	1.744	1.744	13.095	>	4.171	yes
Resid	58	7.724	0.133				
Error	30	3.659	0.122				
LOT	28	4.065	0.145	1.090	<	1.854	no

Table E.14 Analysis of Variance Table for the Final Adequate Model for the Natural Log of the Boron Quantity (Y) as a Linear Function of Leaf Stage (X1)

	DOF	Sum Sqs.	Mean Sqs.	Fcalc		Fcrit	Signif?
Total	61	733.16				$\alpha_{risk} = 0.05$	
Model	2	727.17	363.58	3582	>	3.316	yes
c0	1	651.79	651.79	6422	>	4.171	yes
c1	1	75.376	75.376	742.65	>	4.171	yes
Resid	59	5.988	0.101				
Error	30	2.224	0.074				
LOT	29	3.765	0.130	1.279	<	1.847	no

Table E.15 Analysis of Variance Table for the Final Adequate Model for the Natural Log of the Manganese Quantity (Y) as a Linear Function of Leaf Stage (X1) and Solution Manganese Concentration (X3)

	DOF	Sum Sqs.	Mean Sqs.	Fcalc		Fcrit	Signif?
Total	61	946.32				$\alpha_{risk} = 0.05$	
Model	3	934.59	311.53	1541	>	2.922	yes
c0	1	879.69	879.69	4351	>	4.171	yes
c1	1	53.388	53.388	264.06	>	4.171	yes
c3	1	1.515	1.515	7.493	>	4.171	yes
Resid	58	11.727	0.202				
Error	30	3.009	0.100				
LOT	28	8.718	0.311	1.540	<	1.854	no

Table E.16 Analysis of Variance Table for the Final Adequate Model for the Natural Log of the Iron Quantity (Y) as a Linear Function of Leaf Stage (X1) and Solution Iron Concentration (X3)

	DOF	Sum Sqs.	Mean Sqs.	Fcalc		Fcrit	Signif?
Total	61	1807				$\alpha_{risk} = 0.05$	
Model	3	1802	600.58	6739	>	2.922	yes
c0	1	1741	1741	19531	>	4.171	yes
c1	1	60.721	60.721	681.33	>	4.171	yes
c3	1	0.420	0.420	4.707	>	4.171	yes
Resid	58	5.169	0.089				
Error	30	1.731	0.058				
LOT	28	3.438	0.123	1.378	<	1.854	no

Table E.17 Analysis of Variance Table for the Final Adequate Model for the Natural Log of the Copper Quantity (Y) as a Linear Function of Leaf Stage (X1) and Root-Zone Water Potential (X2)

	DOF	Sum Sqs.	Mean Sqs.	Fcalc		Fcrit	Signif?
Total	61	395.08				$\alpha_{risk} = 0.05$	
Model	3	388.75	129.58	1187	>	2.922	yes
c0	1	329.71	329.71	3020	>	4.171	yes
c1	1	58.007	58.007	531.26	>	4.171	yes
c2	1	1.034	1.034	9.470	>	4.171	yes
Resid	58	6.333	0.109				
Error	30	2.774	0.092				
LOT	28	3.559	0.127	1.164	<	1.854	no

Since these nutrient uptake models were shown to be significantly contributed by the leaf stage of development, then these models were differentiated with respect to this time scale in order to produce models for the inorganic nutrient uptake rates, J_i. This resulted in models for J_i which were identical in form the the corresponding models for $q_{plant,i}$ except that each were multiplied by the parameter for the exponent of the leaf stage, $c_{1,i}$. Since J_i can be calculated as $(c_{1,i}\ q_{plant,i})$, then the experimental values for the nutrient uptake rates could be determined from the experimentally determined nutrient quantities. The differences between these experimental nutrient uptake rates and the standard convection rates determined as $J_{conv,i} = Q_u C_{soln,i}$ were calculated and compared using a t-test to a hypothesized value of zero. Statistically equal values for the critical and calculated t-statistics indicated a convection limitation in the nutrient uptake. Another possibility from this analysis is a result where $J_i > J_{conv,i}$ indicating a diffusion mechanism in addition to the convective supply rate. This rate of diffusion becomes the rate limiting step for the uptake of that particular nutrient. Alternatively, a result of $J_i < J_{conv,i}$ provides evidence that the rate limiting step in the nutrient uptake process is caused by the saturation of the enzymatic sites on the root cell membranes.

In addition to the models for the overall nutrient quantities measure in the plants, the rates of diffusion were modeled for K and Zn as linear functions of the individual nutrient concentration in solution (X1). These nutrients were shown to be diffusion limited by the t-test discussed earlier. The experimental diffusion rates were determined as the differences between J_i and $J_{conv,i}$. Therefore, the diffusion of nutrients to the root surface is in addition to the convective supply rate. By providing evidence that this linear model was adequate in describing the diffusion rate without the requirement of additional terms, then these models combined with the standard convection equation, $J_{conv,i} = Q_u C_{soln,i}$, could be considered the final nutrient uptake models for K and Zn. The analysis of variance results are provided in Tables E.18 and E.19, respectively.

Table E.18 Analysis of Variance Table for the Linear Model Describing the Diffusion Rate of Potassium (Y) as a Function of the Concentration of Potassium in Solution (X1)

	DOF	Sum Sqs.	Mean Sqs.	Fcalc		Fcrit	Signif?
Total	61	308018				$\alpha_{risk} = 0.05$	
Model	2	108188	54094	15.971	>	3.316	yes
d0	1	50507	50507	14.912	>	4.171	yes
d1	1	57680	57680	17.030	>	4.171	yes
Resid	59	199830	3387				
Error	30	91201	3040				
LOT	29	108629	3746	1.106	<	1.847	no

Table E.19 Analysis of Variance Table for the Linear Model Describing the Diffusion Rate of Zinc (Y)

	DOF	Sum Sqs.	Mean Sqs.	Fcalc		Fcrit	Signif?
Total	61	20.394				$\alpha_{risk} = 0.05$	
Model	2	17.531	8.766	180.64	>	3.316	yes
d0	1	17.397	17.397	358.52	>	4.171	yes
d1	1	0.135	0.135	2.774	<	4.171	no
Resid	59	2.863	0.049				
Error	30	1.049	0.035				
LOT	29	1.814	0.063	1.289	<	1.847	no

In addition to the nutrients limited by the rate of diffusion, several nutrients were shown to be limited by the enzymatic activity at the root surface. These included P, Mg, Ca, Na, Mo, B, Mn, Fe, and Cu. These nutrients were shown to be biologically limited by the t-test discussed earlier. The uptake rates for these nutrients were modeled using a linearized function of the Michaelis-Menten equation. This was achieved by taking the inverse of each term. By providing evidence that this linear model was adequate in describing the nutrient uptake rates without the requirement of additional terms, then these models could be considered the final nutrient uptake models for the particular nutrients. The analysis of variance results are provided in Tables E.20 and E.28, respectively.

Table E.20 Analysis of Variance Table for the Model of the Inverse of the Biological Rate of Phosphorus Uptake (Y) as a Linear Function of the Inverse of the Concentration of Phosphorus in Solution (X1)

	DOF	Sum Sqs.	Mean Sqs.	Fcalc		Fcrit	Signif?
Total	34	0.788				$\alpha_{risk} = 0.05$	
Model	2	0.711	0.356	148.25	>	3.592	yes
e0	1	0.686	0.686	285.84	>	4.451	yes
e1	1	0.026	0.026	10.661	>	4.451	yes
Resid	32	0.077	0.0024				
Error	17	0.044	0.0026				
LOT	15	0.032	0.0022	0.899	<	2.308	no

Table E.21 Analysis of Variance Table for the Model of the Inverse of the Biological Rate of Magnesium Uptake (Y) as a Linear Function of the Inverse of the Concentration of Magnesium in Solution (X1)

	DOF	Sum Sqs.	Mean Sqs.	Fcalc		Fcrit	Signif?
Total	34	0.0452				$\alpha_{risk} = 0.05$	
Model	2	0.0417	0.0209	192.75	>	3.592	yes
e0	1	0.0411	0.0411	380.15	>	4.451	yes
e1	1	0.00058	0.00058	5.352	>	4.451	yes
Resid	32	0.0035	0.00011				
Error	17	0.0016	0.00010				
LOT	15	0.0018	0.00012	1.127	<	2.308	no

Table E.22 Analysis of Variance Table for the Model of the Inverse of the Biological Rate of Calcium Uptake (Y) as a Linear Function of the Inverse of the Concentration of Calcium in Solution (X1)

	DOF	Sum Sqs.	Mean Sqs.	Fcalc		Fcrit	Signif?
Total	34	0.0045				$\alpha_{risk} = 0.05$	
Model	2	0.0041	0.0021	163.14	>	3.592	yes
e0	1	0.0040	0.0040	318.26	>	4.451	yes
e1	1	0.00010	0.00010	8.024	>	4.451	yes
Resid	32	0.00040	1.3E-05				
Error	17	0.00011	6.6E-06				
LOT	15	0.00029	2E-05	1.544	<	2.308	no

Table E.23 Analysis of Variance Table for the Model of the Inverse of the Biological Rate of Sodium Uptake (Y) as a Linear Function of the Inverse of the Concentration of Sodium in Solution (X1)

	DOF	Sum Sqs.	Mean Sqs.	Fcalc		Fcrit	Signif?
Total	34	0.481				$\alpha_{risk} = 0.05$	
Model	2	0.444	0.222	190.53	>	3.592	yes
e0	1	0.438	0.438	375.94	>	4.451	yes
e1	1	0.0060	0.0060	5.116	>	4.451	yes
Resid	32	0.037	0.0012				
Error	17	0.023	0.0013				
LOT	15	0.015	0.00097	0.837	<	2.308	no

Table E.24 Analysis of Variance Table for the Model of the Inverse of the Biological Rate of Molybdenum Uptake (Y) as a Linear Function of the Inverse of the Concentration of Molybdenum in Solution (X1)

	DOF	Sum Sqs.	Mean Sqs.	Fcalc		Fcrit	Signif?
Total	34	101254				$\alpha_{risk} = 0.05$	
Model	2	55309	27655	19.261	>	3.592	yes
e0	1	55279	55279	38.502	>	4.451	yes
e1	1	30.171	30.171	0.021	<	4.451	no
Resid	32	45944	1436				
Error	17	19791	1164				
LOT	15	26154	1744	1.214	<	2.308	no

Table E.25 Analysis of Variance Table for the Model of the Inverse of the Biological Rate of Boron Uptake (Y) as a Linear Function of the Inverse of the Concentration of Boron in Solution (X1)

	DOF	Sum Sqs.	Mean Sqs.	Fcalc		Fcrit	Signif?
Total	34	5585				$\alpha_{risk} = 0.05$	
Model	2	5233	2617	238.26	>	3.592	yes
e0	1	5217	5217	475.04	>	4.451	yes
e1	1	16.215	16.215	1.477	<	4.451	no
Resid	32	351.42	10.982				
Error	17	141.67	8.334				
LOT	15	209.75	13.983	1.273	<	2.308	no

Table E.26 Analysis of Variance Table for the Model of the Inverse of the Biological Rate of Manganese Uptake (Y) as a Linear Function of the Inverse of the Concentration of Manganese in Solution (X1)

	DOF	Sum Sqs.	Mean Sqs.	Fcalc		Fcrit	Signif?
Total	34	304.38				$\alpha_{risk} = 0.05$	
Model	2	267.67	133.83	116.65	>	3.592	yes
e0	1	267.59	267.59	233.23	>	4.451	yes
e1	1	0.072	0.072	0.063	<	4.451	no
Resid	32	36.715	1.147				
Error	17	20.562	1.210				
LOT	15	16.153	1.077	0.939	<	2.308	no

Table E.27 Analysis of Variance Table for the Model of the Inverse of the Biological Rate of Iron Uptake (Y) as a Linear Function of the Inverse of the Concentration of Iron in Solution (X1)

	DOF	Sum Sqs.	Mean Sqs.	Fcalc		Fcrit	Signif?
Total	34	27.946				$\alpha_{risk} = 0.05$	
Model	2	26.284	13.142	253.09	>	3.592	yes
e0	1	25.895	25.895	498.69	>	4.451	yes
e1	1	0.389	0.389	7.494	>	4.451	yes
Resid	32	1.662	0.052				
Error	17	0.777	0.046				
LOT	15	0.885	0.059	1.136	<	2.308	no

Table E.28 Analysis of Variance Table for the Model of the Inverse of the Biological Rate of Copper Uptake (Y) as a Linear Function of the Inverse of the Concentration of Copper in Solution (X1)

	DOF	Sum Sqs.	Mean Sqs.	Fcalc		Fcrit	Signif?
Total	34	17727				$\alpha_{risk} = 0.05$	
Model	2	16666	8333	251.16	>	3.592	yes
e0	1	16497	16497	497.23	>	4.451	yes
e1	1	168.91	168.91	5.091	>	4.451	yes
Resid	32	1062	33.177				
Error	17	340.65	20.038				
LOT	15	721.03	48.068	1.449	<	2.308	no

In addition to modeling the biological uptake according to the linearized Michaelis-Menten equation, the back diffusion of these nutrients due to the build up at the root surface was modeled as well. This accumulation of the nutrients was due to the restriction in the uptake caused by the saturation of the active sites. Using the same procedure as the diffusion limited nutrients, the classical diffusion equation was re-formulated into a linear regression equation and the parameters estimated using the method of least squares. The significance of these parameters were then determined using an analysis of variance as shown in Tables E.29 to E.37 below for P, Mg, Ca, Na, Mo, B, Mn, Fe, and Cu, respectively.

Table E.29 Analysis of Variance Table for the Model Describing the Diffusion Rate of Phosphorus (Y) as a Linear Function of the Concentration of Phosphorus in Solution (X1)

	DOF	Sum Sqs.	Mean Sqs.	Fcalc		Fcrit	Signif?
Total	34	10110				$\alpha_{risk} = 0.05$	
Model	2	9916	4958	816.45	>	3.592	yes
d0	1	8777	8777	1445	>	4.451	yes
d1	1	1139	1139	187.52	>	4.451	yes
Resid	32	194.33	6.073				
Error	17	97.931	5.761				
LOT	15	96.396	6.426	1.058	<	2.308	no

Table E.30 Analysis of Variance Table for the Model Describing the Diffusion Rate of Magnesium (Y) as a Linear Function of the Concentration of Magnesium in Solution (X1)

	DOF	Sum Sqs.	Mean Sqs.	Fcalc		Fcrit	Signif?
Total	34	84449				$\alpha_{risk} = 0.05$	
Model	2	81262	40631	408.09	>	3.592	yes
d0	1	68543	68543	688.43	>	4.451	yes
d1	1	12720	12720	127.75	>	4.451	yes
Resid	32	3186	99.564				
Error	17	901.09	53.005				
LOT	15	2285	152.33	1.530	<	2.308	no

Table E.31 Analysis of Variance Table for the Model Describing the Diffusion Rate of Calcium (Y) as a Linear Function of the Concentration of Calcium in Solution (X1)

	DOF	Sum Sqs.	Mean Sqs.	Fcalc		Fcrit	Signif?
Total	34	244742				$\alpha_{risk} = 0.05$	
Model	2	175672	87836	40.694	>	3.592	yes
d0	1	133135	133135	61.681	>	4.451	yes
d1	1	42538	42538	19.708	>	4.451	yes
Resid	32	69070	2158				
Error	17	13452	791.27				
LOT	15	55618	3708	1.718	<	2.308	no

Table E.32 Analysis of Variance Table for the Model Describing the Diffusion Rate of Sodium (Y) as a Linear Function of the Concentration of Sodium in Solution (X1)

	DOF	Sum Sqs.	Mean Sqs.	Fcalc		Fcrit	Signif?
Total	34	329.61				$\alpha_{risk} = 0.05$	
Model	2	99.027	49.513	6.871	>	3.592	yes
d0	1	1.783	1.783	0.247	<	4.451	no
d1	1	97.243	97.243	13.495	>	4.451	yes
Resid	32	230.58	7.206				
Error	17	111.95	6.586				
LOT	15	118.63	7.909	1.098	<	2.308	no

Table E.33 Analysis of Variance Table for the Model Describing the Diffusion Rate of Molybdenum (Y) as a Linear Function of the Concentration of Molybdenum in Solution (X1)

	DOF	Sum Sqs.	Mean Sqs.	Fcalc		Fcrit	Signif?
Total	34	0.016				$\alpha_{risk} = 0.05$	
Model	2	0.0093	0.0046	21.822	>	3.592	yes
d0	1	0.0093	0.0093	43.640	>	4.451	yes
d1	1	7.1E-07	7.1E-07	0.0033	<	4.451	no
Resid	32	0.0068	0.00021				
Error	17	0.0017	0.00010				
LOT	15	0.0051	0.00034	1.585	<	2.308	no

Table E.34 Analysis of Variance Table for the Model Describing the Diffusion Rate of Boron (Y) as a Linear Function of the Concentration of Boron in Solution (X1)

	DOF	Sum Sqs.	Mean Sqs.	Fcalc		Fcrit	Signif?
Total	34	10.015				$\alpha_{risk} = 0.05$	
Model	2	9.992	4.996	6670	>	3.592	yes
d0	1	9.148	9.148	12215	>	4.451	yes
d1	1	0.843	0.843	1126	>	4.451	yes
Resid	32	0.024	0.00075				
Error	17	0.0090	0.00053				
LOT	15	0.015	0.001	1.334	<	2.308	no

Table E.35 Analysis of Variance Table for the Model Describing the Diffusion Rate of Manganese (Y) as a Linear Function of the Concentration of Manganese in Solution (X1)

	DOF	Sum Sqs.	Mean Sqs.	Fcalc		Fcrit	Signif?
Total	34	0.960				$\alpha_{risk} = 0.05$	
Model	2	0.368	0.184	9.938	>	3.592	yes
d0	1	0.0033	0.0033	0.178	<	4.451	no
d1	1	0.365	0.365	19.699	>	4.451	yes
Resid	32	0.592	0.019				
Error	17	0.349	0.021				
LOT	15	0.244	0.016	0.878	<	2.308	no

Table E.36 Analysis of Variance Table for the Model Describing the Diffusion Rate of Iron (Y) as a Linear Function of the Concentration of Iron in Solution (X1)

	DOF	Sum Sqs.	Mean Sqs.	Fcalc		Fcrit	Signif?
Total	34	282.45				$\alpha_{risk} = 0.05$	
Model	2	279.28	139.64	1411	>	3.592	yes
d0	1	239.55	239.55	2421	>	4.451	yes
d1	1	39.735	39.735	401.61	>	4.451	yes
Resid	32	3.166	0.099				
Error	17	1.306	0.077				
LOT	15	1.860	0.124	1.253	<	2.308	no

Table E.37 Analysis of Variance Table for the Model Describing the Diffusion Rate of Copper (Y) as a Linear Function of the Concentration of Copper in Solution (X1)

	DOF	Sum Sqs.	Mean Sqs.	Fcalc		Fcrit	Signif?
Total	34	0.379				$\alpha_{risk} = 0.05$	
Model	2	0.373	0.186	912.55	>	3.592	yes
d0	1	0.369	0.369	1805	>	4.451	yes
d1	1	0.0040	0.0040	19.602	>	4.451	yes
Resid	32	0.0065	0.0002				
Error	17	0.0014	8.4E-05				
LOT	15	0.0051	0.00034	1.667	<	2.308	no

VITA